Universitat Ramon Llull

DOCTORAL THESIS

Title	**New strategies in antimicrobial photodynamic therapy and singlet oxygen detection**
Presented by	**Rubén Ruiz González**
Centre	**IQS School of Engineering**
Department	**Organic Chemistry**
Supervised by	**Prof. Santi Nonell Marrugat**

SUMMARY

Three strategies addressed to give further scope on to the antimicrobial photodynamic therapy field comprise the first part of the thesis. In a first approach, six cationic photosensitisers varying in the net electrical charge and structure have been characterised in solution and their photoinactivation skills have been tested against different types of microorganisms. In a s econd approach, conjugates between a photosensitiser and the antimicrobial peptide Apidaecin 1b have been analysed in a photophysical and mechanistic way, and their properties have been correlated with their bacterial photoinactivation ability. In the last approach, two fluorescent proteins –namely TagRFP and miniSOG- have been expressed in *E. coli* and their phototoxicity has been studied and characterised mechanistically. Moreover, the capacity of miniSOG to photosensitise singlet oxygen formation has been revisited and studied in detail.

In the second part of the thesis, focus has been shifted towards singlet oxygen detection. In the first section, the probing ability of a new dyad comprising a naphthoxazole moiety plus a singlet oxygen chemical trap has been evaluated in solution. In the last section, we develop, test, and discuss the feasibility of a polyacrylamide nanoparticle scaffold as a potential platform for singlet oxygen detection in intracellular systems.

RESUMEN

Tres estrategias destinadas a aportar una mayor perspectiva en el campo de la terapia fotodinámica antimicrobiana componen la primera parte de la tesis. En una primera aproximación, seis fotosensibilizadores catiónicos, con distinta carga eléctrica neta y estructura, han sido caracterizados en disolución y sus propiedades fotoinactivadoras probadas contra diferentes tipos de microorganismos. En una segunda aproximación, conjugados entre un fotosensibilizador y el péptido antimicrobiano Apidaecina 1b han sido analizados fotofísica y mecanísticamente, y sus propiedades correlacionadas con su habilidad fotosensibilizadora en bacterias. En la última aproximación, dos proteínas fluorescentes –TagRFP y miniSOG- han sido expresadas en *E. coli* y se ha estudiado su fototoxicidad así como su mecanismo de acción. Además, se ha reevaluado y estudiado en detalle la capacidad de miniSOG para fotosensibilizar la formación de oxígeno singlete.

En la segunda parte de la tesis, el interés se ha centrado en la detección de oxígeno singlete. En la primera sección, se ha evaluado la capacidad de detección en disolución de una nueva díada compuesta por un naftoxazol y una trampa química de oxígeno singlete. En la última sección, se desarrolla, prueba y discute la viabilidad de nanopartículas de poliacrilamida como plataforma potencial para detección de oxígeno singlete en sistemas intracelulares.

ABBREVIATIONS

ADPA	9,10-anthracene dipropionic acid
AMP	antimicrobial peptide
(a)PDT	(antimicrobial) photodynamic therapy
a.u.	arbitrary units
BHI	brain-heart infusion
BSA	bovine serum albumin
CALI	chromophore-assisted light inactivation
CD	circular dichroism
CFU	colony forming units
(d)PBS	(deuterated) phosphate buffered saline
DABCO	1,4-diazabicyclo[2.2.2]octane
DMSO	dimethylsulfoxide
EDC	1-(3-dimethylaminopropyl)-3-ethylcarbodiimide hydrochloride
EM	electron microscopy
FACS	fluorescence-activated cell sorting
FP	fluorescent protein
GFP	green fluorescence protein
Gdn HCl	guanidinium hydrochloride
His	histidine
IM	inner membrane
IPTG	isopropyl β-D-1-thiogalactopyranoside
IR	infrared
IRF	instrument's response function
LB	lysogeny broth
MDR	multridrug-resistant
MeOH	methanol
Met	methionine
miniSOG	mini singlet oxygen generator
MRSA	methicillin-resistant *Staphylococcus aureus*
***m*-THPP**	5,10,15,20-tetrakis(m-hydroxyphenyl)-21H,23H-porphine
NaN$_3$	sodium azide
NDM-1	New Delhi metallo-beta lactamase
NHS	N-hydroxysuccinimide
NMB	new methylene blue
NMe$_3$MeO-TBPo	2,7,12-tris(trimethyl-*p*-tolyl)–17-(*p*-(methoxymethyl)phenyl)porphycene
NPN	1-N-phenylnaphthylamine
NPs	nanoparticles

$^1O_2$ ($^1\Delta_g$)	singlet oxygen
OD	optical density
OM	outer membrane
PDI	photodynamic inactivation
PDR	pandrug-resistant
PDT	photodynamic therapy
PN(S)	phenalenone (-2-sulfonate)
PS	photosensitiser
Py$_3$MeO-TBPo	2,7,12-tris(α-pyridinio-p-tolyl)–17-(p-(methoxymethyl)phenyl)porphycene
RFP	red fluorescent protein
ROS	reactive oxygen species
rt	room temperature
SOSG	singlet oxygen sensor green
Spp	species
TCSPC	time-correlated single photon counting
THF	tetrahydrofuran
TMPyP	5,10,15,20-tetrakis(N-methyl-4-pyridyl)-21H,23H-porphine
TPP	5,10,15,20-Tetraphenyl-21H,23H-porphine
TPPo	2,7,12,17-tetraphenylporphycene
TPPS	meso-tetrakis(4-sulfonatophenyl)-porphyrin
Trp	tryptophan
TRPD	time-resolved phosphorescence detection
TSB	tryptic soy broth
Tyr	tyrosine
UA	uric acid
UV	ultraviolet
VIS	visible
XDR	extensively-drug resistant

INDEX

Chapter I.

General introduction

Living in a microbial world

"The number of these animals in the scurf of a man's teeth, are so many that I believe they exceed the number of men in a kingdom. [...] Some of these are so exceedingly small that millions of millions might be contained in a single drop of water. I was much surprised at this wonderful spectacle, having never seen any living creature comparable to those for smallness; nor could I indeed imagine that nature had afforded instances of so exceedingly minute animal proportions."

-Antony van Leeuwenhoek

(1684; letter to the Royal Society of London)

Bacteria have been encountered on every recondite surface on Earth, and almost all bacteria possess at least one alternative energy-generating system if the preferred route is unavailable. Ecologists have discovered bacteria in places no one thought a creature could live, and not only do they tolerate these places, but they thrive. Extremophiles live in environments of extraordinary harshness to human standards (very high/low temperatures, huge salt concentrations, etc.) where few other living beings can survive.[1,2]

Though tiny, bacteria occupy the Earth in enormous numbers. The total population of bacteria is estimated to reach 10^{30} and the mass of these cells approaches 1×10^{15} kg. Of these, the overwhelming majority lives in the soil. Just to provide a couple of extra figures and as an update of van Leeuwenhoek comparison, the number of microorganisms in a teaspoon of soil can be compared to the number of humans currently living in Africa. Or, in another rough estimation, dental plaque is so densely packed that one gram will contain namely the same number of humans that have ever populated the Earth![3]

We are microbe magnets since we are born. Evolutionarily, we are meant to attract these bugs because that's the initial signal to activate our immune system.[4] Although animals and bacteria have different forms and lifestyles, they recognise one another and are able to coexist. Most organisms have about 1/3 of their genes in common. For instance, in the human genome 37% genes are similar to those in

bacteria and archaea. Another 28% are similar to genes in unicellular eukaryotes. Thus, a full 65% of human genes show similarity to those of microbes.[5]
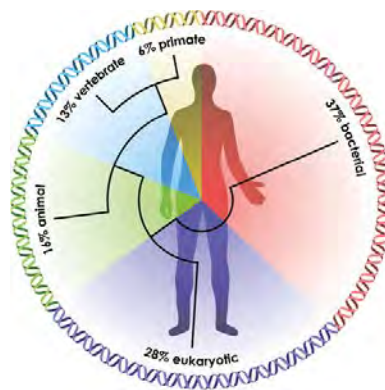
Figure 1. Human genomic signature through phylogenetic analysis. Drawing (from ref [5]) sorts out human genes relative to percentage of the genome that arose at a series of stages in biological evolution.

The human body is, thus, both an organism and a complex ecosystem, whose inhabitants comprise *ca.* 1000 different species belonging to 200 genera. The human microbiota (the collection of microbes that live on and inside us) consists of about 100 trillion microbial cells that outnumber our ''human'' cells 10 to 1, and that provide a wide range of metabolic functions that we lack.[6] If we consider ourselves as supraorganisms encompassing these microbial symbionts, by far the majority of genes in the system are microbial (over 23,000 genes constitute the human genome while *ca.* 8,000,000 genes present in the human microbiome –which refers to the collective genomes of the microbes that colonise a determined habitat, in this case the human body-).[7]

Bacteria

"Ce qui est vrai pour le colibacille est vrai pour l'éléphant"

-Jacques Monod

(Biologist; Nobel Prize 1965)

Bacteria are self-sufficient packets of life, the smallest independently living creatures on Earth. Most bacteria are between 0.5 and 1.5 μm in diameter and 1 to 2 μm long, bacterial volumes ranging, thus, from 0.02 to 400 μm^3.[8] Still, extreme cases appear: huge *Thiomargarita namibiensis* reaches 750 μm while *Francisella tularensis* is as small as 0.2 μm.[9,10] One of many advantages in being small involves the ability to sense environmental changes with an immediacy that large multicellular organisms lack. Bacteria need only be big enough to hold their vital enzymes, proteins, and genetic machinery. Its simple architecture allows for rapid reproduction, which aids adaptation. Bacterial metabolism is a model of efficiency because of a large surface-to-volume ratio that the aforementioned smallness creates.[8] No part of a bacterial cell is very far from the surface where nutrients enter and undesired products exit. Finally, small size contributes to massive bacterial populations that dwarf the populations of any other biota. On the other hand, microbiology's slow acceptance was partly due to the minuscule dimensions of microbes. Antony van Leewenhok reported the first thorough pictures of the '*very little animalcules*' in the end of XVIIth century; but not until the naissance of electron and fluorescence microscopy did their inner structures (nucleoids, ribosomes, cell walls and membranes, flagella) become discernible.[11]

In a microscope, bacteria exhibit several different shapes: spheres (coccus), rods (bacillus), spirals (spirillum), corkscrews (spirochaete), and boomerangs (vibrio). When bacteria grow, the cell wall prevents any increase in size contrary to multicellular organisms.[12,13]

Bacteria grow by splitting into two new cells by binary fission. Bacteria do not always live as free-floating specimens. As cell numbers increase, certain species align or form clusters. Furthermore, if bacterial populations find a surface with a little moisture and some nutrients they settle and form thin, flat

sheets and swarm forming what we call bacterial biofilms (Figure 2).[14,15] Thus, they tend to form communities which display attributes of multicelullarity, with a vast diversity in population, architecture and activities. These groups of cells are held in place by an extracellular matrix and can use intercellular signaling for communication.[16]

Figure 2. Biofilms formed by *Bacillus subtilis* (strain NCIB 3610). Image from reference [5].

Until the late 1970s, microbiologists identified bacteria through enzyme activities, end products, nutrient needs, and morphology. In 1977 C arl Woese proposed a classification based on the use of ribosomal ribonucleic acid (rRNA) fragments. Because the genetic information in rRNA is unique to each species, it can act as a type of bacterial fingerprint. This analysis led to a new hierarchy of living things with bacteria, archaea, and eukaryotes comprising the three domains shown in Figure 3b that substituted classical kingdom-like phylogeny tree (Figure 3a).[17,18]
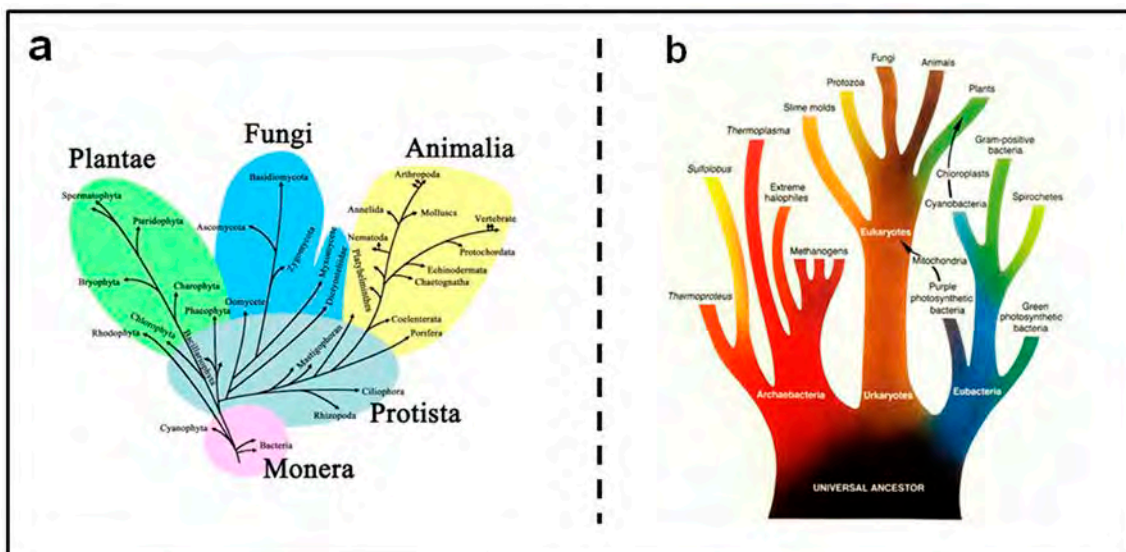
Figure 3. Classical (a) and molecular (b) phylogenia representation. Adapted from ref [19] and http://www.astronoo.com/en/news/tree-of-life.html (retrieved April 2013)

In a different approach, bacteria are usually classified in two main categories regarding their differences in structure. Gram-positive bacteria (Figure 4 right) are surrounded by an outer wall, which is separated from the plasma membrane by a p eriplasmic space. This 20-80 nm thick wall acts as a protective mesh constituted mainly by peptidoglycan layers, which are traversed by negatively charged lipoteichoic and teichuronic acids anchored in the membrane. This architecture doesn't act strictly as a permeability barrier, since macromolecules with molecular weight up to 60,000 Da can diffuse through the inner membrane (IM). On the other hand, Gram-negative bacteria (Figure 4 left) are endowed with an additional 10-15 nm thick densely packed structural layer, external to the peptidoglycan network, whose constituents (e.g., lipoproteins, lipopolysaccharides) confer the outer surface highly negative charges. This highly organised system –called outer membrane (OM)- inhibits the penetration of compounds with molecular weight larger than 600-700 Da.[20]
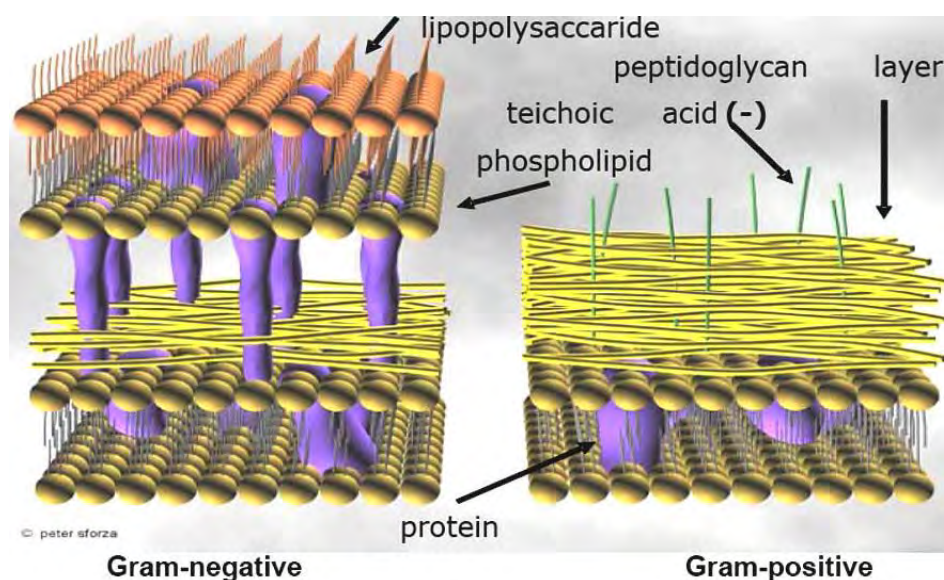
Figure 4. Gram-positive and Gram-negative bacteria structure. Image from ref [20].

Bad bugs, no drugs

"Bacteria have been around for billions of years. Then we steal some antibacterial drugs from fungi and think we can do us in for good."

-Stephen Jay Gould
(1941-2002; Evolutionary biologist)

There is a p reconceived concept that associates bacteria with pathogenesis and, in the end, with deleterious effects (*e.g.* bioterrorism, infections concomitant to natural catastrophes, organisms resistant to antibiotics, etc.). However, the vast majority of microorganisms are not necessarily bad, indeed.

Besides oxygenating the early Earth, loads of bacterial activities shape the ecology of the planet, thus helping to sustain human life. In soil, several bacteria replenish nitrogen that higher organisms need or regulate the carbon cycle through the Earth's organic and inorganic matter; they help metabolise food, block dangerous pathogens and even help develop the immune response.[21,22] Humans and animals also come with a full complement of gut flora that sometimes provides the host living system with metabolic capabilities that do n ot possess by themselves.[23-25] In addition to aiding our digestive system, gut microorganisms also influence distant parts of the body, including the brain.[5]

Moreover, our understanding of microbes has allowed us to use their features in our profit. Among others, we can track disease outbreaks or monitor pollution; we can use them to clean up our wastes and decontaminate (sulfide removal, oil spills…);[26,27] they can provide important and useful chemical compounds;[28-31] preparation of many daily products (food and beverages) are aided by microbes;[32] they have enabled the development of revolutionary tools for bioengineering such as PCR;[33] or we now manage that medically important compounds such as human insulin can be processed in large scale by recombinant bacteria.[34]

Despite we have exemplified in the previous paragraphs that bacteria are not always to be related with deleterious effects, the truth is that pathogenic microorganisms have become a u niversal threat. Today infectious disease is the second most important killer in the world, number three in developed

nations and fourth in the USA. It is the third leading cause of death in Europe and despite existing antibiotic therapies and vaccines, infectious diseases remain the leading cause of mortality and morbidity. Worldwide, 17 million people die each year from bacterial infections.[35]

In total, there are *ca.* 1,400 known species of human pathogens (including viruses, bacteria, fungi, protozoa and helminths), but they account for much less than 1% of the total number of microbial species on the planet.[3] The issue of prevention and control of infectious diseases remains open and a series of highly virulent pathogens are emerging both in and beyond the hospital setting. Penicillin and subsequent development and synthesis of other antibiotics were one of the most sounded scientific highlights of the 20th century as a tool of prevention and control of infectious diseases worldwide. Fleming's first paper on penicillin was published in 1929. Penicillin was put into common use in the early 1940s but by 1944 half of all clinical *Staphylococci* species (hereafter *spp*) isolates were resistant to this proclaimed "miracle drug." Still, by the 1980s, pharmaceutical companies were convinced that there were enough antibiotics and that it was about time to shift focus to more threatening clinical problems such as cancer, diabetes and heart or degenerative diseases.

Paradoxically, concomitant with the rise of antibiotic-resistant bacteria, approval of new antibiotics has dramatically slowed (Figure 5). And not on only that: the number of truly novel compounds with new mechanism of action remains small.[36] Of great significance, nearly all major pharmaceutical companies have withdrawn from or greatly downsized their antibiotic research and development (R+D) programs over the past two decades, and the egress from the market is actively continuing.
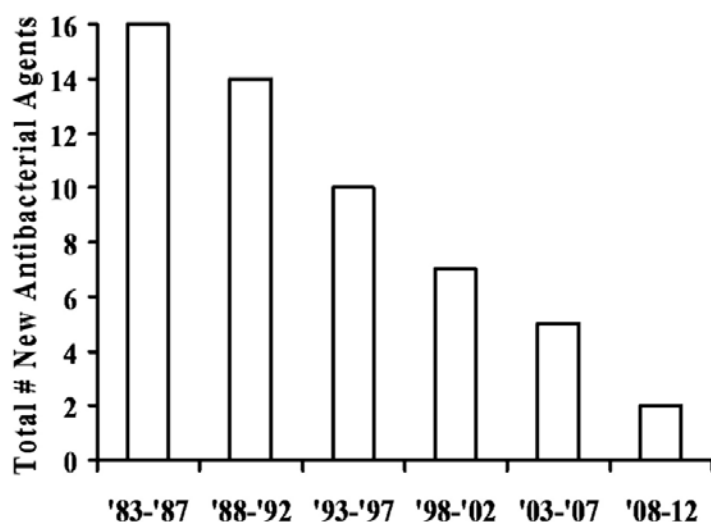
Figure 5. Number of antibacterial agents approved by the US FDA per 5-year period (from reference [37])

Microorganisms, however, had a different opinion. The extensive and inappropriate use of antibiotics gradually has led to a worrying resurgence of morbidity and mortality from new and old infectious diseases.

Figure 6. Stop to the abuse of antibiotics usage. Image adapted from http://www.flickr.com/photos/mbradbury/1847123974/ (retrieved April 2013)

The problem of antimicrobial resistance is not specific to bacteria. Medically important viruses (e.g., HIV, influenza), fungi (e.g., *Candida*, *Aspergillus*), and parasites (e.g., malaria) also develop resistance. However, a unique convergence of events has created an enormous public health concern regarding antibiotic resistance in bacteria making it the primary focus of most research in the field. Today, many bacteria are already resistant to common antibiotics. Antimicrobial resistance is a co nsequence of

continued misuse and overuse of antibiotics (both in humans and animals, Figure 6) combined with the natural and constant growth of resistance over time and the remarkable genetic plasticity of bacteria.[36,38,39]

Harmonised definitions with which to describe and classify the different patterns of bacterial resistance found in healthcare-associated environments comprise three categories: multidrug-resistant (MDR), extensively-drug resistant (XDR) and pandrug-resistant (PDR) bacteria.[40] Up to date, The naisement of the so called "superbugs" or ESKAPE pathogens (*Enterococcus faecium*, *Staphylococcus aureus*, *Klebsiella pneumoniae*, *Acinetobacter baumanii*, *Pseudomonas aeruginosa*, *Escherichia coli* and *Enterobacter spp*) cause serious and life-threatening infections. Indeed, they are extremely difficult and in many cases impossible to effectively treat.[41]
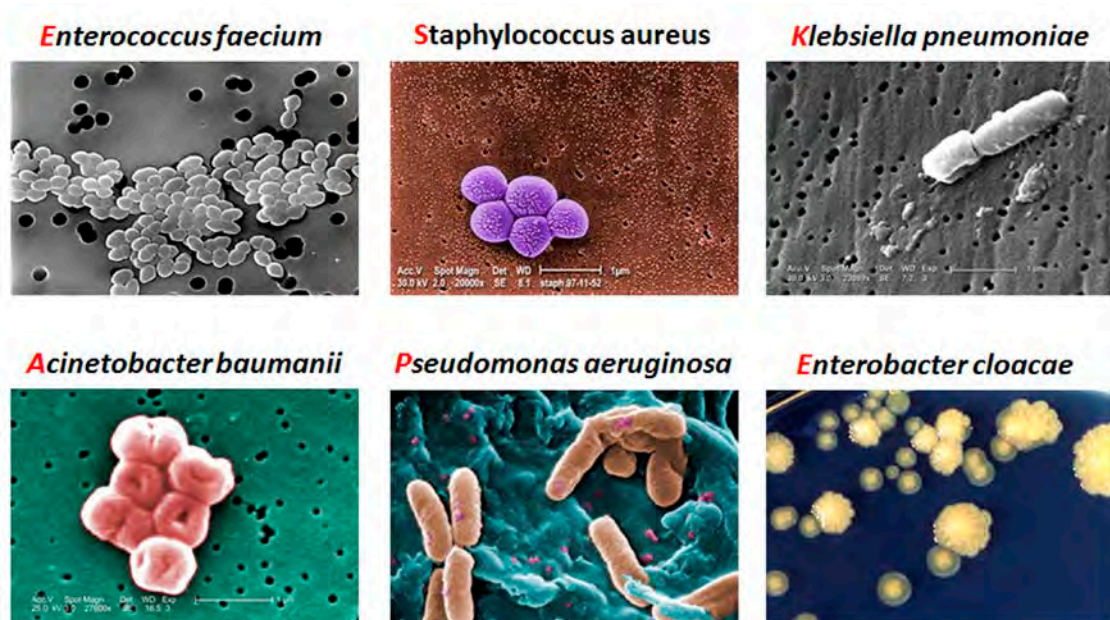
Figure 7. SEM micrographs depicting ESKAPE pathogens. Images were obtained from the Public Health Image Library of the centers for disease control and prevention (http://phil.cdc.gov/Phil/default.asp; retrieved April 2013).

Ten years ago, concern was centred on Gram-positive bacteria, particularly methicillin-resistant *S. aureus* and vancomycin-resistant *Enterococcus spp*. Now, however, consensus exist that MDR Gram-negative bacteria pose the greatest risk. Not only is the increase in resistance of Gram-negative bacteria faster than in Gram-positive bacteria, but also there are fewer new and developmental antibiotics active against Gram-negative bacteria. The increase in resistance of Gram-negative bacteria is mainly due to mobile genes on plasmids that can readily spread through bacterial populations.[42]

Therapeutic options for ESKAPE pathogens are extremely limited such that clinicians are often forced to use obsolete drugs, such as colistin, that are associated with significant toxicity and for which there is a lack of robust data to guide dosage regimen or duration of therapy.[43] For example, more people now die of MRSA infection in U.S.A. than of HIV/AIDS, emphysema, Parkinson's disease and homicide together.[37] XDR *Klebsiella* or XDR *Acinetobacter* bacteria kill up to 50% of infected patients despite treatment with last resort drugs, and resistance rates for these pathogens continue to climb. As a final threatening example, all strains of *Klebsiella* and *E. coli* containing the New Delhi metallo-beta-lactamase (NDM-1) enzyme are resistant to all antibiotics except colistin and tigecycline, and 10% of these strains are even resistant to these drugs, making them truly pan resistant. XDR *Acinetobacter* strains that are resistant to colistin are now being reported.[42]

We must increase our efforts to preserve the activity of available antibiotics, or at least expand as much as possible the period of their use, whilst intense research efforts should be focused on the development and introduction into clinical practice of new antimicrobial agents or therapies.

Photodynamic therapy

"I don't understand it Dr. von Tappeiner, the paramecia were all wiggling just fine a minute ago, but now these over by the window seem to be dead."

-Oscar Raab (1900)

The origin of photosensitisation as a science is usually attributed to the work of Oscar Raab at the end of 19th century. Although there are several accounts of photosensitisation reactions in the writings of the Egyptians, Indians and Chinese dating to at least 30 centuries ago, the modern era is conveniently recognised to begin in the year 1900.

Oscar Raab was a medical student of Hermann von Tappeiner at the Ludwig-Maximilian University in Munich. Raab was involved in a study of the toxicity of acridine towards paramecia. In the winter semester of 1897-98, Raab found that the apparent toxicity that he measured depended on the time of day when he performed his experiment. Near midday the toxicity was the greatest. Raab realised that one of the variables in his work was the amount of light in the laboratory, and he subsequently demonstrated that paramecia in acridine solutions were inactivated more effectively if the solutions were kept near a bright window, than if they were prevented from light. The surprising result was published in 1900 and stimulated further activity in the field. It was the first report regarding what they called "photodynamic action". Since then, a lot has been learnt about this effect ant the development of its use in therapies is a fact.[44]

The photodynamic therapy (PDT) concept comprises the action of three components: a photosensitiser (PS), a light source of appropriate wavelength, and oxygen. The interaction between light and the PS leads to the generation of reactive oxygen species (ROS), e.g. singlet oxygen ($^1O_2$), by two possible mechanisms involving either the interaction of the PS with the oxidizable substrate (e.g., by electron-transfer) -type I- or with oxygen (by energy- or electron-transfer) -type II- reactions. Almost every cell component is a potential target for these ROS, as they react readily with proteins, carbohydrates, cell-membrane components, and nucleic acids resulting in cytotoxicity.[45] PDT is a highly

selective modality as (a) hyperproliferating cells selectively uptake PSs and (b) cell death is spatially limited to regions where light of the appropriate wavelength is applied.

Every PS molecule participates in multiple cycles of oxygen activation so that low doses are required so as to achieve the therapeutic effect. Excited species are generated by photon absorptions and, generally, they exhibit very short lifetimes limiting this way the possible reactions that occur. There are different pathways of returning the energy delivered by irradiation. Either through radiative means (fluorescence, phosphorescence) or thermal pathways (intersystem crossing (ISC), internal conversion, etc.); but they can also react with neighbouring compounds. In this second scenario, another classification can be also done. When energy transfer is mediated through proton or electron with the biological substrate it is known as Type I mechanism; on the contrary, if oxygen is the primary acceptor this process is called Type II mechanism (see Scheme 2). Both mechanisms occur simultaneously and the efficiency of each process hinges on the respective value relative to oxygen and substrate concentration and to the reaction constant rates and also on the triplet state deactivation kinetics.[46]
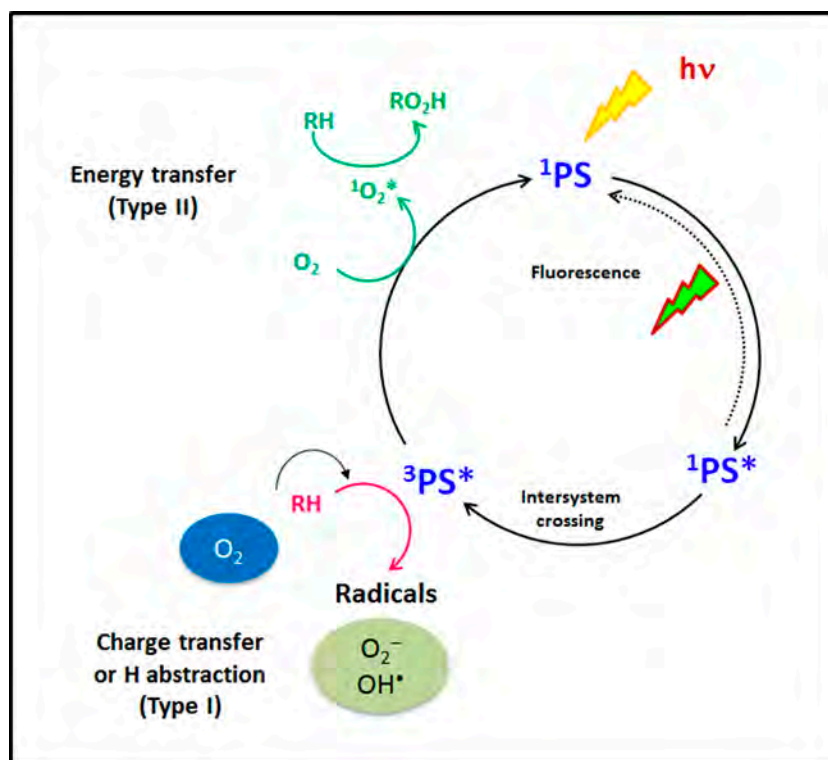


Scheme 1. Photophysical ROS generation cycle.

PDT was established and remains a successful modality for a varied pool of malignancies ranging from cancer to macular degeneration, going through dermatological affections and odontological

25

diseases.[47,48] But photodynamic inactivation (PDI) has been transformed recently to an antimicrobial discovery and development platform.

We have described the PS as the agent able to generate the ROS that will lead to the desired therapeutical effect. Despite their clinical application, several problems aroused from the first generation PSs. For instance, porfimer sodium (Photofrin[®;] the first clinically approved PS) provoked severe dermatological photosensitivity for several weeks due to its low selectivity; also the photosensitising drug was an inseparable mixture of porphyrin oligomeric compounds with the subsequent chemical characterisation difficulties. Based on these and other problems encountered in the clinical use of Photofrin and other first generation PSs, several ideal features were regarded for the ideal PS:

• Pure chemical compound and photochemical stability.

• Preferential location and selective retention at the target tissue.

• Single compound, with known and constant composition whose synthesis is affordable, high performance and scalable.

• Effective generator of $^1O_2$ and other ROS.

• Appropriate photophysical properties: *e.g.* high quantum yield of triplet formation (Φ_T), high quantum yield of $^1O_2$ formation (Φ_Δ) and high triplet state energy (enough to achieve $^1O_2$ formation).

• Low toxicity and negligible dark cytotoxicity.

• Rapid drug clearance in healthy tissue and minimal skin photosensitivity.

• High coefficient of absorption in the red / near infrared in order to achieve maximum penetration into tissues.

• Soluble in biological fluids (allowing administration via parenteral). If not, easy to incorporate into a hydrophilic transport system capable of circulating in the bloodstream.

• Susceptible to become drug through a simple and stable formulation.
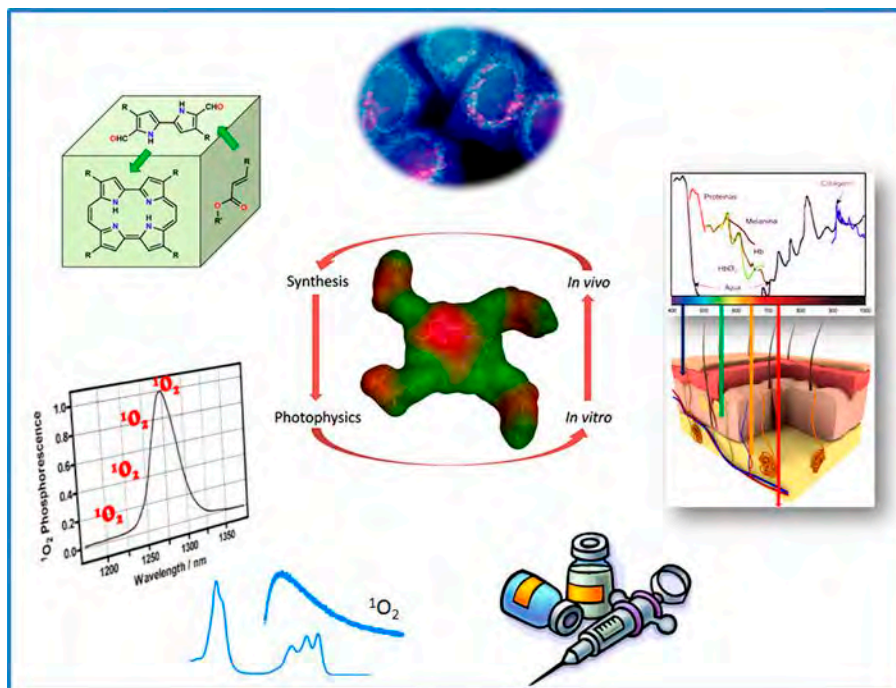
Scheme 2. Summary of desired properties for an ideal PS.

Trying to improve the properties of their predecessors in compliance with the aforementioned properties new families of PSs have been born: the so-called 2nd generation PSs. Among them stand porphycenes, porphyrins, chlorins, bacteriochlorins, phthalocyanines, aza-porphyrins, naphthocyanines, texaphyrins or purpurins.[49]
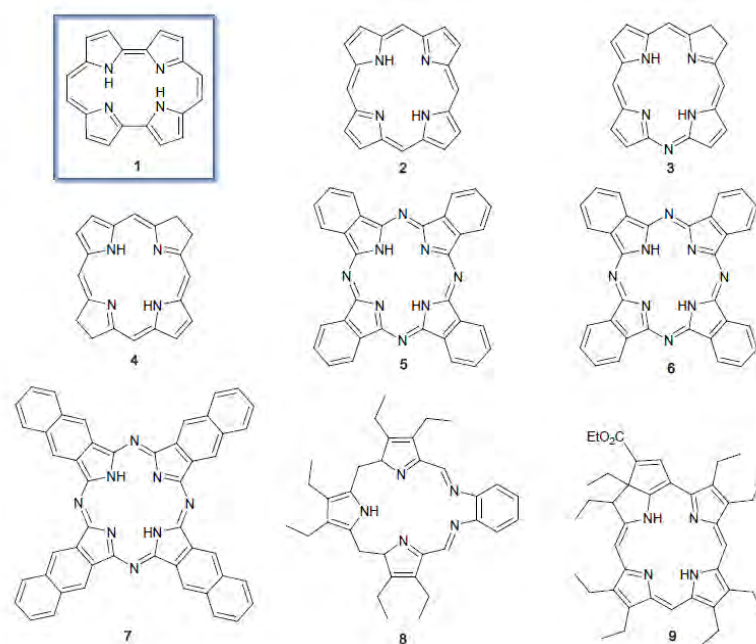
Scheme 3. Families of 2nd generation PSs. 1) Porphycene, 2) Porphyrin, 3) Chlorin, 4) Bacteriochlorin, 5) Phthalocyanine, 6) Azaporphyrin, 7) Naphthalocyanine, 8) Texaphyrin, 9) Purpurin

Singlet oxygen

Molecular oxygen (O_2) is a ubiquitous and often adventitious participant in organic photochemical reactions. O_2 is ubiquitous because samples are saturated with air, which means that unless purged, they contain a certain concentration of dissolved O_2 that at room temperature (rt) and 1 atm of air typically falls in the order of ~ millimolar. O_2 is adventitious because attempts of purging it may not succeeded completely, thus leading to unexpected reactions.

Singlet oxygen ($^1O_2$) is defined as the lowest excited electronic state of molecular oxygen and has been present in the scientific community for over 80 years. Its intrinsically atypical but appealing physico-chemical properties and behaviour (due to the unique electronic structure of the dioxygen molecule with a spin triplet in its ground state), makes $^1O_2$ remain at the forefront of research in different disciplines.[50,51] $^1O_2$ is definitely of great interest. Firstly, due to its high reactivity toward organic substrates as a synthetic reagent.[52] Secondly, as an intermediate in oxygenation reactions of polymers.[53] Thirdly, and probably the most appealing up to date, as a member of the ROS family that takes active part in a range of biological events. A great variety of biological molecules (*i.e.* proteins, DNA and lipids) can suffer oxidation processes by $^1O_2$, leading to a plethora of deleterious effects that can ultimately result in cell death, degenerative diseases, etc.[54] Over the years, insight has been gained in the rules that control $^1O_2$ generation, the characters involved and the energy requirements. More recent studies have focused on assessing the $^1O_2$ involvement during cellular signaling upon its generation in sub-lethal amounts, studying its role in cell regulation events (*i.e.* mediation of immune response, cell transduction or gene expression). Also, we are learning how to use it in our profit, for instance, destroying malignant cells as a therapy (*i.e.* PDT).[48] Still many gaps are to be closed and better understanding about $^1O_2$ is needed. In this sense, delivering the proper amount of $^1O_2$ within a therapy is crucial for its success, but it is not something we can fully control nor monitor yet.

As mentioned in the previous paragraph, the ground state of O_2 is a triplet, paramagnetic because of two parallel electronic spins. When excited, oxygen gets to two different metastable electronically excited singlet states. The higher-energy state ($^1\Sigma_g$) is deactivated to the so called $^1\Delta_g$ stated very rapidly. So rapidly that it has no chance to react. $^1\Delta_g$, namely called singlet oxygen (hereafter $^1O_2$), decays slower,

thus allowing for interaction and reactivity. $^1O_2$ lies *ca.* 94 kJ·mol^{-1} above the ground state, energy corresponding to an infrared wavelength of 1270 nm, where it emits light (Scheme 4).
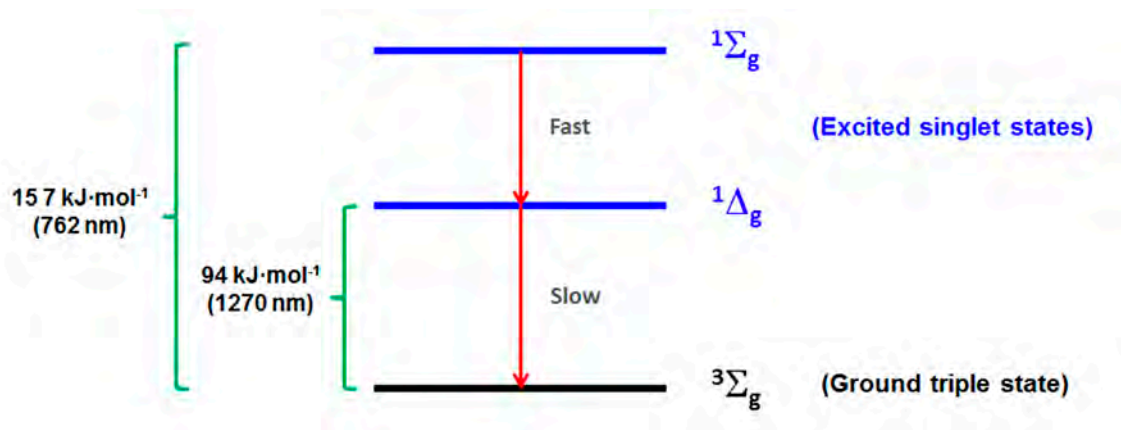
Scheme 4. Energetic representation of $^1O_2$ excited singlet states.

Because $^1O_2$ in solution deactivates by transferring its electronic energy to solvent vibrations, its lifetime depends strongly on the medium. Thus, solvents with high vibrational frequencies provide the most efficient relaxation. It is for this reason that the lifetime is shortest in water (which has a strong OH vibration) followed by solvents with CH groups. In deuterated solvents the quenching rate constant decreases by approximately an order of magnitude because the corresponding vibrations shift to lower frequency. This results in lifetimes increasing from 3-4 μs in water up to 65 μs in D_2O.

There are two major sources of $^1O_2$: photochemical and "chemical". One of the most common sources of $^1O_2$ requires energy transfer (ET) from an excited PS, as seen in Scheme 5.
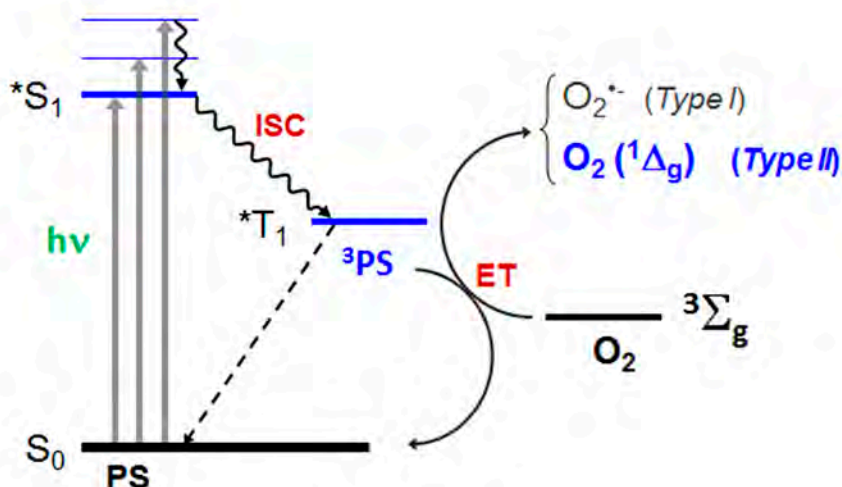
Scheme 5. Representation of $^1O_2$ formation through energy transfer with an excited ^{3}PS.

30

The role of the PS is to absorb the light and be converted to an electronically excited state (usually the first excited triplet state, T_1); then transfers its energy to molecular oxygen, producing $^1O_2$ and regenerating the PS as we previously showed in detail in Scheme 1. Three are the requirements for a molecule to be able to photosensitise the production of $^1O_2$ efficiently: (A) have a good ability to populate the excited triplet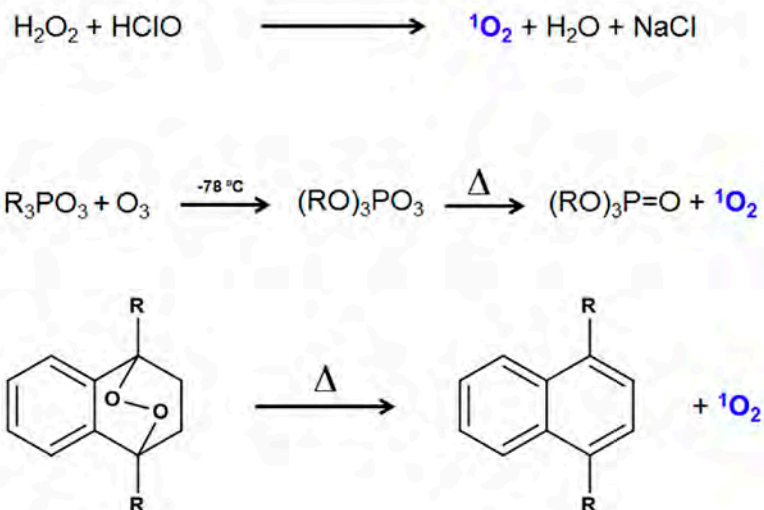 state (high ISC quantum yield), (B) the energy of its triplet state must be higher than 94 $kJ \cdot mol^{-1}$.and (C) energy transfer must occur efficiently.

Although not included in Schemes 1 and 5 for the sake of simplicity, $^1O_2$ can also be generated from the fluorescent (singlet, S_1) state of a PS. This phenomenon is less frequent and requires that the S_1-T_1 energy gap exceeds the excitation energy of $^1O_2$ (94 $kJ \cdot mol^{-1}$) so that oxygen can elicit this spin allowed intersystem crossing.[50,51] This discovery led to the finding that it is possible to achieve Φ_Δ values higher than unity if both S_1-T_1 and T_1-S_0 energy gaps of the PS are around 94 $kJ \cdot mol^{-1}$. For instance, rubrene is reported to have a Φ_Δ value of 1.8 in toluene and oxygen pressure of 10 atm. Perylene, pyrene or 1,3-diphneylisobenzofuran are other examples.[50] Still, most PSs do not have such a large S_1-T_1 energy gap and the utterly high oxygen pressure requirements make their feasibility in PDT unviable.

Hence, for most PSs, the role of oxygen quenching of S_1 is limited to enhancement of the triplet quantum yield, and the main pathway of $^1O_2$ generation is oxygen quenching of T_1. Because the intramolecular $T_1 \rightarrow S_0$ transition is spin-forbidden, T_1 states generally have long lifetimes, allowing mostly for complete quenching by ground-state oxygen in air-saturated solution. From now on, we will focus only in this majority event when dealing with photosensitised $^1O_2$ formation.

Chemical sources of $^1O_2$ are quite diverse (Scheme 6). The oldest is the reaction of HClO with H_2O_2, which produces $^1O_2$ in nearly quantitative yields. Other sources of $^1O_2$ are phosphite ozonides (produced by reaction of ozone with phosphites) and decomposition of hydrotrioxides. Peroxomolybdates are also able to produce $^1O_2$ in good yields. One of the cleanest methods of producing $^1O_2$ without other reactive oxidants is the decomposition of aromatic (particularly substituted naphthalene) endoperoxides. These compounds undergo the reverse reaction to give $^1O_2$ and the aromatic compound in near-quantitative yields.

$$H_2O_2 + HClO \longrightarrow {}^1O_2 + H_2O + NaCl$$

$$R_3PO_3 + O_3 \xrightarrow{-78\,°C} (RO)_3PO_3 \xrightarrow{\Delta} (RO)_3P{=}O + {}^1O_2$$

Scheme 6. Chemical sources of singlet oxygen.

A drawback of chemical sources is that many substrates do not trap $^1O_2$ efficiently, so that a large excess of the reagent must be used to obtain appreciable substrate conversions. Moreover, since many of the sources use strong oxidising agents, undesired side reactions may also occur. Still, this system renders useful whenever light cannot be used or just for mechanistic purposes.

Due to the characteristic reactivity of $^1O_2$, photooxygenation is a valuable complement of oxidation methods. $^1O_2$ is a synthetically useful electrophilic reagent which, in many cases, allows stereospecific and regiospecific introduction of O_2 into organic substrates. In industry, the reaction is applied to production of perfumes and aromas by oxidation of terpenes or terpenols. The singlet spin multiplicity significantly increases reactivity with respect to triplet (ground state) oxygen. Main reactions are briefly summarised in the following paragraphs.

[4+2] cycloaddition: $^1O_2$ reacts with the s-cis conformations of 1,3-dienes to form endoperoxides. The reactions are characterised by a negligible solvent effect and they can be stereospecific. The synthetic importance of this reaction relies on the great variety of transformations available to the endoperoxide products.

Ene reaction: In this reaction, olefins with allylic hydrogens are oxidised to allylic hydroperoxides concomitant with a shift of the double bond. These allylic hydroperoxides can be easily converted to allylic alochols, key intermediates in several synthetic transformations. The synthetic utility of the ene

32

reaction is increased by tits unique stereochemistry and regiochemistry since the double bond always shifts to the allylic position.

[2+2] cycloaddition: [2+2] cycloadditions with $^1O_2$ occur with electron-rich substrates or with olefins in which the competing ene reactions are structurally precluded. The products are dioxetanes, characteristic by their ability to decompose with light emission.

Sulfide photooxidation: The photooxidative behaviour of sulphides was examined more than 50 years ago and reported as a new method of making sulfoxides. The quantum efficiency of product formation is sensitive to both temperature and the identity of the solvent. While pretty efficient in methanol it does not proceed properly in benzene. But efficiency in aprotic solvents, however, increases as the temperature is lowered.

Reactivity towards aminoacids: Biomolecules react in the same way other molecules do, but many of the initial products are unstable and cannot be isolated. Special attention has been gained since the obvious use of $^1O_2$ in biological media as we will later see.
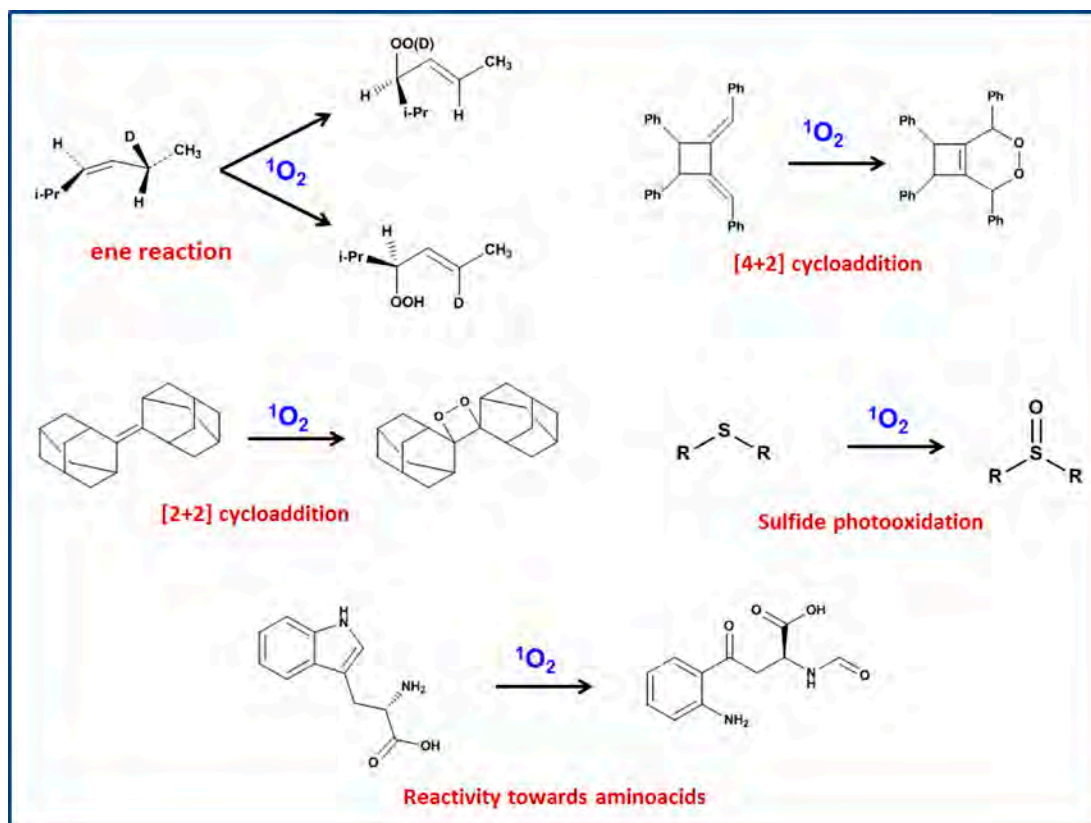
Scheme 7. Representative selection of chemical reactivity of $^1O_2$ with organic molecules.

33

Aside from $^1O_2$ deactivation through chemical reaction (*i.e.* reaction with chemical traps as we will see in chapter IV) physical pathways are very common for deactivation of $^1O_2$. Hereafter we will refer as "quenching" to the concept of deactivation of an excited molecule to its ground state without chemical reaction with the deactivating molecule (quencher). In some case, competition between chemical and physical deactivation pathways occur. There are two major mechanisms of physical quenching:

Energy transfer: this process is typified by carotenes. Carotenes participate in a reverse reaction of that by which $^1O_2$ is formed by the PS. Carotene's triplet excitation energy lies below that of $^1O_2$ so that the reaction is exothermic. Moreover, the rate constant for this reaction is in the diffusional limit rate, that is, in the order of $1 \cdot 10^{10}$ $M^{-1} \cdot s^{-1}$, meaning that reaction occurs with every collision. Thus, carotene family become extremely efficient physical $^1O_2$ quenchers. This quenching may be the reason for the very important role played by carotenes in protecting against oxidative photodamage in photosynthetic systems.

$$\text{carotene} + {}^1O_2 \rightarrow {}^3\text{carotene} + {}^3O_2$$
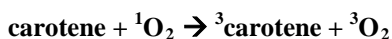
Charge transfer: electron-rich compounds make up the second class of physical quenching molecules. Partial charge transfer from these compounds appears to catalyse the intersystem crossing of $^1O_2$ to the ground state. Complete electron transfer to $^1O_2$ has been observed but only with extremely strong electron donors. However, complete transfer is not a requirement for quenching.

$$Q + {}^1O_2 \rightarrow {}^+Q\text{-}\text{-}O_2^{\cdot -} \rightarrow Q + {}^3O_2$$
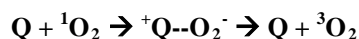
Sodium azide (NaN_3) and DABCO (diazabicyclo[2.2.2]octane) are examples of charge-transfer quenchers. DABCO has a particularly low oxidation potential for an amine and quenches $^1O_2$ very efficiently without itself undergoing any reaction. Hydrazines also are very efficient quenchers. Finally, NaN_3 is a water soluble quencher which has been frequently used in biological studies; however, it is not as inert chemical and it can undergo reactions itself via the azido radical; it is also a potent metalloenzyme poison, which limits its usefulness in biological systems. Certain reactive phenols do also undergo a mixture of reaction and quenching; vitamin E (α-tocopherol) is a particularly reactive example and the ratio of reaction/quenching hinges on the solvent.

35

Objectives of the thesis

AIM OF THE STUDY

In the present study we aim at two main objectives:

- The study of different novel approaches towards antimicrobial photodynamic therapy that can give insight for the development of feasible strategies to overcome antibiotic resistance as well as help understand the mechanisms underneath bacterial cell death upon singlet oxygen-mediated photokilling.

- The study and/or development of new probes that elicit better singlet oxygen detection either in solution or in intracellular systems.

References

1. Pakchung, A. A. H.; Simpson, P. J. L.; Codd, R. Life on Earth. Extremophiles continue to move the goal posts. *Environ. Chem.* **2006***, 3*, 77-93.

2. Pikuta, E. V.; Hoover, R. B.; Tang, J. Microbial extremophiles at the limits of life. *Crit. Rev. Microbiol.* **2007***, 33*, 183-209.

3. AnonymousMicrobiology by numbers. *Nat Rev Micro* **2011***, 9*, 628-628.

4. Palmer, C.; Bik, E. M.; DiGiulio, D. B.; Relman, D. A.; Brown, P. O. Development of the human infant intestinal microbiota. *PloS Biol.* **2007***, 5*, 1556-1573.

5. McFall-Ngai, M.; Hadfield, M. G.; Bosch, T. C. G.; Carey, H. V.; Domazet-Lošo, T.; Douglas, A. E.; Dubilier, N.; Eberl, G.; Fukami, T.; Gilbert, S. F.; Hentschel, U.; King, N.; Kjelleberg, S.; Knoll, A. H.; Kremer, N.; Mazmanian, S. K.; Metcalf, J. L.; Nealson, K.; Pierce, N. E.; Rawls, J. F.; Reid, A.; Ruby, E. G.; Rumpho, M.; Sanders, J. G.; Tautz, D.; Wernegreen, J. J. Animals in a bacterial world, a new imperative for the life sciences. *Proceedings of the National Academy of Sciences* **2013***, 110*, 3229-3236.

6. Hamady, M.; Knight, R. Microbial community profiling for human microbiome projects: Tools, techniques, and challenges. *Genome Research* **2009***, 19*, 1141-1152.

7. Weinstock, G. M. Genomic approaches to studying the human microbiota. *Nature* **2012***, 489*, 250-256.

8. Brock, T. D.; Madigan, M. T.; Martinko, J. M.; Parker, J. *Biology of microorganisms, Seventh edition;* Prentice-Hall, Inc., 113 Sylvan Avenue, Route 9W, Englewood Cliffs, New Jersey 07623, USA London, England, UK: 113 Sylvan Avenue, Route 9W, Englewood Cliffs, New Jersey 07623, USA London, England, UK, 1994; , pp 1296.

9. Schulz, H.; Jorgensen, B. Big bacteria. *Annu. Rev. Microbiol.* **2001***, 55*, 105-137.

10. Duda, V. I.; Suzina, N. E.; Polivtseva, V. N.; Boronin, A. M. Ultramicrobacteria: Formation of the concept and contribution of ultramicrobacteria to biology. *Microbiology* **2012***, 81*, 379-390.

11. Callaway, E. Cell biology: Bacteria's new bones. *Nature* **2008***, 451*, 124-126.

12. Cabeen, M.; Jacobs-Wagner, C. Bacterial cell shape. *Nat. Rev. Microbiol.* **2005***, 3*, 601-610.

13. Young, K. D. The selective value of bacterial shape. *Microbiology and Molecular Biology Reviews* **2006***, 70*, 660-703.

14. Kolter, R.; Greenberg, E. P. Microbial sciences: The superficial life of microbes. *Nature* **2006***, 441*, 300-302.

15. Kolter, R. Biofilms in lab and nature: a molecular geneticist's voyage to microbial ecology. *Int. Microbiol.* **2010***, 13*, 1-7.

16. Irie, Y.; Parsek, M. R. Quorum sensing and microbial biofilms. *Curr. Top. Microbiol. Immunol.* **2008***, 322*, 67-84.

17. Woese, C. R. Bacterial evolution. *Microbiological Reviews* **1987***, 51*, 221-271.

18. Woese, C. R.; Kandler, O.; Wheelis, M. L. Towards a natural system of organisms: proposal for the domains Archaea, Bacteria, and Eucarya. *Proceedings of the National Academy of Sciences* **1990***, 87*, 4576-4579.

19. Uchiyama, Y.; Takeuchi, R.; Kodera, H.; Sakaguchi, K. Distribution and roles of X-family DNA polymerases in eukaryotes. *Biochimie* **2009***, 91*, 165-170.

20. Jori, G.; Coppellotti, O. Inactivation of pathogenic microorganisms by photodynamic techniques: Mechanistic aspects and perspective applications. *Anti-Infective Agents in Medicinal Chemistry* **2007**, *6*, 119-131.

21. Whitman, W. B.; Coleman, D. C.; Wiebe, W. J. Prokaryotes: The unseen majority. *Proc. Natl. Acad. Sci. U. S. A.* **1998**, *95*, 6578-6583.

22. Barea, J.; Pozo, M. J.; Azcón, R.; Azcón-Aguilar, C. Microbial co-operation in the rhizosphere. *Journal of Experimental Botany* **2005**, *56*, 1761-1778.

23. Sears, C. A dynamic partnership: Celebrating our gut flora. *Anaerobe* **2005**, *11*, 247-251.

24. Zoetendal, E. G.; Vaughan, E. E.; De Vos, W. M. A microbial world within us. *Mol. Microbiol.* **2006**, *59*, 1639-1650.

25. O'Hara, A.; Shanahan, F. The gut flora as a forgotten organ. *EMBO Rep.* **2006**, *7*, 688-693.

26. Cohen, Y. Bioremediation of oil by marine microbial mats. *International Microbiology* **2002**, *5*, 189-193.

27. Neves, L. C. M. D.; Miyamura, T. T. M. O.; Moraes, D. A.; Penna, T. C. V.; Converti, A. Biofiltration methods for the removal of phenolic residues. *Appl. Biochem. Biotechnol.* **2006**, *129-132*, 130-152.

28. Hagedorn, S.; Kaphammer, B. Microbial biocatalysis in the generation of flavor and fragrance chemicals. *Annu. Rev. Microbiol.* **1994**, *48*, 773-800.

29. Liese, A.; Villela Filho, M. Production of fine chemicals using biocatalysis. *Curr. Opin. Biotechnol.* **1999**, *10*, 595-603.

30. Chattopadhyay, A.; Bhatnagar, N.; Bhatnagar, R. Bacterial insecticidal toxins. *Crit. Rev. Microbiol.* **2004**, *30*, 33-54.

31. Kuhn, D.; Blank, L. M.; Schmid, A.; Buehler, B. Systems biotechnology - Rational whole-cell biocatalyst and bioprocess design. *Eng. Life Sci.* **2010**, *10*, 384-397.

32. Johnson, M.; Lucey, J. Major technological advances and trends in cheese. *J. Dairy Sci.* **2006**, *89*, 1174-1178.

33. Bartlett, J. S.; Stirling, D. In *A short history of the polymerase chain reaction;* Bartlett, J. S., Stirling, D., Eds.; Humana Press: 2003; Vol. 226, pp 3-6.

34. Graumann, K.; Premstaller, A. Manufacturing of recombinant therapeutic proteins in microbial systems. *Biotechnology Journal* **2006**, *1*, 164-186.

35. St Denis, T. G.; Dai, T.; Izikson, L.; Astrakas, C.; Anderson, R. R.; Hamblin, M. R.; Tegos, G. P. All you need is light: antimicrobial photoinactivation as an evolving and emerging discovery strategy against infectious disease. *Virulence* **2011**, *2*, 509-520.

36. Boucher, H. W.; Talbot, G. H.; Bradley, J. S.; Edwards, J. E.; Gilbert, D.; Rice, L. B.; Scheld, M.; Spellberg, B.; Bartlett, J. Bad Bugs, No Drugs: No ESKAPE! An Update from the Infectious Diseases Society of America. *Clinical Infectious Diseases* **2009**, *48*, 1-12.

37. Infectious Diseases Society of America (IDSA) Combating antimicrobial resistance: Policy recommendations to save lives. *Clin. Infect. Dis.* **2011**, *52*, S397-S428.

38. Khachatourians, G. Agricultural use of antibiotics and the evolution and transfer of antibiotic-resistant bacteria. *Can. Med. Assoc. J.* **1998**, *159*, 1129-1136.

39. McEwen, S. A. Antibiotic use in animal agriculture: What have we learned and where are we going? *Anim. Biotechnol.* **2006**, *17*, 239-250.

40. Magiorakos, A. P.; Srinivasan, A.; Carey, R. B.; Carmeli, Y.; Falagas, M. E.; Giske, C. G.; Harbarth, S.; Hindler, J. F.; Kahlmeter, G.; Olsson-Liljequist, B.; Paterson, D. L.; Rice, L. B.; Stelling, J.; Struelens, M. J.;

37

Vatopoulos, A.; Weber, J. T.; Monnet, D. L. Multidrug-resistant, extensively drug-resistant and pandrug-resistant bacteria: an international expert proposal for interim standard definitions for acquired resistance. *Clin. Microbiol. Infect.* **2012***, 18*, 268-281.

41. Rice, L. B. Federal funding for the study of antimicrobial resistance in nosocomial pathogens: No ESKAPE. *Journal of Infectious Diseases* **2008***, 197*, 1079-1081.

42. Kumarasamy, K. K.; Toleman, M. A.; Walsh, T. R.; Bagaria, J.; Butt, F.; Balakrishnan, R.; Chaudhary, U.; Doumith, M.; Giske, C. G.; Irfan, S.; Krishnan, P.; Kumar, A. V.; Maharjan, S.; Mushtaq, S.; Noorie, T.; Paterson, D. L.; Pearson, A.; Perry, C.; Pike, R.; Rao, B.; Ray, U.; Sarma, J. B.; Sharma, M.; Sheridan, E.; Thirunarayan, M. A.; Turton, J.; Upadhyay, S.; Warner, M.; Welfare, W.; Livermore, D. M.; Woodford, N. Emergence of a new antibiotic resistance mechanism in India, Pakistan, and the UK: a molecular, biological, and epidemiological study. *Lancet Infect. Dis.* **2010***, 10*, 597-602.

43. Falagas, M. E.; Kasiakou, S. K.; Saravolatz, L. D. Colistin: The revival of polymyxins for the management of multidrug-resistant Gram-negative bacterial infections. *Clinical Infectious Diseases* **2005***, 40*, 1333-1341.

44. Bonnett, R. *Chemical aspects of photodynamic therapy (Advanced Chemistry Texts, V. 1);* Gordon and Breach Science Publishers: Amsterdam, 2000; , pp 305.

45. Redmond, R. W.; Gamlin, J. N. A compilation of singlet oxygen yields from biologically relevant molecules. *Photochem. Photobiol.* **1999***, 70*, 391-475.

46. Wilson, B. C.; Patterson, M. S. The physics, biophysics and technology of photodynamic therapy. *Phys. Med. Biol.* **2008***, 53*, 61-109.

47. Babilas, P.; Schreml, S.; Landthaler, M.; Szeimies, R. M. Photodynamic therapy in dermatology: state-of-the-art. *Photodermatol. Photoimmunol. Photomed.* **2010***, 26*, 118-132.

48. Agostinis, P.; Berg, K.; Cengel, K. A.; Foster, T. H.; Girotti, A. W.; Gollnick, S. O.; Hahn, S. M.; Hamblin, M. R.; Juzeniene, A.; Kessel, D.; Korbelik, M.; Moan, J.; Mroz, P.; Nowis, D.; Piette, J.; Wilson, B. C.; Golab, J. Photodynamic therapy of cancer: An update. *CA Cancer. J. Clin.* **2011***, 61*, 250-281.

49. Garland, M. J.; Cassidy, C. M.; Woolfson, D.; Donnelly, R. F. Designing photosensitizers for photodynamic therapy: strategies, challenges and promising developments. *Future Med Chem* **2009***, 1*, 667-691.

50. Schweitzer, C.; Schmidt, R. Physical mechanisms of generation and deactivation of singlet oxygen. *Chem. Rev.* **2003***, 103*, 1685-1758.

51. Ogilby, P. R. Singlet oxygen: there is indeed something new under the sun. *Chem. Soc. Rev.* **2010***, 39*, 3181-3209.

52. Hoffmann, N. Photochemical reactions as key steps in organic synthesis. *Chem. Rev.* **2008***, 108*, 1052-1103.

53. Gonçalves, E. S.; Ogilby, P. R. "Inside" vs "Outside" photooxygenation reactions: Singlet -oxygen-mediated surface passivation of polymer films. *Langmuir* **2008***, 24*, 9056-9065.

54. Redmond, R. W.; Kochevar, I. E. Spatially resolved cellular responses to singlet oxygen. *Photochem. Photobiol.* **2006***, 82*, 1178-1186.

Chapter II.

General instruments, methods & techniques

Steady state measurements

INSTRUMENTS

Equipment: Absorption spectra were recorded on a double beam Cary 6000i spectrophotometer (Varian, Palo Alto, CA), equipped with a 110 mm diameter integrating sphere and high performance photomultiplier tube for transmittance measurements. Fluorescence excitation and emission spectra were registered in a Spex Fluoromax-4 spectrofluorometer (Horiba Jobin-Yvon, Edison, NJ).

Light sources: Sorisa Photocare using a 35 mW·cm^{-2} fluence rate was used in probe conversion assays in Chapter IV (1st section). Light wavelength was chosen depending on the type of experiment, namely, blue (475 ± 15 nm), green (535 ± 15 nm) or red (635 ± 15 nm). Paterson red Lamp BL1000A (630 ± 30 nm) was used for experiments in Chapter IV (2nd section). Fluence rates were routinely measured using a power meter.

METHODS

Fluorescence quantum yield: The fluorescence quantum yield (Φ_F) is defined as the number of photons emitted by the sample *per* absorbed photon. The fluorescence intensity integrated over the entire emission spectrum was measured as a function of the sample absorption factor (1-10^{-Abs}) for the sample and a suitable reference (ref; *i.e.* with a similar emission spectrum as the sample), excited at the same wavelength. Φ_F values were determined using Equations (1-3).

$$\Phi_F(sample) = \Phi_F(ref) \times \left(\frac{F_{sample}}{F_{ref}}\right) \times \left(\frac{\beta_{ref}}{\beta_{sample}}\right) \times \chi \qquad (1)$$

$$\beta = 1 - 10^{-Abs} \qquad (2)$$

$$\chi = \frac{n_{ref}^2}{n_{sample}^2} \qquad (3)$$

where ***F*** stands for the value of the integrated fluorescence and ***n*** is the refractive index of the solvent used in each case.[1] Absorbance of the sample and the reference are to be less than 0.05 arbitrary units (a.u.) in the overlap region between absorption and emission to avoid inner filter effects.

Time-resolved measurements

INSTRUMENTS

Equipment: Time-resolved fluorescence and phosphorescence measurements were carried out using a customised PicoQuant Fluotime 200 fluorescence lifetime system and its FluoFit 4.0 software for the data analysis. For fluorescence assays, excitation was achieved by means of picosecond diode lasers or LEDs (PicoQuant, 10 MHz repetition rate) and the counting frequency was always below 1 %. For direct $^1O_2$ phosphorescence detection, a diode-pumped pulsed Nd:YAG laser (FTSS355-Q, Crystal Laser, Berlin, Germany) working at 10 kHz repetition rate at 532 nm (12 mW, 1.2 μJ per pulse) or at 355 nm (5 mW, 0.5 uJ per pulse) was used for excitation. A 1064 nm rugate notch filter (Edmund Optics, U.K.) was placed at the exit port of the laser to remove any residual component of its fundamental emission in the near-IR region. The luminescence exiting from the side of the sample was filtered by two long-pass filters of 355 and 532 nm (Edmund Optics, York, U.K.) and two narrow bandpass filters at 1275 nm (NB-1270-010, Spectrogon, Sweden; bk-1270-70-B, bk Interferenzoptik, Germany) to remove any scattered laser radiation. A near-IR sensitive photomultiplier tube assembly (H9170-45, Hamamatsu Photonics Hamamatsu City, Japan) was used as the detector at the exit port of the monochromator. Photon counting was achieved with a multichannel scaler (PicoQuant's Nanoharp 250).

Transient absorption experiments in the UV-VIS region were carried out using a home-built nanosecond laser flash photolysis system. In this instrument, either the 2nd harmonic (532 nm) or the 3rd harmonic (355 nm) of a Continuum Surelite I-10 Nd:YAG laser (10 Hz, 5 ns pulse width, 1-10 mJ *per* pulse) was directed to the sample. In other experiments, the 355 nm the the Nd:YAG laser was used to pump a Continuum OPO laser to produce laser pulses in the 400-700 nm region. Changes in the sample absorbance were detected using a Hamamatsu R928 photomultiplier to monitor the intensity variations of an analysing beam produced by a 75 W short arc Xe lamp (USHIO) and spectral discrimination was obtained using a PTI 101 monochromator. The signal was fed to a Lecroy Wavesurfer 454 oscilloscope for digitising and averaging (typically 3-10 shots) and finally transferred by a GPIB interface (National Instruments) to a PC computer for data storage and analysis. The TTL sync output of the laser was used to trigger the oscilloscope. The energy of the laser pulse was varied by neutral density filters and

measured with a pyroelectric energy meter (RJP 735 and RJ 7610) from Laser Precision Corp. The system was controlled by the in house-developed LKS sofware (LabView, National Instruments).

A schematic representation of our setup is depicted in Scheme 1:
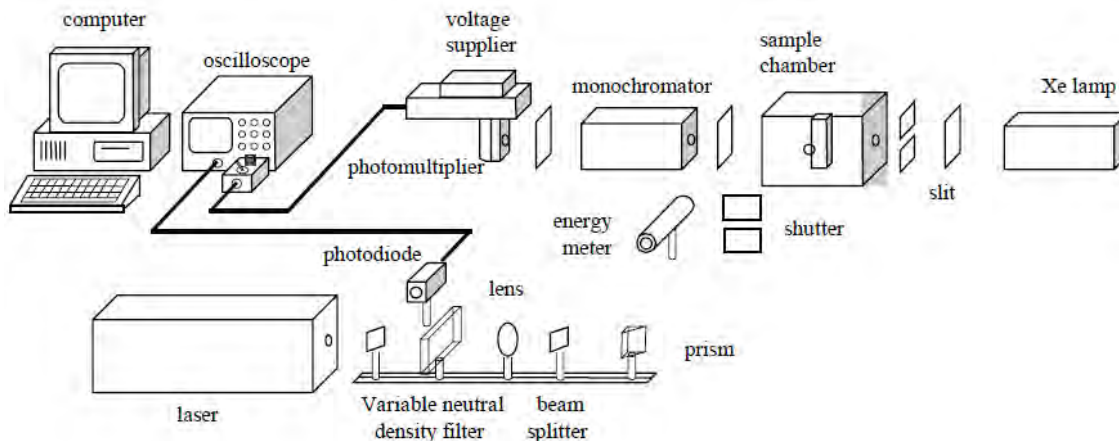
Scheme 1 Experimental setup for nanosecond UV-VIS laser flash photolysis. Image adapted from ref.[2]

GENERAL TECHNIQUES

The time-resolved techniques involve the observation, of excited states or other reaction intermediates generated upon pulsed-laser irradiation of a sample.

Time-Correlated Single Photon Counting (TCSPC): It is the most commonly used technique for singlet state lifetime determination. It is based on the detection of single photons of a periodical light signal, the measurement of the detection times of the individual photons and the reconstruction of the waveform from the individual time measurements. TCSPC technique makes use of the fact that for low-level, high-repetition-rate pulses, the produced light intensity is so low that the probability of detecting one photon in one signal period is less than one. Therefore, is not necessary to seek for the possibility of detecting several photons in one signal period. It is sufficient to record the photons, measure their time in the signal period, and build up a histogram of the photon times.[3]

For fluorescence measurements, an instrument's response function (IRF) is needed because the response of the electronics can be convoluted with the chromophore's decay spectrum. In the absence of chromophore, any decay measured will be the solely the result of the electronics. This is not necessary for samples with lifetimes approaching 1.0 μs. To achieve the IRF signal a sample able to scatter excitation light into the photomultiplier is needed. Diluted solutions of commercially available Ludox is an option, but whatever scattering sample may work.

Time-resolved Near-IR phosphorescence detection (TRPD): This technique is commonly used for directly and specifically monitoring $^1O_2$ formation and decay, the measurement of its lifetime (τ_Δ) and its quantum yield of formation (Φ_Δ). It is based on the detection of the weak $^1O_2$ phosphorescence, centred at 1275 nm (Scheme 2) and has its major potential in homogeneous systems.[2]
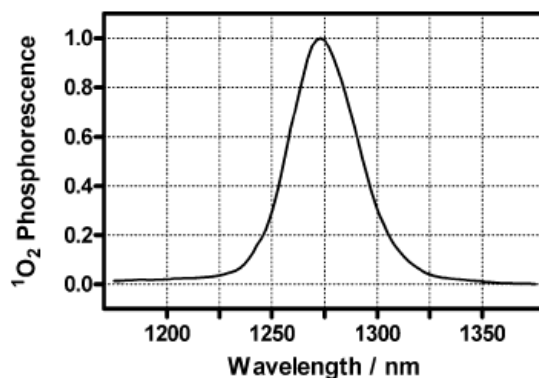
Scheme 2. Near-IR phosphorescence spectrum of $^1O_2$. Image taken from ref.[3]

Direct $^1O_2$ luminescence was detected by means of PicoQuant Fluotime 200 system but with a different customisation respect to TCSPC measurements, as described in the previous section.

UV-VIS nanosecond laser flash photolysis: this technique addresses to the measurement of triplet states of photochemical and photophysical phenomena. There are many experimental setups for the detection of triplet-triplet absorption spectra, but two elements are common. First, an exciting source to produce the triplet state species is required. Second, each experiment has a monitoring light source to probe their absorbance. Triplet states can be generated in several ways; however, two are the main methods for achieving substantial triplet state populations: photolysis with light and radiolysis with ionising radiation.[4] In the case of study, excitation is achieved by means of a nanosecond pulsed Nd:YAG laser.

43

GENERAL METHODS

Singlet state decay kinetics (τ_S): A solution of the sample in the proper solvent was prepared ensuring that the absorbance of the sample was less than 0.05 in the overlap region between absorption and emission to avoid inner filter effects. The deconvolution of the TCSPC fluorescence signal with the IRF signal yields the singlet lifetime (τ_S).

Assessing $^1O_2$ formation and decay kinetics: $^1O_2$ lifetimes were obtained and assigned by fitting Equation (4) to the time-resolved phosphorescence signals (S_t) detected at 1275 nm,

$$S_t = a \times \left(e^{-t/\tau_\Delta} - e^{-t/\tau_T} \right)$$

(4)

where **a** is the zero-time amplitude of the signal and τ_T and τ_Δ are the actual lifetimes of the PS' triplet state and $^1O_2$, respectively.

$^1O_2$ luminescence quantum yield (Φ_Δ): Optically matched solutions of sample and reference were measured and the time-resolved phosphorescence signals analysed. The amplitude (a) is proportional to Φ_Δ (Equation 5),

$$a = k \cdot \times \Phi_\Delta \times \frac{\tau_\Delta}{\tau_\Delta - \tau_T} \times \left(1 - 10^{-Abs} \right)$$

(5)

Thus, the relationship between amplitudes (from sample and reference, respectively) together with Φ_Δ (ref) renders the Φ_Δ (sample) value, as represented in Equation (6)

$$\Phi_\Delta \ (sample) = \Phi_\Delta \ (ref) \times \frac{a_{sample}}{a_{ref}}$$

(6)

This result is only valid if both –sample and reference- show the same τ_T and τ_Δ values. May this condition not be fulfilled, one needs to make a correction taking into account the aforementioned changes in lifetimes, rendering Equation (7):

$$\Phi_\Delta(sample) = \Phi_\Delta(ref) \times \frac{\left(\dfrac{a}{1-10^{-Abs}}\right)_{sample}\left(\dfrac{\tau_\Delta}{\tau_\Delta - \tau_T}\right)_{ref}}{\left(\dfrac{a}{1-10^{-Abs}}\right)_{ref}\left(\dfrac{\tau_\Delta}{\tau_\Delta - \tau_T}\right)_{sample}} \qquad (7)$$

Assessing reaction rate constants: The rate constant for $^1O_2$ quenching (k_q) by a quencher (Q) was determined by measuring the $^1O_2$ lifetime as a function of the quencher concentration. $^1O_2$ was generated by an external PS and the concentration of the sample was varied. A plot of the reciprocal lifetime vs the concentration of the sample afforded k_q as the slope of the linear-fit Equation (8).

$$\frac{1}{\tau_\Delta} = \frac{1}{\tau_\Delta^0} + k_q[Q], \qquad (8)$$

where τ_Δ° is the $^1O_2$ lifetime in the neat solvent.

Microbiological measurements

GENERAL MATERIALS

Chemicals. Phosphate buffer saline (PBS) or deuterated PBS (dPBS) solutions were prepared dissolving the required amount of a PBS tablet (Sigma) in 100 mL milliQ water o deuterium oxide (Fluka). isopropyl β-D-1-thiogalactopyranoside (IPTG), arabinose and disodium carbenicillin were purchased from Sigma and used as received. Growth media and agar were purchased from Scharlau.

Microbial strains: The microbial strains used for the PDI experiments in *Chapter 3.1* were*: Staphylococcus aureus* (CECT239) and methicillin-resistant strain of *S. aureus* (ATCC BAA-44) as Gram-positive bacteria; *Escherichia coli* (CECT101) and *Pseudomonas aeruginosa* (ATCC 25668) as Gram-negative bacteria; *Candida albicans (*ATCC 10231) and *Candida krusei* (ATCC 6258) as yeasts. For spectroscopic measurements in Chapter 3.2 we used *E. coli* (CECT101). *E. coli* strain BL21 (DE3) and *E. coli* DH5α were the strains used in Chapter 3.3.

Light sources: The light source used in the inactivation experiments was selected in order to provide the highest possible overlap between the irradiation range and the absorption spectrum of the PSs. Different light sources were used. MRSA and *P. aeruginosa* inactivation (corresponding to Chapter 3.1) were irradiated with red light (600 -750 nm) with the Waldmann PDT 1200 lamp (Waldmann; Medizintechnik) with a fluence rate at the level of the samples of 40 mW·cm^{-2}. A CW 532 nm laser beam (Cobolt Samba, Sweden) was used at low power density (40 mW·cm^{-2}) for irradiation of TagRFP expressing *E. coli* in Chapter 3.3. Sorisa Photocare using a 35 mW·cm^{-2} fluence rate was used for the rest of PDI experiments (Chapters 3.1 and 3.3). Fluence rates were routinely measured using a power meter. Light wavelength was chosen depending on the type of experiment, namely, blue (475 ± 15 nm), green (535 ± 15 nm) or red (635 ± 15 nm).

GENERAL METHODS

Microbial growth and protein induction: Bacterial cells were aerobically grown overnight at 37 ºC in brain-heart infusion (BHI), lysogeny broth (LB) broth or tryptic soy broth (TSB) to stationary phase. A reinoculum was then grown in fresh LB medium at 37 ºC to an optical density at 600 nm (OD$_{600}$) of 0.2

(start of log phase). TagRFPHis expression was induced with 50 µM solution of IPTG and miniSOGHis expression with 0.1 % arabinose for 1 hour at 37 °C to an attenuance value of ca. 0.6-0.7 at 600 nm or 0.35 at 660 nm, corresponding to *ca.* 10^8 colony forming unit per milliliter ($CFU \cdot mL^{-1}$).[5] If protein expression was not required cells were grown directly to the previous attenuance values. The cell suspensions were then centrifuged (5 min, 3000 rpm) and resuspended with sterile PBS or dPBS at pH 7.4 at the same concentration.

Candidas spp were grown overnight at 35 ºC in Sabouraud broth, and then subcultivated in new Sabouraud medium at 35ºC in an orbital shaking incubator at 130 rpm to an $OD_{600} = 0.7$, corresponding to *ca.* 10^7 CFU/mL. The suspensions were then centrifuged (5 min, 3500 rpm) and resuspended with sterile PBS at pH 7.4 at the same concentration for phototoxicity experiments.

Cultures were maintained by two weeks of subcultures in agar-medium in the presence of the appropriate amount of antibiotics in the media when required (100 µg/mL disodium carbenicillin).

Spectroscopic measurements in cell suspensions: Spectroscopic measurements were recorded on the systems previously described. Cell suspension samples were prepared as follows: bacterial suspensions were incubated in the dark with the desired amount of PS for the required contact time; when required, bacterial samples were centrifuged, excess PS removed and samples resuspended in PBS or dPBS to a final concentration of $\sim 5 \times 10^8$ $CFU \cdot mL^{-1}$. The suspensions were gently stirred during the measurements to avoid cell settlement.

Photodynamic inactivation protocol: Cell suspensions in PBS were incubated in the dark at rt for 30 min with the appropriated amount of PS. Centrifugation (3 min, 12000 rpm) of aliquots was used to remove the excess of PS that was not taken up by the bacteria when experiments required it. Then, bacterial suspensions aliquots were placed in 96-well plates. The wells were illuminated from the top of the plates by light of the selected wavelenght. At the time points when the desired light doses had been delivered, aliquots were thoroughly mixed before sampling to avoid the settlement of bacteria. Light-alone controls (without PS) were also performed for all experimental conditions in order to rule out any inactivation effect due to the light and heating effects. For determination of population reduction, aliquots were serially diluted, streaked on nutrient agar plates and incubated in the dark for 18 h at 37 ºC (bacterial cells and *C. krusei*) or for 36 h at 30 ºC (*C. albicans*). Experiments were carried out in triplicate for each condition.

47

References

1. Montalti, M.; Credi, A.; Prodi, L.; M.T, G. *Handbook of photochemistry;* CRC Press: 2006.

2. Nonell, S.; Braslavsky, S. E. Time-resolved singlet oxygen detection. *Methods Enzymol.* **2000***, 319*, 37-49.

3. Jiménez-Banzo, A.; Ragàs, X.; Kapusta, P.; Nonell, S. Time-resolved methods in biophysics. 7. Photon counting vs. analog time-resolved singlet oxygen phosphorescence detection. *Photochem. Photobiol. Sci.* **2008***, 7*, 1003-1010.

4. Carmichael, I.; Hug, G. L. Triplet-Triplet absorption spectra of organic molecules in condensed phases. *Journal of Physical and Chemical Reference Data* **1986***, 15*, 1-250.

5. Demidova, T. N.; Hamblin, M. R. Effect of cell-photo sensitizer binding and cell density on microbial photoinactivation. *Antimicrob. Agents Chemother.* **2005***, 49*, 2329-2335.

Chapter III.

New strategies in antimicrobial photodynamic therapy

*"the future of humanity and microbes will likely evolve as episodes [...] of our wits versus their genes"*

\- Joshua Lederberg

(Zoologist; Nobel Prize 1959)

Introduction

We have previously introduced the emerging threat due to global diffusion of new antimicrobial infections as well as the continuously increasing resistance of pathogens against many of the commonly used antibiotics. Enhanced efflux pumps, loss of porins, antibiotic inactivation by enzymes and, most worrying, gene transfer codifying resistance to antibiotic among species are several of these strategies bacteria have developed or refined in the latest years (Scheme 1).[1]
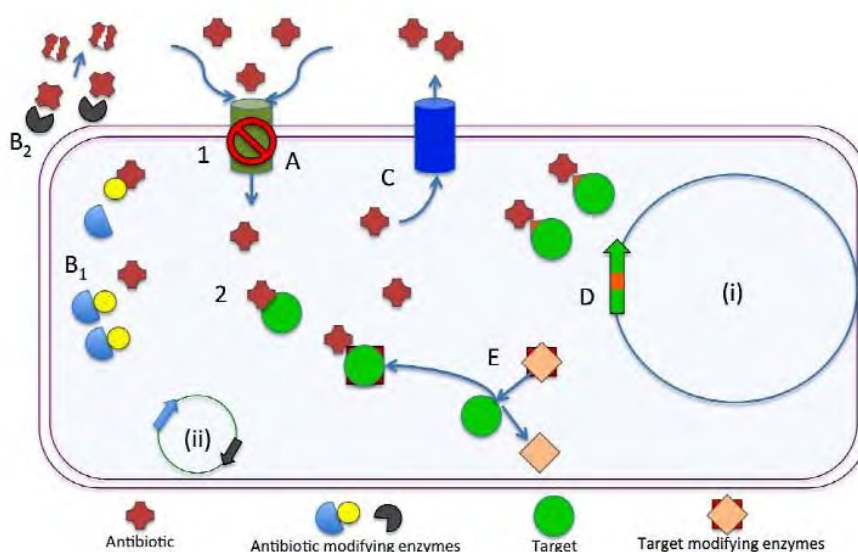
Scheme 1. Representation of the most common antibiotic resistance mechanisms. 1: Entrance of the antibiotic through porins. 2: Binding to the target. A: Loss of porins. B: Antibiotic inactivating enzymes (modification, B1, or hydrolysis, B2). C: Enhanced efflux. D: Pre-transcriptional modification of the target. E: P ost-translational modification of the target. (i) Bacterial chromosome bearing the gene encoding the target. (ii) Resistance plasmid bearing genes encoding for modifying enzymes**.** Image from reference **[1]**

In the past time immense efforts led to new natural and semi-synthetic antibiotics. Development of novel antimicrobial agents, derivatisation of currently known active molecules to overcome resistance, and the development of potentiators of commonly used antimicrobials represent current areas of investigation. For instance, the propagation of DNA extracted directly from environmental samples in laboratory-grown bacteria provides a means to study natural products encoded in the genomes of uncultured bacteria. Tetarimycin A, a tetracyclic MRSA-active antibiotic, was found this way.[2]

It is foreseeable that, in spite of the immense expenditure, the therapeutic success will soon be only minimal. Past and current policies for dealing with resistance have been only partially effective. Thus, an imperious effort to the development of novel approaches to the problem is badly needed.[3] Several

alternatives to antibiotic treatments will be briefly reported in the following paragraphs. Some of them are not novel, but their use was eclipsed mainly due to two causes: insufficient understanding among researchers at the moment of its discovery and the advent of antibiotics.

- Use of polymicrobial vaccines: alternative in early stages of development. Koch's postulates are the reference and have proven useful for vaccination against several diseases, but they do not adequately consider the pathogenesis of microbes with multiple virulence factors or polymicrobial infections. Even if a vaccination attempt successfully blocks virulence factor for one pathogen (i.e. a toxin), virulence could potentially be complemented by another factor produced by a neighbouring species in the polymicrobial community. Microbes can benefit from virulence factors of other organisms or strains during coinfection to enhance their own pathogenesis and colonisation. The eradication of one species from the polymicrobial community may be insufficient to reduce overall disease, as another organism present may fill the niche left behind.[4] A vaccine composed of a multivalent cocktail of antigenic proteins from all microbes involved in disease pathology is expected to be required, making the approach still far from its use. In line with this idea, more modest attempts rely on the idea to use inhibitors of bacterial virulence functions. The rationale for this concept is that antivirulence drugs would deprive pathogenic bacteria of their virulence functions, which would enable their elimination by the body's immune system.

- Synbiotic approach: an overwhelming number of polymicrobial diseases are propagated on abiotic surfaces, such as intravenous and urinary catheters, stents, artificial heart valves, parenteral nutrition feeding tubes, pacemakers and orthopedic devices (e.g. prostheses). These implants may serve as sources of chronic infection and can potentially serve as a source of inoculation into the bloodstream, leading to sepsis. In these cases a failure of antimicrobial therapy requires an alternative treatment strategy, given the evidence that the administration of antibiotics may actually increase overgrowth by potentially pathogenic microorganisms.[4] A synbiotic is defined as the combination of a probiotic and a prebiotic: an oligosaccharide indigestible by humans but able to be fermented by beneficial gut bacteria therefore promoting their growth and displacing the pathogenic colonies.[4-6]

- Antimicrobial peptides: Antimicrobial peptides (hereafter AMPs) are small biological molecules (<10 kDa) with direct antimicrobial activity, including enzymatically synthesised compounds and

ribosomal-synthesised AMPs, provide effective microbial defence for all organisms from bacteria to mammals.[7] Bacteriocins are a specific subgroup of AMPs that are produced by bacteria themselves and active against other bacteria.[8,9] But AMPs can also be originated from fungi, plants and animals. Among the main drawbacks –to overcome if desired as a feasible therapy- is that the proteinaceous nature of AMPs makes them vulnerable to proteolytic enzymes and also the membrane-target makes the possibility of acquiring resistance in the middle/long term.

- <u>Miscellaneous treatments</u>: here we include a repertoire of minority options that –in specific cases- can be useful. Examples include the use of vacuum-assisted closure, hyperbaric oxygen treatment and maggot debridement therapies. These techniques –in combination with conventional surgical treatments- have been proven to aid in the recovery and clearance of wound infections.[4]

- <u>Phage therapies</u>: Bacteriophages were first identified in 1915 and were used as antimicrobial agents from 1919 onwards. Despite its initial successes and widespread application, their efficacy remained controversial. Although they were replaced by antibiotics in the west countries, bacteriophages remained a common therapeutic approach in parts of eastern Europe (especially in Georgia) where they are still in use. Bacteriophages are bacterial viruses that invade bacterial cells and, in the case of lytic ones, disrupt bacterial metabolism and cause the bacterium to lyse. It has been well established that phages can kill microorganisms which are resistant to many or all broad spectrum modern antibiotics. This effect has been shown both *in vitro* and *in vivo* and reflects the fact that phage mechanisms of bacterial killing differ radically from those of antibiotics. Despite its many advantages, its world-wide use is still to come. Some problems arise from controversial proof of efficacy and problems of stability/viability of some preparations in the beginning. Advanced purification techniques together with careful selection for lytic phages are key points in their feasibility for their potential common use.[10]

Figure 1. Electron micrograph of bacteriophages attached to bacterial cell. (from Dr. Graham Beards ; Wikimedia Commons / Public Domain)

- <u>Antimicrobial PDT</u>: While the photodynamic effect was initially discovered in paramecia, the use in the microbial field was stopped due to the incapacity of typical antitumor PSs (neutral or anionic) to perform against Gram-negative bacteria. The better understanding of the system and the new developments in the photodynamic field have re-emerged antimicrobial PDT (hereafter aPDT) as a very promising strategy, particularly for the treatment of superficial and localised infectious diseases. Advantages over traditional antibiotics include a broad-spectrum activity (also against antibiotic-resistant *spp*) and the lack of development of resistance mechanisms due to the multi-target process; one extra attractive feature peculiar to PDT as an antibacterial treatment is the possibility that the generated ROS may chemically destroy many of secreted virulence factors (especially those that are proteins).[11]
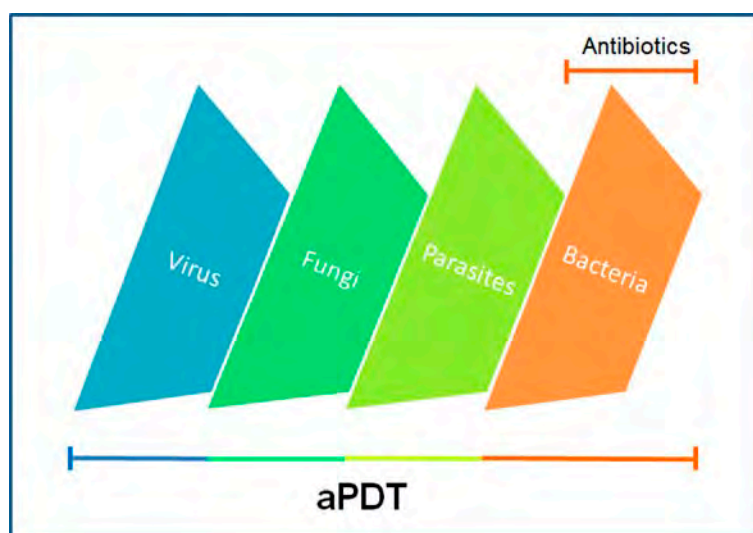
Scheme 2. aPDT broad spectra of action.

Moreover, aPDT it has gained use as research tool: to help identify the photochemical and photophysical mechanisms involved in inactivation, to develop potent and clinically compatible PS, to understand how photoinactivation is affected by key microbial phenotypic elements (multidrug resistance and efflux, virulence and pathogenesis determinants, biofilms), to explore novel delivery platforms inspired by current trends in pharmacology and nanotechnology and to identify photoinactivation applications beyond the clinical setting such as environmental disinfectants.[12]

In line with the first objective of the thesis we have focused our study in 3 different aPDT-based approaches:

a) 3rd generation cationic PSs.

While new families of PS have been developed and tailored, still many conventional 2nd generation PSs tend to aggregate in aqueous media due to π-stacking and hydrophobic interactions, resulting in self-quenching of their photoexcited states. Thus, the photodynamic effect becomes significantly weaker. The concept of '3rd generation PSs' evolved as a combination of the 2nd generation PSs associated to any drug-delivery system which allows enhanced transport into the desired target.[13] Examples of such delivery strategies comprise the use of emulsions or encapsulations with nanoparticles (NPs) and liposomes or association with antibodies or other biomolecules. However, they carry the risk of associated loss of photodynamic effect as well. When one considers the delivery strategy, the final receiver must be borne in mind. Gram-positive and Gran-negative bacteria differ in the composition of their bacterial wall, implying different susceptibility to PDT treatments. This fact, however, was only observed and understood in the 1990s, leading to a turning point in the use of aPDT.[14] As previously described, the absence of external membrane in Gram-positive bacteria allows the entrance of conventional PS (neutral and anionic) while the highly organised and negatively charged outer membrane of Gram-negative bacteria retains them outside the outer membrane in most cases, preventing them from causing inner-cell damage upon illumination. The use of cell wall-disrupting agents such as EDTA or cationic polypeptides such as polymixin B was the next improvement step in this sense.[15,16] However, the crucial discovery was the verification that PSs with intrinsically cationic charges at physiological pH were capable of achieving photoinactivation in both types of bacteria without the need for any co-administered agent.[17,18] Cationicity, thus, can be presented itself as a potential delivery tool for the objective to targeting Gram-negative bacteria through a simplistic way minimising, *a priori*, loss of activity. Their overall positive charge ensures accumulation at the poly-anionic microbial cell surfaces in both types of bacteria.

### b) PSs conjugated to antimicrobial peptides

An alternative approach to improve the susceptibility of Gram-negative bacteria to the photodynamic action of neutral PSs involves the covalent attachment of the PS to AMPs. AMPs are components of the innate defence system of many organisms and they are being considered a promising source of new antibiotics.[19] Beyond the presence of several cationic amino acids, a s ubstantial proportion of hydrophobic amino acid residues permit most AMP to fold into an amphipathic structure that inserts into

the phospholipid bilayer of the cell membranes. After insertion, AMPs act by either disrupting the physical integrity of the membrane or translocating across the membrane to hit internal bacterial targets.[20] This multi-target mode of action promises both low susceptibility to antibiotic resistance and a broad spectrum of activity against a variety of microorganisms. Among AMPs, the family of short proline-arginine rich peptides attracts particular interest because of some unique features, such as a higher activity against Gram-negative bacteria, a relative stability against proteolysis, and a very low toxicity against mammalian cells. Apidaecin 1b, an insect 18-residue long peptide belonging to this family, is effective against a large number of Gram-negative bacteria and a few Gram-positive bacteria,[21] where it acts by a non-pore-forming mechanism only partially elucidated. Mutagenesis[22,23] and structure-activity relationship studies[24] have identified the C-terminal half of apidaecin as essential for its antimicrobial activity and several studies have shown that the peptide is able to translocate a fluorescent tag into a bacterial cell.

c) Fluorescent proteins as genetically encoded PSs.

Because the PS is delivered from the cell exterior it has not been possible so far to separately study the contributions of external and internal damage, nor has it been possible to control the location of the PS and thus the primary site of photodamage.[25] The small size of bacteria (Figure 2) precludes the use of fluorescence microscopy techniques due to the limited spatial resolution of this technique.
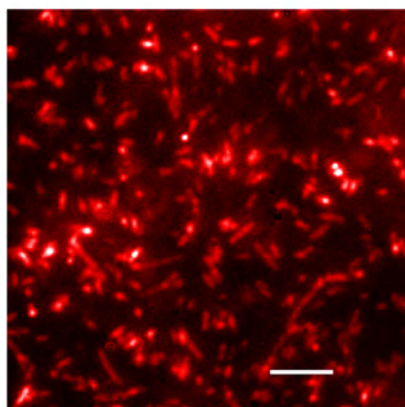

Figure 2. Fluorescence image of TagRFP-expressing bacteria upon laser illumination at 532 nm (scale bar 5 μm)

Electron microscopy (EM) has the necessary resolution and has recently revealed progression of envelope damage inflicted during irradiation.[26] On the other hand, time-resolved studies of the formation and decay of $^1O_2$ have been instrumental in establishing the coexistence of externally-bound and internalised PS molecules in *E. coli*.[27] Still, a sound understanding of the role of drug location in the mechanism of cell death has been elusive to date.

55

Since the discovery of the fluorescent proteins (FPs), novel variants have been engineered to tailor its properties. The development of mutants able to generate reactive oxygen species is pursued as a tool in microscopy, chromophore-assisted light inactivation (CALI) or PDT. Genetically encoded $^1O_2$ PS that are able to express inside the cell can be a solution both to the issue of PS location in aPDT mechanistic studies and as mere photosensitising agents.

KillerRed was the first genetically encoded ROS fluorescent protein and it has led to a plethora of successful studies especially in the CALI field,[28,29] but its *sex-appeal* was partially lost when it was discovered it was not a purely $^1O_2$ PS.[30,31] Previous studies in the group have shown that some green and red FPs are able to photosensitise $^1O_2$ (Scheme 3).[32-34]
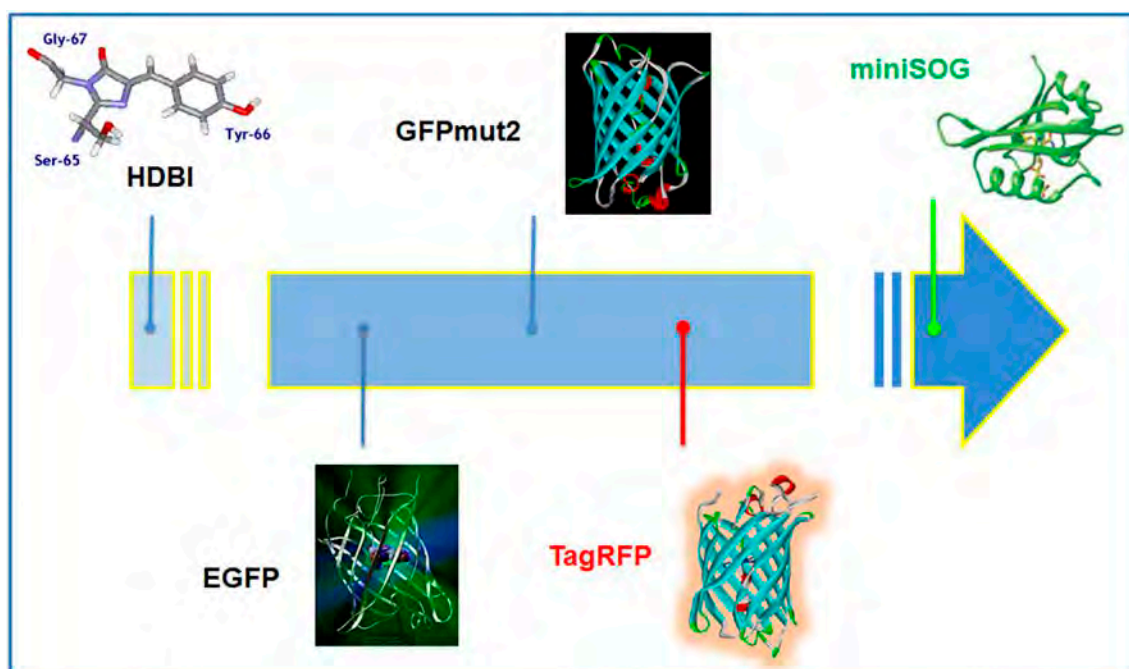

Scheme 3. Towards efficient genetically-encoded $^1O_2$ production by FPs. Graphical representation of the studies performed in the group over the years.

Firstly we have approached TagRFP, a monomeric orange FP generated from the wild-type red fluorescent protein (RFP) from sea anemone *Entacmaea quadricolor*.[35] It possesses bright fluorescence with excitation/emission maxima at 555 and 584 nm, respectively and it was recently reported to be a purely $^1O_2$ generator that is able to sensitise $^1O_2$ with a Φ_Δ value of 0.004.[36] Flavin-binding FPs have recently gained attention due to its smaller size and the maturation of the chromophore without the presence of oxygen.[37] We have also focused our attention to miniSOG (for mini Singlet Oxygen Generator), a recently-reported flavin-binding FP claimed to produce $^1O_2$ with high yield.[38-40]
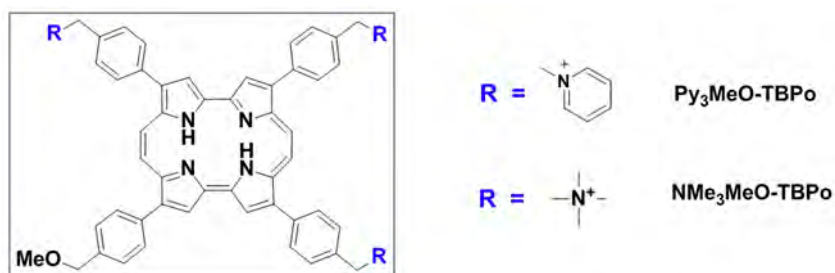
3rd generation cationic PSs

AIM OF THE STUDY

In the present study we analyse the photophysical properties as well as their behaviour against typical Gram-positive and Gram-negative bacteria of selected members of two families of cationic PSs as potential 3rd generation PSs.
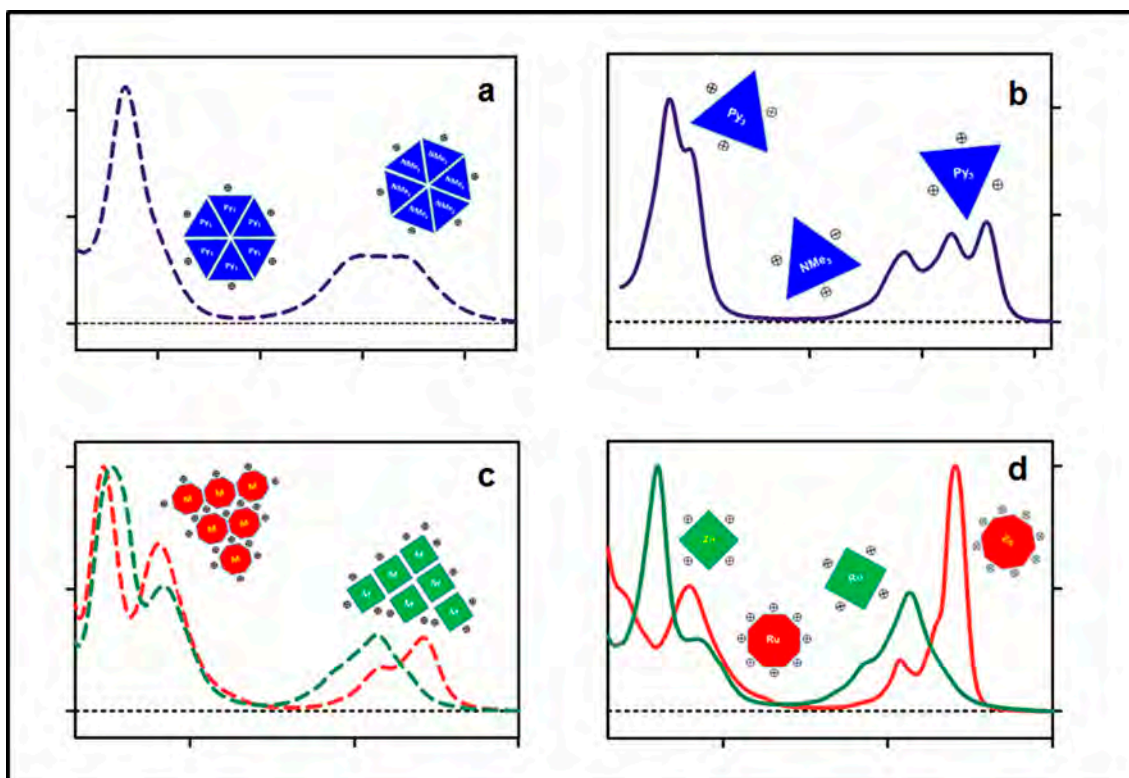
Graphical Abstract 1. Representation of the different behaviour of the tricationic porphycenes (a,b) or dendrimeric phthalocyanines (c,d) either in aggregated (a,c) or disaggregated (b,d) form.

Porphycenes have long been shown as an interesting family of PS due to the appealing optical and photochemical properties conferred by their lower molecular symmetry as compared to porphyrins. A new tricationic porphycene, namely, 2,7,12-tris(trimethyl-*p*-tolyl)–17-(*p*-(methoxymethyl)phenyl) porphycene (**NMe₃MeO-TBPo**) is compared against its predecessor, 2,7,12-tris(α-pyridinio-*p*-tolyl)–17-(*p*-(methoxymethyl)phenyl) porphycene (**Py₃MeO-TBPo**), in order to unravel the effect of different substituents on PDI activity (Scheme 4).

Scheme 4. Representation of tricationic porphycenes of study

On the other hand, we have also explored phthalocyanines bearing dendrimeric substituents (zero and first generation). Dendrimer-encapsulated chromophores are attractive for PDT because the inner chromophores are partially shielded from media while maintaining their photoactive form. Four highly charged dendrimeric phthalocyanines varying in degree of ionicity (4 or 8 positive charges) and coordinating metal (zinc or ruthenium) are presented as potential photosensitising agents in terms of antimicrobial activity (Scheme 5).
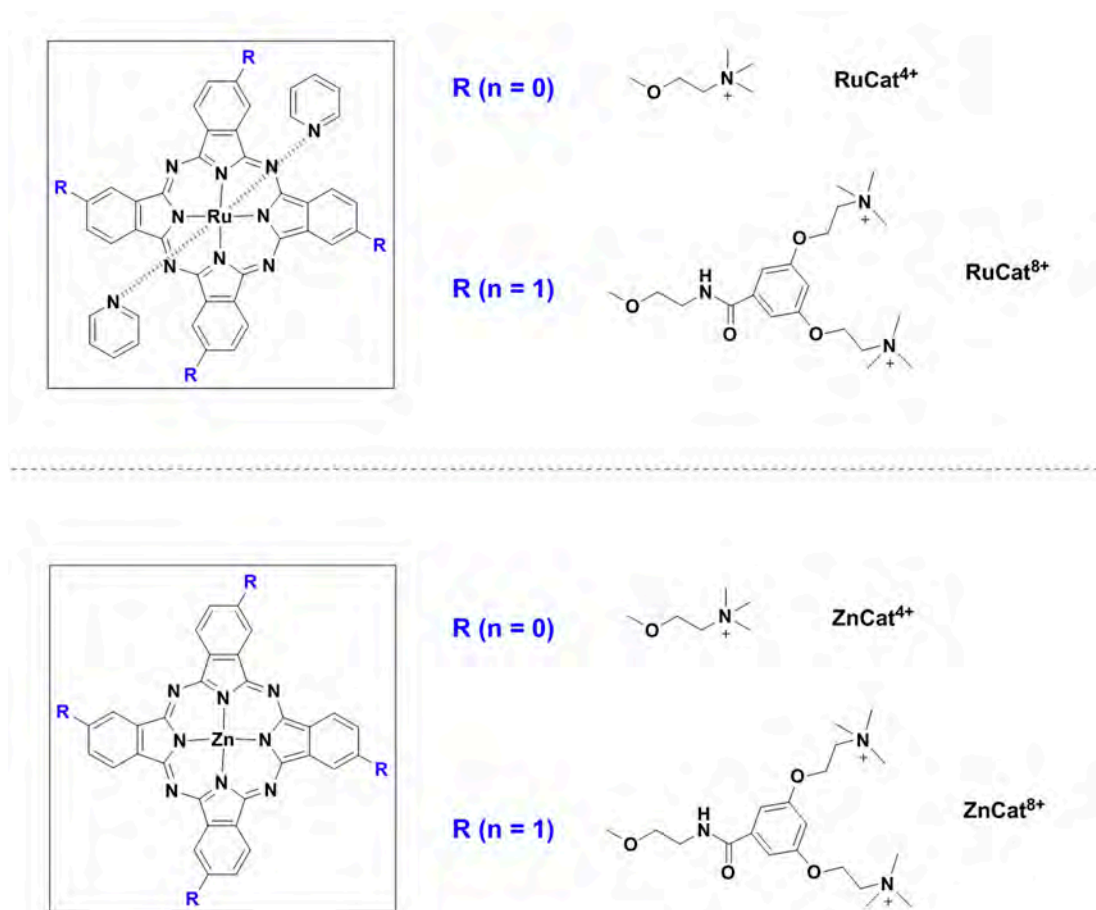

Scheme 5. Representation of zero (n = 0) and first (n = 1) generation of dendrimeric cationic ruthenium (upper scheme) or zinc (lower scheme) phthalocyanines of study.

58

RESULTS

Photophysical characterisation of porphycene derivatives.

The main photophysical properties of **NMe₃MeO-TBPo** are summarised in Table 1 and compared to those already reported for **Py₃MeO-TBPo** and the parent 2,7,12,17-tetraphenylporphycene (**TPPo**).[41,42] Figure 3 shows a compilation of spectral differences between both compounds. In panels a,c comparison of the absorption spectra of **NMe₃MeO-TBPo** and **Py₃MeO-TBPo** in methanol (MeOH) and water can be seen, respectively. The profile remains similar for both compounds and in line with that of other porphycene derivatives. Only a small red shift can be observed for **NMe₃MeO-TBPo**. Namely, a main band in the Soret region plus a small shoulder and three bands in the Q-region can be distinguished in MeOH while a remarkable loss of structure occurs (especially in the Q-region) in aqueous media due to aggregation effects. However, the absorption coefficient values are smaller in both media for **NMe₃MeO-TBPo**.
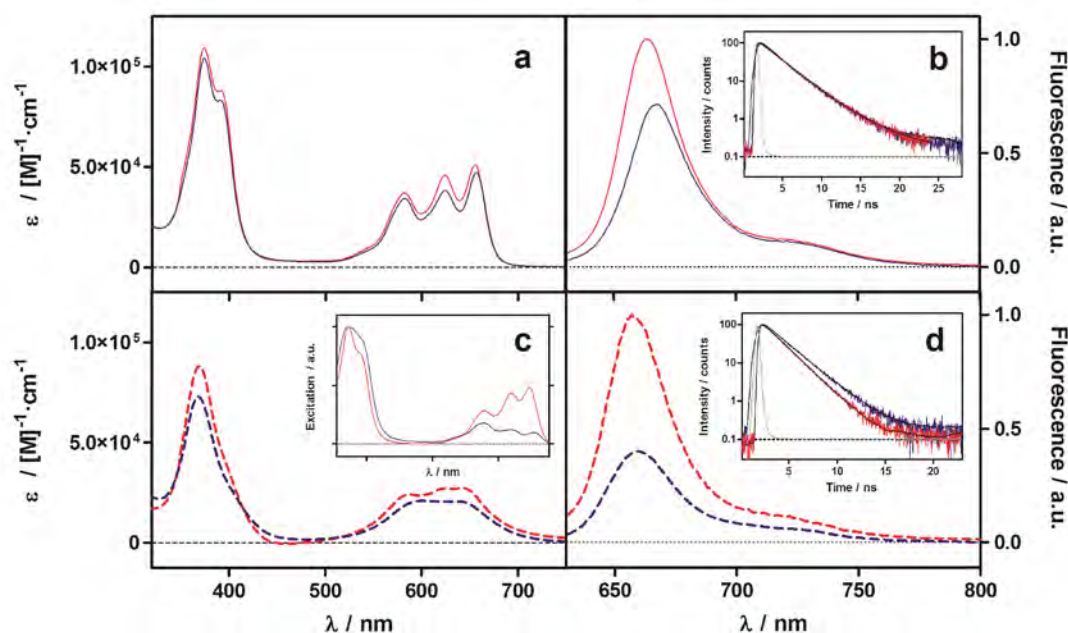
Figure 3. Absorption (a,c) and fluorescence spectra of **Py₃MeO-TBPo** (red) and **NMe₃MeO-TBPo** (blue) in MeOH (a,b) and water (c,d) (solid and dotted line, respectively). Insets: Excitation spectra of the fluorescence at 700 nm (c). Time-resolved fluorescence decays (b,d). Signal, signal fit and instrument response function at 700 nm upon excitation at 375 nm.

Regarding fluorescence measurements (panels b,d), Φ_F values are smaller for **NMe₃MeO-TBPo** both in MeOH and water (1.4 and 2.5-fold, respectively; Table 1). Cresyl violet in MeOH ($\Phi_F = 0.54$)[43] was the chosen reference (see methodology in chapter II). Again, no significative spectral changes can be

59

observed between both compounds. While minor spectral shifts occur due to solvatochromic effect, both compounds in both media exhibit the same fluorescence emission spectra profile, again characteristic of porphycenes (a main band and a weaker vibrational overtone at lower energy that are the mirror image of the $S_1 \leftarrow S_0$ absorption transition).[44] This result let us hypothesise that the aggregates are not emissive. The fluorescence excitation spectra in water (inset panel c) match that of the compounds in MeOH, clearly confirming that only the monomers are fluorescent.

As for the singlet state kinetics, fluorescence decays are monoexponential, consistent with the previous observation that only the monomeric species are fluorescent.[42] The lifetime values are equal in MeOH for both compounds, only a tiny difference being found in aqueous media where the lifetime is slightly longer for **NMe₃MeO-TBPo** (Table 1).

$^1O_2$ signals were detected through direct observation of the $^1O_2$ luminescence at 1275 nm – maximum of $^1O_2$ phosphorescence- for samples excited at 532 nm (Figure 4). Analysis of the signals for **NMe₃MeO-TBPo** resulted in decay lifetimes that matched the literature $^1O_2$ lifetime values in neat water and MeOH, respectively. No rising signal could be observed, thus triplet lifetime could not be assessed through direct luminescence neither in water or MeOH.
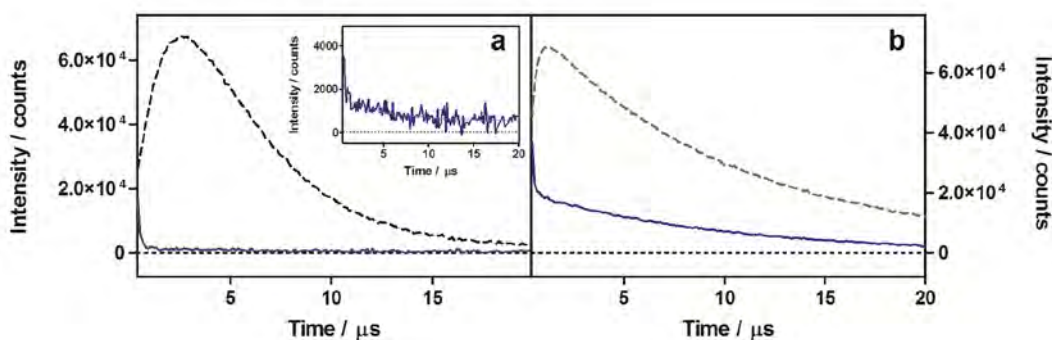
Figure 4. $^1O_2$ luminescence signals observed at 1275 nm for optically matched solutions at 532 nm of **NMe₃MeO-TBPo** (solid lines) and reference PSs (dashed lines) in water (a) or in MeOH (b). Inset: magnification of **NMe₃MeO-TBPo** signal in water. 5,10,15,20-tetrakis(m-hydroxyphenyl)-21H,23H-porphine (**m-THPP**) in water (a) and 5,10,15,20-tetrakis(N-methyl-4-pyridyl)-21H,23H-porphine (**TMPyP**) in MeOH (b) are the chosen PSs.

Comparison of the intensity of the $^1O_2$ signals shown by **NMe₃MeO-TBPo** to that of optically-matched solutions of reference PSs (**TMPyP;** $\Phi_\Delta = 0.74$ in **w**ater; **m-THPP;** $\Phi_\Delta = 0{,}69$ in MeOH)[45,46] are depicted in Figure 4 and yielded the Φ_Δ values reported in Table 1. Once again, the comparison rendered slightly smaller values for **NMe₃MeO-TBPo** respect to **Py₃MeO-TBPo**.

Table 1. Summary of photochemical properties of the porphycenes of study.

Compound	Solvent	λ_{Abs} / nm[a]	λ_{Fluo} / nm[b]	Φ_F[c]	τ_S / ns	Φ_Δ[d]	τ_Δ / μs
TPPo[e]	Toluene	659 (5.0·10^4)	667	0.150	4.8	0.230	-
Py₃MeO-TBPo	MeOH	655 (5.1·10^4)	664	0.075	2.6	0.193	10.0
	Water	644 (2.6·10^4)	657	0.005	1.8	0.004	3.7
NMe₃MeO-TBPo	MeOH	657 (4.7·10^4)	669	0.054	2.4	0.180	9.6
	Water	641 (2.0·10^4)	660	0.002	2.0	0.003	4.1

[a] maximum of the lowest-energy absorption band with ε values (M^{-1}·cm^{-1}) in brackets. [b] maximum of the fluorescence band. [c,d] values at 532 nm. [e] Data from reference [41]

Photoinactivation studies of porphycene derivatives

As a first approach, porphycene **NMe₃MeO-TBPo** was tested against representative members of the Gram-positive and Gram-negative families (namely *E. coli* and *S. aureus*) as well as against two *Candida spp* (*albicans* and *krusei*). Population reductions up to 6-log$_{10}$ in colony forming units per millilitre (CFU/mL) could be achieved in a light-dose and PS-concentration dependent fashion (Figure 5). Results were comparable to those previously reported for **Py₃MeO-TBPo** while slightly less harmful. Dark controls revealed less than 1-log$_{10}$ reduction in CFU/mL at the assayed concentrations (data not shown).
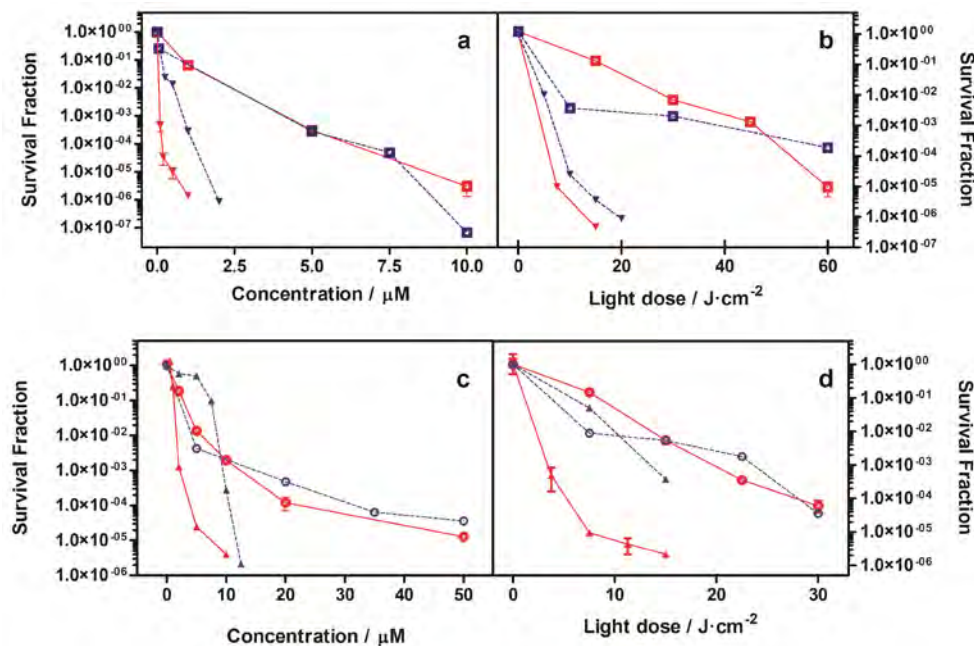
Figure 5. Bacterial (a,b) and yeast (c,d) survival curves with **Py₃MeO-TBPo** (red solid line) and **NMe₃MeO-TBPo** (blue dashed line) upon red LED light (635 ± 15 nm) irradiation. (a) Light doses: 30 J·cm^{-2} (**Py₃MeO-TBPo**) and 20 J·cm^{-2} (**NMe₃MeO-TBPo**) against *S. aureus* (filled inverted triangles); 60 J·cm^{-2} against *E. coli* (open squares). (b) Bulk concentrations: 2 μM against *S. aureus*; 5 μM against *E. coli*. (c) Light doses: 15 J·cm^{-2} (**Py₃MeO-TBPo**) and 22.5 J·cm^{-2} (**NMe₃MeO-TBPo**) against *C. krusei* (filled triangles); 30 J·cm^{-2} (**Py₃MeO-TBPo**) and 22.5 J·cm^{-2} (**NMe₃MeO-TBPo**) against *C. albicans* (open circles). (d) Bulk concentrations: 10 μM against *C. krusei*; 20 μM (**Py₃MeO-TBPo**) and 35 μM (**NMe₃MeO-TBPo**) against *C. albicans*.

The ability of **NMe₃MeO-TBPo** as photosensitising agent was also assessed against more resistant strains, namely MRSA and *P. aeruginosa*. Over 6-$\log_{10}$ reduction in CFU/mL was achieved against MRSA for both porphycenes at concentrations below 0.75 μM keeping a light dose constant (Figure 6 a). Keeping the concentration constant at 0.5 μM, a population reduction up to 6-$\log_{10}$ CFU/mL could be achieved increasing the light dose to *ca.* 20 J·cm^{-2}. A difference *ca.* 1-$\log_{10}$ CFU/mL was encountered when samples were centrifugated, the excess of PS removed, and bacteria resuspended in neat PBS prior to irradiation. This trend could be observed for both PSs under almost all conditions assayed.
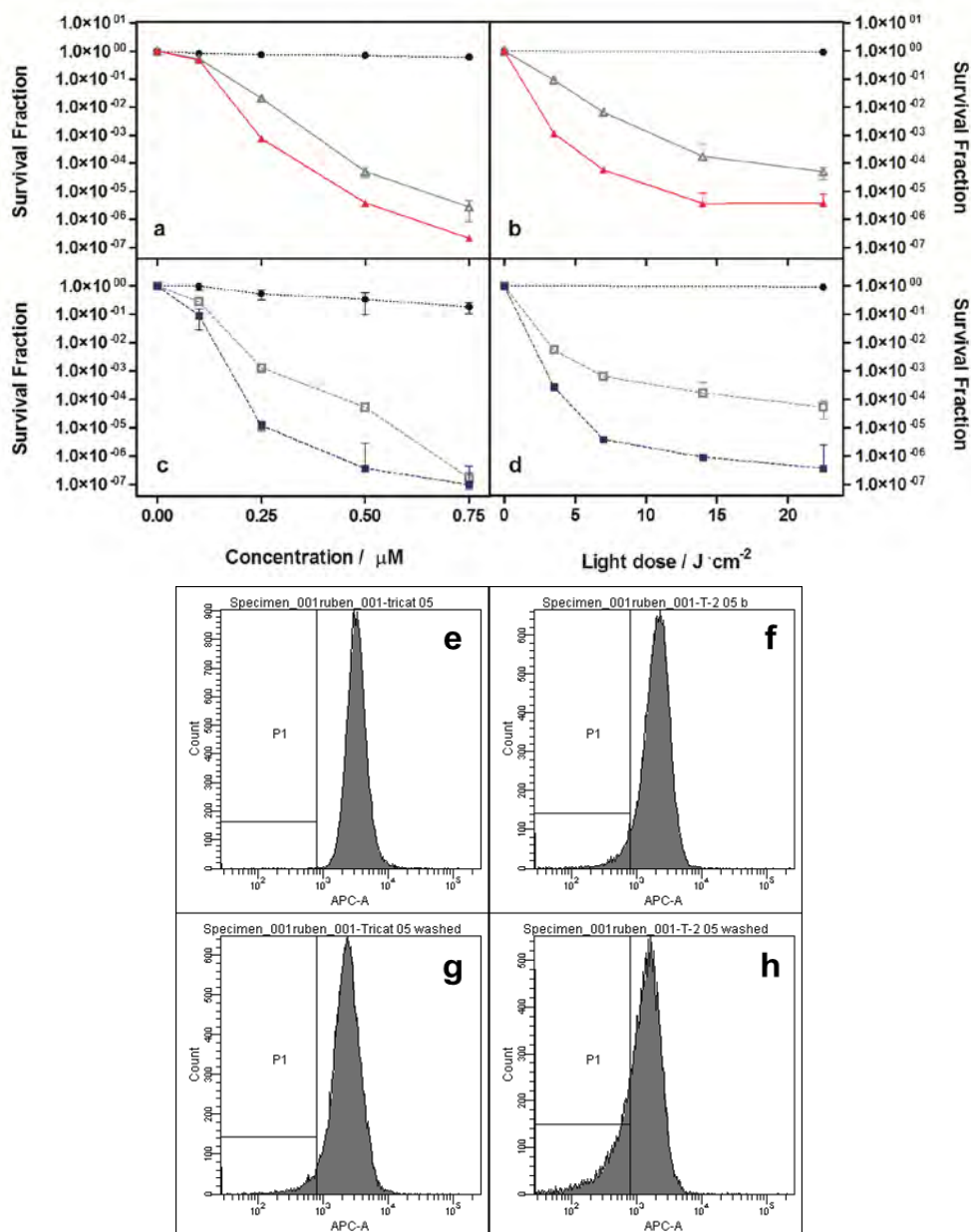
Figure 6. Bacterial photoinactivation and uptake studies. **Py₃MeO-TBPo** (a,b; solid line) and **NMe₃MeO-TBPo** (c,d; dashed line) survival curves against MRSA before (filled symbol) and after (open symbol) removing the excess of PS from the solution before irradiation. Light-dose was maintained at 7.5 J·cm^{-2} (a,c) and bulk concentration of 0.5

μM was assayed (b,d). FACS population distribution of cells incubated with 0.5 μM **Py₃MeO-TBPo** (e,g) or **NMe₃MeO-TBPo** (f,h) for 30 min before (e,f) and after (g,h) removing the excess of PS.

Fluorescence-activated cell sorting (FACS) flow cytometry experiments were carried out in order to correlate the binding of the PS with the photokilling efficiency. Samples incubated with 0.5 μM porphycene for 30 min were analysed removing or not the PS excess. Panels e-h in Figure 6 show the overall profile of the FACS distributions. The clear shift of the maximum to lower populations and the overall lower fluorescence intensity are indicative of partial removal of the PS (see data in Table 2).

Figure 7 shows the results correponding to analogue experimentes assayed against Gram-negative *P. aeruginosa*. We were gladly surprised to also achieve *ca*. 6-log$_{10}$ reduction for both PSs in the two series of experiments, although higher doses either of light or concentration were required.
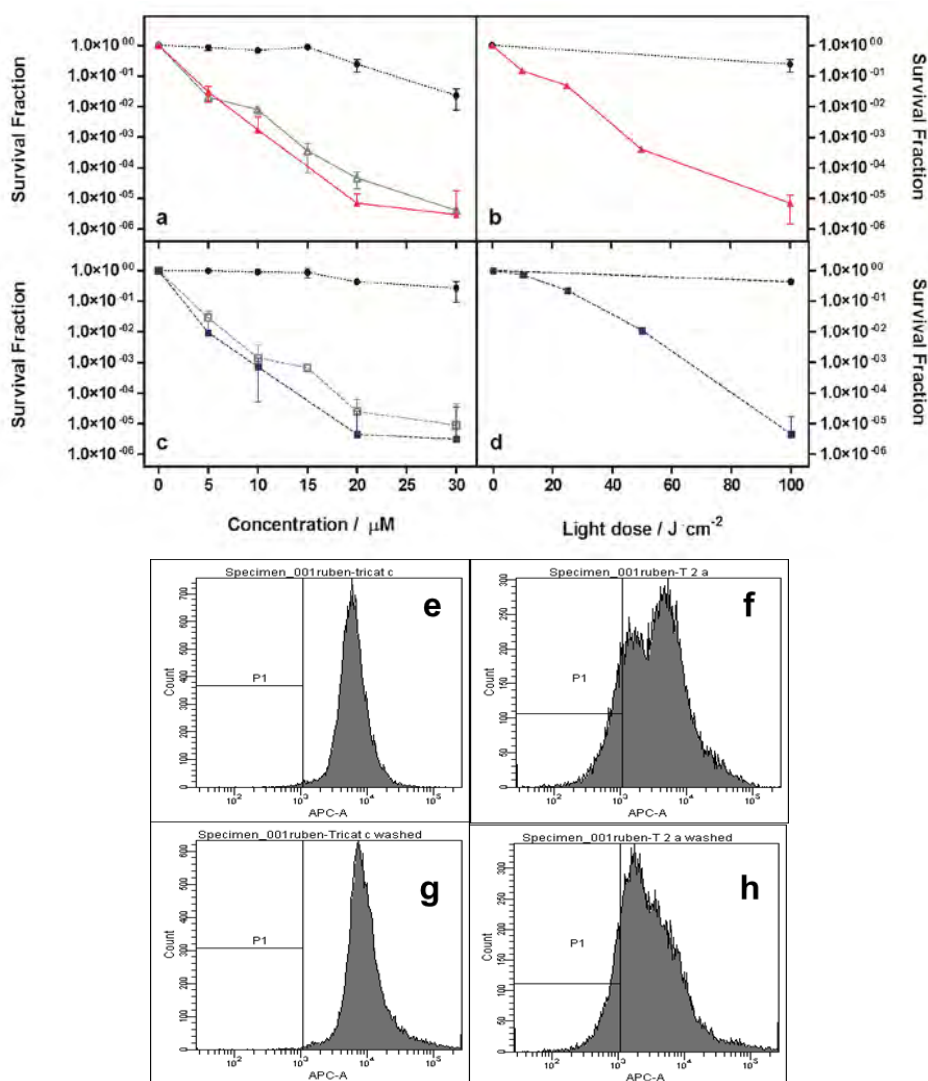

Figure 7. Bacterial photoinactivation and uptake studies. **Py₃MeO-TBPo** (a,b; solid line) and **NMe₃MeO-TBPo** (c,d; dashed line) survival curves against *P. aeruginosa* removing (empty symbol) or not (filled symbol) the PS

excess from the solution before irradiation. Light-dose was maintained at 100 J·cm^{-2} (a,c) and bulk concentration of 20 μM was assayed (b,d). FACS population distribution of cells incubated with 0.5 μM **Py$_3$MeO-TBPo** (e,f) or **NMe$_3$MeO-TBPo** (g,h) for 30 min before (e,g) and after (f,h) removing the excess of PS.

In this case, differences removing or not the excess of PS were less evident and differences only in the experimental errors were in the data set. FACS analysis was carried out for the optimum conditions, namely incubation with 20 μM PS for 30 min in the absence of light. Fluorescence measurements of the cell populations analysed rendered the results included in Table 2. As can be seen, and consistent with the survival curves, no significative difference in cell binding could be obtained removing or not the PS excess. Interestingly, the population profiles were not as narrow as for MRSA. This was especially noticeable for the case of **NMe$_3$MeO-TBPo** where 2 different populations could be observed.

Table 2. FACS fluorescence distribution upon uptake experiments.

Compound	PS removal	Fluorescence Intensity / Counts	
		MRSA	*P. aeruginosa*
Py$_3$MeO-TBPo	NO	2600 ± 900	4200 ± 1000
	YES	2100 ± 400	4300 ± 2000
NMe$_3$MeO-TBPo	NO	2600 ± 700	2600 ± 900
	YES	2000 ± 900	2600 ± 700

Photophysical characterisation of dendrimeric charged phthalocyanines.

A compilation of the photophysics of the 4 dendrimeric charged phthalocyanines is summarised in Table 3. As we will see in the following paragraphs, the different behaviour between organic and aqueous solvents has very much to do with aggregation issues.

Figure 8 shows the normalised absorption spectra of all four phthalocyanines in tetrahydrofuran (THF), water and dimethylsulfoxide (DMSO). As previously anticipated, marked changes appear due to the degree of aggregation that they exhibit in each solvent. Aside from minor peak shifts derived from solvatochromic effects, the important changes rely in the relative intensities of the bands in each region. The spectrum in DMSO is taken as representative for the monomeric form, characterised by a narrow and intense red Q band.[47] The general trend for three out of the four compounds is that they tend to disaggregate in aqueous media. This is not completely clear for compound **ZnCat^{4+}** (Panel a) whose Soret

band, but not the Q region, resembles that in DMSO. Both ruthenium compounds pretty much completely disaggregate in water. In spite of having the same charges as their zinc analogues, the presence of the apical pyridil groups seems to prevent aggregation.
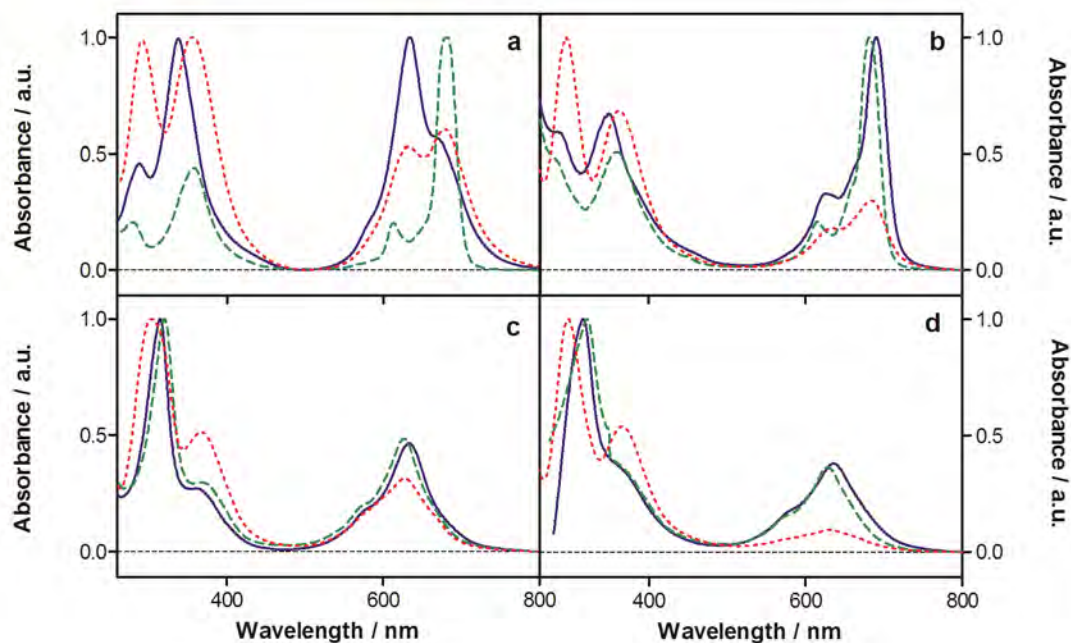
Figure 8. Normalised absorption spectra of dendrimeric cationic phthalocyanines in DMSO (green dashed line), THF (red dotted line) and water (blue solid line). **ZnCat^{4+}** (a), **ZnCat^{8+}** (b), **RuCat^{4+}** (c) and **RuCat^{8+}** (d).

Fluorescence of the compounds was also studied in the same series of solvents. As observed in Figure 9 and Table 3, there is a huge difference in behaviour depending on the nature of the central metal ion, only zinc phthalocyanines being fluorescent. Moreover, a great difference in Φ_F values can be encountered for a given compound depending on the medium, once again due to aggregation.
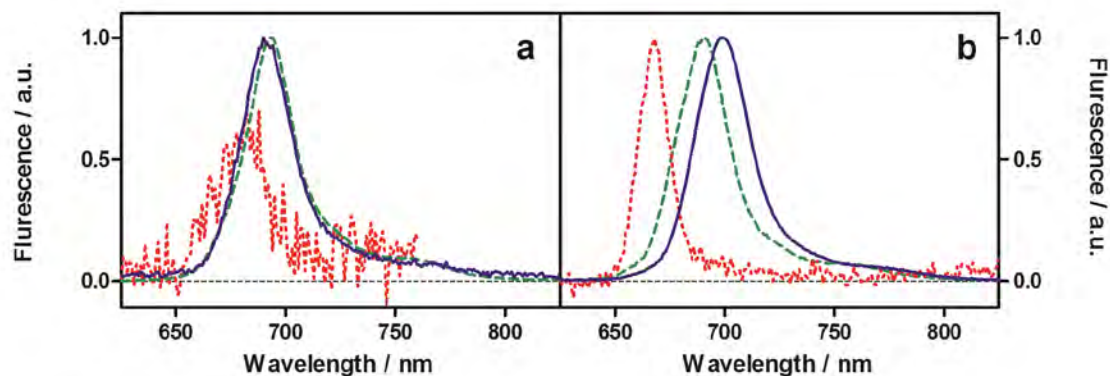
Figure 9. Normalised fluorescence spectra of dendrimeric cationic phthalocyanines in DMSO (green dashed line), THF (red dotted line) and water (blue solid line). **ZnCat^{4+}** (a), **ZnCat^{8+}** (b)

Especially significant is the case of **ZnCat^{8+}** that shows Φ_F values two orders of magnitude different in THF and water (Table 3). Similarly, the fluorescence of both **ZnCat^{4+}** and **ZnCat^{8+}** was completely lost in PBS. Fluorescence decay kinetics were also studied.

Finally, the ability of the phthalocyanines to sensitise the production of $^1O_2$ was studied both in THF and in aqueous media. Φ_Δ measurements were performed by direct observation of $^1O_2$ luminescence at 1275 nm (as described above for porphycene derivatives), exciting either at 532 nm (for RuCats) or at 355 nm (for ZnCats). In line with the fluorescence results, the photosensitising properties of the phthalocyanines hinged on the degree of aggregation, being more efficient when less aggregated. This effect was –once again- especially exagerated for compound **ZnCat^{8+}** whose Φ_Δ value in water was two orders of magnitude higher than in THF (Table 3). The τ_Δ values indicate that RuCats are better $^1O_2$ quenchers than ZnCats, as their τ_Δ values are shorter than reported in the literature for the solvents used (21 μs in THF and 64 μs in D$_2$O).[48] This effect has previously been reported for other ruthenium dendrimeric derivatives, although to a lesser extent.[49]

Table 3. Summary of photochemical properties of the dendrimeric phthalocyanines of study.

Compound	Solvent	λ_{Abs} / nm	λ_{Fluo} / nm	Φ_F [a]	Φ_Δ [b]	τ_Δ / μs
ZnCat^{4+}	THF	679	688	$< 1\cdot10^{-4}$	0.002	20.8
	D$_2$O	634	692	0.035	0.022	62.8
ZnCat^{8+}	THF	684	667	0.002	0.004	21.0
	D$_2$O	690	698	0.538	0.119	64.0
RuCat^{4+}	THF	628	-	$< 1\cdot10^{-4}$	0.011	19.7
	D$_2$O	633	694	$< 1\cdot10^{-3}$	0.015	45.3
RuCat^{8+}	THF	631	-	$< 1\cdot10^{-4}$	0.001	19.4
	D$_2$O	636	694	$< 1\cdot10^{-3}$	0.017	38.7

[a] Rhodamine 6G as reference (Φ_F (ethanol) = 0.94).[50] [b] 5,10,15,20-Tetraphenyl-21*H*,23*H*-porphine (TPP ; Φ_Δ (THF) = 0.62) and meso-tetrakis(4-sulfonatophenyl)-porphyrin (TPPS ; Φ_Δ (D$_2$O) = 0.64) as references.[46]

Photoinactivation studies of dendrimeric charged phthalocyanines

All 4 dendrimers were assayed against *E. coli* to assess their potential use as photosensitising agents (Figure 10). Dark toxicity was below 1-log$_{10}$ CFU/mL for the ZnCat compounds and **RuCat^{8+}**, but *ca.* 2-log$_{10}$ CFU/mL for **RuCat^{4+}** at concentrations above 5 μM. A remarkable difference in PDI efficiency was also displayed depending on the coordinated metal. Undoubtedly, ZnCats performed far better than their

ruthenium analogues. *Ca.* 6-log$_{10}$ CFU/mL reductions were achieved at concentrations as low as 2.5 μM for **ZnCat^{4+}** and 5 μM for **ZnCat^{8+}** at 30 J·cm^2 light dose. In contrast, a more modest reduction was obtained when using **RuCat^{4+}** in even more demanding conditions (*ca.* 5-log$_{10}$ reduction at best with 5 μM and 60 J·cm^2, but with dark toxicity over 1-log$_{10}$ reduction). Compound **RuCat^{8+}** caused only a modest 2-log$_{10}$ CFU/mL reduction even at 50 μM and 100 J·cm^2; data not shown).

An interesting effect could be observed for all families of compounds at high concentration: instead of achieving higher killing efficiency the efficiency worsened. Aggregation above a concentration threshold could be a plausible explanation to this behaviour.
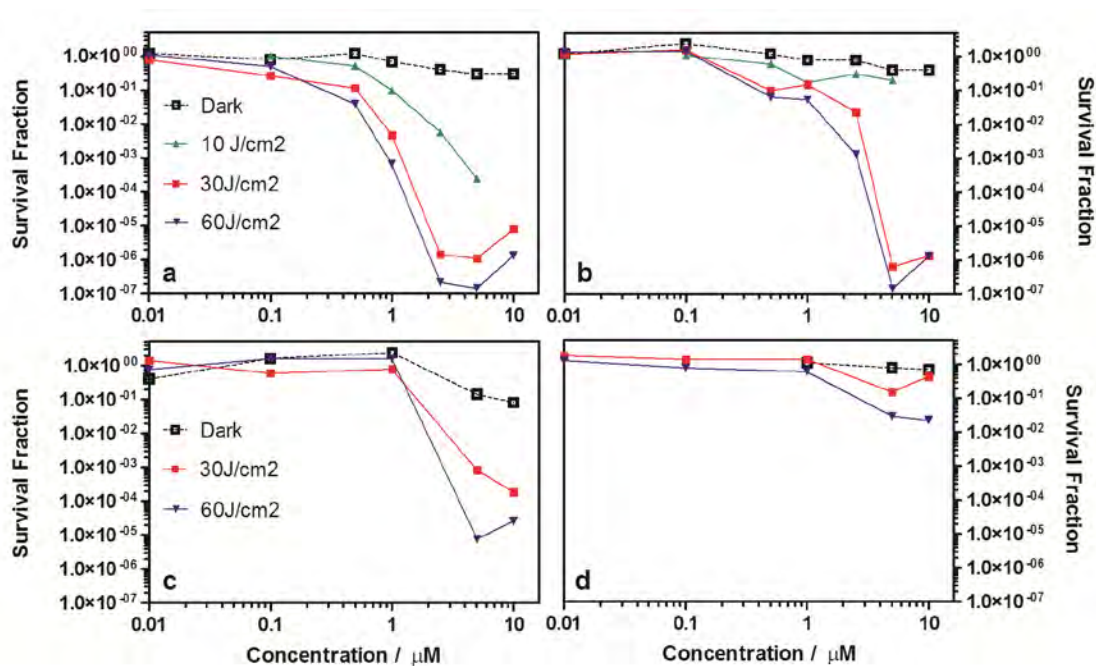
Figure 10. *E. coli* photoinactivation studies with **ZnCat^{4+}** (a), **ZnCat^{8+}** (b), **RuCat^{4+}** (c) and **RuCat^{8+}** (d) upon red LED light (635 ± 15 nm) irradiation. Different concentrations were used at different light doses: 10 J·cm^{-2} (triangles), 30 J·cm^{-2} (filled squares), and 60 J·cm^{-2} (inverted triangles). Dark toxicity is represented with empty squares.

DISCUSSION

Porphycene is a structural isomer of porphyrin and constitutes an interesting new class of 2nd generation PS. Porphycene derivatives show higher absorption values than porphyrins in the red spectral region ($\lambda > 600$ nm, $\varepsilon \sim 50000$ $M^{-1} \cdot cm^{-1}$) owing to the lower molecular symmetry.[44] Photophysical and photobiological properties of porphycene derivatives make them excellent candidates as PSs and have proven interesting in several recent studies addressing not only antimicrobial but also tumor targets.[42,51-53]

Based on the encouraging results obtained with the first cationic aryl porphycene **Py$_3$MeO-TBPo** against a wide variety of pathogenic *spp* both in vivo and in animal model[42] a second member of the family of the tricationic porphycenes was synthesised in order to further investigate in the properties of the family. Decades of research on porphycenes has built the knowledge that most dramatic photophysical changes arise either by increasing the conjugation (electronic circulation of the core) or with the introduction of heteroatoms to the porphycene core.[44] Thus, one would not expect remarkable changes due to the presence of trimethylammonium groups instead of pyridynium groups. Spectral changes were not huge; however, a general decrease in the photophysical parameters of study for **NMe$_3$MeO-TBPo** was found. Moreover, a remarkable decrease in the Φ_F value was observed not fully in line with the decrease in the τ_s. A notorious decrease in the ε value was also observed. Still, both **Py$_3$MeO-TBPo** and **NMe$_3$MeO-TBPo** photophysics lie far from those of parent **TPPo**. For instance, the τ_s values are almost half faster as compared to **TPPo** in toluene (4.8 ns), that can be attributed both to new deactivation pathways due to intermolecular interactions consequence of aggregation but also to the higher degrees of freedom conferred by the periferical residues.

The PDI experiments resulted in a similar antimicrobial efficiency for both tricationic porphycenes with slight differences depending on the microbial type. In the case of *Candida spp*, **Py$_3$MeO-TBPo** clearly outperformed **NMe$_3$MeO-TBPo**. The reverse situation was found for MRSA and *P. aeruginosa* even though the difference between both compounds was below 1-$\log_{10}$. One remarkable difference was the significative dark toxicity of **Py$_3$MeO-TBPo** at the highest concentration needed to photoinactivate *P. aeruginosa*. More significative is the fact that **Py$_3$MeO-TBPo** had previously been unable to inactivate *P. aeruginosa* at 100 μM porphycene concentration and light dose up to 100 $J \cdot cm^{-2}$.[42] However, both light source and, especially, cell strain (ATCC 19660 vs ATCC 25668) were markedly different. In fact, it is described that ATCC 19660 strain is especially virulent when inoculated in an area of burned skin,

producing septicemia in mice while strain ATCC 25668 is sensitive to common antibiotics such as carbenicillin or gentamicin.[54]

The second result to debate is the outcome regarding removal of the unbound PS prior to irradiation. In the case of MRSA the difference was *ca.* 1-log_{10} in performance for both PSs; however, little loss of efficiency occurred when same experiments were tested for *P. aeruginosa*. Overall, no clear effects can be attributed to the difference in charge density among Gram-positive and Gram-negative bacteria. In fact, previous studies for **Py₃MeO-TBPo** also showed no significative differences between inactivation curves recorded either in the presence of excess of PS or after three washings.[42]

As far as the bacterial wall in Gram-negative is much more densely packed and negatively charged it is expected that the cationic PS will be better attached and less PS will be lost after centrifugation step as compared to the same experiment in Gram-positive bacteria. This hypothesis seems to correlate with the data obtained in our flow cytometry studies (bearing in mind the high error associated with the mean fluorescence intensity; Table 2). Thus, the positive charges on the PS appear to promote a tight electrostatic interaction with negatively charged sites at the outer surface of the Gram-negative bacteria. The fact that the efficiency of the photoinactivation processes is not highly altered seems to indicate that only the PS bound to the cells is involved in the photodynamic effect.

Dendrimer-encapsulated chromophores are attractive for PDT because the bulky substituents prevent aggregation of the macrocycle. Their large dimensions should allow prolonged circulation in the blood and higher accumulation of dendronised PSs in the tumor tissues via the so-called enhanced permeation retention effect.[55] We have assessed the potential of four different cationic dendrimeric phthalocyanines as potential antibacterial PSs. The study of the photophysics revealed substantial differences among them, the ZnCats dendrimers showing superior properties than the RuCats. This behaviour perfectly correlates with the results obtained in the PDI treatments against *E. coli*. While **ZnCat⁴⁺** and **ZnCat⁸⁺** achieved bacterial reduction over 6-log_{10} CFU/mL at low concentration/light doses this is not the case for RuCats, especially for the octacationic compound.

The incorporation of positive charges in PSs has been a benchmark in the reemerging of aPDT as a potential platform to fight antibiotic-resistant microbials. Still, cationicity is not a straightforward property and caution is to be borne in mind since most PSs are comprised of a highly hydrophobic core. In spite of the solubility in aqueous media that cationicity confers, one must not forget the fact that

69

aggregation is likely to be present. And most of the times aggregation means loss of photodynamic potential. The photophysical studies summarised in Tables 1 a nd 3 clearly exemplify that some photophysical properties can decrease up to two orders of magnitude (i.e. Φ_F or Φ_Δ values). It is interesting to note that the disaggregated form –and thus the one that exhibits best photophysical properties- corresponds to opposite media depending on the family of the studied compounds. Thus, for porphycenes the best performance in cuvette is found in organic-like media, while for the dendrimeric compounds the most powerful skills arise in aqueous media.

Results show that both cationic porphycenes as well as ZnCats perform nicely against *E. coli*, reaching 6-$\log_{10}$ reduction in CFU/mL at concentrations 5 µM or lower. We infer three different issues in the explanation: A) there must be different localisation of the active compounds so that in all cases they are disaggregated (no matter where or how). B) In line with the previous statement, the hydrophobicity/hydrophilicity balance must be an important factor. C) Finally, but not least important, the number and distribution of charges in the compounds is also a key parameter. Some studies have attempted to establish relationships between PDI efficiency and the overall charge of the PSs. The study of Caminos *et. al* showed that the photosensitising efficiency of a series of meso-substituted cationic porphyrins against *E.coli* , followed the trend $(PS)^{3+} > (PS)^{4+} \gg (PS)^{2+} > (PS)^{+}$.[56] In our case, a shallow comparison would point out that **ZnCat⁴⁺** outperforms them all while tricationic **Py₃MeO-TBPo** and **NMe₃MeO-TBPo,** and **ZnCat⁸⁺** work more or less with the same efficiency. However, it is very risky to extrapolate the results as different families with markedly different behaviour are being compared. Thus, no extra conclusions should be taken without further investigation under same conditions.

Photokilling efficiency among dendrimers seems to go in line with the photophysics of the compounds. In general, ZnCats showed better properties, namely higher Φ_F and Φ_Δ values. However, behaviour in the presence of cells should be further studied. In order to correlate the promising results in killing efficiency one could hypothesise that in the presence of bacteria ZnCats will be able to disaggregate in order to exhibit their best photophysical behaviour. On the contrary, RuCats will probably have worse affinity towards *E. coli*. Especially, this is expected for **RuCat⁸⁺** whose killing efficiency rendered extremely poor.

CONSLUSIONS

Six different cationic PSs have been assayed against bacterial cultures in order to correlate its photochemical behaviour in cuvette with their photokilling efficiency. The differences arising from their macrocyclic inner structure renders different behaviour in solution towards aggregation. While porphycene family seems to disaggregate more in organic solvents dendrimeric phthalocyanines present better skills in aqueous media. Still, best candidates in both families achieve a similar photoinactivation efficiency towards *E. coli*, indicating disaggregation when uptaken and consequent different localisation. The more complete study of tricationic porphycenes renders a higher affinity towards Gram-negative organisms as deduced from the photoinactivation and flow cytometry results comparing experiments removing or not the excess of PS. Finally, the different amount of charges seem to have an important effect, while further conclusions cannot be obtained since different conditions have been used.

SPECIFIC EXPERIMENTAL SECTION

Chemical synthesis. 2,7,12-Tris(r-pyridinio-p-tolyl)-17-(p-(methoxymethyl)phenyl) porphycene (**Py₃MeO-TBPo**) was synthesised as previously described[42] and its analogue 2,7,12-tris(trimethylamonioum -p-tolyl)-17-(p-(methoxymethyl)phenyl) porphycene (**NMe₃MeO-TBPo**) with small variation in the last step. Purity of **NMe₃MeO-TBPo** was confirmed by thin layer chromatography using a pre-coated TLC plate (Silica gel C18 0.25 mm; Macherey-Nagel) in a t rifluoroacetic acid/acetonitrile mixture (20:80), providing a unique spot at R_f = 0.26. ^{1}H-NMR (δ/ ppm, d_6-MeOD): 10.02 (brs, 4H), 9.98 (brs, 4H) 8.58 (d, 6H), 8.38 (d, 2H), 7.84 (d, 2H), 8.06 (d, 6H); 4.86 (s, 6H), 4.58 (s, 2H); 3.72 (s, 2H), 3.59 (s, 2H), 3.30 (s, 27H).

UV/Vis (MeOH): 657 (46483), 626 (41129), 584 (32590), 393(80599), 377 (102543)

HRMS (ESI-TOF) m/z $C_{58}H_{64}N_7O_1^{3+}$ [M-3Br] found, 290.5054.

Flow Cytometry. The interaction of PSs with bacteria was evaluated by flow cytometry. For these experiments, the bacteria were subjected to the same treatments used for PDI experiments, but instead of being illuminated after incubation and washing they were analysed with a FACSCantoTm II flow cytometer. Samples were excited with the 488 nm laser, and fluorescence emission signals were recorded at wavelengths higher than 670 nm. The bacteria population was isolated from instrument noise by setting electronic gates on the dual-parameters dot plots of forward scatter against side scatter. For each sample, 20000 events were acquired and analysed with the FACSDiva software (BD). Samples not incubated with the PSs were used to determine the cell background fluorescence.

AMP-PS conjugates[i]

AIM OF THE STUDY

Binding to a cationic antimicrobial peptide offers the attractive prospect of improving both the water solubility and the localisation of the photoactive drug in bacteria. In this work we have compared a number of free and apidaecin-conjugated PSs differing in structure and charge.

We report the photophysical characterisation and relation to the phototoxicity studies against *E. coli* and MRSA of new conjugates in which apidaecin and its C-terminal octapeptide were modified at the N-terminus with neutral or charged porphyrin and porphycene PSs.

Our results indicate that the conjugation of *per se* ineffective highly hydrophobic PSs to a cationic peptide produces a photosensitising agent effective against Gram-negative bacteria. Apidaecin cannot improve the phototoxic activity of cationic PSs, which mainly depends on a very high yield of singlet oxygen production in the surroundings of the bacterial outer membrane. Apidaecin−PS conjugates appear most promising for treatment protocols requiring repeated washing after sensitiser delivery.
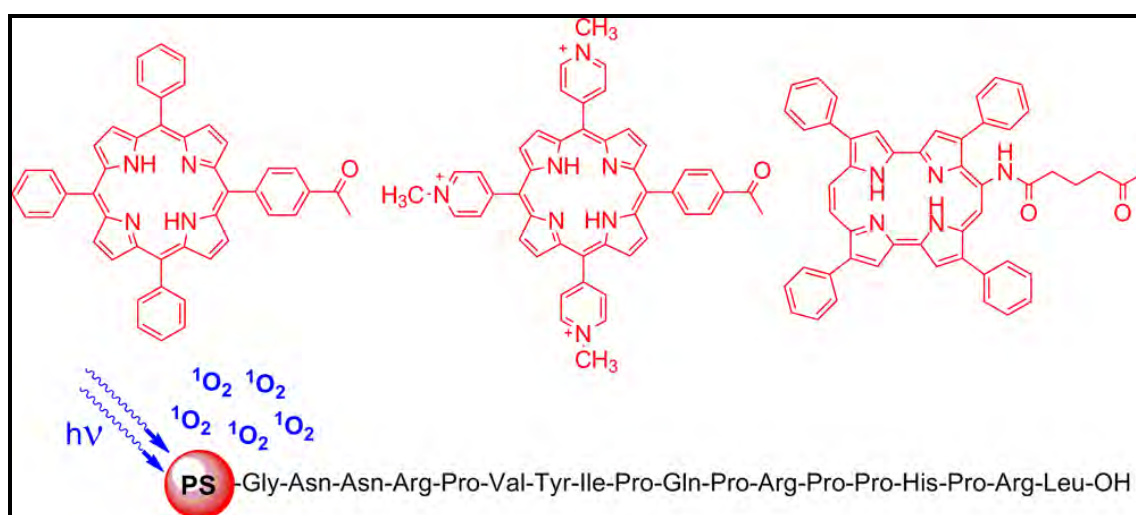
Graphical Abstract 2. Representation of the combination of different PSs and Apidaecin 1b seeking synergistic effects for enhanced aPDT treatments.

RESULTS

Conjugates description.

4 conjugates comprised by Apidaecin 1b and 4 different PSs (two neutral porphyrins, a tricationic porphyrin and a neutral porphycene) were the basis of the study (Scheme 6). Further details on the synthesis, purification and characterisation of the compounds can be found in reference [57].

a, R = -OCH$_3$ **b**, R= -OH

c, R = -Gly-Asn-Asn-Arg-Pro-Val-Tyr-Ile-Pro-Gln-Pro-Arg-Pro-Pro-His-Pro-Arg-Leu-OH

d, R = -Gly-Pro-Arg-Pro-Pro-His-Pro-Arg-Leu-OH

e, R = -Gly-Asn-Asn-Arg-Pro-Val-Tyr-Ile-Pro-Gln-Pro-Arg-Pro-Pro-His(N^{π}CH$_3$)-Pro-Arg-Leu-OH
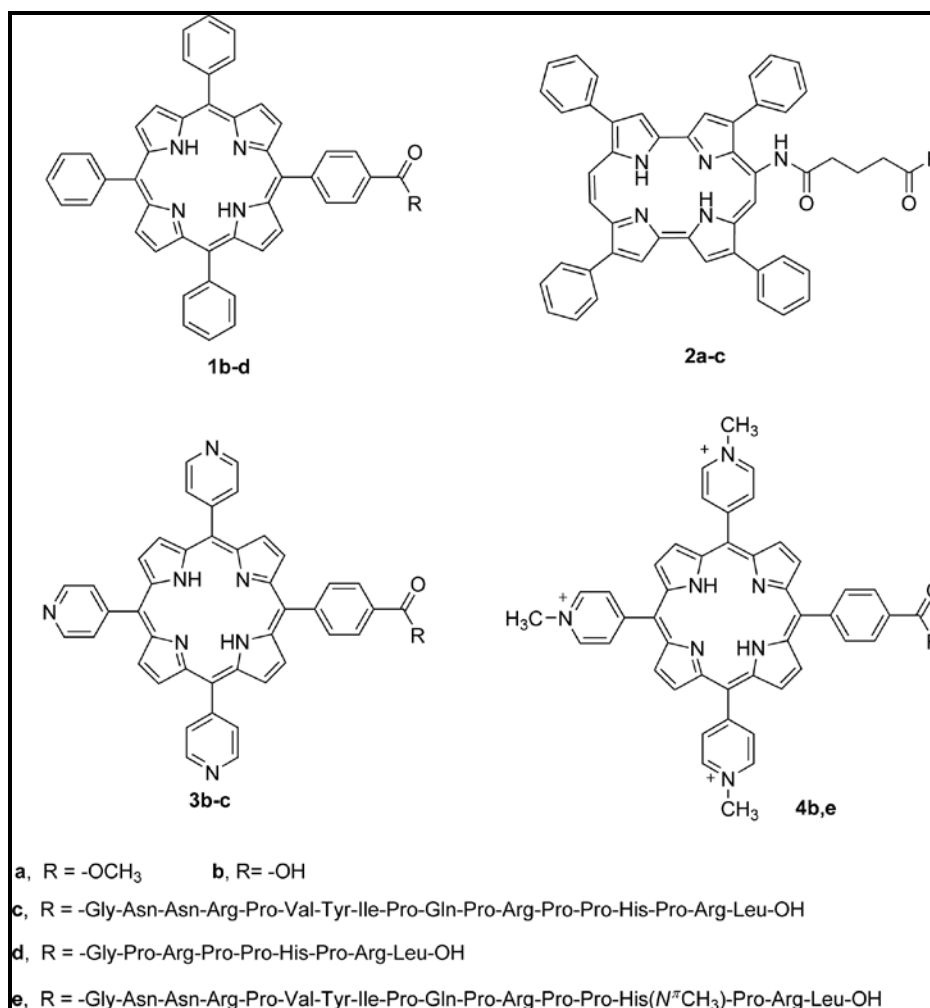
Scheme 6. Structure of the PSs of study and the conjugated peptides

Absorption and fluorescence of the conjugates.

The spectroscopic and photophysical properties of the PSs and their conjugates were measured in aqueous and organic media and in cell suspensions in order to assess structural and environmental effects as well as their correlation with antibacterial activity.

MeOH. Figures 11 and 12 show the absorption and fluorescence spectra of the free PSs and of their peptide conjugates in MeOH.
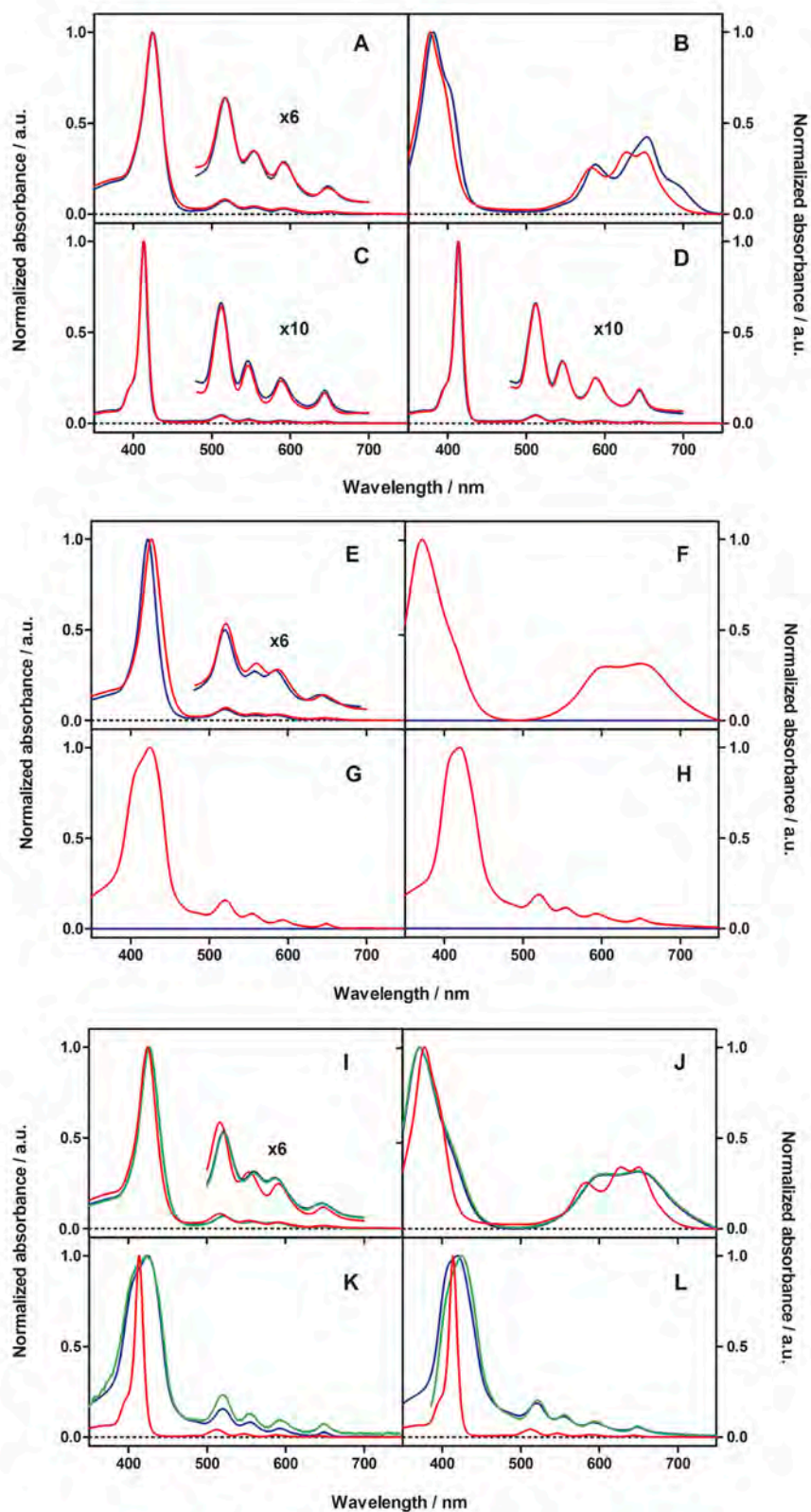
Figure 11. Absorption spectra in MeOH (A−D), PBS (E−H), and *E. coli* suspensions (I−L), normalised to facilitate their comparison. The concentration is 5 μM for all compounds. MeOH: (A) 4e (red) and 4b (blue); (B) 2c (red) and 2a (blue; dichloromethane (DCM) as solvent); (C) 1d (red) and 1b (blue); (D) 1c (red) and 1b (blue). PBS: (E) 4e (red) and 4b (blue); (F) 2c (red) and 2a (blue); (G) 1d (red) and 1b (blue); (H) 1c (red) and 1b (blue). *E. coli* suspensions (green): (I) 4e; (J) 2c; (K) 1d; (L) 1c. Spectra in MeOH (red) and PBS (blue) are given for comparison.
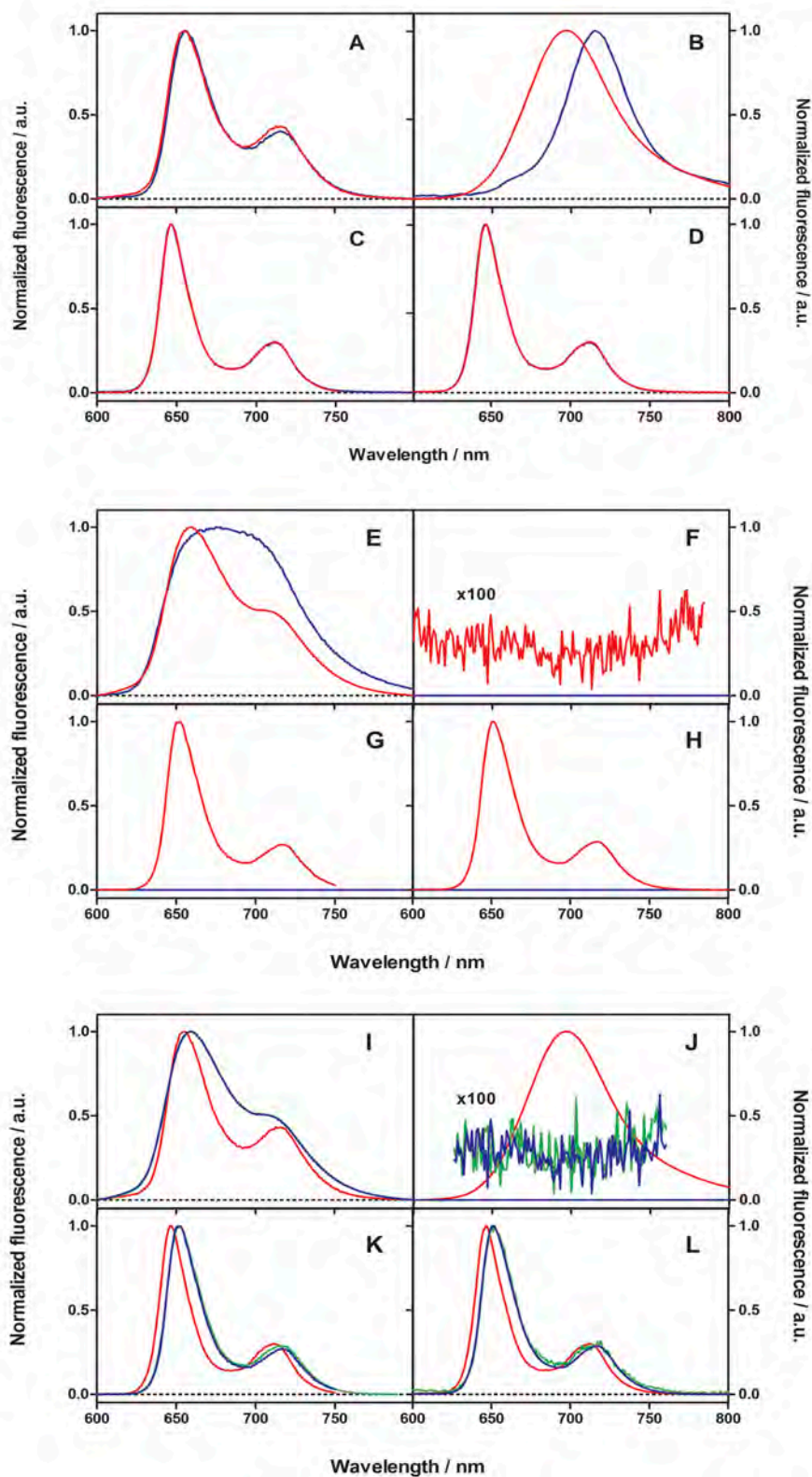
Figure 12. Emission spectra in MeOH (A–D), PBS (E–H), and *E. coli* suspensions (I–L), normalised to facilitate their comparison. The concentration is 5 µM for all compounds. MeOH: (A) 4e (red) and 4b (blue); (B) 2c (red) and 2a (blue; DCM as solvent); (C) 1d (red) and 1b (blue); (D) 1c (red) and 1b (blue). PBS: (E) 4e (red) and 4b (blue); (F) 2c (red) and 2a (blue); (G) 1d (red) and 1b (blue); (H) 1c (red) and 1b (blue). *E. coli* suspensions (green): (I) 4e; (J) 2c; (K) 1d; (L) 1c. Spectra in MeOH (red) and PBS (blue) are given for comparison.

While the spectra of porphyrins are essentially insensitive to conjugation (panels A, C, D), clear changes can be observed for the porphycene (panel B). In turn, the Φ_F value does not change appreciably for the porphyrins while it drops by *ca.* 50% for the porphycene (Table 4). Finally, all porphyrins show monoexponential fluorescence decay kinetics and conjugation does not change the lifetime values either (Table 4). Again, the situation is different for the porphycenes in that the conjugate **2c** shows biexponential kinetics unlike the free porphycene **2a** (Table 4) and on average the singlet state decays faster (Table 4).

Table 4. Fluorescence properties of the peptide conjugates and model compounds in MeOH, PBS and in *E. coli* suspensions. (Fractional amplitudes in parentheses)

Compound	$\lambda_{F, max}$ / nm			Φ_F		τ_S / ns		
	MeOH	PBS	*E. coli*	MeOH[a]	PBS[b]	MeOH	PBS	*E. coli*
1b	647	ns[c]	-	0.040	ns	10.1	ns	-
1c	647	651	651	0.050	0.006	9.8	10.7 (0.82) 3.1 (0.18)	10.5 (0.46) 7.5 (0.33) 3.1 (0.21)
1d	646	652	652	0.044	0.006	9.8	6.1 (0.61) 2.6 (0.39)	5.9 (0.11) 4.9 (0.48) 2.5 (0.41)
2a	715	ns	-	0.030[d]	-	1.46[d]	-	-
2c	697	-	-	0.016	<$1 \cdot 10^{-3}$	0.9 (0.94) 9.6 (0.06)	-	0.9 (0.75) 5.2 (0.25)
4b	656	675	-	0.022	0.008	7.9	4.2	-
4e	655	660	660	0.024	0.018	8.1	4.2 (0.49) 7.1 (0.51)	4.2 (0.48) 7.1 (0.52)

[a] Cresyl violet as standard (Φ_F (MeOH) = 0.54).[43] [b] TMPyP as standard (Φ_F (PBS) = 0.017).[58] [c] Not soluble. [d] In toluene.

Aqueous solutions (PBS). Porphyrin **4b** is water soluble as a consequence of its positively- and negatively-charged groups. It remains water soluble after conjugation (**4e**) with small but clear shifts in the position of the Soret and Q absorption bands and changes in their relative intensities (Figure 11E). The fluorescence spectrum of **4b** shows a single, structureless broadband (Figure 11E), a behaviour strikingly different from that in MeOH but in line with that of the related tetracationic **TMPyP**.[59] Conjugation to the peptide (**4e**) leads to partial recovery of the two well-resolved fluorescence bands observed in MeOH. The fluorescence decay kinetics of **4b** is monoexponential, albeit with lifetime much

shorter than in MeOH. For the conjugate **4e** two decay components can be observed, whose lifetimes are close to those of **4b** in MeOH and in PBS, respectively (Table 4). The kinetics are independent of concentration over 3 orders of magnitude (Figure 13).
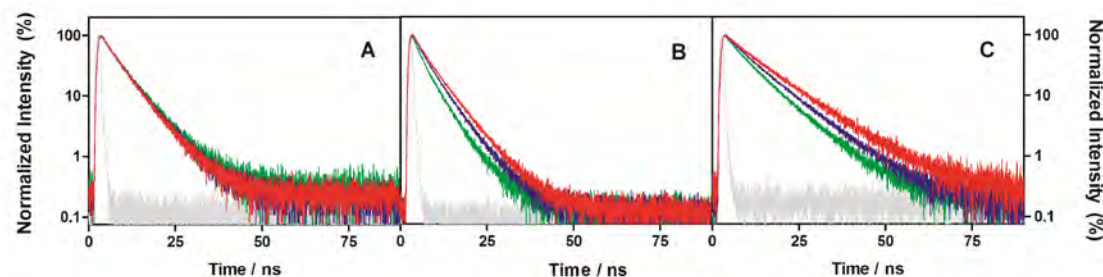
Figure 13. Time-resolved fluorescence at 660 nm in MeOH and IRF (grey) upon excitation at 405 nm, normalised to facilitate their comparison. A) **4e** at 5 μM (red), 0.5 μM (blue) and 0.05 μM (green). B) **1d** at 5 μM (red), 0.5 μM (blue) and 0.05 μM (green). C) **1c** at 5 μM (red), 0.5 μM (blue) and 0.05 μM (green).

On the other hand, porphyrin **1b** and porphycene **2a** are insoluble in water and therefore no fluorescence can be recorded in this solvent. Conjugation to the peptides (**1c, 1d** and **2c**, respectively) renders them water-soluble but the spectroscopic and photophysical properties change substantially relative to MeOH: the absorption spectra show broadening of the Soret band and loss of structure in the Q region (Figure 11F-H) and the fluorescence is dramatically quenched. In addition, the fluorescence spectra of **1c-1d** are slightly red shifted (Figure 12G,H), and the decays are biexponential (Table 4) and show a clear concentration trend (Figure 13B,C).

E. coli suspensions. The conjugate **4e** shows in cell suspensions the same absorption and fluorescence properties as in PBS (Figures 11I-12I and Table 4). On the other hand, there are evident changes for conjugates **1c** and **1d** relative to PBS, particularly in the absorption spectrum and in the fluorescence kinetics, which show a third decay component not present in PBS or in MeOH (Table 4). Finally, porphycene conjugate **2c** shows a very similar absorption spectrum in PBS and in *E. coli* suspensions (Figure 11J). However, while we could record no fluorescence in PBS, we were nevertheless able to observe extremely weak biexponential fluorescence decay in cell suspensions (Figures 12, and Table 4).

Singlet oxygen production and decay. All free and conjugated PSs were able to photosensitise the formation of $^1O_2$ in MeOH as evidenced by its phosphorescence at 1275 nm. The quantum Φ_Δ values were in the 0.6-0.7 range for the porphyrins and 0.1-0.3 for the porphycenes (Table 5). The kinetics of $^1O_2$ production matched the results of laser flash photolysis experiments for the triplet PS decay (data not

79

shown). Likewise, an excellent match was found between the observed lifetime of $^1O_2$ and literature values. In PBS, only porphyrins **4b** and **4e** retained their high ability to produce $^1O_2$. All other compounds experienced a decrease of the Φ_Δ value by 20-30-fold (porphyrins **1c** and **1d**) or even 100-fold (porphycene **2c**; Table 5). Inspection of the kinetics of $^1O_2$ reveals that production of $^1O_2$ by conjugate **4e** is as fast as by the free porphyrin **4b** (Table 5), yet for the conjugates **1c**, **1d** and **2c** it is one order of magnitude slower. On the other hand, the lifetime of $^1O_2$ for all conjugates in dPBS is shorter than the value expected in this solvent (65 μs),[60] which is actually observed only for the free porphyrin **4b**. When *E. coli* suspensions were studied, the $^1O_2$ signals showed essentially the same pattern as in PBS solutions (Table 5).

Table 5. Kinetics of singlet oxygen production (Φ_Δ) and decay (τ_Δ) of the peptide conjugates and model compounds in air-saturated MeOH, PBS and *E. coli* suspensions.

Compound	Φ_Δ		τ_Δ / μs		
	MeOH[a]	PBS[b]	MeOH	PBS[c]	*E. coli*[d]
1b	0.63	Ns[e]	9.8[f]	ns	-
1c	0.70	0.020	9.8	3.0 / 43[g]	2.3
1d	0.66	0.036	9.5	45[g]	-
2a	0.26[h]	ns	-	ns	-
2c	0.14	0.001	9.8	42[g]	-
4b	0.69	0.73	9.6	3.6 / 60[g]	3.6
4e	0.67	0.89	9.6	3.6 / 36[g]	3.6

[a] TMPyP as reference (Φ_Δ (MeOH) = 0.74).[46] [b] TPPS as reference (Φ_Δ (water) = 0.69).[46] [c] Literature value 3.5 μs in PBS and 65 μs in dPBS.[61] [d] In PBS. [e] Not soluble. [f] Literature value 10.4 μs.[61] [g] In dPBS. [h] In toluene.

DISCUSSION

In a p revious communication it has already been shown that the conjugate **1c** is endowed with antibacterial activity upon light activation.[57] In this work we have extended the investigations towards other porphyrin-apidaecin conjugates, containing either neutral or cationic groups in order to assess the effects of structural modifications. Porphycene, a structural isomer of porphyrin, was also included in the study for its larger absorption coefficients in the red part of the spectrum, where light can deeply penetrate in tissues (Scheme 6). Because positively-charged PSs are effective in PDT against Gram-negative bacteria without the addition of outer membrane-disrupting agents,[62] we hypothesised that a conjugate between apidaecin and a ca tionic porphyrin could further promote the uptake of the PS in Gram-negative bacteria, thereby reducing the minimum effective dose. Moreover, in order to establish whether the antimicrobial peptide is able to direct the PS against specific bacterial targets, we synthesised also a conjugate between porphyrin **1b** and a short cationic nonapeptide (GPRPPHPRL) corresponding to the C-terminal segment of apidaecin.

Although the mode of action of apidaecin has not been determined in detail, several evidences suggest that this peptide enters *E. coli* cells by a non-pore forming mechanism and, once inside the cell, it interacts with components of the protein synthesis machinery, impairing protein synthesis and folding. The full-length apidaecin sequence is very important and the C-terminal nonapeptide does not possess any antibacterial activity[63] nor is able to translocate a fluorescent cargo into bacterial cells.[64] Thus, most probably, the conjugate with this cationic peptide (**1d**) can effectively bind to the bacterial cell wall without being able to reach the cytosol.

Efficient PSs for PDT must have appropriate photophysical properties, such as an intense red-light absorption band and a high quantum yield of generation of both the long-lived excited triplet state and cytotoxic ROS, in particular $^1O_2$. To establish whether the peptide moiety negatively affects the PS photosensitising efficiency, the porphyrin-peptide conjugates were submitted to a detailed photophysical characterisation.[ii]

[ii] For the sake of a more complete discussion, correlation with phototoxicity results as well as with FACS and circular dichroism (CD) spectroscopy has been included even though they were conducted by our collaborators in the Biology and Chemistry departments of the University degli studi di Padova. Further data can be found in the published article *J.Med.Chem.* **2013**. Vol.56. pp 1052-1063

The fluorescence properties and the $^1O_2$ production ability of the peptide conjugates **1c-d** and **4e** in MeOH (Tables 4 and 5) are essentially identical to those of free PSs, demonstrating that the peptide moiety exerts no influence on the PS photosensitising efficiency in this solvent. Only in the case of porphycene **2a** changes can be observed in the absorption spectrum and a reduction by about 50% of the Φ_F value of the PS and in $^1O_2$ production after conjugation to the peptide, which may be ascribed to interactions between the peptide and the macrocyclic core.

The situation is different in aqueous environment where the photophysical data change considerably relative to MeOH for all conjugates and particularly for those containing a neutral PS. The decrease in Φ_F value, the concentration dependence of the fluorescence kinetics, and the slow kinetics of $^1O_2$ production in **1c-d** and **2c** reveal the presence of intermolecular interactions as observed also by CD spectroscopy (data not shown). Such interactions account also for the 20-fold lower production of $^1O_2$ in PBS relative to MeOH (Table 5). Nevertheless, following illumination (with blue light for **1c-d** and red light for **2c**) the conjugates resulted phototoxic against *E. coli* cells, inducing a decrease of survival of 3-4 $\log_{10}$ at 15 μM concentration (data not shown). On the other hand, the unconjugated PS **2a** was completely ineffective towards *E. coli* (data not shown), consistently with data previously reported for **1b**[57] and other neutral porphyrins, which are unable to diffuse through the highly organised outer membrane of Gram-negative bacteria.[65]

Peptide conjugates **1c-d** and **2c** associate efficiently to *E. coli* cells, as suggested by the observation that repetitive washing of bacteria treated with conjugates, before illumination, caused only a moderate reduction of phototoxicity (data not shown). In the case of **1c-d** this is also supported by the flow cytometry results (data not shown). Porphycene was not fluorescent enough for FACS studies but the detection of fluorescence by time-resolved techniques in the *E.coli* suspensions, but not in PBS (Table 4), is taken as proof for binding.

A deeper understanding of the type of binding/association of **1c-d** to *E. coli* cells was obtained by analysing the fluorescence decay kinetics: unlike PBS or MeOH, three decay components were observed in cell suspensions, which suggest multiple binding sites (Table 4). The match between two of the three observed lifetimes with those detected in PBS indicates that one binding site is located in an aqueous-like environment. Thus, the third decay component suggests that an additional binding site exists where the conjugates experience a less hydrophilic environment. However, the phototoxicity, the photophysical and

flow cytometry results for the apidaecin conjugate **1c** and its truncated analogue **1d** are so similar that it is difficult to propose a different localisation of these conjugates in *E. coli* cells. Most probably both conjugates can diffuse through the OM and localize in different environments, but since the C-terminal apidaecin fragment is unable to translocate a PS across the cytoplasmic membrane, we are led to conclude that the apidaecin conjugate is also not able to reach the bacterial targets of apidaecin in cytosol.

The conjugate between the cationic porphyrin **4e** and apidaecin possess a +6 net positive charge, well distributed along the whole molecule that is expected to discourage the aggregation phenomena observed in conjugates **1c** and **2c**. In confirmation of this, the far-UV CD spectrum of **4e** in water is very similar to that of the free peptide and no dichroic signal, indicative of porphyrin-porphyrin interactions, was detected in the Soret band region (Figure 11 A and B). Aggregation can also be ruled out by the lack of concentration effects on the decay kinetics (Figure 13). It can therefore be safely concluded that the major differences observed between **4b** and **4e** (Table 4) are due to interactions between apidaecin and the porphyrin within the conjugate.

Comparison of the fluorescence spectrum, quantum yield and kinetics for **4b** and **4e,** reveals that two populations of conjugates coexist, in which the porphyrin is either exposed to water or shielded from it by the peptide. This conclusion is consistent with the well-known solvent-polarity effects on the fluorescence of tetra-pyridinium porphyrins.[59] Nevertheless the production of $^1O_2$ was very high in PBS, comparable or even higher than that in MeOH (Table 5). In fact, the conjugate **4e** caused total photokilling of *E. coli* cells at a concentration (10 μM) at which **1c** induced a strong (4-$\log_{10}$) but incomplete reduction of cell survival. The cationic porphyrin **4b** proved to be even more potent than its apidaecin conjugate **4e**.

The $^1O_2$ lifetime data in Table 2, particularly in dPBS, indicate that apidaecin is able to quench $^1O_2$. Thus, because $^1O_2$ molecules are generated in the vicinity of apidaecin, some of them will be quenched by the peptide during their lifetime rather than by cell components. The washing of the cells before illumination, to remove the unbound or weakly associated PS, caused a tremendous reduction of photokilling of *E. coli* cells and under these conditions **4b** became the least efficient PS (data not shown). Flow cytometry measurements showed that only unwashed cells exhibited red fluorescence slightly above the background after incubation with these compounds (data not shown).

Thus, the results indicate that **4b** and **4e** associate very weakly to *E. coli* cells and the killing of unwashed cells is caused mainly by $^1O_2$ generated by the PS molecules not associated or loosely associated to bacteria. Several reports of PDT on Gram-negative bacteria have pointed out that if $^1O_2$ can be generated in sufficient quantities near to the bacterial OM, it will be able to diffuse into the cell to inflict damage to vital structure. Our photophysical data thus support this hypothesis.

CONCLUSIONS

Binding to an AMP offers the attractive prospect of enhancing both the water solubility of the PS and the efficiency of the PDT treatments through a synergistic effect. In this work we have compared a number of free and apidaecin-conjugated PSs differing in structure and charge. Our results confirm previous findings that the conjugation of *per se* ineffective highly hydrophobic PSs to a cationic peptide produces a photosensitising agent effective against Gram-negative bacteria. The apidaecin ability to penetrate Gram-negative bacteria is lost after conjugation to a bulky PS, but the amphiphilic character conferred by the peptide enforces the binding of the PS to the bacterial OM.

Apidaecin-PS conjugates appear most promising for treatment protocols requiring repetitive washing after sensitiser delivery, where the most active cationic PSs, such as **4b** and its apidaecin conjugate **4e**, are rapidly washed out. On the other hand apidaecin cannot improve the phototoxic activity of the cationic porphyrin, which is mainly determined by a very high yield of singlet oxygen production in the surroundings of the bacterial outer membrane.

Killing bacteria from the inside: genetically encoded $^1O_2$ production[iii]

AIM OF THE STUDY

In the present study we explore the use of TagRFP and miniSOG as genetically encoded PSs in aPDT not only as antimicrobial agents but also as "Trojan horses" that shed light on cell death mechanisms underlying bacterial photoinactivation treatments. Moreover, for miniSOG the $^1O_2$ generation mechanism has been analysed in further detail and the Φ_Δ value has been reassessed ($\Phi_\Delta = 0.03 \pm 0.01$) using two alternative and independent methods. We provide further insight into the photochemistry of miniSOG and we ascertain the reasons for the discrepancy in Φ_Δ values (reported value of $\Phi_\Delta = 0.47 \pm 0.01$). In addition, we find that cumulative irradiation of miniSOG increases its Φ_Δ value ca. 10-fold due to a photoinduced transformation of the protein
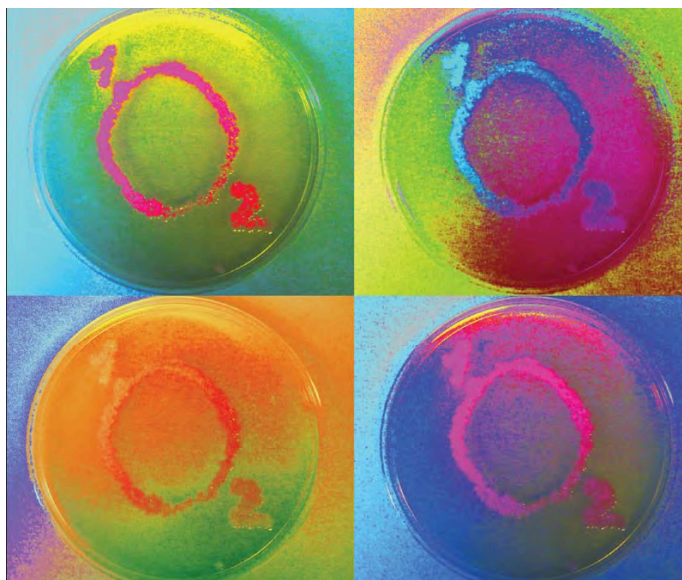
Graphical Abstract 3. TagRFP and miniSOG, fluorescent proteins capable of photosensitising the production of singlet oxygen have been expressed in *E. Coli*. Photophysics and mechanistic aspects of photoinduced cell death have been thoroughly studied and discussed.

RESULTS

Photodynamic inactivation studies.

When *E. coli* BL21 (DE3) cells expressing TagRFP in the cytosol were irradiated (535 ± 15 nm) no significant damage was observed for light doses below 750 J·cm^{-2}. However, a population reduction of *ca.* 4-log$_{10}$ in CFU/mL was achieved after a light dose of 3200 J·cm^{-2} in dPBS suspensions (*ca.* 2.5-log$_{10}$ CFU/mL reduction in normal PBS; Figure 14A). *E. coli* cells transformed with pET20b control plasmid, devoid of the TagRFP sequence, were tested under the same experimental conditions. As shown in Figure 1A, a reduction less than 0.5-log$_{10}$ CFU/mL was observed in all cases. In addition, non-irradiated bacteria expressing TagRFP did not significantly lose viability (data not shown). These negative controls confirm that damage is inflicted by photodynamic effect, *i.e.*, by the combination of light, oxygen and TagRFP acting as PS.

A similar experiment was performed with *E. coli* DH5α cells expressing miniSOG in the cytosol. A population reduction of over 1-log$_{10}$ units was achieved after light doses as mild as 2.5 J·cm^{-2} and up to 3.5-log$_{10}$ units was observed after 12 J·cm^{-2} treatment (Figure 14B). As above, an enhancement of photoinduced cell death was observed when the experiment was performed in dPBS. No damage was observed at maximum light dose without miniSOG. Moreover, no damage could be effected to bacteria expressing miniSOG in the absence of light (data not shown).
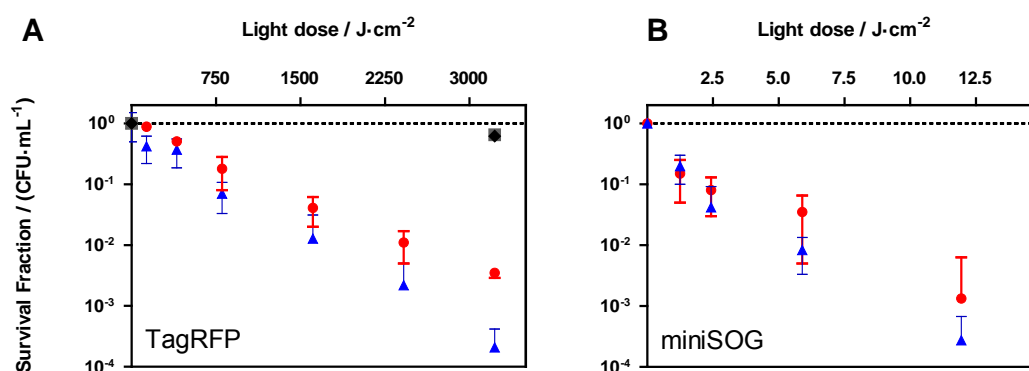
Figure 14. A) Photoinactivation of *E. coli* BL21 (DE3) expressing TagRFP in the cytosol upon irradiation with 532-nm laser light. Light-dose dependence on cell death transformed with pET20TagRFPhis in PBS (red circles) or dPBS (blue triangles). Control with pET20b in PBS (black diamonds) or dPBS (grey squares). B) Light-dose dependence (475± 15 nm LED irradiation) on bacterial cell death in *E. coli* DH5α expressing miniSOG in PBS (red circles) and dPBS (blue triangles).

Mechanistic studies.

In order to obtain further insight into the mechanism of cell death photosensitised by both FPs, several additional assays were performed. First, we focused on the cytoplasmic cell membrane. Damage to the bacterial IM can be tracked spectroscopically through absorbance measurements at 260 nm.[66,67] The results of this assay are shown in Figure 15 (red circles), where the 260 nm absorbance of the supernatants of irradiated bacteria suspensions is plotted as a function of the light dose. Data have been normalised against the values for non-irradiated samples. In both cases (TagRFP- and miniSOG-expressing bacteria) a clear growth in the 260 nm absorbance can be observed almost from the outset.

In a second series of assays, the integrity of the OM was assessed after PDI treatments. The fluorescent probe 1-N-phenylnaphthylamine (NPN) increases its fluorescence upon binding to cells with a damaged OM.[67,68] As shown in Figure 15 (blue circles), there is a markedly different behaviour between TagRFP- and miniSOG-expressing bacteria. For TagRFP, no increase in NPN fluorescence was observed relative to dark control suspensions. However, over two-fold increase in NPN fluorescence was observed in miniSOG-tagged bacteria. NPN fluorescence measurements in water and in lysed cells served as further controls (data not shown).
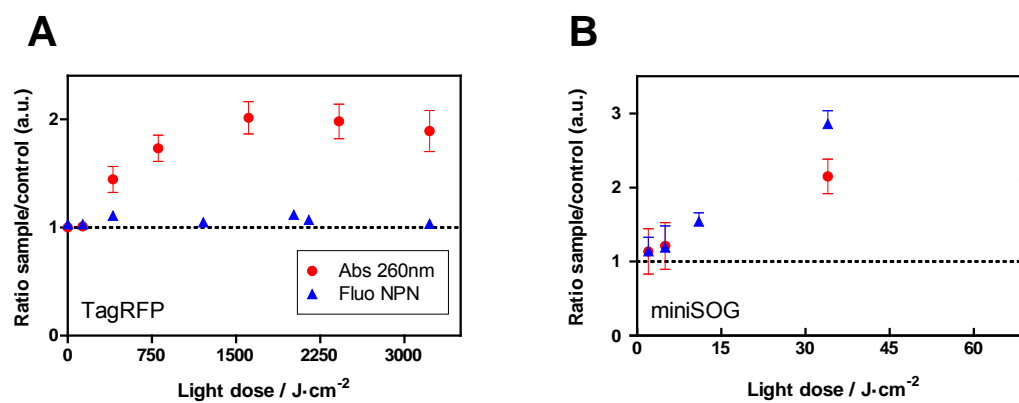
Figure 15. Bacterial cell envelope integrity assays after different aPDT light-dose treatments. Red circles: absorbance of supernatants at 260 nm. Blue triangles: fluorescence of NPN. Data are normalised to values measured for non-irradiated samples. A)TagRFP in *E. coli* BL21 (DE3), laser irradiation at 532 nm; B) miniSOG in *E. coli* DH5α. LED irradiation at 475 nm.

Finally, damage to genomic DNA from genomic *E. coli* cells was studied. DNA from irradiated cells was extracted by standard procedures and electrophoresis of the extracts was run in a 0.6 % agarose gel. As shown in Figure 16, no differences could be observed between samples irradiated at the maximum light dose and dark controls.
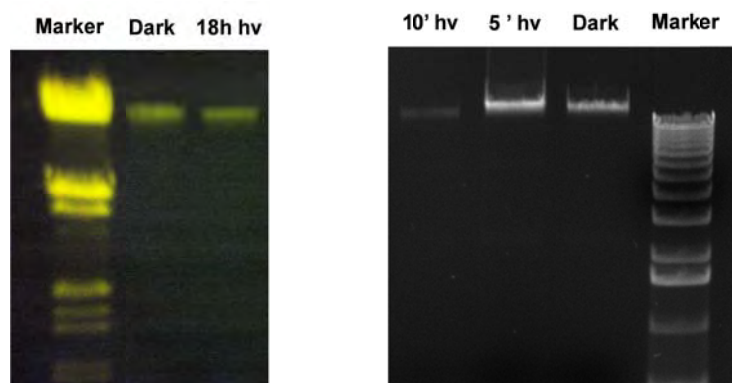
Figure 11. Agarose electrophoresis (0.6% agarose) of extracted genomic DNA samples. Left image) Line 1: Lambda DNA/EcoRI+HindIII Marker; Line 2: TagRFP DNA dark control; Line 3: TagRFP irradiated sample (2400 J·cm^{-2}). Right image) Line 1: miniSOG irradiated sample (12 J·cm^{-2}); Line 2: miniSOG irradiated sample (6 J·cm^{-2}); Line 3: miniSOG DNA dark control Line 4: Marker.

Unravelling $^1O_2$ generation by miniSOG.

Parallel to the PDI and mechanistic studies carried out with miniSOG expressed in *E. coli*, further characterisation was undergone with purified miniSOG since the photophysical properties of this flavoprotein had not been explored in much detail.

The absorption and fluorescence spectra of purified miniSOG in PBS pH 7.4 are slightly blue-shifted relative to those of FMN and show more vibronic structure (Figure 17), indicating tight binding of the chromophore to the protein. This is consistent with both the reported small dissociation constant of 170 ± 8 pM [40] and with the environmental restrictions to the chromophore motion resulting from its confinement and interactions within the active pocket of the protein. [69] The fluorescence of miniSOG shows distinct features from that of FMN, namely lifetime 5.1 ns vs. 4.3 ns; (Figure 17b, inset), and quantum yield $\Phi_F = 0.37$,[40] vs. $\Phi_F = 0.22$[70], respectively.
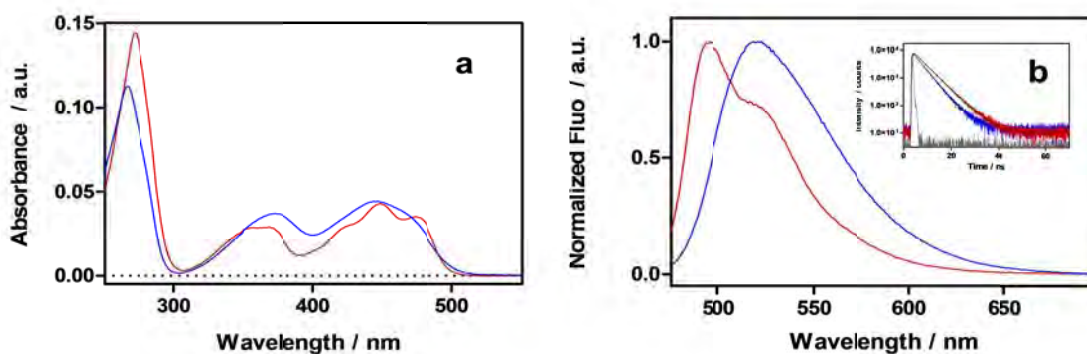
Figure 12. Basic photophysics of FMN (blue line) and miniSOG (red line) in solution. (a) Absorption spectra. (b) Normalised fluorescence spectra. $\lambda_{exc} = 450$ nm; Inset: Time-resolved fluorescence decay at 500 nm and IRF (grey) upon excitation at 375 nm.

The triplet state of miniSOG was investigated using nanosecond laser flash photolysis (for experimental details consult Chapter II). Upon excitation of oxygen-free solutions at 355 nm, a transient signal with lifetime of 35 μs was observed at 300 and at 700 nm (Figure 18a-b), with a decay rate that was accelerated by oxygen (3 μs in aerated solutions; Figure 18c). This transient signal is therefore ascribed to the triplet state of miniSOG. For comparison, the triplet lifetime of FMN was 42 μs and the transient absorbance was two-fold larger for an optically-matched solution (Figure 18a-b).
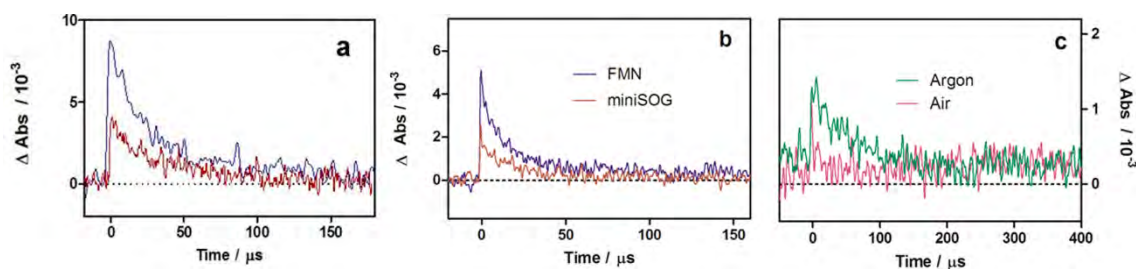
Figure 18. Transient absorption decays of FMN (blue line) and miniSOG (red line) observed at 300 nm (a) and 700 nm (b) for argon-saturated optically-matched solutions excited at 355 nm. Transient absorbance decays for argon-saturated solutions (green line) or aerated solutions (pink) of miniSOG observed at 300 nm and excited at 475 nm (c).

As the previously reported Φ_Δ value of miniSOG ($\Phi_\Delta = 0.47 \pm 0.05$ [40]) was determined by an indirect method based on the fluorescence photooxidation of 9,10-anthracene dipropionic acid (ADPA), we have now measured it by directly monitoring the phosphorescence of $^1O_2$ at 1275 nm in a time-resolved manner.[71] For these studies, miniSOG was dissolved at a concentration of 2.5 μM either in PBS or in a mixture of dPBS and PBS (9:1) since deuteration increases the $^1O_2$ lifetime and thus facilitates its detection.[72] Upon pulsed excitation at 355 nm, clear $^1O_2$ phosphorescence signals could be detected in both media (Figure 19). Comparison of the intensity of the miniSOG $^1O_2$ signal to that of optically-matched reference solutions of FMN and phenalenone-2-sulfonate (PNS; $\Phi_\Delta = 1$),[73] at the excitation wavelength of 355 nm and in the same solvent,[74] yielded $\Phi_\Delta = 0.03 \pm 0.01$ irrespective of solvent deuteration.
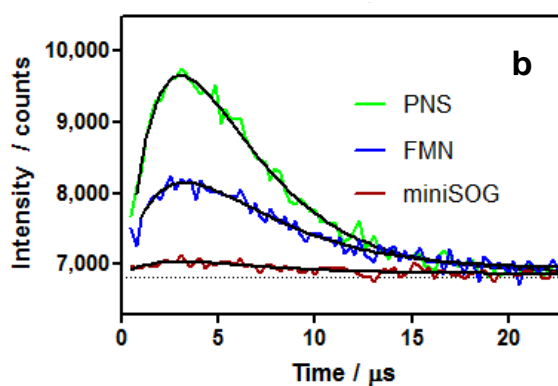
Figure 9. MiniSOG-photosensitised $^1O_2$ formation. $^1O_2$ phosphorescence signals for optically-matched solutions of the reference photosensitiser PNS (top, green line), FMN (middle, blue line) and miniSOG (bottom, red line) excited at 355 nm in PBS; the intensities are proportional to the Φ_Δ values.

To resolve the discrepancy between the reported and the measured values we used an alternative $^1O_2$ chemical trap. Uric acid (UA) was chosen as it reacts with $^1O_2$ through a different mechanism than ADPA.[75,76] Using UA we obtained $\Phi_\Delta = 0.03 \pm 0.01$ both in PBS and in dPBS upon excitation at 450 nm (Figure 20), fully in line with the value measured by time-resolved $^1O_2$ phosphorescence (Table 6).
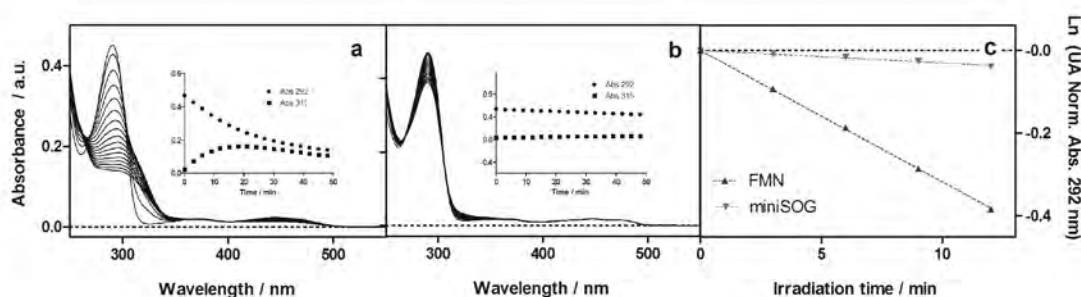
Figure 20. Singlet oxygen quantum yield determination using UA as probe. Spectral variations of optically-matched solutions of FMN (a) and miniSOG (b) in the presence of UA 50 μM upon excitation at 450 nm. Insets: time-dependent absorbance variations at 292 and 315 nm. (c) Comparison of UA bleaching rate at 292 nm in the presence of miniSOG (red) or FMN (blue).

Table 6. MiniSOG Φ_Δ values obtained by different techniques

Method	Φ_Δ	
	PBS	**dPBS**
Luminescence	0.03±0.01	0.03±0.01
Uric Acid	0.03±0.01	0.03±0.01
ADPA	0.42±0.02	0.18±0.02

91

Next series of experiments were carried out to ascertain the ADPA mismatching results. When oxygen-depleted solutions of miniSOG or FMN were blue-irradiated in the presence of increasing amounts of ADPA formation of new long-lived transient species could be readily observed, whose absorbance increased in an ADPA-concentration dependent manner (Figure 21a-b). In addition, we observed that, in the presence of ADPA, the fluorescence of miniSOG was partially quenched and the spectrum lost its vibronic structure (Figure 21c).
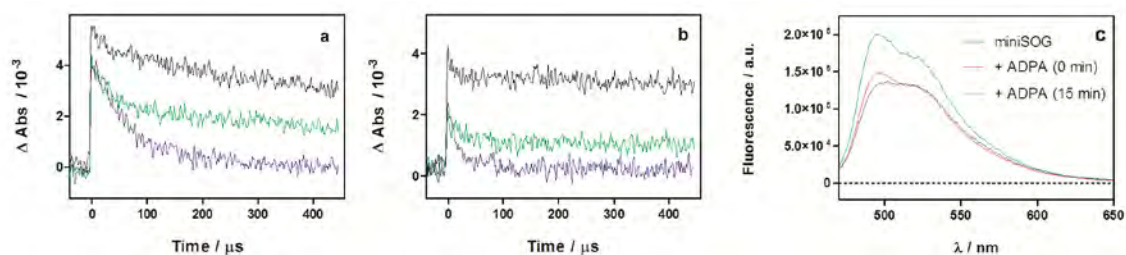
Figure 210. Transient absorption of (a) FMN and (b) miniSOG in deaerated PBS solutions in the presence of increasing amounts of ADPA (0 μM, blue line; 12 μM, green line; 60 μM, black line). λ_{exc} = 475 nm; λ_{obs} = 300 nm. (c) MiniSOG fluorescence time-dependent changes upon addition of 20 μM ADPA. λ_{exc} = 450 nm.

Finally, we have further assessed the involvement of electron-transfer processes in ADPA degradation by studying the photooxidation of ADPA by 4-diphenyl-6-(4′-methoxyphenyl)pyrylium tetrafluoroborate, which acts as an electron acceptor and does not generate $^1O_2$.[77] Figure 22 unequivocally shows that ADPA fluorescence gradually disappears upon irradiation of this type I PS.
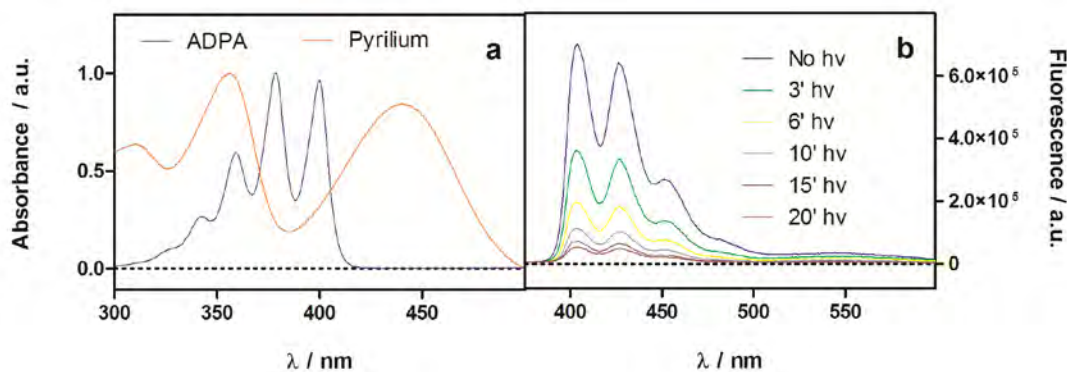
Figure 22. (a) Absorption spectra of ADPA (blue) and 2,4-diphenyl-6-(4′-methoxyphenyl)pyrylium tetrafluoroborate (Pyrilium; orange). (b) ADPA fluorescence photobleaching upon blue light irradiation in the presence of Pyrilium. λ_{exc} = 355 nm.

The results above led us to the necessity of performing a series of experiments focused on studying the effect of the protein environment on miniSOG's $^1O_2$ photosensitisation efficiency. First, miniSOG was denatured in a 6 M solution of guanidinium hydrochloride (Gdn HCl)[78] (Figure 23a-b). The $^1O_2$

photosensitisation efficiency increased over 10-fold upon protein denaturation (Figure 23c), coming close to the value for free FMN.
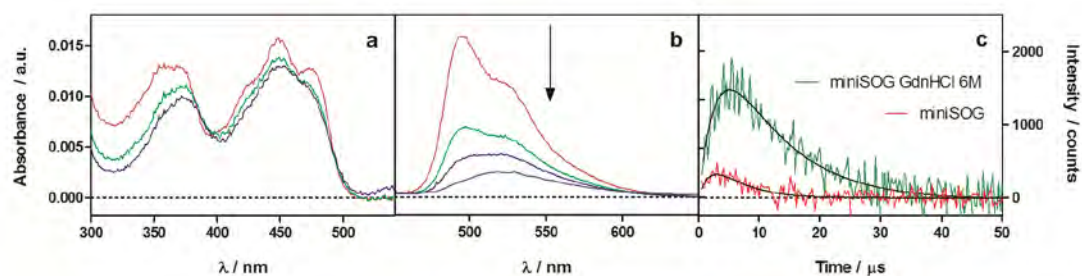
Figure 11. Absorption (a) and fluorescence (b) spectral changes of 2.5 µM miniSOG in Gdn HCl 6 M PBS over time. λ_{exc} = 355 nm. The initial resolved vibronic structure of miniSOG is progressively lost as the protein denatures and FMN is released. Note that, unlike other flavoproteins, denaturation results in loss of fluorescence as free FMN has a lower fluorescence quantum yield than miniSOG. (c) Time-resolved near IR phosphorescence of $^1O_2$ photosensitised by folded (red line) or denatured (green line) miniSOG in PBS.

As far as miniSOG contains a l arge number of aminoacids that are effective $^1O_2$ quenchers, measurements of $^1O_2$ upon cumulative irradiation of miniSOG were carried out. We were rewarded to observe that the amplitude of the $^1O_2$ signal, and therefore the Φ_Δ value, increased *ca.* 10-fold after irradiation (taking into account the small absorbance decrease upon irradiation) in a light-dose dependent manner (Figure 24c). Absorption and fluorescence measurements rule out any contribution of protein denaturation to this effect (Figure 24a-b).
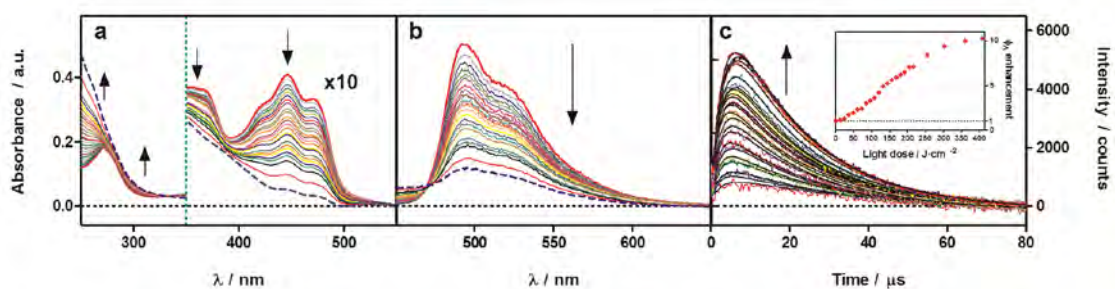
Figure 12. Absorption (a) and fluorescence (b) changes of 2.5 µM tag-less miniSOG in dPBS upon cumulative irradiation at λ_{exc} = 355 nm. Fluorescence was probed at λ_{exc} = 400 nm. c) Effect of cumulative irradiation of miniSOG on its $^1O_2$ photosensitisation ability in dPBS. λ_{exc} = 355 nm; λ_{obs} = 1275 nm. Inset: Φ_Δ enhancement.

In contrast, photolysis of free FMN leads to a decrease in the $^1O_2$ phosphorescence signal (Figure 25). As a final remark, removal of the His-tag did not change the Φ_Δ value (data not shown).
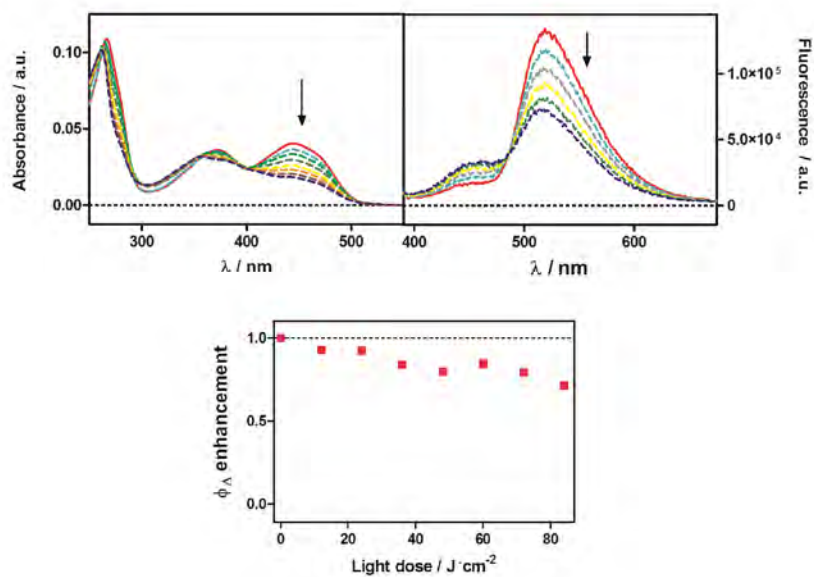
Figure 13. Absorption (a) and fluorescence (b) changes of FMN in dPBS upon cumulative irradiation at λ_{exc} = 355 nm. Fluorescence was acquired at λ_{exc} = 355 nm. (c) Relative enhancement of Φ_Δ values taking into account absorbance decrease.

DISCUSSION

Photoinactivation studies.

We report an approach to the issue of PS location in aPDT mechanistic studies by using two genetically-encoded $^1O_2$ PSs that have been expressed in the cytoplasm of two *E. coli* strains. It is known that some green and red FP variants are able to photosensitise $^1O_2$.[32,34,36] In our first approach, we have chosen TagRFP as a PS because, unlike other FPs such as KillerRed,[28,30,31] it is able to photosensitise the production of $^1O_2$ but not of other ROS,[36] and is therefore uniquely suited to ascertain the role of $^1O_2$ in bacterial cell death. Our observation of *ca*.1-$\log_{10}$ population reduction difference between PBS- and dPBS-suspended cells is consistent with a $^1O_2$ lifetime of 3.5 μs in H_2O and 65 μs in D_2O.[72] Such enhancement of oxidative damage upon deuteration has long been used as a mechanistic test for the involvement of $^1O_2$. This also agrees with our previous report that TagRFP is a pure $^1O_2$ PS[36] and constitutes the first report showing that cytoplasmic location of a $^1O_2$ PS is sufficient to induce bacterial cell death following light irradiation. Regarding the light dose used, it is orders of magnitude higher than that used in typical aPDT treatments[25] but comparable to that in CALI assays[79] and –again- in line with the low quantum yield of $^1O_2$ generation by TagRFP ($\Phi_\Delta = 0.004 \pm 0.001$).[36]

As for miniSOG, similar correlation was observed since deuterotopic effects could be observed in the PDI treatments. However, the light dose required was orders of magnitude lower than that used in previous PDI treatments with TagRFP, but comparable to the those of KillerRed.[80]

Mechanistic studies

When bacterial IM is compromised, leaching-out of low molecular-weight species and DNA and RNA fragments occurs, which are also able to permeate the external membrane. Release of such intracellular components can be, thus, conveniently monitored by spectroscopic means, and the onset of UV absorption at 260 nm in the supernatant is taken as a strong indication of membrane damage. According to the results, photodynamic damage to the inner cell membrane occurs in both cell types.

It is well known that Gram-negative bacteria are markedly more resistant to PDI treatments than Gram-positive *spp* due to the highly organised structure of its cell envelope.[81] Specifically, many studies have shown that the presence of an additional OM prevents many PSs from reaching and/or binding to the IM, resulting in lowered photosensitisation efficiency.[81] The OM is, thus, a typical target in Gram-

negative bacteria.[82] According to the data presented in Figure 2B, it looks clear that the more efficient photosensitising properties of miniSOG result in a significant amount of $^1O_2$ being able to reach the OM and inflict damage, which is not the case for TagRFP-tagged bacterial experiments.

Finally experiments regarding DNA damage indicate that FP-induced photodamage to genomic DNA does not occur to any measurable extent. Our results are in line with those of previous studies where it was concluded that DNA damage is not the primary cause of bacterial cell photoinactivation.[25,83] However, we cannot exclude that a lethal effect may be produced by localised DNA damage that could not be detected in our assay.[84]

Overall, TagRFP photodamage seems to occur mainly in the cytoplasm and IM. No damage of the OM or of genomic DNA could be observed. These observations are markedly different to those reported for an external PS.[67] As for miniSOG, its enhanced ability to sensitise $^1O_2$ makes it inflict more severe damage that also affects the OM viability. Thus, not only the amount but also the site where $^1O_2$ is primarily generated proves crucial for inflicting different types of cell damage. It is relevant to recall that the latest estimates of the radial diffusion distance of $^1O_2$, which represents its sphere of activity, are about 155 nm and 550 nm in H_2O and D_2O, respectively.[72] These distances are below the typical size of a bacterial cell.

Unravelling $^1O_2$ generation by miniSOG

Basic photophysical properties of miniSOG are markedly different to those of FMN. The characteristic vibronic absorption and fluorescence spectra of miniSOG indicate tight binding of the chromophore to the protein. This is consistent both with the reported small dissociation constant of 170 ± 8 pM[40] and with the environmental restrictions to the chromophore motion resulting from its confinement and interactions within the active pocket of the protein.[69]

The most novel aspect of miniSOG is its stronger photosensitisation ability compared to FPs from the green fluorescen protein (GFP) family.[40] We have herein confirmed this superior ability by comparing the photoinduced cell death of *E. coli* bacteria expressing either miniSOG or TagRFP. Consistent with our expectations, miniSOG clearly outperformed TagRFP (*vide supra*). The higher photosensitisation ability of miniSOG was initially explained by its apparently higher Φ_Δ value (0.47 ± 0.05[40]) very close to that of free FMN in solution ($\Phi_\Delta = 0.51$).[85] However, when we performed direct measurements of $^1O_2$ phosphorescence or indirect Φ_Δ quantification with UA we got a value ~ 15-fold smaller ($\Phi_\Delta = 0.03 \pm$

0.01) -irrespective of solvent deuteration- that, *per se*, was unable to explain the behaviour overall and, thus, further investigations were required.

The reported Φ_Δ value for miniSOG was arrived at using ADPA as $^1O_2$ probe.[40] Specifically, Φ_Δ was determined by comparing the rates of ADPA photooxidation sensitised by miniSOG and by the reference FMN, the loss of ADPA being monitored by fluorescence. It was found that the rates of ADPA photooxidation were very similar, a result that we have reproduced in our laboratory. Surprisingly, when we repeated the experiment in dPBS the ratio of photooxidation rates decreased to *ca.* 1/3, corresponding to an apparent Φ_Δ value of ~ 0.18. This lower value is totally unexpected if ADPA photooxidation occurs exclusively through a $^1O_2$ reaction (as the longer $^1O_2$ lifetime in dPBS would increase the rate of ADPA photooxidation)[86] and suggests that a more complex mechanism is involved. In view of the results above, we were led to conclude that processes other than reaction with $^1O_2$ contributed significantly to ADPA photooxidation by miniSOG. Photooxidation reactions may occur through two mechanisms: type-I, where the PS reacts directly with the substrate, or type-II, where $^1O_2$ is formed instead.[87] Indeed, it has been reported that, in addition to their reaction with $^1O_2$, anthracene derivatives can be oxidised by electron-transfer processes.[88]

Support of the previous statements was achieved thanks to the series of experiments performed. First, flash photolysis experiments revealed the formation of new species that we assigned to semioxidised forms of ADPA, in line with previous reports for other anthracene derivatives.[89] Next, miniSOG alteration in the presence of ADPA (without irradiation) strongly suggests that ADPA binds to miniSOG as observed for other anthracene derivatives that bind to proteins through electrostatic and hydrophobic interactions thereby interfering in some cases with protein function.[90,91] Finally, we could support that direct photoinduced electron transfer reactions can contribute to ADPA photooxidation with the degradation of ADPA in the presence of a purely electron-transfer PS such as 4-diphenyl-6-(4′-methoxyphenyl)pyrylium tetrafluoroborate. It is well documented that flavins are able to undergo electron transfer reactions with suitable electron donors.[92,93] The observations above indicate that photooxidation of ADPA results from both $^1O_2$ and electron-transfer processes, the latter facilitated by the binding of ADPA to the protein. Thus, in addition to generating $^1O_2$, miniSOG is capable of photooxidising substrates by type-I mechanisms as well, which should be taken into account by researchers using miniSOG as a genetically-encodable $^1O_2$ source.

97

Our observations upon miniSOG denaturation point to a strong effect of the protein environment on $^1O_2$ photosensitisation efficiency. The high increase of the Φ_Δ value upon denaturation highlights the effect of protein residues, which could either modulate the excited states of FMN in the folded protein and therefore affect the quantum yield of $^1O_2$ production, or quench a fraction of $^1O_2$ molecules before they can diffuse into the bulk medium.

As to the first possibility, it is well established that the photosensitised production of $^1O_2$ occurs in three steps, each with its own efficiency: first the PS's triplet state must be populated by ISC from the originally photoexcited singlet excited state; second, the triplet-state molecules must be trapped by oxygen before they decay; finally, ET from the triplet sensitiser to oxygen must take place.[74] Regarding the first process, it has been reported that the protein environment can modulate ISC in flavoproteins by electrostatic effects.[69] Consistent with this, we do observe smaller triplet transient absorbance signals for miniSOG than for free FMN (data not shown) and a higher fluorescence quantum yield. ISC in miniSOG would therefore be less efficient than in free FMN, although this effect alone fails to account for the 15-fold decrease in Φ_Δ. The triplet lifetime data likewise indicate that oxygen trapping of miniSOG's triplet state is almost as efficient as for FMN in water, which also rules out the second process as an important factor. Finally it must be recalled that oxygen quenching of triplet excited states can occur by either ET, producing $^1O_2$, or electron transfer, yielding the superoxide radical anion. The lack of any evidence for radical formation in transient absorption experiments suggests that the electron transfer pathway is of minor importance.

Our data, thus, suggest that $^1O_2$ production by the flavin inside the protein is probably not much different from that in the bulk aqueous solution. Even though FMN is located at about 10-15 Å of the protein surface, the triplet lifetime of miniSOG, similar to that of FMN, indicates that the chromophore is accessible to oxygen. Therefore, the most relevant cause for the difference in measured Φ_Δ may be attributed to a substantial fraction of the nascent $^1O_2$ molecules being quenched on their way off the protein.[94,95] This notion is supported by the fact that miniSOG contains a large number of aminoacids that are effective $^1O_2$ quenchers (Figure 25): tryptophan (Trp; x1), histidine (His; x1), tyrosine (Tyr; x3), methionine (Met; x2) (Figure 3a), plus the His-tag (x6) used for purification.
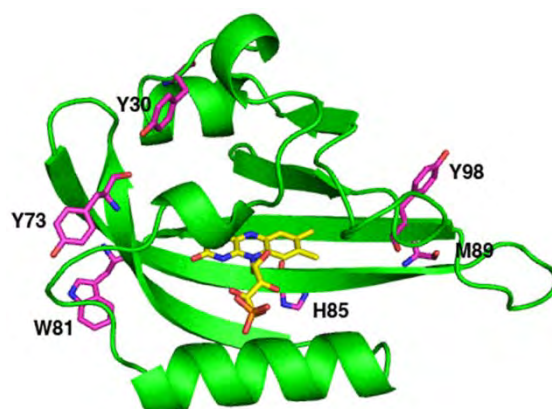
Figure 14. MiniSOG's molecular model based on the structure of iLOV protein (PBD ID: 4eet), built using the Swiss-model server (http://swissmodel.expasy.org/). The backbone of miniSOG is shown as a green ribbon, FMN as orange sticks, and the aminoacids that may quench $^1O_2$ as magenta sticks.

As for the increase of the Φ_Δ value upon cumulative irradiation, experiments both for miniSOG and free FMN seem to indicate progressive photoinactivation of the aminoacids responsible for $^1O_2$ quenching, discarding the build-up of FMN photoproducts of higher Φ_Δ value. Respect to the fact that the miniSOG mutant lacking the His-tag showed the same Φ_Δ than miniSOG itself was not totally unexpected since this tag is far away from the site of $^1O_2$ production. This is relevant for drawing comparisons between miniSOG's photochemistry as a purified protein in solution with that as a fusion partner in a cell. It is worth to note that redox-active aminoacids (Trp, Tyr) that are involved in electron transfer reactions in some flavoproteins are also present in miniSOG's sequence.[96] However, these residues are not in the chromophore vicinity (Figure 14), and are not likely to participate in direct electron transfer reactions with FMN (see ref [97] and references therein). For example, replacement of Trp81 by phenylalanine (Phe) does not improve $^1O_2$ photosensitisation ($\Phi_\Delta = 0.01$), which seems to rule out the direct participation of this residue in electron transfer reactions.

CONCLUSIONS

Purely endogenous $^1O_2$ produced by genetically-encoded photosensitising proteins expressed in the bacterial cytosol is able to induce bacterial cell death. Photodamage seems to occur mainly in the bacterial membrane, the extent of which correlates with the photosensitising efficiency of the protein. Both TagRFP and miniSOG can induce damage in the IM, but only miniSOG in the OM. No damage of genomic DNA could be observed. Our observations are markedly different to those reported for an external photosensitiser.[67] Thus, the site where $^1O_2$ is primarily generated proves crucial for inflicting different types of cell damage.

Moreover, we have unravelled the photochemical $^1O_2$ generation of the fluorescent protein miniSOG. Our most important result is the revision of the Φ_Δ value, which we have determined to be 0.03 ± 0.01, *ca.* 15-fold lower than reported previously.[40] We have accounted for potential reasons for the discrepancy, namely the contribution of electron transfer processes to ADPA oxidation, and the increase of Φ_Δ upon cumulative irradiation. Regarding the first point, a contribution of electron-transfer processes to the photodynamic activity of miniSOG in biological media should not be excluded *a priori*. As to the second one, increase of Φ_Δ upon irradiation may prove advantageous for EM imaging and other potential uses of miniSOG. A recent communication in which miniSOG is shown to outperform commercial fluorescent tag ReAsH (for resorufin arsenical hairpin) in EM experiments suggests that this may indeed be the case.[38] As a final remark, it is worth pointing out that the screening method used to evolve miniSOG was based on evaluating the photobleaching of a fused fluorescent protein. Photobleaching can be due not only to $^1O_2$, but also to other ROS and radical reactions. Thus, there is still scope to improve the value of Φ_Δ by screening with another, more specific method that selects for singlet oxygen-generating mutants. Detection of $^1O_2$ phosphorescence at 1275 nm as described within this work is thus highly suited to develop new and better miniSOG variants.

This work supports the potential of genetically-encoded strategies in mechanistic studies of aPDT, and using appropriate gene transfer methods could be extended to therapeutic strategies.

SPECIFIC EXPERIMENTAL SECTION

Chemical Compounds: UA, PN, Gdn·HCl and NPN were purchased from Sigma; FMN was purchased from Chemochroma and ADPA from Chemodex. All these reagents were used as received. PNS was resynthesised according to the published method in reference.[73]

Cell membrane integrity assessment protocol: After photodynamic treatments, samples were centrifuged (13000 rpm, 10 min) and the supernatant was monitored by UV-vis spectroscopy in order to measure the absorbance values at 260 nm, which indicates leakage of small cellular components due to inner membrane damage.[16] Supernatant of non-irradiated cells was also measured as control and normalisation factor. To test the integrity of the outer membrane, the pellet was resuspended and NPN was added to a final concentration of 15 μM.[14, 17] Fluorescence spectra were readily measured after NPN addition upon excitation at 350 nm. Cell lysate (3 x 1 minute sonication) was used as a positive control (data not shown).

DNA purification and electrophoresis: Genomic DNA was extracted immediately after photodynamic treatments by means of a Wizard Genomic DNA Purification Kit (Promega). DNA samples were gently mixed with 3 μL of Loading Buffer 6x and analysed by agarose gel electrophoresis (0.6 % agarose in TBE buffer). The nucleic acid stain Sybr Green (1 mg/mL; Invitrogen) was incorporated during preparation of agarose gel. The Lamda DNA/EcoRI + Hind III Marker (BioRad) was used as molecular weight marker (0.5 mg/mL) with DNA fragments between 564 and 21,226 bp.

Protein protocols: miniSOG expression and purification were performed by our collaborators Sara H. Mejías and Aitziber L. Cortajarena following reference [98] with minor modifications. For denaturation, miniSOG was adjusted to a concentration of 2.5 μM in a 6 M solution of Gdn HCl (PBS or dPBS) according to a well-established protocol.[78] The solution was stirred over time and, periodically, absorption and fluorescence spectra were acquired in order to assess the degree of denaturation.

Φ_Δ using UA as a $^1O_2$ probe: In the presence of $^1O_2$, UA forms an intermediate that undergoes an additional degradation step to allantoin.[99] As a result, absorbance at 292 nm decays with biexponential kinetics. The degradation of the intermediate is known to be oxygen-independent, so only the first decay (k_1) reflects the reaction with singlet oxygen. The reaction can also be monitored at 315 nm, with the difference that the intermediate formation (k_1) appears as an increase of absorbance.[76]

101

References

1. González-Zorn, B.; Escudero, J. A. Ecology of antimicrobial resistance: humans, animals, food and environment. *Int Microbiol* **2012**, *15*, 101-109.

2. Kallifidas, D.; Kang, H. S.; Brady, S. F. Tetarimycin A, an MRSA-active antibiotic identified through induced expression of environmental DNA gene clusters. *J. Am. Chem. Soc.* **2012**, *134*, 19552-19555.

3. Infectious Diseases Society of America (IDSA) Combating antimicrobial resistance: Policy recommendations to save lives. *Clin. Infect. Dis.* **2011**, *52*, S397-S428.

4. Peters, B. M.; Jabra-Rizk, M. A.; O'May, G. A.; Costerton, J. W.; Shirtliff, M. E. Polymicrobial interactions: impact on pathogenesis and human disease. *Clin. Microbiol. Rev.* **2012**, *25*, 193-213.

5. Quigley, E. M. M. Prebiotics and probiotics; modifying and mining the microbiota. *Pharmacol. Res.* **2010**, *61*, 213-218.

6. Quigley, E. M. Gut microbiota and the role of probiotics in therapy. *Current Opinion in Pharmacology* **2011**, *11*, 593-603.

7. Sang, Y.; Blecha, F. Antimicrobial peptides and bacteriocins: alternatives to traditional antibiotics. *Animal Health Research Reviews* **2008**, *9*, 227-235.

8. Riley, M. A.; Robinson, S. M.; Roy, C. M.; Dennis, M.; Liu, V.; Dorit, R. L. Resistance is futile: the bacteriocin model for addressing the antibiotic resistance challenge. *Biochem. Soc. Trans.* **2012**, *40*, 1438-1442.

9. Cotter, P. D.; Ross, R. P.; Hill, C. Bacteriocins - a viable alternative to antibiotics? *Nat. Rev. Microbiol.* **2013**, *11*, 95-105.

10. Kutter, E.; De Vos, D.; Gvasalia, G.; Alavidze, Z.; Gogokhia, L.; Kuhl, S.; Abedon, S. T. Phage Therapy in Clinical Practice: Treatment of Human Infections. *Curr. Pharm. Biotechnol.* **2010**, *11*, 69-86.

11. Hamblin, M. R.; Hasan, T. Photodynamic therapy: a new antimicrobial approach to infectious disease? *Photochemical & Photobiological Sciences* **2004**, *3*, 436-450.

12. St Denis, T. G.; Dai, T.; Izikson, L.; Astrakas, C.; Anderson, R. R.; Hamblin, M. R.; Tegos, G. P. All you need is light: antimicrobial photoinactivation as an evolving and emerging discovery strategy against infectious disease. *Virulence* **2011**, *2*, 509-520.

13. Garland, M. J.; Cassidy, C. M.; Woolfson, D.; Donnelly, R. F. Designing photosensitizers for photodynamic therapy: strategies, challenges and promising developments. *Future Med Chem* **2009**, *1*, 667-691.

14. Malik, Z.; Ladan, H.; Nitzan, Y. Photodynamic Inactivation of Gram-Negative Bacteria - Problems and Possible Solutions. *Journal of Photochemistry and Photobiology B-Biology* **1992**, *14*, 262-266.

15. Bertoloni, G.; Rossi, F.; Valduga, G.; Jori, G.; Lier, J. E. V. Photosensitizing activity of water- and lipid-soluble phthalocyanines on Escherichia coli. *FEMS Microbiol. Lett.* **1990**, *71*, 149-156.

16. Nitzan, Y.; Gutterman, M.; Malik, Z.; Ehrenberg, B. Inactivation of Gram-Negative Bacteria by Photosensitized Porphyrins. *Photochem. Photobiol.* **1992**, *55*, 89-96.

17. Wilson, M. Photolysis of Oral Bacteria and its Potential Use in the Treatment of Caries and Periodontal Disease. *J. Appl. Bacteriol.* **1993**, *75*, 299-306.

18. Merchat, M.; Bertolini, G.; Giacomini, P.; Villanueva, A.; Jori, G. Meso-substituted cationic porphyrins as efficient photosensitizers of gram-positive and gram-negative bacteria. *J Photochem Photobiol B.* **1996**, *32*, 153-157.

19. Hancock, R. E. W. The end of an era? *Nature Reviews Drug Discovery* **2007**, *6*, 28-28.

20. Jenssen, H.; Hamill, P.; Hancock, R. E. W. Peptide Antimicrobial Agents. *Clinical Microbiology Reviews* **2006**, *19*, 491-511.

21. Li, W. F.; Ma, G. X.; Zhou, X. X. Apidaecin-type peptides: biodiversity, structure-function relationships and mode of action. *Peptides* **2006**, *27*, 2350-2359.

22. Casteels, P.; Romagnolo, J.; Castle, M.; Casteels-Josson, K.; Erdjument-Bromage, H.; Tempst, P. Biodiversity of apidaecin-type peptide antibiotics. Prospects of manipulating the antibacterial spectrum and combating acquired resistance. *J. Biol. Chem.* **1994**, *269*, 26107-26115.

23. Taguchi, S.; Mita, K.; Ichinohe, K.; Hashimoto, S. Targeted Engineering of the Antibacterial Peptide Apidaecin, Based on an In Vivo Monitoring Assay System. *Applied and Environmental Microbiology* **2009**, *75*, 1460-1464.

24. Gobbo, M.; Biondi, L.; Filira, F.; Gennaro, R.; Benincasa, M.; Scolaro, B.; Rocchi, R. Antimicrobial peptides: Synthesis and antibacterial activity of linear and cyclic drosocin and apidaecin 1b analogues. *J. Med. Chem.* **2002**, *45*, 4494-4504.

25. Jori, G.; Coppellotti, O. Inactivation of pathogenic microorganisms by photodynamic techniques: Mechanistic aspects and perspective applications. *Anti-Infective Agents in Medicinal Chemistry* **2007**, *6*, 119-131.

26. Pudziuvyte, B.; Bakiene, E.; Bonnett, R.; Shatunov, P. A.; Magaraggia, M.; Jori, G. Alterations of Escherichia coli envelope as a consequence of photosensitization with tetrakis(N-ethylpyridinium-4-yl)porphyrin tetratosylate. *Photochem. Photobiol. Sci.* **2011**, *10*, 1046-1055.

27. Ragàs, X.; Agut, M.; Nonell, S. Singlet oxygen in Escherichia coli: New insights for antimicrobial photodynamic therapy. *Free Radic. Biol. Med.* **2010**, *49*, 770-776.

28. Bulina, M. E.; Chudakov, D. M.; Britanova, O. V.; Yanushevich, Y. G.; Staroverov, D. B.; Chepurnykh, T. V.; Merzlyak, E. M.; Shkrob, M. A.; Lukyanov, S.; Lukyanov, K. A. A genetically encoded photosensitizer. *Nat. Biotechnol.* **2006**, *24*, 95-99.

29. Waldeck, W.; Mueller, G.; Wiessler, M.; Toth, K.; Braun, K. Positioning effects of KillerRed inside of cells correlate with DNA strand breaks after activation with visible light. *Int. J. Med. Sci.* **2011**, *8*, 97-105.

30. Serebrovskaya, E. O.; Edelweiss, E. F.; Stremovskiy, O. A.; Lukyanov, K. A.; Chudakov, D. M.; Deyev, S. M. Targeting cancer cells by using an antireceptor antibody-photosensitizer fusion protein. *Proc. Natl. Acad. Sci. U. S. A.* **2009**, *106*, 9221-9225.

31. Vegh, R. B.; Solntsev, K. M.; Kuimova, M. K.; Cho, S.; Liang, Y.; Loo, B. L.; Tolbert, L. M.; Bommarius, A. S. Reactive oxygen species in photochemistry of the red fluorescent protein "Killer Red". *Chem. Commun.* **2011**, *47*, 4887-4889.

32. Jiménez-Banzo, A.; Nonell, S.; Hofkens, J.; Flors, C. Singlet oxygen photosensitization by EGFP and its chromophore HBDI. *Biophys. J.* **2008**, *94*, 168-172.

33. Ragàs, X.; Jiménez-Banzo, A.; Sanchez-Garcia, D.; Batllori, X.; Nonell, S. Singlet oxygen photosensitisation by the fluorescent probe Singlet Oxygen Sensor Green (R). *Chem. Commun.* **2009**, *20*, 2920-2922.

34. Jiménez-Banzo, A.; Ragàs, X.; Abbruzzetti, S.; Viappiani, C.; Campanini, B.; Flors, C.; Nonell, S. Singlet oxygen photosensitisation by GFP mutants: oxygen accessibility to the chromophore. *Photochem. Photobiol. Sci.* **2010**, *9*, 1336-1341.

35. Merzlyak, E. M.; Goedhart, J.; Shcherbo, D.; Bulina, M. E.; Shcheglov, A. S.; Fradkov, A. F.; Gaintzeva, A.; Lukyanov, K. A.; Lukyanov, S.; Gadella, T. W.; Chudakov, D. M. Bright monomeric red fluorescent protein with an extended fluorescence lifetime. *Nat. Methods* **2007**, *4*, 555-557.

36. Ragàs, X.; Cooper, L. P.; White, J. H.; Nonell, S.; Flors, C. Quantification of photosensitized singlet oxygen production by a fluorescent protein. *Chemphyschem* **2011**, *12*, 161-165.

37. Drepper, T.; Eggert, T.; Circolone, F.; Heck, A.; Krauss, U.; Guterl, J. K.; Wendorff, M.; Losi, A.; Gartner, W.; Jaeger, K. E. Reporter proteins for in vivo fluorescence without oxygen. *Nat. Biotechnol.* **2007**, *25*, 443-445.

38. Boassa, D.; Berlanga, M. L.; Yang, M. A.; Terada, M.; Hu, J.; Bushong, E. A.; Hwang, M.; Masliah, E.; George, J. M.; Ellisman, M. H. Mapping the subcellular distribution of alpha-synuclein in neurons using genetically encoded probes for correlated light and electron microscopy: implications for Parkinson's disease pathogenesis. *J. Neurosci.* **2013***, 33*, 2605-2615.

39. Qi, Y. B.; Garren, E. J.; Shu, X.; Tsien, R. Y.; Jin, Y. Photo-inducible cell ablation in Caenorhabditis elegans using the genetically encoded singlet oxygen generating protein miniSOG. *Proc. Natl. Acad. Sci. U. S. A.* **2012***, 109*, 7499-7504.

40. Shu, X.; Lev-Ram, V.; Deerinck, T. J.; Qi, Y.; Ramko, E. B.; Davidson, M. W.; Jin, Y.; Ellisman, M. H.; Tsien, R. Y. A genetically encoded tag for correlated light and electron microscopy of intact cells, tissues, and organisms. *PLoS Biol.* **2011***, 9*, e1001041.

41. Rubio, N.; Prat, F.; Bou, N.; Borrell, J. I.; Teixido, J.; Villanueva, A.; Juarranz, A.; Canete, M.; Stockert, J. C.; Nonell, S. A comparison between the photophysical and photosensitising properties of tetraphenyl porphycenes and porphyrins. *New Journal of Chemistry* **2005***, 29*, 378-384.

42. Ragàs, X.; Sánchez-García, D.; Ruiz-González, R.; Dai, T.; Agut, M.; Hamblin, M. R.; Nonell, S. Cationic porphycenes as potential photosensitizers for antimicrobial photodynamic therapy. *J. Med. Chem.* **2010***, 53*, 7796-7803.

43. Magde, D.; Brannon, J. H.; Cremers, T. L.; Olmsted, J. Absolute luminescence yield of cresyl violet - Standard for the red. *J. Phys. Chem.* **1979***, 83*, 696-699.

44. Stockert, J. C.; Cañete, M.; Juarranz, A.; Villanueva, A.; Horobin, R. W.; Borrell, J. I.; Teixido, J.; Nonell, S. Porphycenes: facts and prospects in photodynamic therapy of cancer. *Curr. Med. Chem.* **2007***, 14*, 997-1026.

45. Wilkinson, F.; Helman, W. P.; Ross, A. B. Quantum yields for the photosensitized formation of the lowest electronically excited singlet state of molecular oxygen in solution. *J. Phys. Chem.* **1993***, 22*, 113-262.

46. Redmond, R. W.; Gamlin, J. N. A compilation of singlet oxygen yields from biologically relevant molecules. *Photochem. Photobiol.* **1999***, 70*, 391-475.

47. Anonymous *Phthalocyanines: Properties and Applications (Vol. 3);* VCH Publishers, Inc: 1989; , pp 1-303.

48. Gorman, A. A.; Rodgers, M. A. J. In *Singlet Oxygen;* Scaiano, J. C., Ed.; Handbook of organic photochemistry; Boca Raton: CRC Press, 1989; Vol. II, pp 229-247.

49. Hahn, U.; Setaro, F.; Ragas, X.; Gray-Weale, A.; Nonell, S.; Torres, T. Microenvironment-switchable singlet oxygen generation by axially-coordinated hydrophilic ruthenium phthalocyanine dendrimers. *Phys. Chem. Chem. Phys.* **2011***, 13*, 3385-3393.

50. Montalti, M.; Credi, A.; Prodi, L.; M.T, G. *Handbook of photochemistry;* CRC Press: 2006; .

51. García-Díaz, M.; Nonell, S.; Villanueva, A.; Stockert, J. C.; Canete, M.; Casado, A.; Mora, M.; Sagrista, M. L. Do folate-receptor targeted liposomal photosensitizers enhance photodynamic therapy selectivity? *Biochim. Biophys. Acta* **2011***, 1808*, 1063-1071.

52. Ruiz-González, R.; Acedo, P.; Sánchez-García, D.; Nonell, S.; Cañete, M.; Stockert, J. C.; Villanueva, A. Efficient induction of apoptosis in HeLa cells by a novel cationic porphycene photosensitizer. *Eur. J. Med. Chem.* **2013***, 63*, 401-414.

53. Soriano, J.; García-Díaz, M.; Mora, M.; Sagrista, M. L.; Nonell, S.; Villanueva, A.; Stockert, J. C.; Canete, M. Liposomal temocene (m-THPPo) photodynamic treatment induces cell death by mitochondria-independent apoptosis. *Biochim. Biophys. Acta* **2013**.

54. AnonymousATCC - Pseudomonas Aeruginosa (Schroeter) Migula. *http://www.lgcstandards-atcc.org/en.aspx* (accessed May/12, 2013).

55. Li, W. S.; Aida, T. Dendrimer porphyrins and phthalocyanines. *Chem. Rev.* **2009***, 109*, 6047-6076.

56. Caminos, D. A.; Spesia, M. B.; Durantini, E. N. Photodynamic inactivation of Escherichia coli by novel meso-substituted porphyrins by 4-(3-N,N,N-trimethylammoniumpropoxy)phenyl and 4-(trifluoromethyl)phenyl groups. *Photochem. Photobiol. Sci.* **2006**, *5*, 56-65.

57. Dosselli, R.; Gobbo, M.; Bolognini, E.; Campestrini, S.; Reddi, E. Porphyrin-apidaecin conjugate as a new broad spectrum antibacterial agent. *ACS Med. Chem. Lett.* **2010**, *1*, 35-38.

58. Reddi, E.; Ceccon, M.; Valduga, G.; Jori, G.; Bommer, J. C.; Elisei, F.; Latterini, L.; Mazzucato, U. Photophysical properties and antibacterial activity of meso-substituted cationic porphyrins. *Photochem. Photobiol.* **2002**, *75*, 462-470.

59. Vergeldt, F. J.; Koehorst, R. B. M.; Vanhoek, A.; Schaafsma, T. J. Intramolecular Interactions in the ground and excited-state of tetrakis(N-Methylpyridyl)porphyrins. *J. Phys. Chem.* **1995**, *99*, 4397-4405.

60. Ogilby, P. R.; Foote, C. S. Chemistry of Singlet Oxygen .36. Singlet molecular oxygen (1-Delta-G) Luminescence in solution following pulsed laser excitation - Solvent deuterium isotope effects on the lifetime of singlet oxygen. *J. Am. Chem. Soc.* **1982**, *104*, 2069-2070.

61. Scaiano, J. C. *CRC Handbook of Organic Photochemistry;* CRC Press: Boca Raton,Florida, 1989; Vol. 1.

62. Jori, G. Far-red-absorbing photosensitizers: their use in the photodynamic therapy of tumours. *J. Photochem. Photobiol. A.* **1992**, *62*, 371-378.

63. Dutta, R. C.; Nagpal, S.; Salunke, D. M. Functional mapping of apidaecin through secondary structure correlation. *Int. J. Biochem. Cell Biol.* **2008**, *40*, 1005-1015.

64. Czihal, P.; Hoffmann, R. Mapping of Apidaecin regions relevant for antimicrobial activity and bacterial internalization. *International Journal of Peptide Research and Therapeutics* **2009**, *15*, 157-164.

65. George, S.; Hamblin, M. R.; Kishen, A. Uptake pathways of anionic and cationic photosensitizers into bacteria. *Photochem. Photobiol. Sci.* **2009**, *8*, 788-795.

66. Chen, C. Z.; Cooper, S. L. Interactions between dendrimer biocides and bacterial membranes. *Biomaterials* **2002**, *23*, 3359-3368.

67. Spesia, M. B.; Caminos, D. A.; Pons, P.; Durantini, E. N. Mechanistic insight of the photodynamic inactivation of Escherichia coli by a tetracationic zinc(II) phthalocyanine derivative. *Photodiagnosis Photodyn Ther.* **2009**, *6*, 52-61.

68. Loh, B.; Grant, C.; Hancock, R. E. Use of the fluorescent probe 1-N-phenylnaphthylamine to study the interactions of aminoglycoside antibiotics with the outer membrane of Pseudomonas aeruginosa. *Antimicrob. Agents Chemother.* **1984**, *26*, 546-551.

69. Schüttrigkeit, T. A.; Kompa, C. K.; Salomon, M.; Rüdiger, W.; Michel-Beyerle, M. E. Primary photophysics of the FMN binding LOV2 domain of the plant blue light receptor phototropin of Avena sativa. *Chem. Phys.* **2003**, *294*, 501-508.

70. Valle, L.; Vieyra, F. E.; Borsarelli, C. D. Hydrogen-bonding modulation of excited-state properties of flavins in a model of aqueous confined environment. *Photochem. Photobiol. Sci.* **2012**, *11*, 1051-1061.

71. Jiménez-Banzo, A.; Ragàs, X.; Kapusta, P.; Nonell, S. Time-resolved methods in biophysics. 7. Photon counting vs. analog time-resolved singlet oxygen phosphorescence detection. *Photochem. Photobiol. Sci.* **2008**, *7*, 1003-1010.

72. Ogilby, P. R. Singlet oxygen: there is indeed something new under the sun. *Chem. Soc. Rev.* **2010**, *39*, 3181-3209.

73. Nonell, S.; González, M.; Trull, F. R. 1h-Phenalen-1-One-2-Sulfonic Acid - an Extremely Efficient Singlet Molecular-Oxygen Sensitizer for Aqueous-Media. *Afinidad* **1993**, *50*, 445-450.

74. Nonell, S.; Braslavsky, S. E. In *Time-resolved singlet oxygen detection;* Methods in enzymology; Academic Press INC: San Diego; San Diego, CA 92101-4495 USA, 2000; Vol. 319, pp 37-49.

75. Matsuura, T.; Saito, I. Photoinduced reactions—XXI : Photosensitized oxygenation of N-unsubstituted hydroxypurines. *Tetrahedron* **1968**, *24*, 6609-6614.

76. Rabello, B. R.; Gerola, A. P.; Pellosi, D. S.; Tessaro, A. L.; Aparício, J. L.; Caetano, W.; Hioka, N. Singlet oxygen dosimetry using uric acid as a chemical probe: Systematic evaluation. *J. Photochem. Photobiol. A.* **2012**, *238*, 53-62.

77. Miranda, M. A.; Garcia, H. 2,4,6-Triphenilpyrylium tetrafluoroborate as an electron-transfer photosensitizer. *Chem. Rev.* **1994**, *94*, 1063-1089.

78. Munro, A.; Noble, M. In *Fluorescence Analysis of Flavoproteins;* Chapman, S. K., Reid, G. A., Eds.; Flavoprotein Protocols; Humana Press Inc.: Totowa, NJ, 1999; Vol. 131, pp 25-48.

79. McLean, M. A.; Rajfur, Z.; Chen, Z.; Humphrey, D.; Yang, B.; Sligar, S. G.; Jacobson, K. Mechanism of chromophore assisted laser inactivation employing fluorescent proteins. *Anal. Chem.* **2009**, *81*, 1755-1761.

80. Waldeck, W.; Mueller, G.; Wiessler, M.; Brom, M.; Toth, K.; Braun, K. Autofluorescent proteins as photosensitizer in eukaryontes. *Int. J. Med. Sci.* **2009**, *6*, 365-373.

81. Jori, G.; Fabris, C.; Soncin, M.; Ferro, S.; Coppellotti, O.; Dei, D.; Fantetti, L.; Chiti, G.; Roncucci, G. Photodynamic therapy in the treatment of microbial infections: basic principles and perspective applications. *Lasers Surg. Med.* **2006**, *38*, 468-481.

82. Segalla, A.; Borsarelli, C. D.; Braslavsky, S. E.; Spikes, J. D.; Roncucci, G.; Dei, D.; Chiti, G.; Jori, G.; Reddi, E. Photophysical, photochemical and antibacterial photosensitizing properties of a novel octacationic Zn(II)-phthalocyanine. *Photochem. Photobiol. Sci.* **2002**, *1*, 641-648.

83. Schafer, M.; Schmitz, C.; Horneck, G. High sensitivity of Deinococcus radiodurans to photodynamically-produced singlet oxygen. *Int. J. Radiat. Biol.* **1998**, *74*, 249-253.

84. Ashkenazi, H.; Pechatnikov, I.; Nitzan, Y. Low-intensity photosensitization may enhance RecA production. *Curr. Microbiol.* **2006**, *52*, 317-323.

85. Baier, J.; Maisch, T.; Maier, M.; Engel, E.; Landthaler, M.; Baumler, W. Singlet oxygen generation by UVA light exposure of endogenous photosensitizers. *Biophys. J.* **2006**, *91*, 1452-1459.

86. Foote, C. S.; Clennan, E. L. In *Properties and Reactions of Singlet Dioxygen;* Liebman, J. L., Ed.; Blackie Academic and Professional: Glasgow, 1995; Vol. 1, pp 105-140.

87. Foote, C. S. Definition of type-I and type-Ii photosensitized oxidation. *Photochem. Photobiol.* **1991**, *54*, 659-659.

88. Kotani, H.; Ohkubo, K.; Fukuzumi, S. Photocatalytic oxygenation of anthracenes and olefins with dioxygen via selective radical coupling using 9-mesityl-10-methylacridinium ion as an effective electron-transfer photocatalyst. *J. Am. Chem. Soc.* **2004**, *126*, 15999-16006.

89. Shida, T. *Electronic absorption spectra of radical ions;* Physical sciences data; Elsevier science publishers: 1988; Vol. 34, pp 1-446.

90. Wilson, A. J.; Hong, J.; Fletcher, S.; Hamilton, A. D. Recognition of solvent exposed protein surfaces using anthracene derived receptors. *Org. Biomol. Chem.* **2007**, *5*, 276-285.

91. Wilson, A. J. Inhibition of protein-protein interactions using designed molecules. *Chem. Soc. Rev.* **2009**, *38*, 3289-3300.

92. Crovetto, L.; Braslavsky, S. E. Photoinduced electron transfer to triplet flavins. Correlation between the volume change-normalized entropic term and the Marcus reorganization energy. *J Phys Chem A* **2006**, *110*, 7307-7315.

93. Barbieri, Y.; Massad, W. A.; Díaz, D. J.; Sanz, J.; Amat-Guerri, F.; García, N. A. Photodegradation of bisphenol A and related compounds under natural-like conditions in the presence of riboflavin: Kinetics, mechanism and photoproducts. *Chemosphere* **2008**, *73*, 564-571.

94. Chin, K. K.; Trevithick-Sutton, C. C.; McCallum, J.; Jockusch, S.; Turro, N. J.; Scaiano, J. C.; Foote, C. S.; Garcia-Garibay, M. A. Quantitative determination of singlet oxygen generated by excited state aromatic amino acids, proteins, and immunoglobulins. *J. Am. Chem. Soc.* **2008***, 130*, 6912-6913.

95. Jensen, R. L.; Arnbjerg, J.; Ogilby, P. R. Reaction of singlet oxygen with tryptophan in proteins: a pronounced effect of the local environment on the reaction rate. *J. Am. Chem. Soc.* **2012***, 134*, 9820-9826.

96. Kao, Y. T.; Tan, C.; Song, S. H.; Ozturk, N.; Li, J.; Wang, L.; Sancar, A.; Zhong, D. Ultrafast dynamics and anionic active states of the flavin cofactor in cryptochrome and photolyase. *J. Am. Chem. Soc.* **2008***, 130*, 7695-7701.

97. Kao, Y. T.; Saxena, C.; He, T. F.; Guo, L.; Wang, L.; Sancar, A.; Zhong, D. Ultrafast dynamics of flavins in five redox states. *J. Am. Chem. Soc.* **2008***, 130*, 13132-13139.

98. Shaner, N. C.; Campbell, R. E.; Steinbach, P. A.; Giepmans, B. N. G.; Palmer, A. E.; Tsien, R. Y. Improved monomeric red, orange and yellow fluorescent proteins derived from Discosoma sp. red fluorescent protein. *Nat Biotech* **2004***, 22*, 1567-1572.

99. Ammann, E. C.; Lynch, V. H. Purine metabolism by unicellular algae. 3. The photochemical degradation of uric acid by chlorophyll. *Biochim. Biophys. Acta* **1966***, 120*, 181-182.

Chapter IV.

New strategies for $^1O_2$ detection

The real voyage of discovery consists not in seeking new landscapes but in having new eyes"

\- Marcel Proust

Introduction

With all this previous considerations, it lo oks clear that $^1O_2$ measurement is a goal of general interest for the scientific community. In fact, over the years a great effort has been made in developing techniques and/or methods able not only to detect but also to quantify the generation of $^1O_2$. As a general idea, high sensitivity and selectivity towards $^1O_2$, high signal-to-noise ratio, and ease of measurement are a must for any candidate probing system. So far, $^1O_2$ detection methods can be sorted into two groups: 1) physical detection, given by direct measurement of near-infrared $^1O_2$ phosphorescence at 1275 nm and 2) chemical probes that, in the presence of $^1O_2$, undergo a reaction with a subsequent great magnification of a measurable physical property, such as absorption, fluorescence or chemiluminescence.

$^1O_2$ can be detected through its intrinsic phosphorescence with maximum centered at 1275 nm.[1] This is a robust, specific, noninvasive and direct method; but it suffers from weak signal due to the lower efficiency particularly in biological media, where the lifetime of $^1O_2$ is very short (3.1 μs)[2] and the phosphorescence quantum yield is very small, *ca.* 10^{-7}.[3]

Among the chemical traps, UA is a good alternative that has recently gained atention.[4,5] In the presence of $^1O_2$, UA forms an intermediate that undergoes an additional degradation step to allantoin.[6] As a result, absorbance at 292 nm decays with biexponential kinetics. As a drawback, it is not convenient for *in vivo* measurements due to the difficulty of measuring absorption in the UV region without interferences of biological components. Plus tracking the bleaching of a physical property is less desirable than tracking its enhancement.

Another approach has been the development of chemiluminescent probes, believed to be one of the most sensitive methods in $^1O_2$ detection. Compared with fluorescence, chemiluminescence does not require excitation light, so background fluorescence and scattered light interference are eliminated. The set of widely-used chemiluminescence probes includes 2-methyl-6-phenyl-3,7-dihydroimidazo [1,2-a] pyrazin-3-one, and its derivatives.[7,8] More recently developed chemiluminescence probes, include tetrathiafulvalene[9] and probes based on s table dioxetane precursors[10]. Tetrathiafulvalene is a strong electron donor that enhances its reaction with $^1O_2$ and it offers improved sensitivity and good ratiometric correlation between $^1O_2$ and chemiluminescence. Dioxetane-based traps comprehend the reaction of $^1O_2$ with a p recursor (sporoadamantyl-substituted vinyl ether) that can form a d ioxetane, $^1O_2$ chemical trap

that can be used for quantification purposes by chemiluminescence after addition of a chemical trigger. Again, the lack of water solubility and the short emission wavelength are the main drawbacks when assessed in detection of $^1O_2$ in biosamples.

Another commonly used $^1O_2$ trap system consists of molecules able to react with $^1O_2$ through photochemical endoperoxidation reactions. In the presence of $^1O_2$, anthracene (or acene-like) or furan derivatives specifically react with $^1O_2$ to form an endoperoxide.[11] This reaction is accompanied by a decrease in absorbance which can be used as a signal of $^1O_2$ production. Again, such detection is not very sensitive since it is based on an absorbance measurement. However, lately, the fluorescence bleaching of anthracene has also been used as $^1O_2$ reporter with good results.[12,13] Unfortunately, anthracene fluorescence is observed in the blue, which is difficult to monitor in living systems due to overlap with cell autofluorescence.[14]

Fluorescent probing of $^1O_2$ is probably the most studied and developed technique. Fluorometric assays were firstly based on the use of the chemically reduced, non-fluorescent forms of highly fluorescent dyes such as fluorescein and rhodamine that when properly oxidised to the parent dye molecule, resulted in a notorious increase in fluorescence intensity.[15] However, these dihydro-compounds are highly photosensitive compounds (they tend to be autoxidised producing a large background fluorescence even in the absence of ROS) and lack selectivity for $^1O_2$.

In later studies, it was concluded that the fluorescence properties of fluorescein derivatives were controlled by a photoinduced electron transfer process from the benzoic acid moiety to the xanthene ring.[16-18]. Thus, it paved the way to devise a new general approach: a two-component system comprised of a $^1O_2$ trapping moiety coupled to a light-emitting chromophore. Several probes have been developed following this principle: DPAX and DMAX,[16,19] MTTA-Eu^{3+} [20] and more recently SOSG (for Singlet Oxygen Sensor Green),[21] use an anthracene moiety to trap $^1O_2$. In their native state, the luminescence of the emitting moiety is quenched by the anthracene by an electron-transfer process. Oxidation of the anthracene by $^1O_2$ eliminates this quenching channel and the probe becomes luminescent. The same concept has been recently used to develop a near-infrared probe, His-Cy, where anthracene has been replaced by a histidine and a cyanine is chosen as fluorophore.[22] A common drawback for all the above probes is that the fluorescence increases only moderately after reaction with $^1O_2$, *e.g.*, from less than two-fold for His-Cy[22] to *ca.* 10-fold for SOSG. Moreover, since electron-transfer reactions are strongly

dependent on solvent polarity, false positive signals arise that merely reflect location of the probe in a less-polar microenvironment rather than reaction with $^1O_2$, *e.g.*, when the probe is in hydrophobic pockets of proteins.[23] In addition, the presence of an anthracene moiety in the structure is potentially misleading since anthracene is itself a $^1O_2$ PS that may auto-oxidize the probe, which further complicates its use.[24]

Most $^1O_2$ probes have in common that they have been envisaged to measure $^1O_2$ in solution or in extracellular systems. As a consequence, when interest was drawn to measuring $^1O_2$ intracellularly and the available probes were tested in this context they failed, needed harsh/not physiological conditions, or were not successful enough.[14,20,23] Recently, a synthetic $^1O_2$ sensitive construct has been reported to successfully perform in intracellular systems. However, the synthetic complexity of the system – comprised by a photocleavable moiety, two fluorophores and a cholesterol unit to achieve cell internalisation (Scheme 1)- makes it far from being the ideal and accessible $^1O_2$ probe.[25]
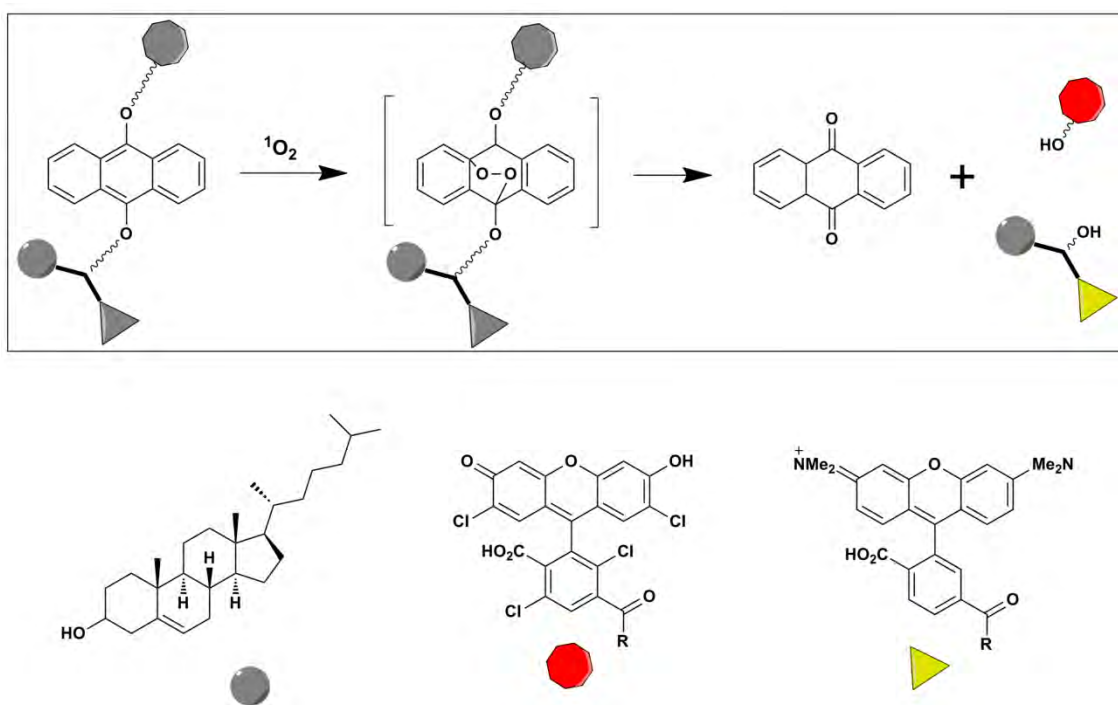
Scheme 1. Representation of the system described in ref [25]. An anthracene moiety is coupled to two fluorophores (whose fluorescence is initially quenched) and a cholesterol unit to enhance cell penetration. In the presence of $^1O_2$ an unstable endoperoxide breaks liberating the fluorophores that recover their inner fluorescence.

For the sake of measuring $^1O_2$ intracellularly, extra features are requested from the probing candidates that need to be borne in mind during their design, *i.e.* stability, ease of uptake, and lack of toxicity. Inside the cell, the $^1O_2$ produced will encounter mainly an aqueous-like environment, what means that the probe must be water soluble and non-toxic in working concentrations for good and viable cell internalisation. Most $^1O_2$ probes are highly hydrophobic and, thus, lack water solubility and ease of

110

cell uptake. Although new water-soluble chemical probes have been developed,[13,19,21,26,27] problems associated with dye toxicity or cell uptake are also being encountered. On the other hand, the $^1O_2$ lifetime in water and inside cells is very short.[28] This results in the immediate quenching of a large fraction of the $^1O_2$ produced, hence reducing the emission signal to the threshold of detection by physical methods. In addition, it is extremely difficult for the physical method to monitor the accumulation of $^1O_2$ production during, for instance, a PDT process. Another important feature of $^1O_2$ measurement is its spatial localisation. Even considering that the $^1O_2$ probe could be successfully internalised, still its targeting to the subcellular region where $^1O_2$ will be located is a great handicap (or goal). Microscopy has been used to achieve resolution in a spatio-temporal manner, but the resolution limit is very close to the diffraction limit. Still, interesting approaches have been achieved in this respect.[29-31]

There is an emerging trend to the use of polyacrylamide NPs in cellular and *in vivo* drug delivery,[32-34] sensing[35,36] and imaging[37] and successful examples of the system have recently been published in several fields.[38-40] Their first and well-known advantage is the biocompatibility and ease of delivery into cellular systems. While dyes usually rely on passive uptake by cells, NPs design elicits a more targeted delivery of the probe, especially as they can easily be chemically tailored for enhanced targeting to cells and subcellular compartments. Another property of NPs is their ability to be encapsulated/conjugated with a vast variety of molecules. The loaded NPs can be used in aqueous solution regardless of the hydrophobicity of the drug/probe. NPs thus become potential carriers and physical protectors of the cargo. The dye molecule will be shielded from the chemical and biological environment in the physiological system while, simultaneously, the physiological system will also be protected from the potential toxicity of the dye molecules.

Some previous approaches have been tried to combine $^1O_2$ chemical probing with the advantages of using biocompatible carriers. Steinbeck *et al.,*[41] used micron-sized glass beads coated with 9,10-diphenylanthracene, a well-known $^1O_2$ chemical trap. Although they demonstrated that $^1O_2$ was produced from the cells, its huge size (1.6 μm) is likely to perturb the cells, thus, limiting its use *in vivo*. More recently, Cao et al.[42] reported the results of a system composed by another common $^1O_2$ chemical probe, 9,10-dimethyl anthracene, entrapped in a permeable silica matrix (ORMOSIL) leading to NPs able to detect $^1O_2$ while maintaining the advantages of being a biocompatible carrier. Further studies of its performance in intracellular systems have not been published to date. With all this shown, it is clear that there is not a perfect detection method for $^1O_2$ and room exists for new findings in this area.

Naphthoxazole-based ^{1}O$_2$ fluorescent probes[i]

AIM OF THE STUDY

In this study we report the synthesis and photochemical behaviour of a new family of photoactive compounds in order to assess its potential as singlet oxygen probes. The candidate dyads are composed by a singlet oxygen trap plus a naphthoxazole moiety linked through an unsaturated bond. In the native state, the inherent great fluorescence of the naphthoxazole moiety is quenched; but in the presence of ^{1}O$_2$, generated by the addition and appropriate irradiation of an external PS, a photooxidation reaction occurs leading to the formation of a new chemical entity whose fluorescence is two orders of magnitude higher than that of the initial compound, at the optimal selected wavelength. The presented dyads outperform the commonly used indirect fluorescent singlet oxygen probes in terms of fluorescence enhancement maintaining the required specificity for singlet oxygen detection in solution.
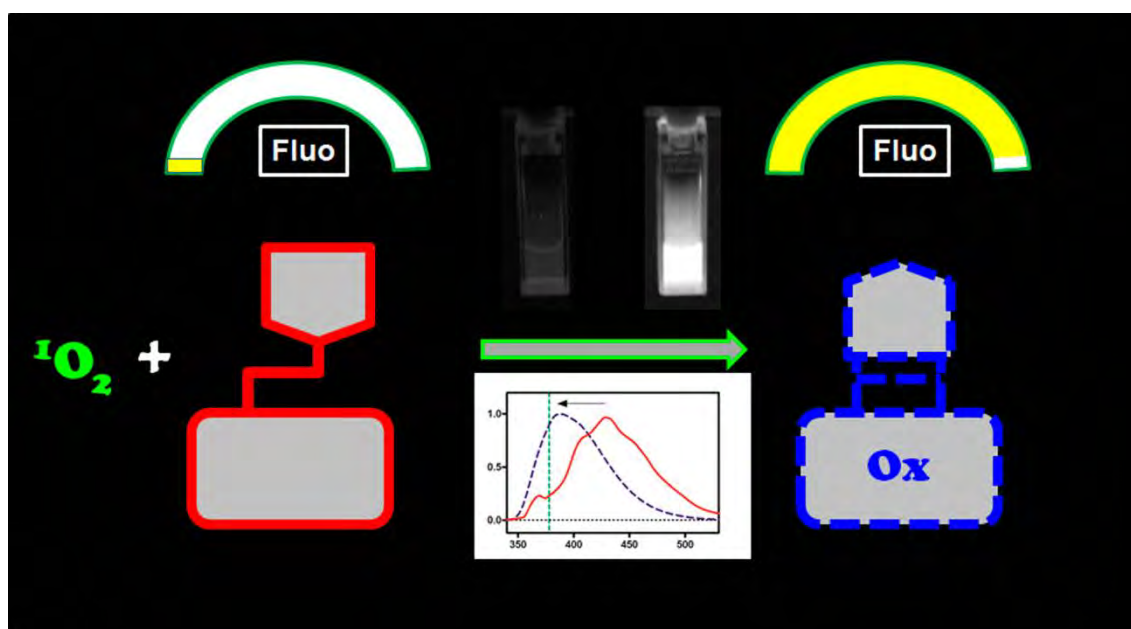
Graphical Abstract 1. Conjugation of a fluorescent and a ^{1}O$_2$-trapping moieties leads to a dyad with a low fluorescence in its native state. In the presence of ^{1}O$_2$ a new photooxidised chemical entity is born, leading to a fluorescence enhancement over two orders of magnitude at the optimal selected wavelength.

112

RESULTS

Naphthoxazole dyads description.

2-(2-(Furan-2-yl)ethyl)naphtho[1,2-d]oxazole, **FN-I1**, contains a naphthoxazole linked to a furan through a saturated ethyl bridge. In 2-(furan-2-yl)naphtho[1,2-d]oxazole, **FN-I2**, the furan moiety is bonded directly to the position 2 of the oxazole ring, whereas in (E)-2-(2-(furan-2-yl)vinyl)naphtho[1,2-d]oxazole, **FN-4**, the naphthoxazole and the furan are conjugated through an unsaturated ethylidene link. In the control molecule, (E)-2-(4-methylstyryl)naphtho[1,2-d]oxazole, **FN-7**, the furan ring of **FN-4** has been replaced by a non-reactive tolyl group. Two candidates could be used as singlet oxygen sensors, namely **FN-I2** and **FN-4**, since their fluorescence is boosted by a factor of ca. 135 and 300, respectively, upon reaction with $^1O_2$. Four described compounds are depicted in Scheme 2.

2-(2-(furan-2-yl)ethyl)naphtho[1,2-*d*]oxazole
FN-I1

2-(furan-2-yl)naphtho[1,2-*d*]oxazole
FN-I2

(*E*)-2-(2-(furan-2-yl)vinyl)naphtho[1,2-*d*]oxazole
FN-4

(*E*)-2-(4-methylstyryl)naphtho[1,2-*d*]oxazole
FN-7
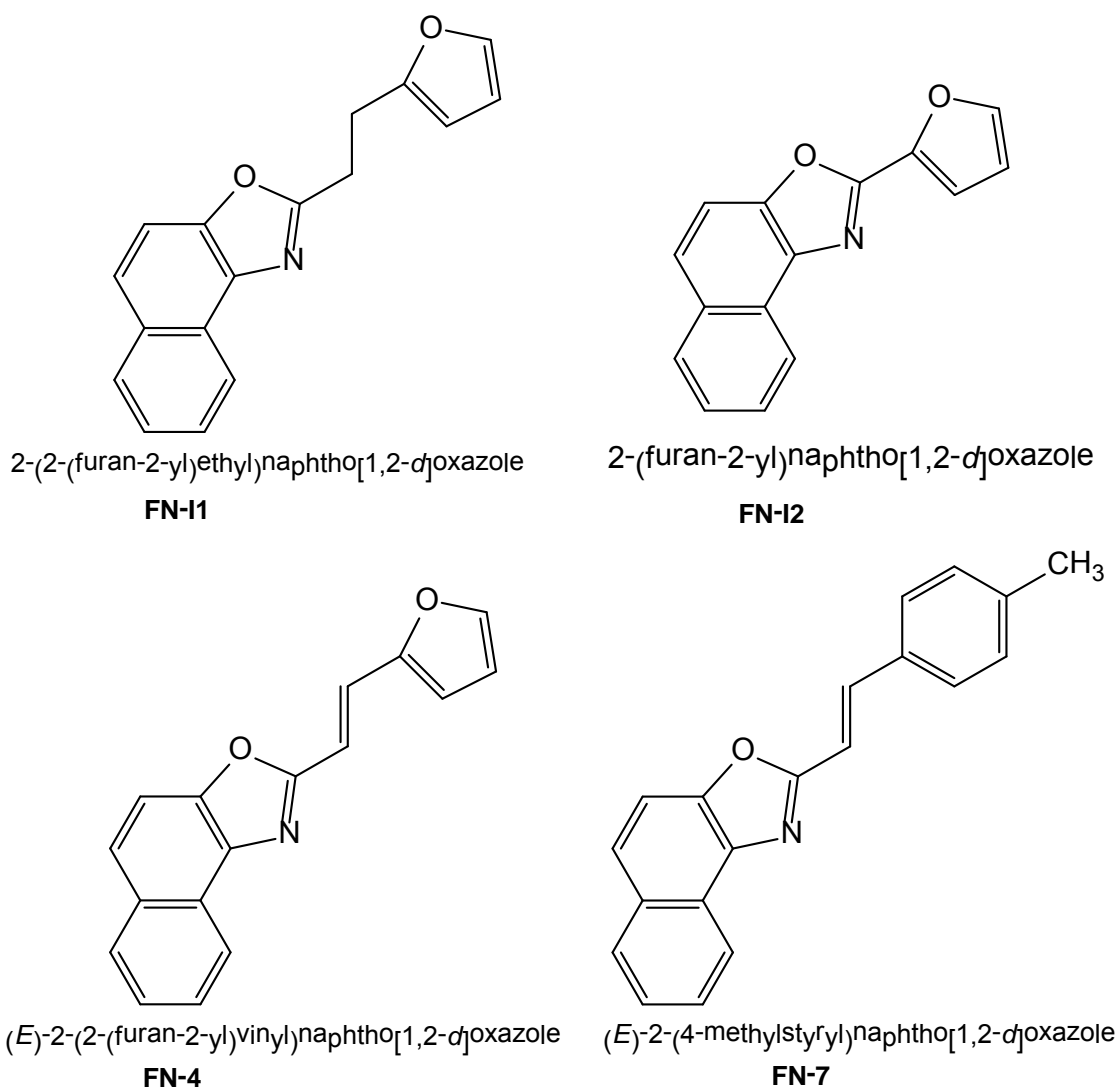
Scheme 2. Chemical structures of the four naphthoxazole derivatives of study.

Photophysical characterisation

FN-4 is a dyad composed by a furan ring linked to a naphthoxazole moiety through an ethylidene group. The absorption spectrum is dominated by a main band with maximum at 367 nm and a second weaker band at 314 nm (Figure 1a) that compares reasonably well with the values of 387 and 314 nm obtained from TD-DFT calculations using G09W. The position of the bands follows no obvious trend with the solvent polarity (data not shown). The high values of molar absorptivity, *ca.* $3 \cdot 10^4 \cdot M^{-1} cm^{-1}$ in all solvents except in water, and the molecular orbital analysis of the minimum energy structure obtained from DFT calculations, indicate a π,π^* transition. A similar behaviour of the absorption properties was observed for **FN-I2** (data not shown), in which the furan ring is linked directly to the naphthoxazole moiety, and for **FN-7**, in which a non-reactive tolyl substituent replaces the furan moiety. When the linker is saturated (**FN-I1**) spectral bands shift substantially to the blue (λ_{max} = 322 nm) and become more structured. These results correlate with the distinct degree of electronic coupling between the aromatic moiety and the naphthoxazole fluorophore. Similar trends are observed in the maximum of the fluorescence spectra (Figure 2b), consistent with the reports for related benzoxazole derivatives.[43]
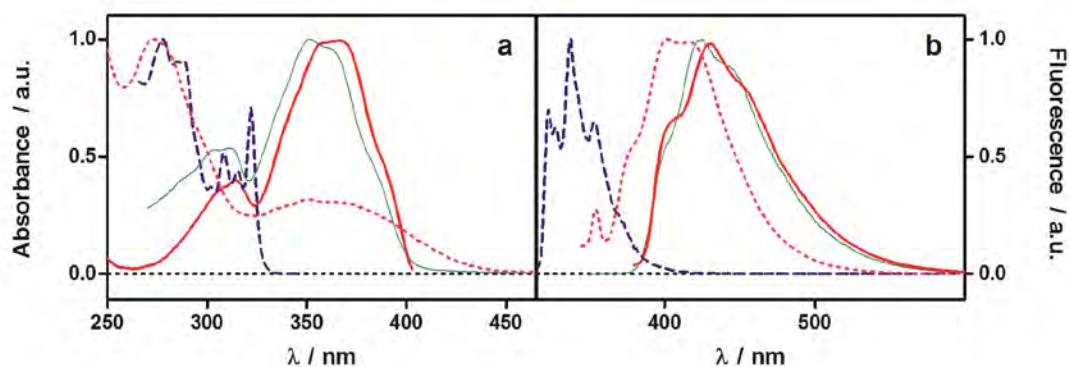
Figure 1. Normalised absorption (a) and fluorescence (b) spectra of **FN-4** (thick solid), **FN-I1** (dashed), **FN-I2** (dotted) and **FN-7** (thin solid) in MeOH**.**

Aryl oxazoles typically exhibit a very high Φ_F value, in the 0.7-1.0 range [44,45]. Among all studied compounds, this is observed only for **FN-I1** ((Φ_F = 0.93 in MeOH). In contrast, **FN-4** and **FN-7** show high Φ_F values in low-polarity solvents only, the quantum yield decreasing by 1-2 orders of magnitude as the solvent polarity increases (Figure 2). However, for (E)-4-(2-(naphtho[1,2-d]oxazol-2-yl)vinyl)benzonitrile (**FN-7CN**), an **FN-7** analogue in which the methyl group is replaced by the strong

electron-attractor cyano group, the fluorescence quantum yields are close to 1 in all solvents, irrespective of their polarity (A. L. Zanocco, unpublished data). Finally, **FN-I2** is scantly fluorescent even in non-polar solvents (Figure 2). These results indicate that electron-rich aromatic moieties can act as effective quenchers of naphthoxazole fluorescence in conjugated dyads and, particularly, in polar protic environments, likely due to a charge-transfer interaction. Thus, furyl-oxazole dyads fulfill the first condition requested for a potential $^1O_2$ probe, namely that the fluorescence is severely quenched in their native form, thus deserving further scrutiny.
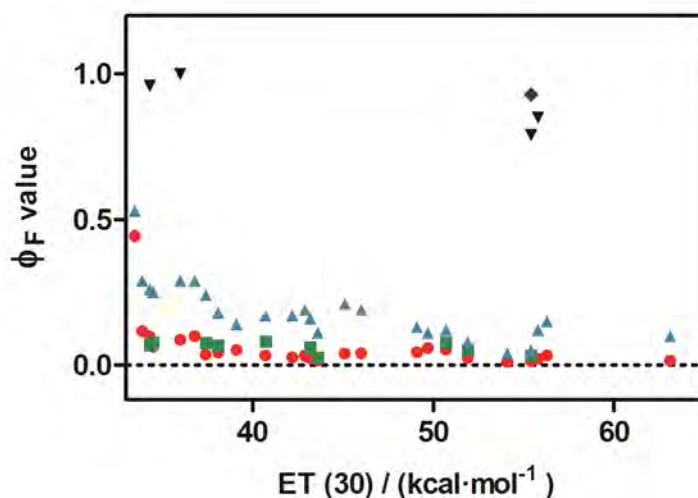
Figure 2. Correlation of Φ_F values with the solvent polarity (represented by the ET(30) values) for the dyads **FN-4** (red circles), **FN-I2** (green squares), **FN-7** (light blue triangles), **FN-7CN** (black inverted triangles) and **FN-I1** (dark blue diamond)

Reactivity towards singlet oxygen

The ability of the dyads to react with $^1O_2$ has been studied by monitoring changes in their absorption and fluorescence properties. No changes could be recorded for **FN-I1** and **FN7**, as expected. In the case of **FN-4**, reaction with $^1O_2$ in MeOH caused bleaching of the main band at 367 nm and the growth of a new band in the 325-350 nm region (Figure 3a). The clear isosbestic point at 348 nm suggests a clean transformation to a single photoproduct (hereafter **FN-4OX**). This was confirmed by HPLC experiments that, after 95% **FN-4** (t_r = 14.3 min) consumption, show the formation of a main product at t_r = 8.3 min and several minor secondary products (data not shown). Experiments to identify reaction products are in progress; however, furan is well known to selectively react with $^1O_2$ through an endoperoxidation reaction, followed by methanolysis of the endoperoxide.[46-48]
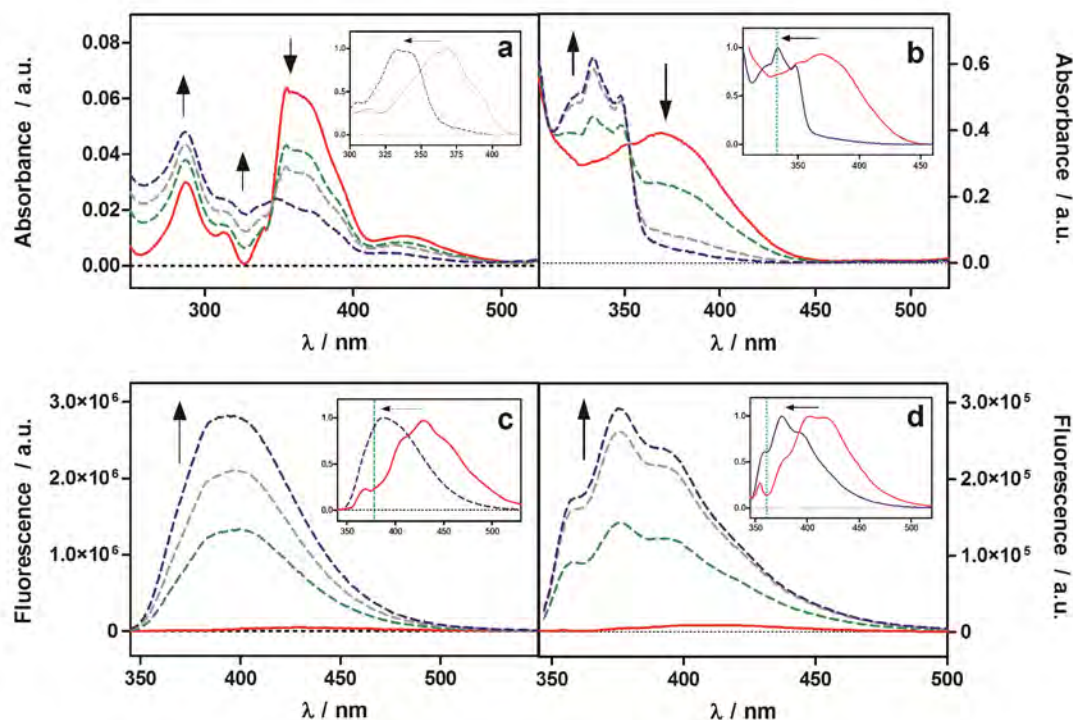
115

Figure 3. Absorption (a,b) and fluorescence (c,d) spectra of **FN-4** (a, c) and **FN-I2** (b, d) before (solid line) and after (dashed lines) reaction with $^1O_2$. The PS was NMB 1 μM, the irradiation wavelength was 635 ± 15 nm, and the experiments were carried out in aerated MeOH. Insets show normalised excitation (a, b) and fluorescence (c, d) spectra to facilitate their comparison.

Involvement of $^1O_2$ in the process was unequivocally demonstrated by the inhibitory effect of selective $^1O_2$ quenchers (data not shown). Most effective were α-terpinene and sodium azide that inhibited the **FN-4** photo-oxidation by *ca.* 90%. DABCO was able to diminish the **FN-4** consumption to a lesser extent. A strong fluorescence increase and a concomitant shift of the fluorescence peak to the blue could also be observed (Figure 3c), the excitation spectra of the original and final fluorescence bands being markedly different, implying that they correspond to different chemical entities (Figure 3a, inset). The spectral overlap is minimised at 330 nm, which suggests that this excitation wavelength should be chosen to maximise the fluorescence of **FN-4OX**. As shown in Figure 4 the fluorescence intensity at 378 nm is enhanced by more than 300-fold. Compared to SOSG, the fluorescence enhancement of **FN-4** is 30-fold larger.

In a similar fashion to that observed for **FN-4**, emission of **FN-I2** also increases considerably upon reaction with $^1O_2$ in MeOH (Figure 3d), concomitant with the bleaching of the low-energy absorption band at 367 nm (Figure 3b). Both the absorption and fluorescence spectra reveal the appearance of new bands shifted to the blue. The absorption spectra show a clear isosbestic point at 352 nm, suggesting the

formation of a single photoproduct as for **FN-4**. Excitation at 333 nm maximises the system emission, which increases by a factor *ca*. 135 at 363 nm (Figure 4).
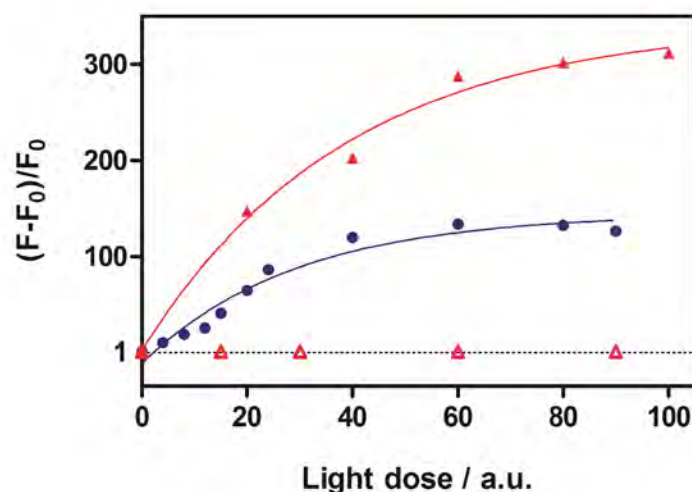
Figure 4. Fluorescence enhancement of **FN-4** (solid red triangles; λ_{exc} = 330 nm; λ_{obs} = 378 nm) and **FN-I2** (solid blue circles; λ_{exc} = 333 nm; λ_{obs} = 363 nm.) upon external generation of $^1O_2$ in MeOH. Open red triangles stand for **FN-4** fluorescence intensity changes upon cumulative irradiation at 355 nm. *F* stands for the fluorescence intensity at each point of study while *F$_0$* refers to the background fluorescence.

The rate constant for $^1O_2$ quenching by the dyads (k_q) was determined by time-resolved detection of $^1O_2$ phosphorescence at 1275 nm.[1,49] Increasing concentrations of the dyads enhanced the decay rate of $^1O_2$ in a linear fashion. The slope of the plots afforded the k_q values, which are collected in Table 1.

Table 1. Summary of photophysics, $^1O_2$ production and reactivity data for the compounds of study in MeOH.

Compound	λ_{exc}/ nm	ε / $M^{-1} \cdot cm^{-1}$	Φ_F	k_q / $M^{-1} \cdot s^{-1}$	Φ_Δ [a]
N-4	367	30060	0.014	9.1×10^5	0.003
FN-I1	322	13940	0.930[b]	1.9×10^7	0.070
FN-I2	342	31721	0.032	2.1×10^7	0.009
FN-7	351	32516	0.050	0.0033[c]	0.004

[a] PN in MeOH (Φ_Δ = 1.0) was used as standard; λ_{exc} = 355 nm.[50] [b] naphthalene in ethanol (Φ_F = 0.21) was used as reference [51] Excitation wavelength was λ_{exc} = 280 nm for **FN-I1**. [c] acetonitrile as solvent

Interestingly, the value for **FN-4** (vinyl bridge) is 20-fold smaller than that for **FN-I1** (ethyl bridge) and for **FN-I2** (direct link), and about 40-fold smaller than for isolated 2-methylfuran (k_q = 9.9x10^7 M^{-1}s^{-1} in MeOH [52]), which confirms the strong electronic delocalisation of the furan ring across the vinyl bridge

117

in **FN-4**. Notice that the fluorescence enhancements do not correlate with k_q. Finally, the low k_q value for **FN-7** confirms that naphthoxazole derivatives lacking the furyl substituent are essentially unreactive towards $^1O_2$.

Self-sensitisation of $^1O_2$ by the dyads and reactivity towards other ROS

A drawback of SOSG is the growth of fluorescence due to self-sensitisation of $^1O_2$ (19). Other dyads lack selectivity towards $^1O_2$ and react also with different ROS. We investigated whether the naphthoxazole dyads suffered from the same problems. All dyads sensitised the production of $^1O_2$, although with very small quantum yields (Φ_Δ, Table 1 and Figure 5). Nevertheless, Figure 4 show that the fluorescence of **FN-4** does not increase upon cumulative irradiation in MeOH and that of **FN-I2** actually decreases (data not shown).
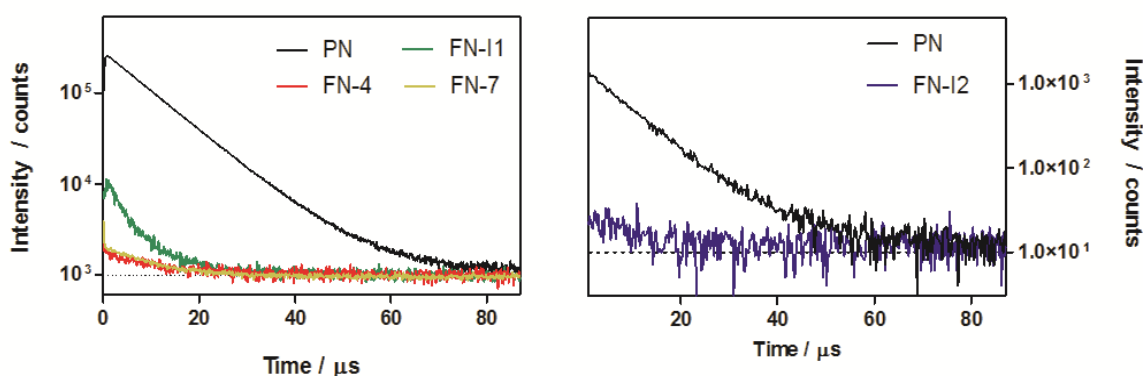
Figure 5. $^1O_2$ phosphorescence signals upon excitation at 355 nm and observation at 1275 nm. Amplitudes of the dyads' decays were compared to that of PN used as standard.

Reactivity towards other ROS was also tested for **FN-I2** and **FN-4** with negative results for both superoxide (KO_2) and H_2O_2 (Figure 6).
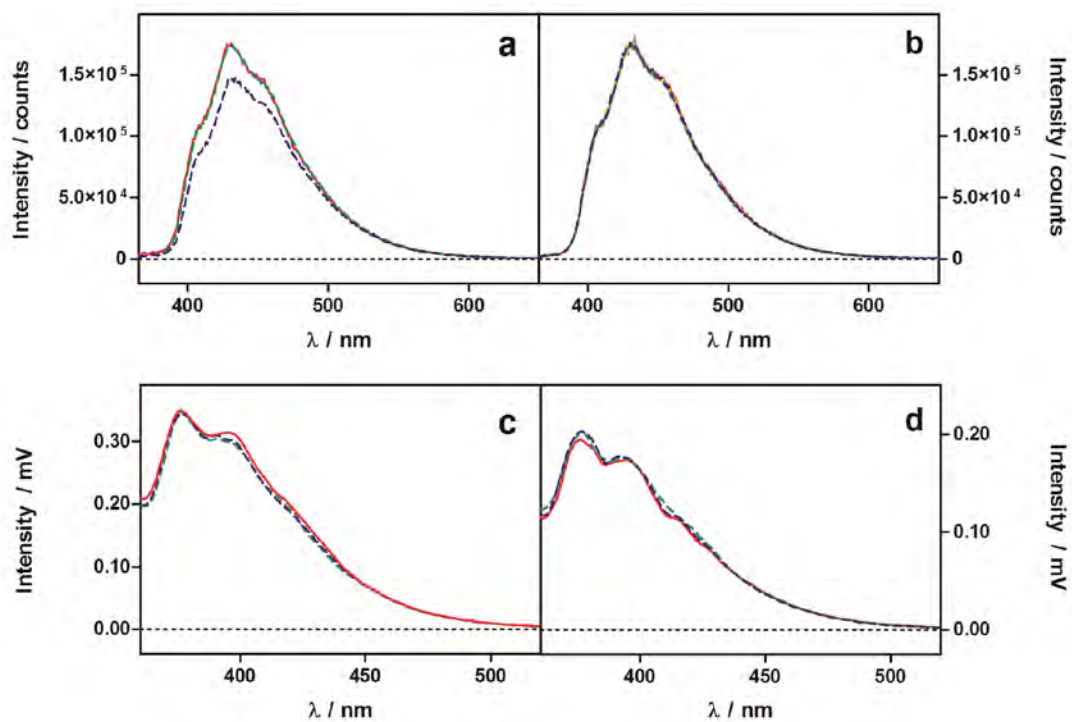
Figure 6. Fluorescence changes of methanolic solutions of **FN-4** upon addition of H_2O_2 (a) or KO_2 (b). Analogous results are presented for **FN-I2** (c, d).

DISCUSSION

The results above demonstrate that the new family of naphthoxazole dyads represented by compounds **FN-4** and **FN-I2** outperform any other fluorescent probe currently available for monitoring $^1O_2$. The key novelty of the system relies on the fact that the fluorophore in the photooxidation adduct is different from that in the initial species. Thus, spectral changes arise that elicit the selection of optimal excitation wavelengths to enhance the fluorescence of the photoproducts. Enhancement factors up to 310-fold have been observed, that compare favorably with the 2-fold observed recently for His-Cy or with the 10-fold for SOSG. While both dyads are able to self-sensitise $^1O_2$, their fluorescence does not increase in the absence of external $^1O_2$ PSs. Finally, a high degree of specificity for $^1O_2$ has been shown for both candidates.

CONCLUSIONS

FN-4 and **FN-I2** are two examples of successful naphthoxazole-based dyads capable of monitoring $^1O_2$ in solution with unprecedented sensitivity. Photooxidation of the trapping moiety leads to the formation of a new chemical entity whose fluorescence is spectrally different from that of the non-irradiated conjugate. Fluorescence enhancement factors up to 310-fold have been observed taking advantage of the change in spectral properties upon photooxidation. Its added selectivity towards $^1O_2$ and the negligible effects of self-sensitisation, make naphthoxazole dyads worth of further development as $^1O_2$ fluorescent probes.

Polyacrylamide nanoparticles as scaffold for $^1O_2$ detection in intracellular systems

AIM OF THE STUDY

We have envisaged a polyacrylamide nanoparticle scaffold that might be able to circumvent many of the general drawbacks of $^1O_2$ intracellular detection while meeting the requirements for a good *in vivo* $^1O_2$ reporter readily compatible with biological systems. Two commercial $^1O_2$ probes, namely 9,10-anthracenedipropionic acid (ADPA) and singlet oxygen sensor green (SOSG) with different working mechanisms have been covalently bound through different size linkers to the nanoparticle core and their detecting performance and biocompatibility have been tested in solution as well as in cells. $^1O_2$ generation has been achieved either by an exogenous PS coadministered with the nanoparticles or by including the PS in the polyacrylamide matrix. The preliminary results show biocompatibility and uptake feasibility with concomitant localisation inside cells. While the system is not yet fully optimised it still serves as proof of concept for the scaffold.
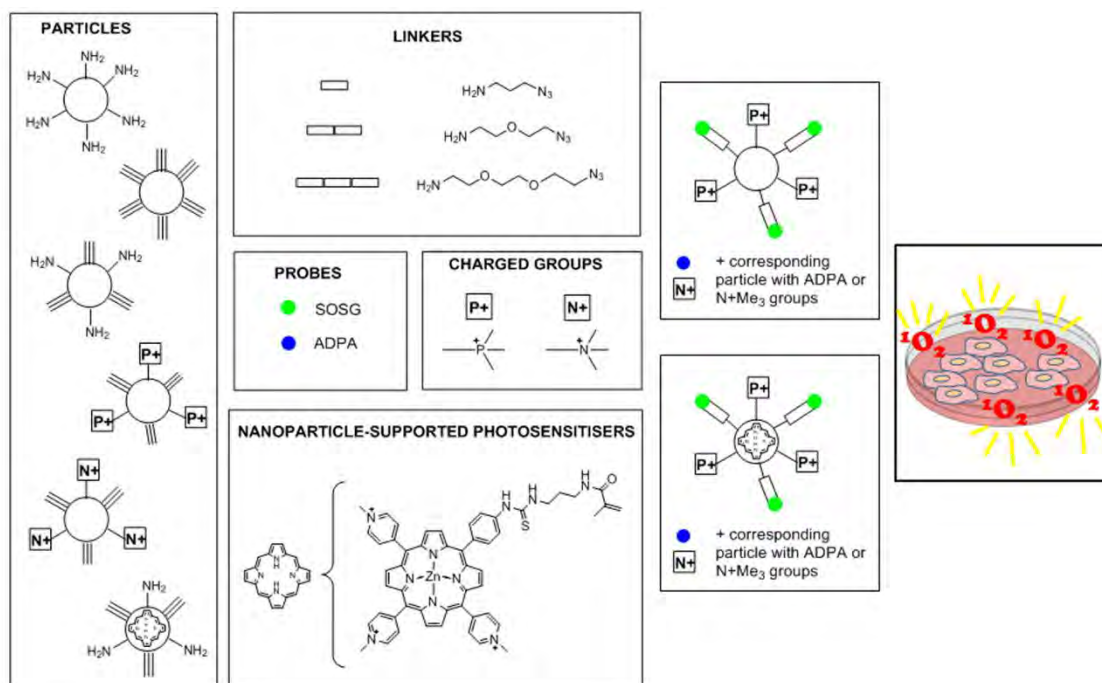
Graphical Abstract 2. Rational of the designed system intended for detecting $^1O_2$ in intracellular systems. Key structures of a versatile system endowed with a polyacrylamide nanoparticle scaffold where different units can be probe is clicked to a generic fluorogenic $^1O_2$ probe through different linkers. Other units such as charged moiety or porphyrin are also shown.

RESULTS

As a primary approach, we developed the simplest scenario where the $^1O_2$ probe is readily attached to the NP scaffold, following the Scheme 3. Amino-derivatised NPs were covalently bound either to ADPA or SOSG.
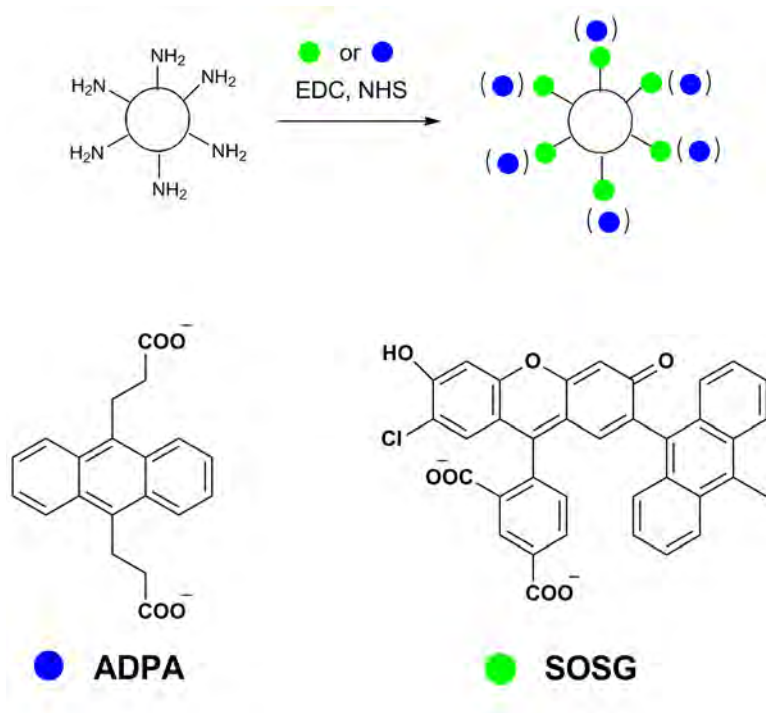
Scheme 3. Rational design of ADPA (blue dots) or SOSG (green dots) probes readily linked to amino-NPs through amide bonds, together with the chemical structures of ADPA and SOSG

Solutions containing 2 mg/mL NPs and 1 μM NMB were irradiated by means of a red light source and fluorescence changes were observed over time. The behaviour of the nano-probes in solution was poor as compared to the free probes, especially for SOSG-NPs, where the fluorescence enhancement was very mild (Figure 7).
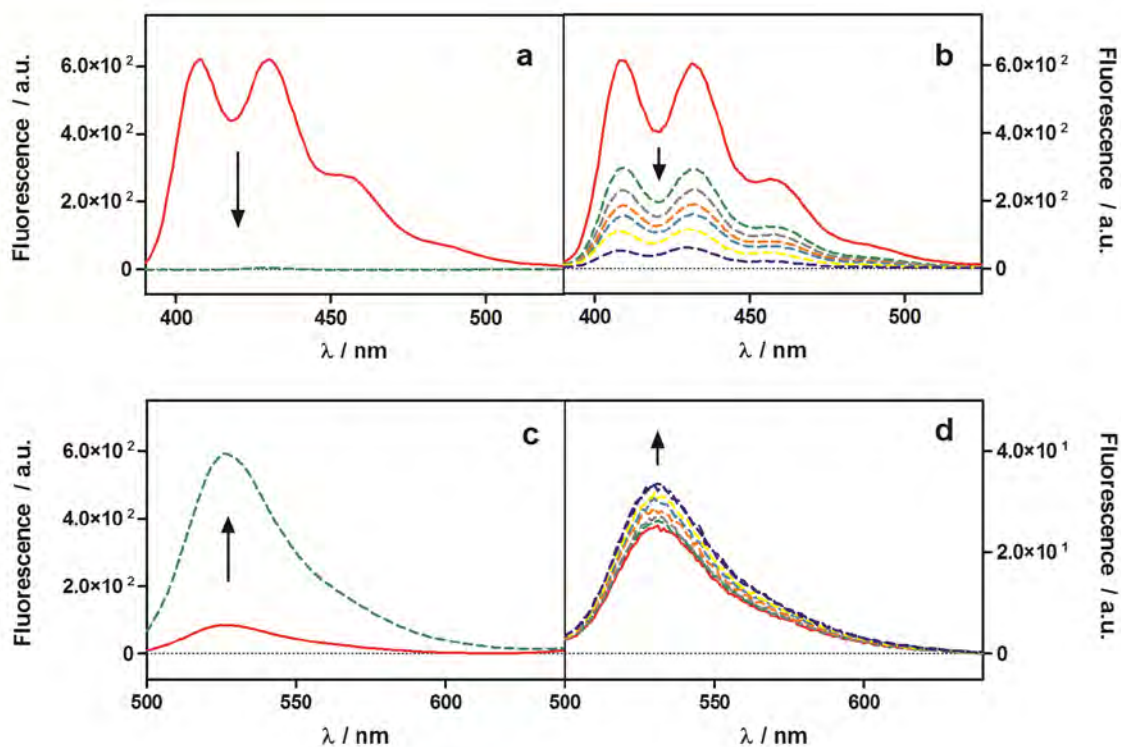
Figure 7. Fluorescence bleaching (a,b) or enhancement (c,d) upon irradiation in the presence of 1 μM of NMB for aqueous solutions of (a) ADPA, (b) ADPA-NPs, (c) SOSG and (d) SOSG-NPs. Solid red line represents basal fluorescence and green dotted line first irradiation time. Extra light doses were given to NP-probe systems to assess their evolution.

The excessive vicinity of the probe to the polyacrylamide matrix could be responsible for the aforementioned low probing efficiency by non-specific interactions of the probe to the NPs. Thus, we decided to include a spacer between the polyacrylamide scaffold and the probe, as can be seen in Scheme 4. In order to be able to include the linker, the polyacrylamide matrix was synthesised exposing alkyl groups in the outer surface so that linkers could be coupled *via* click chemistry. Moreover, all the linkers exposed a terminal amino group allowing them to be bound either to ADPA or SOSG through amide bond.
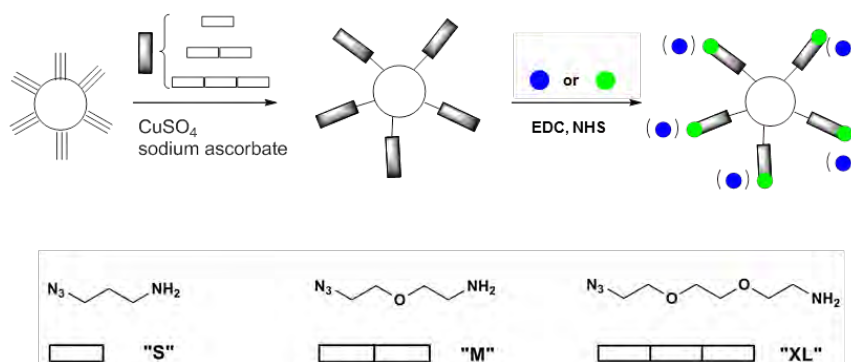
Scheme 4. Rational design of nano-probes including different size linkers between the NP and the probe. Blue dots represent ADPA dye and green dots SOSG.

New scaffolds including linkers of three different lengths were synthesised, characterised and tested in solution, as summarised in Figure 8. For both types of probe, absorption and emission spectra match those of the free probe. In the case of the absorption, a tail in the base line can be seen due to NP scattering. The results in terms of $^1O_2$ sensing are modest and still the free probe outperforms them all. However, for both types of probe, the linker with an intermediate size ("M") seems to provide an acceptable behaviour, at least to serve as a proof of concept of the system. After 10 min irradiation, ADPA-M-NPs were photobleached up to a 90%; and over 95% photobleaching was achieved after 20 min irradiation. For SOSG-M-NPs, a 3.5-fold fluorescence enhancement could be achieved in dPBS and 3-fold when in PBS.
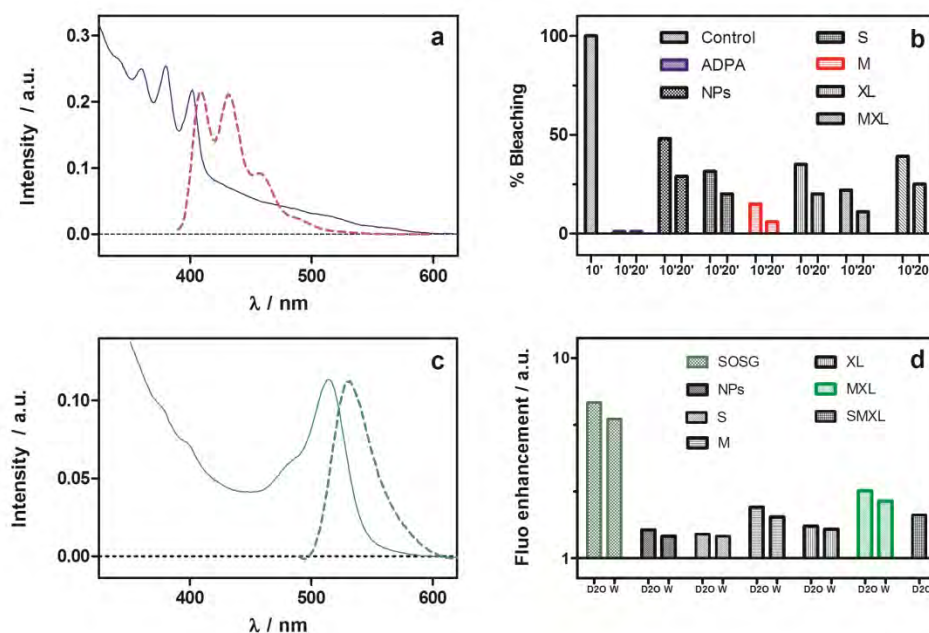
Figure 8. Behaviour in solution of probe-link-NPs. Absorption (solid line) and emission (dashed line) spectra of representative ADPA-M-NP (a) or SOSG-M-NP (c). Probing efficiency in solution of probe-link-NPs was assessed by addition of 1 μM NMB to 1 mg/mL nano-probe solutions and irradiation. ADPA bleaching in % (b) or SOSG fluorescence enhancement (d) was plotted, respectively.

125

In order to discard a problem of inner filter effect due to scattering, solutions of SOSG containing increasing concentrations of plain bare NPs were tested in the presence of 1 μM NMB and irradiated (Figure 9). Our experiment shows that for concentrations below 5 mg/mL SOSG solutions are able to behave almost equally with or without free NPs.
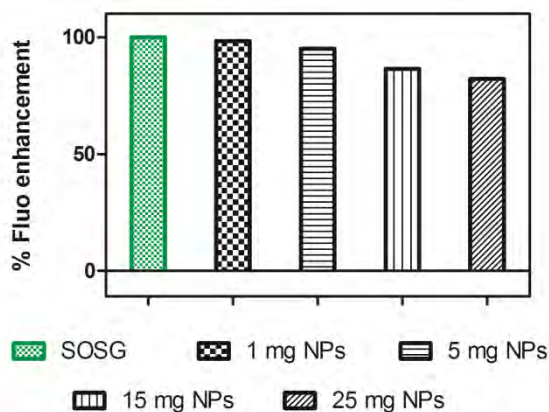
Figure 9. Scattering effect on SOSG conversion.

Once proved the viability of the system, further development was carried out to our best scaffold system: particles with the probe and a medium-size linker (probe-M-NPs). Our next goal was to confer charge to the system so as to be apt to be uptaken by the cells. Two different charged groups were developed: trimethylamoniumbysacrylamide ($-NMe^{3+}$) and trimethylphosphoniumbysacrylamide ($-PMe^{3+}$) and integrated in the system as depicted in Scheme 5. Chemically speaking, the main difference with the previously developed particles is that now the NPs, apart from exhibiting alkyl groups, do also carry the charged functionalised groups. The new particles were characterised and its $^1O_2$ sensing ability resulted comparable to its non-charged analogues.
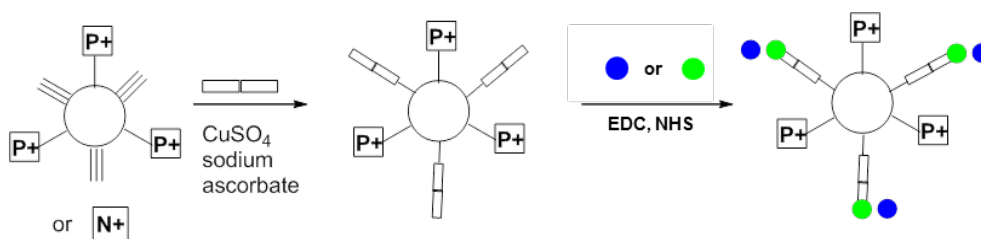
Scheme 5. Rational design of charged nano-probes including the probe and a medium-size linker. Blue dots represent ADPA dye and green dots SOSG.

One of the main problems found in the performance of available probes in living systems is their difficulty to be uptaken by the cells due to interactions with serum proteins.[23] Thus, next stage was to test their behaviour in the presence of bovine serum albumin (BSA). Fluorescence measurements were

registered upon addition of increasing amounts of BSA. In previous reports it has been described that shifts can be observed for SOSG in both absorption and emission spectra in the presence of BSA even at very low concentrations.[23] In contrast, in our system, while partial fluorescence quenching occurs, no fluorescence shifts can be observed as presented in Figure 10. This result seems to point out that interactions of the protein with the nano-probe are minimised, especially for SOSG were even the fluorescence quenching effects are low. Likewise, the efficiency of the probe in the presence of BSA and $^1O_2$ is decreased (data not shown), consistent with the fact that BSA is known to be a good $^1O_2$ quencher.
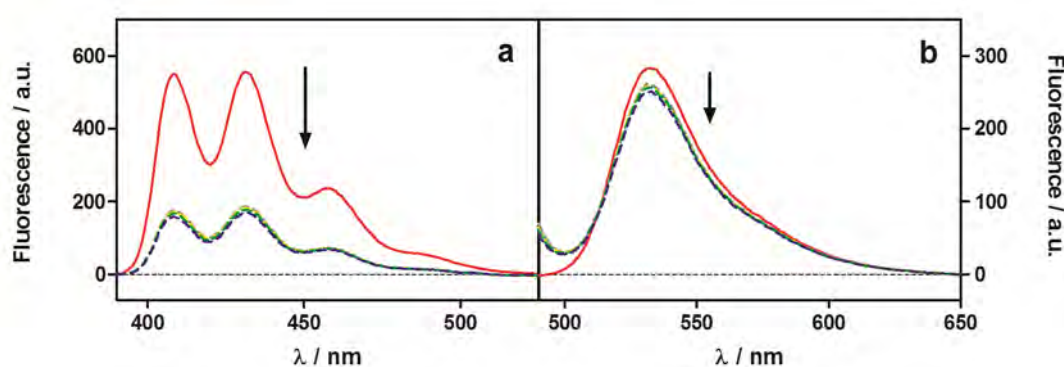
Figure 10. Interaction of probe-link-NPs in the presence of BSA. Figures a and b show fluorescence changes upon addition of BSA up to150 μM to ADPA-M-NPs (a) or SOSG-M-NPs (b).

Another drawback encountered for the $^1O_2$ probes used intracellularly up till now is the difficulty of delivering the probe and the PS to the same subcellular localisation.[14] Taking advantage of the versatility of our system, a new class of nano-probes was designed and synthesised including both the $^1O_2$ probe and the PS, as schematised in Scheme 6.
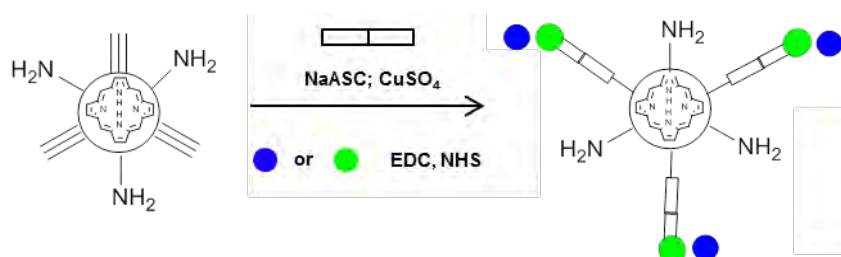
Scheme 6. Rational design of porphyrin-containing NPs including the probe and a medium size linker.

A zinc porphyrin polymerised within the polyacrylamide matrix was chosen as model PS. In Figure 11 it can be observed the absorption and emission resulting from the new constructs.
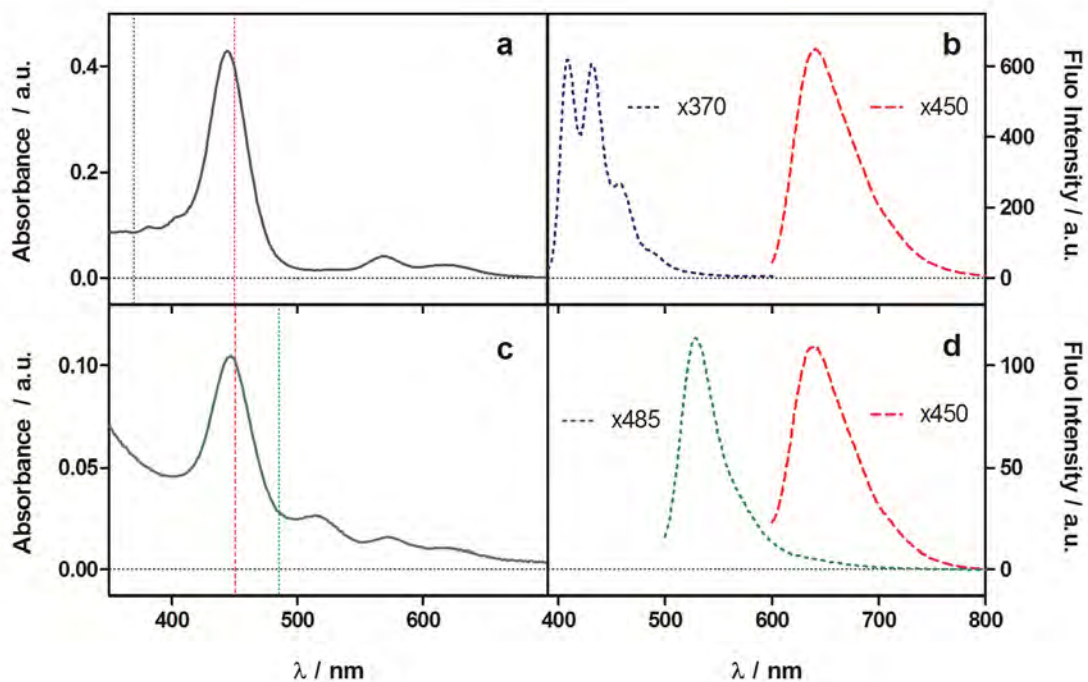
Figure 11. Behaviour in solution of porphyrin loaded probe-link-NPs. Absorption (a,c) and fluorescence (b,d) spectra for the ADPA systems (a,b) or SOSG systems (c,d). Dotted lines correspond to probe fluorescence and dashed lines to porphyrin fluorescence.

Apart from the majority porphyrin absorption bands, shoulders corresponding either to ADPA or SOSG can also be observed, respectively. More interestingly, in both cases the fluorescence from both the porphyrin and the probe is sufficiently well separated. That will confer an extra aid in terms of fluorescence detection intracellularly as fluorescence colocalisation will be possible. Regarding its sensing behaviour, it is even more modest than for the previous system. Comparison between the behaviour of the NPs with and without porphyrin is depicted in Figure 12.
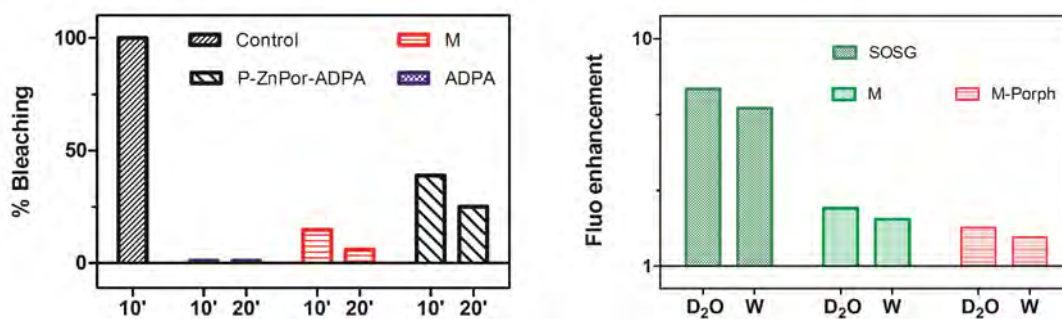
Figure 12. Probing behaviour in solution of porphyrin loaded probe-link-NPs upon irradiation.

DISCUSSION

In order to assess the potential of the polyacrylamide as a scaffold for the development of $^1O_2$ probes for its use in intracellular systems, several items have been studied and are worth of further comments.

One of the requirements to meet for a potential scaffold is versatility. As our final goal was to obtain a general platform able to perform inside a cell independently of the probing molecule, we chose two commercial $^1O_2$ probes, fairly different in mode of action. ADPA is a water-soluble anthracene derivative that in the presence of $^1O_2$ undergoes an endoperoxidation that results in a decrease of both its absorbance and fluorescence.[11,53] On the other hand, SOSG is a dyad composed by a fluorescein moiety whose fluorescence is quenched by photoinduced intramolecular electron transfer due to the presence of a near covalently bound anthracene moiety. In the presence of $^1O_2$, the anthracene suffers an endoperoxidation and, as a result, the electron transfer is blocked leading to great fluorescence enhancement.[23] Chemically speaking, both probes are acidic salts that under proper activation can readily react with amino groups. This is the reason why all the NPs developed presented amino groups either directly on the surface or throughout the linker. Coupling through an amide bond is a fairly straightforward reaction and high yields of reaction were obtained. Moreover, amino derivatisation was easily achieved. When required on the surface, commercial amino-bisacrylamide was used; when needed detached from the surface, linkers were directly connected via click chemistry.

The second requirement is, of course, that the system should work. This was first tested in solution. In the first approach, with the probes readily attached to the NP surface, results were unfruitful and very modest conversion rates were obtained as compared to the virgin probe. Incorporation of spacers of different length improved substantially the result. However, no clear correlation between linker length and probing efficiency was found. For both compounds the medium-size linker NPs performed more efficiently. NPs composed of mixed linkers of different lengths were also synthesised and tested, but without improving the general outcome.

Biocompatibility with living systems is another must. As previously mentioned, one of the main problems dealing with regular $^1O_2$ probes is that they have not been envisaged to act in intracellular systems and many fail due to toxicity, biocompatibility or difficulties in uptake. For instance, SOSG has been proved hard to be internalised in HeLa cells cultures when administered in whole media (including

129

serum proteins). One of the advantages of our system is that NPs presented minimised interaction in the presence of BSA. While still partial fluorescence quenching occurs, no spectral changes arise. Thus, administration and uptake in whole medium has been proven feasible (preliminary results, Figure 13). Cationicity has been shown necessary for polyacrylamide systems to be internalised. Thus, two different cationic groups have been designed and added to the system from the NP synthesis. Thankfully, the incorporation of these groups on the surface of the NP did not affect the global performance of the NPs. Once again, this result elicits more versatility on the system since different subcellular localisations can be targeted.

One of the most interesting approaches developed on the system is the incorporation of both the probe and a reference PS. One of the main problems in detecting $^{1}O_{2}$ is the difficulty to achieve that the probe is present just in the loci where $^{1}O_{2}$ is being produced. By incorporating a porphyrin in the matrix of the NP this problem is overcome. Moreover, dual fluorescent localisation is displayed since porphyrin and probe fluorescent spectra are fairly well separated. It is true that performance in cuvette has proven less efficient that their analogues without porphyrin. However, the PS' concentration loaded in the construct is minor to that of the experiments performed in cuvette. Still we could observe enhancement and the system is closer to reality when administered in cells. Further data has not been provided, but preliminary experiments (Figure 13) show that NPs loaded both with probe and PS are uptaken and colocalisation occurs. Next stage will be to assess the performance upon generation of $^{1}O_{2}$.
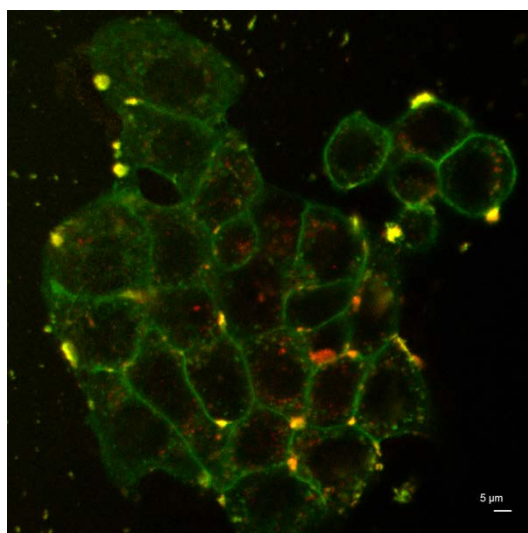
Figure 13. Confocal merged image of HT-29 cells incubated for 18 h with NP-M-SOSG-Porph (2 mg/mL in whole medium). Plasma membranes were stained with Cell Mask Deep Red (5 min; 5 mg/mL; green). Little red dots inside the green circles indicate that smaller NPs have been taken in. Some NPS are aggregated at the surface of the membrane (big red blobs). Big yellowish bright blobs correspond to artifact from the laser light going through both membrane and aggregate. FITC set up (488 nm Ar laser) and Alexa Fluor set up (633 nm HeNe laser).

CONCLUSIONS

In summary, we have designed, synthesised and preliminary proven a multifunctional biodegradable polyacrylamide NP scaffold for $^1O_2$ detection inside cellular systems. By a combination of two different commercial $^1O_2$ chemical probes linked to the polyacrylamide nanocore we obtain an interesting approach to achieving intracellular $^1O_2$ ratiometric measurements. Modification of the polyacrylamide matrix with linkers of different length between the core and the probe enabled changes in sensing response towards $^1O_2$. Moreover, the NP scaffold hampered the interactions between the hydrophobic probes and BSA thus proving minimised efficiency losses when in a cell-like environment. Best candidate positively charged NPs incorporating either SOSG or ADPA were successfully uptaken by cells without appreciable dark toxicity and localisation assessed by the probe basal fluorescence. NPs incorporating a porphyrin PS in the polyacrylamide matrix were also tested and demonstrated both a better colocalisation and the possibility to generate $^1O_2$ *in situ*. Even though the best candidates are far from ideal, we believe the described platform is endowed with potential features to soon become the reference system for intracellular $^1O_2$ measurement.

SPECIFIC EXPERIMENTAL SECTION

Materials.

Chemicals: Acrylamide (99% minimum), ammonium persulsufate, dioctyl sulfosuccinate sodium salt and N,N,N,N-tetramethylethylenediamine were purchased from Sigma-Aldrich. N,N'methylenebis(acrylamide) and Brij 30® were obtained from Fluka Analytical. 1-(3-dimethylaminopropyl)-3-ethylcarbodiimide hydrochloride (EDC) and N-hydroxysuccinimide (NHS) were purchased from Alfa Aesar. Hexane HPLC grade and ethanol analytical grade were obtained from Fisher Scientific. SOSG was purchased from Invitrogen. ADPA was supplied by Chemodex.

Methods.

Synthesis of polyacrylamide NPs: Amino functionalised NPs were synthesised by adopting the free radical microemulsion polymerisation procedure optimised by Chauhan *et al.*[38] Briefly, a final volume of 1.9 mL containing acrylamide (540 mg, 7.60 mmol), N,N-methylenebisacrylamide (150 mg, 1.04 mmol) and N-(3-aminopropyl)methacrylamide hydrochloride (10 mg; mmol; 1% equivalence to acrylamide) in water (1.7 mL) was added to a deoxygenated hexane (42 mL) solution containing Brij 30 (3.08 g, 8.49 mmol) and completely dissolved dioctyl sulfosuccinate sodium salt (1.59 g, 3.58 mmol). To this solution 30 μL of ammonium persulfate (0.4 μmol) in water and 15 μL N,N,N,N-tetramethylethylenediamine (0.1 μmol) were added and the mixture stirred for 2 h under a positive argon pressure at rt. Excess hexane was removed *in vacuo*. The resulting viscous yellow colored solid was washed with ethanol, centrifuged (8 x 50 mL, 10 min, 4500 rpm) and recovered by microfiltration (Whatman Anodisc 25, 0.02 μm, 25 mm filters) to yield the desired NPs. Yield: 86% (602 mg).

To synthesise alkyl functionalised NPs, the above synthesis procedure was followed with the exception of addition of N-(pent-4-yn-1-yl)methacrylamide instead of N-(3-aminopropyl)methacrylamide. To synthesise charged alkyl functionalised NPs, the above synthesis procedure was followed with the exception of extra addition of trimethylamoniumbysacrylamide or trimethylphosphoniumbysacrylamide together with the rest of the acrylamide monomers.

Linker synthesis: (2-azidoethoxy)methanamine hydrochloride (medium linker; "M") and 2-(2-(2-azidoethoxy)ethoxy)ethanamine hydrochloride (large linker; "XL") were synthesised following protocols described in references [54,55]. Short description for "XL" is explained as example. To a stirred solution of tert-butyl (2-(2-(2-aminoethoxy)ethoxy)ethyl)carbamate (10 mmol) in MeOH (50 mL) was added copper (II) sulphate (1 mg), and anhydrous potassium carbonate (2.5 g; 12 mmol) was added, and the mixture

stirred at rt for 24 h . The solvent was removed under reduced pressure and the product purified via column chromatography (1% MeOH: DCM) to yield tert-butyl (2-(2-(2-azidoethoxy)ethoxy)ethyl)carbamate as a colourless oil (2.37 g, 87 %). The obtained product was dissolved in 20 mL ethyl acetate and 10 mL HCl in dioxane were added and the reaction mixture stirred at rt for another 24 h. The solvent was removed under reduced pressure, and the residue washed with diethyl ether yielding "XL". 3-azidopropan-1-amine (Small linker; "S") was synthesised according to reference [56]. Commercially available Boc-propanolamine was converted to the mesylate, which then smoothly underwent direct substitution with sodium azide to give the Boc-protected azide. Removal of the amine protecting group under standard anhydrous conditions gave the azidoethylamine as the hydrochloride salt.

Coupling and purification: coupling between carboxylic dyes and amino groups were performed by standard protocols. Namely, dye-carboxylate was activated for 30 min upon addition of 1 EDC and NHS *per* mg dye followed by addition of the amino-NPs (20 mg in 2 mL NaHCO$_3$). Stirring of the mixture was allowed overnight and dye-NPs were collected after running of the sample through a 8 .3 mL Shepadex PD-10 desalting columns (GE Healthcare) and precipitation in cold ethanol. Coupling of the linker to the NP was achieved using standard click chemistry protocol.[57] Namely, a mixture of the alkyne-NPs, the azide linker (2 equiv.), sodium ascorbate (0.2 equiv.) and copper sulphate (0.2 equiv.) was stirred for 8 hours and subsequently recovered after Shepadex column purification.

Porphyrin: 5-{4-[3-(2-methylpropenamido)propylamino]thiocarbonylamino]phenyl}-10,15,20-tris-[4-(methylpyridinium)-yl]-porphyrinato zinc (II) trichloride was kindly provided by Francesca Giuntini.

NPs characterisation: particle size and size distribution properties of the NPs were measured by PCS, Zetaplus particle size analyzer (Malvern 3000) at 25 ºC and at a scattering angle of 90º. A dilute sample of 1 mg/mL NPs was prepared in Milli-Q water, sonicated for 30 s and filtered (Millex GP, 0.22 μm filter unit) before analysis. The value was recorded as the average of 30 data measurements. Porphyrin and dye loading was quantified using the Beer-Lambert law .

REFERENCES

1. Nonell, S.; Braslavsky, S. E. In *Time-resolved singlet oxygen detection;* Methods in enzymology; Academic Press INC: San Diego; San Diego, CA 92101-4495 USA, 2000; Vol. 319, pp 37-49.

2. Ogilby, P. R. Singlet oxygen: there is indeed something new under the sun. *Chem. Soc. Rev.* **2010**, *39*, 3181-3209.

3. Schweitzer, C.; Schmidt, R. Physical mechanisms of generation and deactivation of singlet oxygen. *Chem. Rev.* **2003**, *103*, 1685-1758.

4. Montaña, M. P.; Massad, W. A.; Amat-Guerri, F.; García, N. A. Scavenging of riboflavin-photogenerated oxidative species by uric acid, xanthine or hypoxanthine: A kinetic study. *J. Photochem. Photobiol. A.* **2008**, *193*, 103-109.

5. Rabello, B. R.; Gerola, A. P.; Pellosi, D. S.; Tessaro, A. L.; Aparício, J. L.; Caetano, W.; Hioka, N. Singlet oxygen dosimetry using uric acid as a chemical probe: Systematic evaluation. *J. Photochem. Photobiol. A.* **2012**, *238*, 53-62.

6. Ammann, E. C.; Lynch, V. H. Purine metabolism by unicellular algae. 3. The photochemical degradation of uric acid by chlorophyll. *Biochim. Biophys. Acta* **1966**, *120*, 181-182.

7. He, Y.; Xing, D.; Yan, G.; Ueda, K. FCLA chemiluminescence from sonodynamic action in vitro and in vivo. *Cancer Lett.* **2002**, *182*, 141-5.

8. Zhu, D. B.; Xing, D.; Wei, Y. D.; Li, X.; Gao, B. Evaluation of the degree of medical radiation damage with a highly sensitive chemiluminescence method. *Luminescence* **2004**, *19*, 278-282.

9. Li, X. H.; Zhang, G. X.; Ma, H. M.; Zhang, D. Q.; Li, J.; Zhu, D. B. 4,5-Dimethylthio-4'-[2-(9-anthryloxy)ethylthio]tetrathiafulvalene, a highly selective and sensitive chemiluminescence probe for singlet oxygen. *J. Am. Chem. Soc.* **2004**, *126*, 11543-11548.

10. MacManus-Spencer, L. A.; Latch, D. E.; Kroncke, K. M.; McNeill, K. Stable dioxetane precursors as selective trap-and-trigger chemiluminescent probes for singlet oxygen. *Anal. Chem.* **2005**, *77*, 1200-1205.

11. Gandin, E.; Lion, Y.; Van de Vorst, A. Quantum yield of singlet oxygen production by xanthene derivatives. *Photochem. Photobiol.* **1983**, *37*, 271-278.

12. Zhang, J.; Sarrafpour, S.; Pawle, R. H.; Thomas, S. W.,3rd Acene-linked conjugated polymers with ratiometric fluorescent response to 1O2. *Chem. Commun.* **2011**, *47*, 3445-3447.

13. Oliveira, M. S.; Severino, D.; Prado, F. M.; Angeli, J. P.; Motta, F. D.; Baptista, M. S.; Medeiros, M. H.; Di Mascio, P. Singlet molecular oxygen trapping by the fluorescent probe diethyl-3,3'-(9,10-anthracenediyl)bisacrylate synthesized by the Heck reaction. *Photochem. Photobiol. Sci.* **2011**, *10*, 1546-1555.

14. Kessel, D.; Price, M. Evaluation of diethyl-3-3'-(9,10-anthracenediyl)bis acrylate as a probe for singlet oxygen formation during photodynamic therapy. *Photochem. Photobiol.* **2012**, *88*, 717-720.

15. Rota, C.; Chignell, C. F.; Mason, R. P. Evidence for free radical formation during the oxidation of 2'-7'-dichlorofluorescin to the fluorescent dye 2'-7'-dichlorofluorescein by horseradish peroxidase: possible implications for oxidative stress measurements. *Free Radic. Biol. Med.* **1999**, *27*, 873-881.

16. Tanaka, K.; Miura, T.; Umezawa, N.; Urano, Y.; Kikuchi, K.; Higuchi, T.; Nagano, T. Rational design of fluorescein-based fluorescence probes. Mechanism-based design of a maximum fluorescence probe for singlet oxygen. *J. Am. Chem. Soc.* **2001**, *123*, 2530-2536.

17. Miura, T.; Urano, Y.; Tanaka, K.; Nagano, T.; Ohkubo, K.; Fukuzumi, S. Rational design principle for modulating fluorescence properties of fluorescein-based probes by photoinduced electron transfer. *J. Am. Chem. Soc.* **2003**, *125*, 8666-8671.

18. Urano, Y.; Kamiya, M.; Kanda, K.; Ueno, T.; Hirose, K.; Nagano, T. Evolution of fluorescein as a platform for finely tunable fluorescence probes. *J. Am. Chem. Soc.* **2005**, *127*, 4888-4894.

19. Umezawa, N.; Tanaka, K.; Urano, Y.; Kikuchi, K.; Higuchi, T.; Nagano, T. Novel fluorescent probes for singlet oxygen. *Angew. Chem. Int. Ed. Engl.* **1999**, *38*, 2899-2901.

20. Song, B.; Wang, G.; Tan, M.; Yuan, J. A europium(III) complex as an efficient singlet oxygen luminescence probe. *J. Am. Chem. Soc.* **2006**, *128*, 13442-13450.

21. Invitrogen - Molecular Probes Singlet Oxygen Sensor Green Reagent. *http://probes.invitrogen.com/media/pis/mp36002.pdf;* (accessed 18/03, 2013).

22. Xu, K.; Wang, L.; Qiang, M.; Wang, L.; Li, P.; Tang, B. A selective near-infrared fluorescent probe for singlet oxygen in living cells. *Chem. Commun.* **2011**, *47*, 7386-7388.

23. Gollmer, A.; Arnbjerg, J.; Blaikie, F. H.; Pedersen, B. W.; Breitenbach, T.; Daasbjerg, K.; Glasius, M.; Ogilby, P. R. Singlet Oxygen Sensor Green(R): photochemical behavior in solution and in a mammalian cell. *Photochem. Photobiol.* **2011**, *87*, 671-679.

24. Ragàs, X.; Jiménez-Banzo, A.; Sanchez-Garcia, D.; Batllori, X.; Nonell, S. Singlet oxygen photosensitisation by the fluorescent probe Singlet Oxygen Sensor Green (R). *Chem. Commun.* **2009**, *20*, 2920-2922.

25. Arian, D.; Kovbasyuk, L.; Mokhir, A. 1,9-Dialkoxyanthracene as a O-1(2)-sensitive linker. *J. Am. Chem. Soc.* **2011**, *133*, 3972-3980.

26. Lindig, B. A.; Rodgers, M. A. J.; Schaap, A. P. Determination of the lifetime of singlet oxygen in water-d2 using 9,10-anthracenedipropionic acid, a water-soluble probe. *J. Am. Chem. Soc.* **1980**, *102*, 5590-5593.

27. Castellano, F. N.; Lakowicz, J. R. A water-soluble luminescence oxygen sensor. *Photochem. Photobiol.* **1998**, *67*, 179-183.

28. Kuimova, M. K.; Botchway, S. W.; Parker, A. W.; Balaz, M.; Collins, H. A.; Anderson, H. L.; Suhling, K.; Ogilby, P. R. Imaging intracellular viscosity of a single cell during photoinduced cell death. *Nature Chemistry* **2009**, *1*, 69-73.

29. Zebger, I.; Snyder, J. W.; Andersen, L. K.; Poulsen, L.; Gao, Z.; Lambert, J. D. C.; Kristiansen, U.; Ogilby, P. R. Direct optical detection of singlet oxygen from a single cell. *Photochem. Photobiol.* **2004**, *79*, 319-322.

30. Snyder, J. W.; Skovsen, E.; Lambert, J. D. C.; Ogilby, P. R. Subcellular, time-resolved studies of singlet oxygen in single cells. *J. Am. Chem. Soc.* **2005**, *127*, 14558-14559.

31. Snyder, J. W.; Skovsen, E.; Lambert, J. D. C.; Poulsen, L.; Ogilby, P. R. Optical detection of singlet oxygen from single cells. *Phys.Chem.Chem.Phys.* **2006**, *8*, 4280-4293.

32. Bechet, D.; Couleaud, P.; Frochot, C.; Viriot, M. L.; Guillemin, F.; Barberi-Heyob, M. Nanoparticles as vehicles for delivery of photodynamic therapy agents. *Trends Biotechnol.* **2008**, *26*, 612-621.

33. Cho, K.; Wang, X.; Nie, S.; Chen, Z.; Shin, D. M. Therapeutic nanoparticles for drug delivery in cancer. *Clin. Cancer Res.* **2008**, *14*, 1310-1316.

34. Janib, S. M.; Moses, A. S.; MacKay, J. A. Imaging and drug delivery using theranostic nanoparticles. *Adv. Drug Deliv. Rev.* **2010**, *62*, 1052-1063.

35. Koo Lee, Y.; Smith, R.; Kopelman, R. Nanoparticle PEBBLE sensors in live cells and in vivo. *Annual Review of Analytical Chemistry* **2009**, *2*, 57-76.

36. Uusitalo, L. M.; Hempel, N. Recent advances in intracellular and in vivo ROS sensing: focus on nanoparticle and nanotube applications. *Int. J. Mol. Sci.* **2012**, *13*, 10660-10679.

37. Ruedas-Rama, M. J.; Walters, J. D.; Orte, A.; Hall, E. A. H. Fluorescent nanoparticles for intracellular sensing: A review. *Anal. Chim. Acta* **2012**, *751*, 1-23.

135

38. Chauhan, V. M.; Burnett, G. R.; Aylott, J. W. Dual-fluorophore ratiometric pH nanosensor with tuneable pKa and extended dynamic range. *Analyst* **2011**, *136*, 1799-1801.

39. Kuruppuarachchi, M.; Savoie, H.; Lowry, A.; Alonso, C.; Boyle, R. W. Polyacrylamide nanoparticles as a delivery system in photodynamic therapy. *Mol. Pharm.* **2011**, *8*, 920-931.

40. Wang, S.; Kim, G.; Lee, Y. K.; Hah, H. J.; Ethirajan, M.; Pandey, R. K.; Kopelman, R. Multifunctional biodegradable polyacrylamide nanocarriers for cancer theranostics--A see and treat strategy. *ACS Nano* **2012**, *6*, 6843-6851.

41. Steinbeck, M. J.; Khan, A. U.; Karnovsky, M. J. Intracellular singlet oxygen generation by phagocytosing neutrophils in response to particles coated with a chemical trap. *Journal of Biological Chemistry* **1992**, *267*, 13425-13433.

42. Cao, Y.; Koo, Y. E.; Koo, S. M.; Kopelman, R. Ratiometric singlet oxygen nano-optodes and their use for monitoring photodynamic therapy nanoplatforms. *Photochem. Photobiol.* **2005**, *81*, 1489-1498.

43. Mac, M.; Tokarczyk, B.; Uchacz, T.; Danel, A. Charge transfer fluorescence of benzoxazol derivatives investigation of solvent effect on fluorescence of these dyes. *J. Photochem. Photobiol. A* **2007**, *191*, 32-41.

44. Machado, A. E. d. H.; de Miranda, J.; Guilardi, S.; Nicodem, D.; Severino, D. Photophysics and spectroscopic properties of 3-benzoxazol-2-yl-chromen-2-one. *Spectrochimica acta.Part A, Molecular and biomolecular spectroscopy* **2003**, *59*, 345-55.

45. Fayed, T. Probing of micellar and biological systems using 2-(p-dimethylaminostyryl)benzoxazole - An intramolecular charge transfer fluorescent probe. *Colloid Surf. , A* **2004**, *236*, 171-177.

46. Foote, C. S.; Wuesthof, M.; Wexler, S.; Burstain, I. G.; Denny, R. Photosensitized oxygenation of alkyl-substituted furans. *Tetrahedron* **1967**, *23*, 2583.

47. Frimer, A. A. The reaction of singlet oxygen with olefins: the question of mechanism. *Chem. Rev.* **1979**, *79*, 359-387.

48. Marinkovic, S.; Brule, C.; Hoffmann, N.; Prost, E.; Nuzillard, J. M.; Bulach, W. Origin of chiral induction in radical reactions with the diastereoisomers (5R)- and (5S)-5-l-menthyloxyfuran-2[5H]-one. *J. Org. Chem.* **2004**, *69*, 1646-1651.

49. Jiménez-Banzo, A.; Ragàs, X.; Kapusta, P.; Nonell, S. Time-resolved methods in biophysics. 7. Photon counting vs. analog time-resolved singlet oxygen phosphorescence detection. *Photochem. Photobiol. Sci.* **2008**, *7*, 1003-1010.

50. Redmond, R. W.; Gamlin, J. N. A compilation of singlet oxygen yields from biologically relevant molecules. *Photochem. Photobiol.* **1999**, *70*, 391-475.

51. Montalti, M.; Credi, A.; Prodi, L.; M.T, G. *Handbook of photochemistry;* CRC Press: 2006; .

52. Wilkinson, F.; Helman, W. P.; Ross, A. B. Rate constants for the decay and reactions of the lowest electronically excited singlet state of molecular oxygen in solution. An expanded and revised compilation. *J. Phys. Chem. Ref. Data* **1995**, *24*, 663-677.

53. Hoebeke, M.; Damoiseau, X. Determination of the singlet oxygen quantum yield of bacteriochlorin a: a comparative study in phosphate buffer and aqueous dispersion of dimiristoyl-L-alpha-phosphatidylcholine liposomes. *Photochem. Photobiol. Sci.* **2002**, *1*, 283-287.

54. Shimokawa, K.; Yamada, K.; Ohno, O.; Oba, Y.; Uemura, D. Design, synthesis, and biological evaluation of biotin-labeled (-)-ternatin, a potent fat-accumulation inhibitor against 3T3-L1 adipocytes. *Bioorg. Med. Chem. Lett.* **2009**, *19*, 92-95.

55. Azagarsamy, M. A.; Yesilyurt, V.; Thayumanavan, S. Disassembly of dendritic micellar containers due to protein binding. *J. Am. Chem. Soc.* **2010**, *132*, 4550-+.

56. Howell, L. A.; Howman, A.; O'Connell, M. A.; Mueller, A.; Searcey, M. Synthesis and evaluation of 9-aminoacridines derived from benzyne click chemistry. *Bioorg. Med. Chem. Lett.* **2009**, *19*, 5880-5883.

57. Kolb, H.; Finn, M.; Sharpless, K. Click chemistry: Diverse chemical function from a few good reactions. *Angewandte Chemie (International ed.)* **2001**, *40*, 2004.

Chapter V.

General Discussion and Outlook

"There must be no barriers to freedom of inquiry.

There is no place for dogma in science.

The scientist is free, and must be free to ask any question,

to doubt any assertion, to seek for any evidence, to correct any errors."

- Robert Oppenheimer

GENERAL DISCUSSION & OUTLOOK

Getting involved in a PhD has made me grow as a scientist and as a person. And not only scientific knowledge has been gained. I find it important to share a couple of thoughts I have obtained throughout my PhD thesis.

Firstly, the realisation of how small we are as compared to science and the scientific world. One has only two hands and a finite time to dig in the infinite vineyard that is science. Reading every Monday over the discoveries in the field –and science in general- has helped me to start every week both enthusiastic about thrilling science and also with the feeling that I am late and at times obsolete in my research. And that tells you the more you think you know, the more humble you must be.

I would like to add a second reflection concerning science in general. After my first research stay in Edinburgh I learnt that science is a lonely world. But it is not only loneliness; it also has to do with frustration and getting stuck many times. Feeling stupid, even. Fortunately to me, a summer later in Hull, I got to read the amazing reading "*The importance of stupidity in scientific research*".[1] I found it utterly revealing and encouraging. At times we forget we have to muddle through a field where we do not have insight. But nobody has insight and that's why it is science research!!

> *"I remember the day when Henry Taube (who won the Nobel Prize two years later) told me he didn't know how to solve the problem I was having in his area. I was a third-year graduate student and I figured that Taube knew about 1000 times more than I did (conservative estimate). If he didn't have the answer, nobody did. That's when it hit me: nobody did. That's why it was a research problem. And being my research problem, it was up to me to solve."*

Focusing, now it's time to shift discussion towards scientific matters. After three lovely years devoted to singlet oxygen, its detection and its application in antimicrobial photodynamic therapy, what have I learn out of it? My first reflection goes towards "classical aPDT", may I call it that way. With this term, I recall the cyclic concept of 1) designing and synthesising the "miracle" PS that will likely solve the problem of antibiotic resistance and outperform all previous last-resort drugs or PSs. 2) Measuring its

138

photophysics in cuvette and its photokilling efficiency in bacterial cultures. 3) Realising it is another PS as good as the others but nothing especially new. Evolution towards 3rd generation PSs, as for me, represents an opportunity to better understand the processes of antimicrobial killing trough the photodynamic effect and unraveling key factors that would allow aPDT as a regular tool in our medical repertoire. But I believe we should be careful in thinking we are getting closer to the "Holy Grail PS". This idea became clear to me in the last congress of the ESP I attended in Geneve (September 2011). Most studies regarding photodynamic inactivation were pretty similar to mine, even though different families of classy PSs with several degrees of complexity were used. Our cationic porphycenes were as good as the rest. However, what I could appreciate is that there was an upcoming shift in direction. Instead of looking for a new drug candidate, "old-fashioned" 2nd generation PSs were being used (or "recycled" somehow) as disinfectant agents in waters in conjunction with white light, to treat malaria, fungi or other parasites where little had been previously done (and thus becoming cool for publication) or to ascertain the relationships of photodynamic effect and immune system. The results obtained in the Chapter III section "cationic PSs as 3rd generation PSs" points out the previous statement. Out of the 6 tested compounds, nice results have been achieved with at least 4 of them, even though they varied in the family of PS, the number of charges and probably in the subcellular localisation. However, little has been improved since first approaches with cationic phenothiazine or porphyrins PSs in terms of photodynamic efficiency.[2,3] Rather, further and more thorough rationalisation regarding charge effects should be undergone, since little focus have been gained in recent years and shallow studies have been performed.[4,5] Out of our 4 good candidates two were tricationic, one tetracationic and one octacationic. Still, big differences among them make it hard to canalize the feasibility of the comparison. Especially regarding mechanistic issues as important limitations are found as far as the PS is delivered externally.

Despite the previous reflections, I believe "classical aPDT" is far from death, but it needs a shift in direction. And one gap looks clear to me: biofilms. If one consults the number of scientific publications resulting from the search "antimicrobial photodynamic therapy" in PUBMED (http://www.ncbi.nlm.nih.gov/pubmed) and compares it with the same search for "microbial biofilms" the result goes as follows:

139
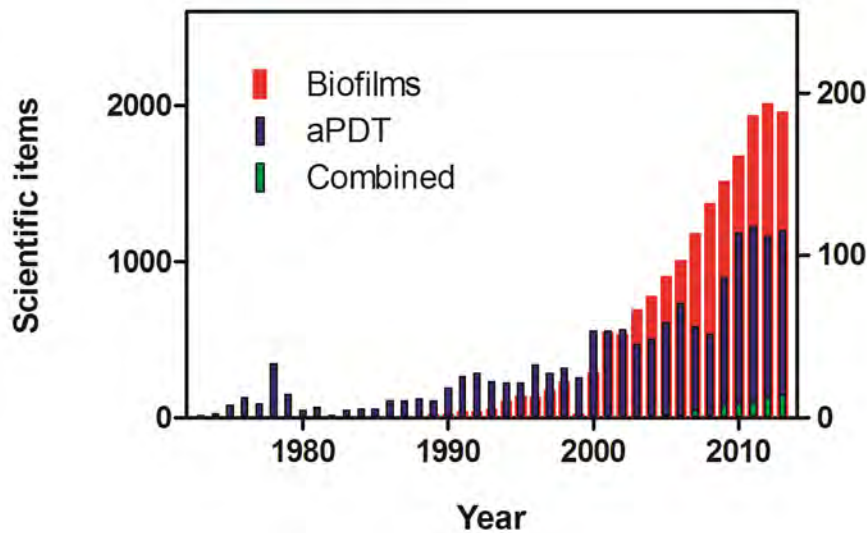
Figure 1. Evolution on scientific publications on "microbial biofilms" (red; left ordinate axis) and "antimicrobial photodynamic therapy" (blue; rightt ordinate axis) and combined topics (green) over the last 40 years. Publications for 2013 have been extrapolated from results up to date and trend.

While both topics seem to be hot spots, if one goes for a combined search of both topics, the result obtained is as surprising as 57 results altogether!! Biofilms have gained a lot of attention since our understanding and the techniques have let us gain a lot of insight in the complex architecture that bacteria build-up in different niches.[6,7] It was previously believed that a single virulence factor sufficiently mediated disease caused by a single organism. While true in some cases, many diseases can no longer be defined as an infection by a single species. And here we include diseases of the oral cavity, otitis media, diabetic foot wound infections, and chronic infection in the cystic fibrosis lung. In these cases, the composition of microbial populations predicts both disease severity and outcome.[8] Thus, if aPDT is meant to go for gold, further aPDT-mediated studies should be addressed. Almost twenty years ago Roberto Kolter (one of the popes on biofilms) saw clear it was about time to move from bacterial cultures to biofilms;[9] now it is time for aPDT to move onwards.

"However, things changed for me in 1994 when, noticing my depressed state, members of my laboratory gave me a fish tank in an effort to draw me out of the blues. As I sat locked-up in the office staring at the tank, I realized that by studying shaken cultures of E. coli I had been barking up the wrong tree. The water in the fish tank remained crystal clear, it was on the surfaces where most microbial activity was occurring."

Introduction of Chapter III intended to offer the reader some background on the approach of AMPs and bacteriocins as possible helpers in the fight against bad bugs. From the outside and within, we are constantly bombarded with a myriad of diverse microbial species. Fortunately, our bodies are equipped with an evolutionarily conserved innate immune defence system that allows us to thwart potential pathogens. AMPs are a unique and assorted group of molecules produced by living organisms of all types, considered to be part of the host innate immunity. These peptides demonstrate potent antimicrobial activity and are rapidly mobilised to neutralize a broad range of microbes, including viruses, bacteria, protozoa, and fungi.[10] Thus, the idea of combining the use of PSs with AMPs in order to seek for a synergistic effect looks promising. In spite of the encouraging results obtained, further studies are necessary: new conjugates assaying other AMPs (magainin, bufforin, etc.), going to animal models (for instance to check if AMPs are degraded before getting to the target) and, importantly, controls in mammalian cells. Recent reports have shown that small modification of AMPs can result in targeting to mammalian cells,[11] fact that could lead to undesired properties for our candidates. Another issue to bear in mind is that conjugation of the PS with other entities sometimes results in loss of efficiency.

Definitely, to me, the approach that employs FPs as genetically-encoded PSs results the most promising and the most elegant of all. What better than a PS that can be built by the bacteria itself with its own machinery. Whenever I come to think of it, it reminds me the idea of a Trojan Horse. Giving bacteria plasmids encoding for tasty FP, letting them grow, making them glow to observe where they are and finally sheding light to kill them or exert localised damage at will!

The beauty of using FPs that are able to generate sufficient amounts of $^1O_2$ is multiple. First, localisation issues: by properly tailoring a plasmid we are able –on paper- to target any protein (and thus any part) of the cell by fusing our FP-gene to that of the protein of interest. Second, tracking issues: FPs are –as their name indicates- fluorescent. And we can take advantage of the property to check the feasibility of the construct and even the life of the protein. Finally, being able to generate $^1O_2$ opens the door to a plethora of unprecedented opportunities. We can finely tune the amount of $^1O_2$ we need to provoke cell death (addressing dosimetry issues, key in clinical success), we can damage selectively a fused protein, we can compare the damage at different *loci* (thus going to selectivity issues) or we can improve the development of probes that can perform in intracellular systems (as far as FPs are not restricted to bacteria).

141

Figure 2. Drawing representing Trojan Horse. (Image from *www.keiththompsonart.com; retrieved April 2013*)

The potential of its use as a therapy could be explored combined with the use of a proper carrier systems (siRNA, phages, etc.). But before anything, new flavin-binding proteins with enhanced capacity to produce $^1O_2$ have to be developed. And also further insight needs to be given. Questions such as why miniSOG ability to sensitise $^1O_2$ is increased upon cumulative irradiation are not fully understood yet.

Shifting to the issue of $^1O_2$ detection I would like to comment first on the fact that it is a recurrent issue and that has had broad interest. Some of the already mentioned reviews regarding the topic clearly show that it has attracted a never-ending interest and pretty beautiful and smart approaches have been published.[12,13] Having had the necessity of quantifying $^1O_2$ myself in different scenarios I have had the chance to experience with many of them what has given me a better idea on what advantages and drawbacks each technique exhibits.

As for me, the number one option has always been direct $^1O_2$ measurement through phosphorescence at 1275 nm. You just need to adjust solutions of the sample and a reference to the same absorbance at the excitation wavelength and let it shine for a certain period of time, depending on the efficiency of the sample as $^1O_2$ generator. If the unknown sample is a chemical substance soluble in organic solvents not many inconvenients will appear. May the sample be water soluble, a bit more patient one will have to be as far as the $^1O_2$ phosphorescence efficiency in aqueous media is low.[14] But with enough sample and using deuterated solvents usually it is enough to solve the measurement. Direct $^1O_2$

phosphorescence detection looked perfect to me until two especial water-like scenarios came to my hands. First, I had the necessity of measuring $^1O_2$ generated by PSs uptaken by living cells. The huge scattering and the amazingly low signals made me realise the limitations of the system. Later on, we found the problem of obtaining a Φ_Δ value much lower for miniSOG than that published. In the latest case, even though we were sure our measurements were correct, we needed at least a second method that would proof us right. These two examples told me it was time for me to get to use indirect $^1O_2$ detection methods. My first approach was the use of the commercially available SOSG. This fluorescent probe has long been used in the topic of assessing $^1O_2$ values in many different systems with pretty nice results.[15] Just to refresh what I previously said, this probe, however, has two important disadvantages. Firstly, it is unable to perform in intracellular systems mainly due to unspecific interactions with other substrates (such as BSA).[16] Secondly, fluorescence enhancement upon reaction with $^1O_2$ in "only" *ca.* 10 times at best. I also had the chance to use another fluorescent probe called ADPA (anthracene dipropionic acid, just to remind you). As commented back in chapter III, it has long been used and its use is fairly standard in the assessment of $^1O_2$ in PSs. One of the most unexpected results was to find that this probe failed to measure $^1O_2$ in proteins due to unspecific interactions with the protein itself. Interaction of anthracene-like molecules with proteins had been previously reported, but not until the necessity of using both systems together did people realise of its inadequacy. Other interesting probe I had the pleasure to play with UA: Another indirect probe, this time not fluorescent. In this case, the $^1O_2$ reactivity is tracked by absorbance due to bleaching of the probe. While useful in cuvette, this system is endowed with several drawbacks. Firstly, it works in the blue part of the spectrum, where many cell components absorb or emit (e.g. mitochondria autofluorescence); second, it is not such a straightforward measuring method, as far as a second order reaction takes place and one must be careful with the kinetics of the bleaching. Finally, the decrease in absorption can be really hard to measure -once again- in living systems.

With the previous background on the topic I was happy to have the opportunity to work with two new $^1O_2$ detection scaffolds, corresponding to the two sections in Chapter IV.

The approach of the naphthoxazole dyads offered a pretty nice surprise. While the first measurements were conducted early on my thesis, not until the last months did we realise the power of the scaffold we had in our hands. At the beginning, we thought the system was "just" another fluorescent dyad in which fluorescent was prevented by photoinduced electron transfer until reaction with $^1O_2$

143

hindered the electron transfer and the fluorescence was thus recovered. The key point was to realize the novelty and usefulness of our system: the presence of two real different chemical entities before and after reaction of the dyad with $^1O_2$. In common fluorescent $^1O_2$ traps such as SOSG, the fluorophore is fluorescein. And it always is. However, in our system the conjugation of the two partners of the dyads makes that, in fact, the native and oxidised photoproducts are not the same. Such fact results in a fluorescent photoproduct that presents also spectral shift respect to the initial compound, thus enabling to choose a wavelength were initial and final products present maximum spectral differences. This double phenomenon explains why we achieve the amazing 310-fold fluorescent enhancement values. And it confers the system with very promising attributes. However, it is no gold all that glitters. First, we have not yet been able to fully ascertain the reasons for the initial quenching of the dyad in its native state. Second, the system presents huge dependence on the solvent polarity (in apolar solvents the probe is fluorescent before irradiation and photoconversion is slowed down and minimised). Finally, its solubility in aqueous media is very poor what hampers its use as a probe in intracellular systems.

In line with the end of the previous sentence, solubility in aqueous media and cell uptake are two of the milestones that a probe has to overcome so as to present itself as a potential $^1O_2$ candidate to perform in intracellular systems. Of course, cell uptake talks about biocompatibility (low toxicity, for instance) and minimised (ideally lack of) interaction with other biological entities such as serum proteins. With these requirements in mind we decided to develop a system whose core would have polyacrylamide NPs that would confer both solubility in aqueous media and biocompatibility (at least by itself). Another attractive point is that it presents affordable chemical synthesis and versatility. Polyacrylamide NPs have long been used in several fields, also as probes for other analytes, so much of the chemistry needed was unravelled.[17,18] The first approaches with direct ADPA and SOSG attachment to the NP didn't render the desired performance. And thus we went for the incorporation of the linkers using the well-established click-chemistry. Despite we have seen the systems are not perfect in terms of fluorescent changes upon conversion, still we decided it was worth giving them a try in cellular systems. The first reason, because we needed to check they really were cell-compatible and that the scaffold was tolerated and uptaken. It was this way we realised we needed to incorporate charges in the system when the cationic porphyrin was not incorporated in the NP matrix. One of the greatness of the system we developed is the versatility as mentioned before. In a first approach, it allows the incorporation of several entities. For instance, we have incorporated the probe and the porphyrin. This idea provides two important factors: it improves the

localisation of the NP (by colocalising both fluorophores) and it puts together the probe and the generation of $^1O_2$, something not achieved up till now. Besides, it opens the door to much more elaborated systems still without introducing too much complexity into the system. For instance, we could include both probes to check both the bleaching of the anthracene moiety and the enhancement of the SOSG fluorescence; we could also try new probes (naphthoxazole-based dyads!!) or even load it with other PSs. However, better performance in cuvette is needed before moving much forward. As mentioned in the corresponding chapter, we are not the first group trying to measure $^1O_2$ in intracellular systems; but none of us has fully succeeded up till now. After all, the main conclusion on this topic can be that none of the kind-of-successful systems published are ideal. Every system is inherently different (and difficult enough) and thus room for new improved $^1O_2$ will always be welcome.

To finish this chapter I would love to give further emphasis on the reality of the bacteria resistant to antibiotics. Sadly, I'm afraid little will be done until cases of the "big monsters" land at home (just to recall, most of the cases of the pan-resistant bacteria are present in India or Pakistan, still far from western Europe). I also believe that people are not fully aware of the risks of misuse and abuse of antibiotics (not only in humans but also in cattle industry). And sadly is such a common use. Together with the improvement in the development of new therapies and drugs, much more should be done regarding raising awareness of the problem on society. And we should take notes on what our neighbours in the USA do in this respect with institutions such as ISDA (Infectious Diseases Society of America). Finally, I would also like to send a message of hope. And it comes from one of the aforementioned therapies: phage therapies. I was astonished by reading that this therapy is being used in Georgia (and other URSS-derived countries) routinely since 1920s!! And you can purchase phage-cocktails as easy as you can get an aspirin. Again, we have much to learn (and reading interesting reviews helps!).[19] Hopefully some research back in this forgotten therapy is being held.

REFERENCES

1. Schwartz, M. A. The importance of stupidity in scientific research. *J. Cell. Sci.* **2008**, *121*, 1771.

2. Merchat, M.; Bertolini, G.; Giacomini, P.; Villanueva, A.; Jori, G. Meso-substituted cationic porphyrins as efficient photosensitizers of gram-positive and gram-negative bacteria. *J Photochem Photobiol B.* **1996**, *32*, 153-157.

3. Wainwright, M.; Phoenix, D. A.; Marland, J.; Wareing, D. R.; Bolton, F. J. A study of photobactericidal activity in the phenothiazinium series. *FEMS Immunol. Med. Microbiol.* **1997**, *19*, 75-80.

4. Caminos, D. A.; Spesia, M. B.; Durantini, E. N. Photodynamic inactivation of Escherichia coli by novel meso-substituted porphyrins by 4-(3-N,N,N-trimethylammoniumpropoxy)phenyl and 4-(trifluoromethyl)phenyl groups. *Photochem. Photobiol. Sci.* **2006**, *5*, 56-65.

5. Alves, E.; Costa, L.; Carvalho, C. M. B.; Tome, J. P. C.; Faustino, M. A.; Neves, M. G. P. M.; Tome, A. C.; Cavaleiro, J. A. S.; Cunha, A.; Almeida, A. Charge effect on the photoinactivation of Gram-negative and Gram-positive bacteria by cationic meso-substituted porphyrins. *Bmc Microbiology* **2009**, *9*.

6. Kolter, R.; Greenberg, E. P. Microbial sciences: The superficial life of microbes. *Nature* **2006**, *441*, 300-302.

7. Irie, Y.; Parsek, M. R. Quorum sensing and microbial biofilms. *Curr. Top. Microbiol. Immunol.* **2008**, *322*, 67-84.

8. Peters, B. M.; Jabra-Rizk, M. A.; O'May, G. A.; Costerton, J. W.; Shirtliff, M. E. Polymicrobial interactions: impact on pathogenesis and human disease. *Clin. Microbiol. Rev.* **2012**, *25*, 193-213.

9. Kolter, R. Biofilms in lab and nature: a molecular geneticist's voyage to microbial ecology. *Int. Microbiol.* **2010**, *13*, 1-7.

10. Sang, Y.; Blecha, F. Antimicrobial peptides and bacteriocins: alternatives to traditional antibiotics. *Animal Health Research Reviews* **2008**, *9*, 227-235.

11. Nakase, I.; Okumura, S.; Katayama, S.; Hirose, H.; Pujals, S.; Yamaguchi, H.; Arakawa, S.; Shimizu, S.; Futaki, S. Transformation of an antimicrobial peptide into a plasma membrane-permeable, mitochondria-targeted peptide via the substitution of lysine with arginine. *Chem. Commun.* **2012**, *48*, 11097-11099.

12. Soh, N. Recent advances in fluorescent probes for the detection of reactive oxygen species. *Anal. Bioanal Chem.* **2006**, *386*, 532-543.

13. Uusitalo, L. M.; Hempel, N. Recent advances in intracellular and in vivo ROS sensing: focus on nanoparticle and nanotube applications. *Int. J. Mol. Sci.* **2012**, *13*, 10660-10679.

14. Schweitzer, C.; Schmidt, R. Physical mechanisms of generation and deactivation of singlet oxygen. *Chem. Rev.* **2003**, *103*, 1685-1758.

15. Flors, C.; Fryer, M. J.; Waring, J.; Reeder, B.; Bechtold, U.; Mullineaux, P. M.; Nonell, S.; Wilson, M. T.; Baker, N. R. Imaging the production of singlet oxygen in vivo using a new fluorescent sensor, Singlet Oxygen Sensor Green (R). *J. Exp. Bot.* **2006**, *57*, 1725-1734.

16. Gollmer, A.; Arnbjerg, J.; Blaikie, F. H.; Pedersen, B. W.; Breitenbach, T.; Daasbjerg, K.; Glasius, M.; Ogilby, P. R. Singlet Oxygen Sensor Green(R): photochemical behavior in solution and in a mammalian cell. *Photochem. Photobiol.* **2011**, *87*, 671-679.

17. Chauhan, V. M.; Burnett, G. R.; Aylott, J. W. Dual-fluorophore ratiometric pH nanosensor with tuneable pKa and extended dynamic range. *Analyst* **2011**, *136*, 1799-1801.

18. Wang, S.; Kim, G.; Lee, Y. K.; Hah, H. J.; Ethirajan, M.; Pandey, R. K.; Kopelman, R. Multifunctional biodegradable polyacrylamide nanocarriers for cancer theranostics--A see and treat strategy. *ACS Nano* **2012**, *6*, 6843-6851.

19. Stone, R. Stalin's Forgotten Cure. *Science* **2002**, *298*, 728-731.

Chapter VI.

Conclusions

As a result of the present work, the following conclusions have been arrived at:

- Tricationic porphycene **NMe₃MeO-TBPo** has slightly improved photoinactivation ability against MRSA and *P. aeruginosa* as compared to its analogue **Py₃MeO-TBPo**, but it is less efficient against *Candida* spp. Dendrimeric phthalocyanines bearing zinc group clearly outperform their ruthenium analogues. Still, all dendrimers except **RuCat⁸⁺** are capable of effectively photoinactivating *E. coli*. Aggregation effects have been observed for all compounds, while differences in behaviour occur depending on the family of PS.

- Photophysical studies on A pidaecin 1b c onjugated to four different PSs indicate binding to the bacterial OM but not improved photophysical properties respect to the parent PS, except for the water solubility conferred by the intrinsic charge of Apidaecin 1b. The reported results are consistent with photoinactivation experiments, FACS analysis, and circular dichroism studies.

- $^1O_2$ production by TagRFP has proven sufficient to exert bacterial cell death in a light dose dependent manner, being the first report on bacterial photokilling via purely $^1O_2$ endogenous production. MiniSOG has been shown to outperform any other reported fluorescent protein in terms of bacterial photoinactivation. Additionally, insight has been gained unravelling mechanistic aspects on bacterial cell death.

- MiniSOG capability of sensitising $^1O_2$ has been revisited and an apparent Φ_Δ value of 0.03 ± 0.01 has been established through direct $^1O_2$ luminescence and indirectly by using uric acid as probe. An increase in the Φ_Δ value of almost an order of magnitude upon cumulative irradiation of miniSOG indicates that its sensitisation ability is hindered by scavengers inside the protein.

- Conjugated naphthoxazole-based dyads have shown an unprecedented fluorescence increase up to 310-fold in the presence of $^1O_2$. This effect can be explained since native and photooxidize species are indeed different chemical entities allowing optimised wavelength selection.

- Polyacrylamide-based NPs linked to $^1O_2$ chemical traps have been successfully developed and tested in solution. Chemical versatility of the system has allowed the inclusion of two different trapping moieties (ADPA or SOG), linkers varying in size, charged groups and even a model porphyrin. Moreover, minimised interactions of the system towards BSA have been observed. Finally, preliminary results in intracellular systems point out on biocompatibility, ease of localisation and lack of toxicity.

Appendices

/

APPENDIX I

This first appendix includes two paragraphs corresponding to a published interview to Professor John Conly by World Health Organization at the end of 2010 related to the World Health Day 2011 dedicated to antimicrobial resistance.

Q: What's special about this new type of resistance labelled as NDM1?

A: NDM1 is an enzyme that confers resistance to one of the most potent classes of antibiotics, known as carbapenems, but what has been observed is different in many ways to what we have seen to date. This new resistance pattern has been reported in many different types of bacteria compared to previously and at least one in 10 of these NDM1-containing strains appears to be pan-resistant, which means that there is no known antibiotic that can treat it. A second concern is that there is no significant new drug development for antimicrobials. Third, this particular resistance pattern is governed by a set of genes that can move easily from one bacterium to another. Fourth, NDM1 has been found in the most commonly encountered bacterium in the human population, *E. coli,* which is the most common cause of bladder and kidney infections. A further concern is that of the two drugs potentially capable of treating an infection due to one of these new multiresistant strains, one of them, colistin, causes toxic effects to the kidney in about a third of people.

Q: Is this the doomsday scenario of a world without antibiotics?

A: Unfortunately yes, with these new multiresistant NDM1-containing strains and their potential for worldwide spread. Doctors will face a terrible dilemma when a pregnant woman develops a kidney infection that spills over into the bloodstream with a pan-resistant strain containing NDM1 and there are no treatment options. We are essentially back to an era with no antibiotics.


APPENDIX II

Not until one gets to know real stories one is not fully aware of the significance of the problem. With this purpose in mind, two representative and shocking real and recent cases have been selected and attached below as part of this second appendix. More information can be found from the main web page of the Infectious Diseases Society of America (IDSA; http://www.idsociety.org/Topic_Antimicrobial_Resistance/)

David Ricci's story
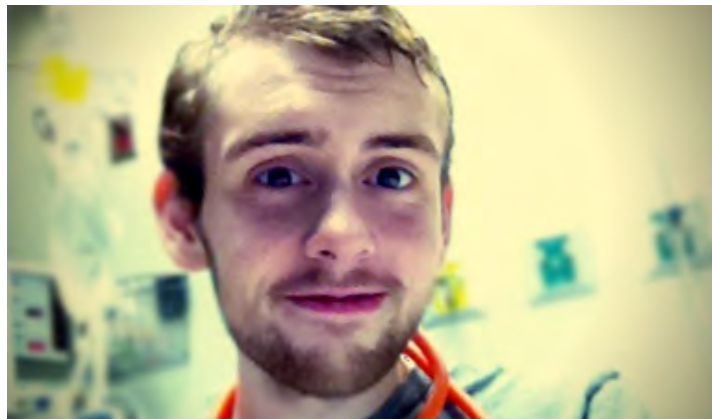
A 19-year-old from the Seattle area battles several NDM-1 positive antibiotic-resistant infections as he recovers from a train accident that cost him his right leg.

"In just one moment my life changed forever. In June 2011 I was 19 years old and working as a volunteer with HIV/AIDS orphans in Calcutta, India, through the social justice organization YWAM, far from my home in the Seattle area. One morning while I was walking to the orphanage, I took a shortcut across some train tracks to avoid the trash-filled roadside. All of the sudden I was hit and dragged by a train, resulting in the brutal amputation of my right leg above the knee.

You never know when it's the biggest day of your life until it's happening. It was as if I was in the middle of a nightmare turned reality; I didn't receive pain relievers until a week after the accident. When I received clearance to be airlifted back home to Seattle after a hazy three weeks of agony, I thought the worst of my journey would be over: Maybe I would need some antibiotics and other treatment, but I could get on with learning how to live with only one leg. Little did I know how wrong I was.

151

When I arrived back in the U.S., I soon learned that my wounds were infected with multiple drug-resistant bacteria (including *Pseudomonas aeruginosa, Klebsiella pneumoniae, Morganella morganii, and Enterococcus*), several of which tested positive for New Delhi metallo-beta-lactamase-1 (NDM-1), a dangerous and recently discovered enzyme that makes bacteria resistant to a whole class of very important antibiotics. I had never heard of any of those bacteria, nor NDM-1, let alone thought that one day I would become infected with them. I remember when the lab results came back, the hospital staff was so concerned by the NDM-1 that everyone went into crisis mode, and I was immediately isolated in my room. After another surgery to remove infected tissue from my residual limb, I was put on broad-spectrum antibiotics as a precaution. They thought the infection was gone, so I was released and returned home to my family.
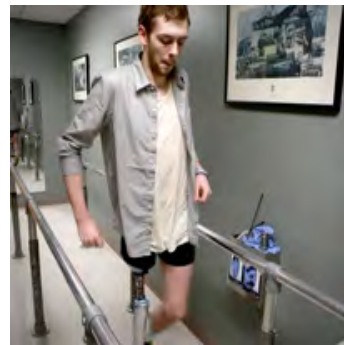
After four weeks at home the pain still hadn't subsided, and my doctor knew something was wrong. Another surgery was required, and the surgeon found the tissue was still infected with the highly drug-resistant bacteria. I began a course of strong antibiotics, including an antibiotic of last-resort called colistin, which is rarely used because it's so toxic. I felt my body shutting down from the toxicity of the treatment. My immune system, kidneys, and liver were failing, and I could feel my body giving up. Top doctors were giving me potent cocktails of the most powerful antibiotics available, and we were not sure if the drugs were even working. To know that the drugs that were strong enough to damage my internal organs might not be powerful enough to fight the bacteria they were intended to treat, made me feel incredibly powerless.

I stopped the antibiotics at the end of September when the infection was thought to be gone. By December, it was back again in the form of a golf ball-sized abscess in my thigh. A biopsy revealed that the resistant bacteria were back full-force, and I underwent another emergency surgery to have more infected tissue removed. The antibiotics I took during this time were even stronger than the first course, and the side effects completely exhausted my body. The treatment was very similar to chemotherapy, making me vomit daily. It felt as though each of my organs were slowly deteriorating. I felt my body dying. When my white blood cell count dropped, I was so weak that normal daily activities were impossible.

Now, eight months after my accident, my wounds are closed, but my worries are not over. My life consists of watchful waiting and praying that the infection, like some awful type of cancer, does not return. I have weekly doctor visits and monthly hospital visits so that we can keep a close watch on my progress. The learning process for my new prosthetic leg has been slow going because I had to restart my physical therapy treatments after every emergency surgery, which removed more of my leg tissue. Plus, losing more and more of my leg to these antibiotic-resistant infections has made it harder to use a prosthetic, since I have less muscle to work with.

My battle is not over, but I'm thankful to be alive. I survived an impossible accident and continue to fight the deadliest of infections. My family, friends, and faith keep me going, and it is for them that I stay optimistic. While things may never be the same as they were before that June morning, I am grateful for life. Recovering from a traumatic accident isn't easy, saying it is exhausting is an understatement. The infections leave my body weak and broken, but I continue to fight every day. I cheated death because I found life too beautiful to resist."

April 2012

Addie Rerecich's story

A healthy 11-year-old girl from Tucson, Ariz., who spent months in the hospital fighting several antibiotic-resistant infections and needed a lung transplant to save her life.

"*Addie will never be the same again, and there's nothing I can do about it.* I thought this as I sat in the hospital watching my 11-year-old daughter's health rapidly fade. She had tubes running all over her body, a special machine had been brought in to help her breathe, and doctors were preparing me for the worst. I was not new to hospital settings, but I've never been invested on such a personal level. As a

153

nurse, I remember learning about drug-resistant organisms, such as methicillin-resistant *Staphylococcus aureus* (MRSA) and *Escherichia coli* (*E. coli*), in school. I preached to my patients and colleagues the importance of using antibiotics properly to avoid promoting the development of life-threatening pathogens. However, as I sat there watching my little girl fight for her life I realized, *dear God, this is happening to us!*

It all started on Mother's Day 2011. I remember Addie being more tired than usual. I didn't think too much of it since she was always such an active kid who loved to swim, run track, and play softball. Those things catch up with you, and I figured on this day she was just worn out. About a week later, Addie mentioned to me that she had been having a lot of pain in her hip. I suspected a pulled muscle but made an appointment with our doctor for the next day just in case. We never made it to that appointment. Instead, her pain continued to increase, and she developed a fever of 103, prompting us to make a trip to the emergency room.

Doctors there saw nothing wrong with her white blood cell counts or other lab results that might indicate she had a bacterial infection, so they sent us home with ibuprofen and a reminder to see our doctor within three days. But Addie didn't get better. I called paramedics and took her to the emergency room one more time before seeking a second opinion at another hospital. Addie walked into the hospital with me on May 19, 2011, and would not pass again through those doors until October, five months later. Those months were a whirlwind, and it started immediately. Doctors ordered a culture of her blood, and found her body was overcome with a *Staphylococcus* infection, a condition called sepsis. The infection had begun growing as an abscess in her hip muscle, and spread into her blood, eventually causing a devastating bacterial pneumonia in her lungs. The abscess in her hip had gone untreated for so long that she had developed a blood clot deep in a vein near the abscess. Unfortunately, part of the clot broke away and caused a pulmonary embolism to her right lung – further complicating matters.

Within 24 hours, my little girl went from happy and healthy to being intubated and hooked to a breathing machine. Her small body was riddled with tubes and wires. She had surgery to remove the abscess from her hip. She was not getting better. Eventually her lungs began to fail entirely, and she had to be placed on a machine called ECMO (extracorporeal membrane oxygenation), which circulated her blood and added oxygen to it, like and external lung. The hope was that taking the pressure off her lungs

would allow them to heal. The machine is usually only needed for five to seven days; Addie was connected to it for three full months.

During this time, Addie's doctors realized her lungs were not getting better– she would need a lung transplant to survive. However, they were unsure they could perform a transplant, because there were so much bacteria running amok in her body. She had developed infections caused by several drug-resistant bacteria – including extended-spectrum beta-lactamase (ESBL)-producing *E. coli*, *Stenotrophomonas maltophilia*, and a resistant form of pneumonia caused by *Enterobacter aerogenes*. Addie's doctors had run out of the most common antibiotics used to treat these serious bacteria so, in desperation, they turned to an antibiotic known as colistin. Colistin is very powerful, but it is also so highly toxic to the kidneys and other organs that doctors rarely use it. We started saying extra prayers.

Our prayers were answered as she responded to this antibiotic therapy and was cleared for a double lung transplant. The transplant went off successfully, but, in the end, our lives will never be the same. When we left the hospital, Addie was in a wheelchair. She had lost the use of her left arm, had almost no vision in her left eye, and had restricted vision in her right eye. She had limited use of her left leg. She had suffered a stroke. She had lost 30 pounds, almost one third of her body weight. She was so weak and debilitated that she couldn't even turn herself side to side in bed. With intensive therapy Addie is improving, but progress is slow, and no one is sure how much function she can regain. She has horrible scars all over her body from the various procedures, tubes, and tests that ultimately saved her life. My once normal, strong, athletic Addie will need medical attention and therapy for the rest of her life. I'm so grateful that she's still with us and that we made it through, but my heart aches when she looks up at me and asks, "Why me?", because I don't have an answer.

Nothing can describe my feelings as a mother sitting helpless as I watched my little girl go from smiling and healthy to near death in less than a day. Antibiotic-resistant infections have devastated my daughter's life and our family's health, wellbeing, and finances. The health care costs from Addie's five-month hospital stay alone came to $6 million**.** We need to take steps now to ensure we are able to more effectively battle these infections in the future and that we have the antibiotics we need to do so. My family and I pray every day that no one else will have to experience what Addie has gone through.

February 2012

APPENDIX III

List of articles derived from the thesis

1. <u>R. Ruiz-González</u>, J.H. White, M. Agut, S. Nonell and C. Flors. *A genetically-encoded photosensitiser demonstrates killing of bacteria by purely endogenous singlet oxygen*. Photochemical & Photobiological Sciences. **2012**. Vol. 9. pp 1403-1486

2. R. Dosselli, R. <u>Ruiz-González</u>, M. Gobbo, S. Nonell and E. Reddi. *Synthesis, characterization and photoinduced cytotoxicity of porphyrin type photosensitizers conjugated to the antimicrobial peptide Apidaecin.* Journal of Medicinal Chemistry. **2012**; Vol. 56, pp 1052-1063

3. <u>R. Ruiz-González</u>; J. H. White; A.L. Cortajarena, L.; M. Agut; S. Nonell; C. Flors. *Fluorescent proteins as singlet oxygen photosensitizers: mechanistic studies in photodynamic inactivation of bacteria.* Proc. SPIE, **2013**, 859609

4. <u>R. Ruiz-González</u>, R. Zanocco, Y. Gidi, A. L. Zanocco, E. Lemp and S. Nonell. Naphthoxazole-*based singlet oxygen fluorescent probes.* Photochemistry and Photobiology. **2013** (DOI: 10.1111/php.12106)

5. <u>R. Ruiz-González</u>, A. L. Cortajarena, S. H. Mejias, M. Agut, S. Nonell and C. Flors. *Singlet oxygen generation by the genetically-encoded tag miniSOG.* Journal of the American Chemical Society. **2013** (under second-round revision)

During the development of the thesis, some contributions to other articles that do not belong to the present work have been performed:

6. X. Ragàs, D. Sánchez-García, R. Ruiz-González, T. Dai, M. Agut, M.R. Hamblin and S. Nonell *Cationic porphycenes as potential photosensitizers for antimicrobial photodynamic therapy*. Journal of Medicinal Chemistry. **2010**. Vol 53. pp 7796-7803

7. R. Ruiz-González, P. Acedo, D. Sánchez-García, S. Nonell, M. Cañete J.C. Stockert and A. Villanueva. *Efficient induction of apoptosis in HeLa cells by a nov el cationic porphycene photosensitizer*. European Journal of Medicinal Chemistry. **2013**. Vol 63. pp 401-414

8. E. Rosas, S.Nonell, R. Ruiz-González, M.C. Llinàs, D. Sánchez-García, E.R. Edelman and M. Balcells. *Selective targeting of microvascular endothelial cells using a n ovel immunoconjugated photosensitizer drug.* Langmuir. **2013** (submitted)

157

A genetically-encoded photosensitiser demonstrates killing of bacteria by purely endogenous singlet oxygen†‡

Rubén Ruiz-González,[a] John H. White,[b] Montserrat Agut,[a] Santi Nonell*[a] and Cristina Flors*[b,c]

TagRFP, a fluorescent protein capable of photosensitizing the production of singlet oxygen, was expressed in *E. coli*. Subsequent exposure to green light induced bacterial cell death in a light-dose dependent manner. It is demonstrated for the first time that intracellular singlet oxygen is sufficient to kill bacteria.

Antimicrobial therapies are being actively sought with the goal to address the increasing resistance of pathogens to antibiotics.[1–4] Antimicrobial photodynamic therapy (aPDT) is regarded as very promising in this respect mainly because its mechanism of action involves non-specific photo-oxidation of cellular components, which strongly reduces the likelihood to develop resistance.[5] In fact, no reports exist describing the selection of aPDT-induced resistant pathogens *in vitro*[6,7] or *in vivo*.[8] After light absorption by a molecular entity acting as photosensitizer (PS), the primary molecular event in the photodynamic action is the generation of reactive oxygen species (ROS) such as singlet oxygen ($^1O_2$), superoxide radical anion, hydrogen peroxide, or hydroxyl radicals. Almost every cell component is a potential target for these ROS, as they react readily with proteins, carbohydrates, cell-membrane components, and nucleic acids.[9]

Despite decades of research, the actual mechanism of cell death triggered by these early photochemical steps is poorly understood and it is not clear whether bacterial death requires damage to the external wall and/or the inner cell components.[10] Crucially, it has been difficult to establish the role of the PS location, and thus the primary site of photodamage, since the small size of bacteria precludes the use of fluorescence microscopy techniques due to the limited spatial resolution of

this technique. Electron microscopy has the necessary resolution and has recently revealed progression of envelope damage inflicted during irradiation.[11] On the other hand, time-resolved studies of the formation and decay of $^1O_2$ have been instrumental in establishing the coexistence of externally-bound and internalized PS molecules in *E. coli*.[12] Because the PS is delivered from the cell exterior it has not been possible so far to separately study the contributions of external and internal damage, nor has it been possible to control the location of the PS. As a result, a sound understanding of the role of drug location in the mechanism of cell death has been elusive to date.

In this communication, we report a solution to the issue of PS location in aPDT mechanistic studies by using a genetically-encoded $^1O_2$ PS that we are able to express inside the cell. We have previously shown that some green and red fluorescent protein variants are able to photosensitize $^1O_2$.[13–15] Here, we have chosen TagRFP as a PS, which, unlike other fluorescent proteins such as KillerRed,[16–19] is able to photosensitize the production of $^1O_2$ but not of other ROS,[15] and is therefore uniquely suited to ascertain the role of $^1O_2$ in bacterial cell death.

E. coli BL21 (DE3) cells readily expressed TagRFP, as judged from the development of red color and its distinctive red fluorescence (Fig. S1, ESI‡). TagRFP seems to be evenly distributed in the bacterial cytosol, and no clear accumulation in specific locations, *e.g.* near the internal membrane, can be clearly appreciated within the diffraction-limited spatial resolution of the fluorescence images. Photodynamic inactivation experiments of *E. coli* expressing TagRFP were subsequently carried out. Cell cultures in exponential growing phase were induced with 50 μM isopropyl β-D-1-thiogalactopyranoside (IPTG) for 1 h. After replacing the growth medium with PBS or deuterated PBS (D-PBS), depending on the experiment, the cells were transferred to an optical non-treated sterile glass chamber and irradiated through the bottom of the chamber by means of a 532 nm CW laser (40 mW cm^{-2}).

No remarkable damage was observed for light doses below 750 J cm^{-2}. However, a population reduction of *ca.* 4-log$_{10}$ in colony-forming units (CFU) per milliliter was achieved after a light dose of 3200 J cm^{-2} in D-PBS suspensions (*ca.* 2.5-log$_{10}$ CFU mL^{-1} reduction in normal PBS; Fig. 1). It is well known that solvent deuteration extends the $^1O_2$ lifetime[20,21] such that the enhancement of oxidative damage upon deuteration has long been used as a mechanistic test for the involvement of $^1O_2$.[22] The light dose used is several orders of magnitude higher than that used in typical aPDT treatments[10] but comparable to that in
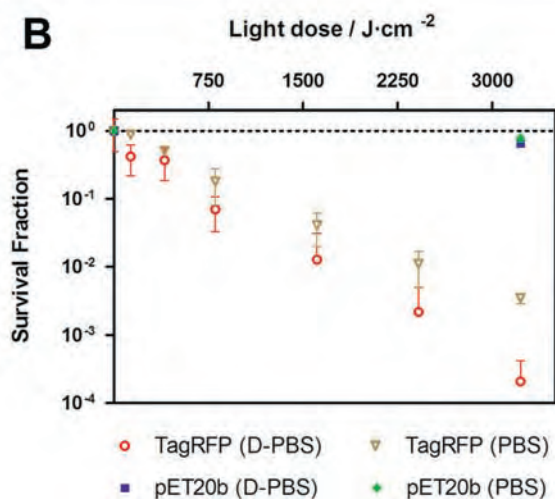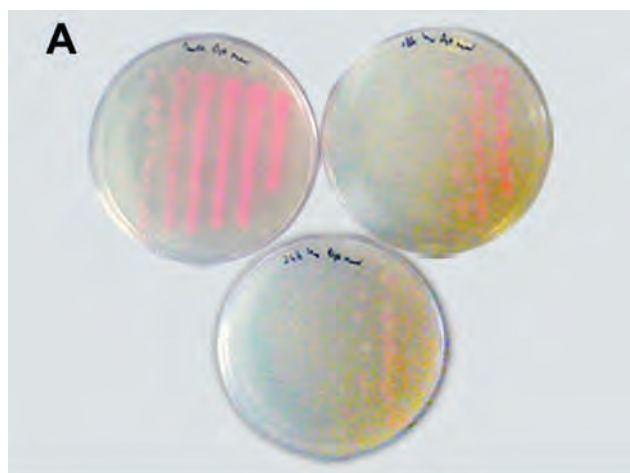
[a] IQS School of Engineering, Universitat Ramon Llull, Vía Augusta 390, E-08017 Barcelona, Spain. E-mail: santi.nonell@iqs.url.edu; Fax: +34 932056266; Tel: +34 932672000
[b] EastChem School of Chemistry, University of Edinburgh, Joseph Black Building, The King's Buildings, West Mains Rd, EH9 3JJ Edinburgh, UK
[c] IMDEA Nanociencia, C/Faraday 9, Ciudad Universitaria de Cantoblanco, 28049 Madrid, Spain. E-mail: cristina.flors@imdea.org; Fax: +34 91 397 6855; Tel: +34 91 397 6851

† Dedicated to Professor Miguel A. Miranda on the occasion of his 60th birthday.
‡ Electronic supplementary information (ESI) available: Bacterial expression and culture conditions. Photodynamic inactivation studies. Spectroscopic measurements and microscopy. Integrity of cell membrane. DNA purification and electrophoresis. See DOI: 10.1039/c2pp25126d

This journal is © The Royal Society of Chemistry and Owner Societies 2012

Photochem. Photobiol. Sci., 2012, **11**, 1411–1413 | 1411

Fig. 1 Photokilling effect of TagRFP in *E. coli* upon irradiation with green laser light. Panel A: Example of viability results after photodynamic treatments in D-PBS. Each column is a 1 : 10 dilution with respect to the one on its right. The initial cell density for every sample was *ca.* 10^8 CFU mL^{-1}. Dark control (upper left); 2400 J cm^{-2} irradiation (upper right) and 3200 J cm^{-2} irradiation (bottom). Panel B: Light-dose dependence on bacterial cell death in *E. coli* transformed with pET20TagRFPhis or pET20b plasmids.

chromophore-assisted light inactivation (CALI) assays,[23] and is consistent with the low quantum yield of $^1O_2$ generation by TagRFP (0.004 ± 0.0001).[15]

E. coli cells transformed with the control pET20b plasmid, devoid of the TagRFP sequence, were tested under the same experimental conditions. As depicted in Fig. 1, a CFU mL^{-1} reduction of less than 0.5-log$_{10}$ units was observed in all cases. Moreover, bacteria expressing TagRFP which were not irradiated did not significantly lose viability (data not shown). These negative controls confirm that damage is inflicted by a photodynamic reaction, *i.e.*, by the combination of light, oxygen and TagRFP acting as photosensitizer.

Our observation of *ca.* 1-log$_{10}$ population reduction difference between PBS- and D-PBS-suspended cells is consistent with a $^1O_2$ lifetime of 3.5 μs in H$_2$O and 65 μs in D$_2$O.[24] This is also in agreement with our previous report that TagRFP is a pure $^1O_2$
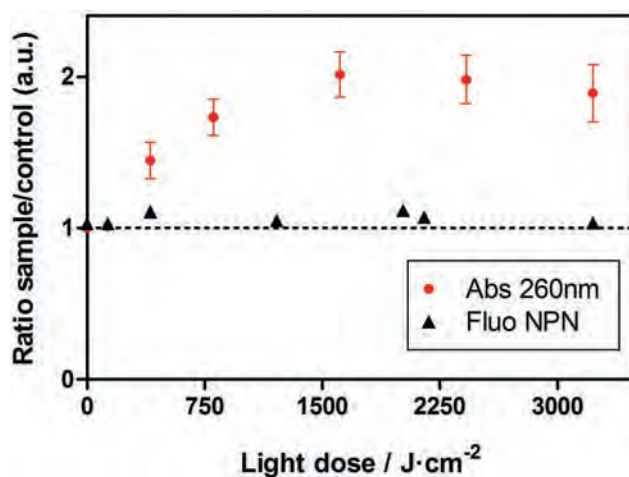
Fig. 2 Bacterial cell envelope integrity assays after different aPDT light dose treatments. Red circles: absorbance of supernatants at 260 nm. Black triangles: fluorescence of NPN. Data are normalized to values measured for non-irradiated samples.

PS[15] and constitutes the first report showing that cytoplasmic location of a $^1O_2$ PS is sufficient to induce bacterial cell death following light irradiation.

In order to obtain further insight regarding the mechanism of cell death photosensitized by TagRFP, several additional assays were performed. First, we focused on the cytoplasmic cell membrane. Damage to the inner bacterial membrane is accompanied by leaching-out of low molecular-weight species in addition to DNA and RNA fragments, which are also able to permeate the external membrane. The release of such intracellular components can be conveniently monitored by spectroscopic means and the onset of UV absorption at 260 nm in the supernatant is taken as a strong indication of membrane damage.[25,26] The results of such assays in our TagRFP-tagged bacteria are shown in Fig. 2 (red circles), where the 260 nm absorbance of the supernatants of irradiated bacteria suspensions is plotted as a function of the light dose. The data have been normalized against the values for non-irradiated samples. A clear growth in the 260 nm absorbance can be observed almost from the outset and a *plateau* value is reached at a light dose of 1600 J cm^{-2}. This indicates that photodynamic damage to the inner cell membrane occurs in our system. Leakage of TagRFP from the bacterial cytosol, measured by fluorescence spectroscopy of supernatant solutions, was observed only after light exposure and in a light-dose dependent manner, consistent with increasing levels of photoinduced bacterial membrane damage (not shown).

In a second series of assays we assessed the integrity of the outer membrane. It is well known that Gram-negative bacteria are markedly more resistant to photodynamic inactivation than Gram-positive species, due to the highly organized structure of its cell envelope.[5] Specifically, many studies have shown that the presence of an additional outer membrane prevents many PSs from reaching and/or binding to the inner membrane, resulting in lowered photosensitization efficiency.[5] The outer membrane is thus a typical target in Gram-negative bacteria.[27,28] The fluorescent probe 1-*N*-phenylnaphthylamine (NPN), which increases its fluorescence upon binding to cells with a damaged outer membrane, was used to this end.[26,29] As shown in Fig. 2 (black

triangles), no increase in NPN fluorescence was observed relative to dark control suspensions, suggesting that no significant damage is inflicted on the outer membrane. NPN fluorescence measurements in water and in lysed cells served as further controls (Fig. S2, ESI‡).

Finally, damage to genomic DNA from *E. coli* cells was studied, since some authors have reported photodamage to genetic material in aPDT.[30,31] DNA from irradiated cells was extracted by standard procedures and electrophoresis of the extracts was run in a 0.6% agarose gel. As shown in Fig. S3, ESI,‡ no differences could be observed between samples irradiated at the maximum light dose and dark controls. This indicates that TagRFP-induced photodamage to genomic DNA does not occur to any measurable extent. Our results are in line with those of previous studies where it was concluded that DNA damage is not the primary cause of bacterial cell photoinactivation.[10,32] However, we cannot exclude that a lethal effect may be produced by localized DNA damage that could not be detected in our assay.[33]

Overall, TagRFP photodamage seems to occur mainly in the inner membrane. No damage of the outer membrane or of genomic DNA could be observed. These observations are markedly different to those reported for an external photosensitizer.[26] Thus, the site where $^1O_2$ is primarily generated proves crucial for inflicting different types of cell damage. It is relevant to recall that the latest estimates of the radial diffusion distance of $^1O_2$, which represents its sphere of activity, are about 155 and 550 nm in H_2O and D_2O, respectively.[21] These distances are below the typical size of a bacterial cell.

In summary, killing of bacteria from purely endogenous $^1O_2$ produced by a genetically-encoded photosensitizing protein has been demonstrated for the first time. Our work provides insight into the mechanism of singlet-oxygen mediated photodamage, namely that cytoplasmic location of a photosensitizer is sufficient for light-induced bacterial cell death. Moreover, this work supports the potential of genetically-encoded strategies for treating bacterial infections with photodynamic therapy, which could be realized by appropriate gene transfer methods.

References

1 K. Konig, M. Teschke, B. Sigusch, E. Glockmann, S. Eick and W. Pfister, *Cell Mol. Biol.*, 2000, **46**, 1297–1303.

2 T. Dai, Y. Y. Huang and M. R. Hamblin, *Photodiagn. Photodyn. Ther.*, 2009, **6**, 170–188.

3 S. K. Sharma, T. Dai, G. B. Kharkwal, Y. Y. Huang, L. Huang, V. J. De Arce, G. P. Tegos and M. R. Hamblin, *Curr. Pharm. Des.*, 2011, **17**, 1303–1319.

4 B. Xing, T. Jiang, W. Bi, Y. Yang, L. Li, M. Ma, C. K. Chang, B. Xu and E. K. Yeow, *Chem. Commun.*, 2011, **47**, 1601.

5 G. Jori, C. Fabris, M. Soncin, S. Ferro, O. Coppellotti, D. Dei, L. Fantetti, G. Chiti and G. Roncucci, *Lasers Surg. Med.*, 2006, **38**, 468–481.

6 L. Costa, J. P. Tome, M. G. Neves, A. C. Tome, J. A. Cavaleiro, M. A. Faustino, A. Cunha, N. C. Gomes and A. Almeida, *Antiviral Res.*, 2011, **91**, 278–282.

7 L. A. Pedigo, A. J. Gibbs, R. J. Scott and C. N. Street in *Proc. SPIE-Int. Soc. Opt. Eng.*, ed D. H. Kessel, SPIE, Washington, 2009, vol. 7380, 73803H.

8 S. A. Lambrechts, T. N. Demidova, M. C. Aalders, T. Hasan and M. R. Hamblin, *Photochem. Photobiol. Sci.*, 2005, **4**, 503–509.

9 R. W. Redmond and J. N. Gamlin, *Photochem. Photobiol.*, 1999, **70**, 391–475.

10 G. Jori and O. Coppellotti, *Anti-Infect. Agents Med. Chem.*, 2007, **6**, 119–131.

11 B. Pudziuvyte, E. Bakiene, R. Bonnett, P. A. Shatunov, M. Magaraggia and G. Jori, *Photochem. Photobiol. Sci.*, 2011, **10**, 1046–1055.

12 X. Ragàs, M. Agut and S. Nonell, *Free Radical Biol. Med.*, 2010, **49**, 770–776.

13 A. Jiménez-Banzo, S. Nonell, J. Hofkens and C. Flors, *Biophys. J.*, 2008, **94**, 168–172.

14 A. Jiménez-Banzo, X. Ragàs, S. Abbruzzetti, C. Viappiani, B. Campanini, C. Flors and S. Nonell, *Photochem. Photobiol. Sci.*, 2010, **9**, 1336–1341.

15 X. Ragàs, L. P. Cooper, J. H. White, S. Nonell and C. Flors, *ChemPhysChem*, 2011, **12**, 161–165.

16 M. E. Bulina, D. M. Chudakov, O. V. Britanova, Y. G. Yanushevich, D. B. Staroverov, T. V. Chepurnykh, E. M. Merzlyak, M. A. Shkrob, S. Lukyanov and K. A. Lukyanov, *Nat. Biotechnol.*, 2006, **24**, 95–99.

17 E. O. Serebrovskaya, E. F. Edelweiss, O. A. Stremovskiy, K. A. Lukyanov, D. M. Chudakov and S. M. Deyev, *Proc. Natl. Acad. Sci. U. S. A.*, 2009, **106**, 9221–9225.

18 R. B. Vegh, K. M. Solntsev, M. K. Kuimova, S. Cho, Y. Liang, B. L. Loo, L. M. Tolbert and A. S. Bommarius, *Chem. Commun.*, 2011, **47**, 4887–4889.

19 W. Waldeck, E. Heidenreich, G. Mueller, M. Wiessler, K. Tóth and K. Braun, *J. Photochem. Photobiol., B*, 2012, **109**, 28–33.

20 C. Schweitzer and R. Schmidt, *Chem. Rev.*, 2003, **103**, 1685–1757.

21 P. R. Ogilby, *Photochem. Photobiol. Sci.*, 2010, **9**, 1543–1560.

22 C. S. Foote and E. L. Clennan, Properties and reactions of singlet dioxygen, in *Active Oxygen in Chemistry*, ed. C. S. Foote, J. S. Valentine, A. Greenberg and J. F. Liebman, Chapman and Hall, London, 1995, p. 66.

23 M. A. McLean, Z. Rajfur, Z. Chen, D. Humphrey, B. Yang, S. G. Sligar and K. Jacobson, *Anal. Chem.*, 2009, **81**, 1755–1761.

24 P. R. Ogilby and C. S. Foote, *J. Am. Chem. Soc.*, 1982, **104**, 2069–2070.

25 C. Z. Chen and S. L. Cooper, *Biomaterials*, 2002, **23**, 3359–3368.

26 M. B. Spesia, D. A. Caminos, P. Pons and E. N. Durantini, *Photodiagn. Photodyn. Ther.*, 2009, **6**, 52–61.

27 A. Segalla, C. D. Borsarelli, S. E. Braslavsky, J. D. Spikes, G. Roncucci, D. Dei, G. Chiti, G. Jori and E. Reddi, *Photochem. Photobiol. Sci.*, 2002, **1**, 641–648.

28 J. Y. Je and S. K. Kim, *Biochim. Biophys. Acta, Gen. Subj.*, 2006, **1760**, 104–109.

29 B. Loh, C. Grant and R. E. Hancock, *Antimicrob. Agents Chemother.*, 1984, **26**, 546–551.

30 R. J. Fiel, N. Datta-Gupta, E. H. Mark and J. C. Howard, *Cancer Res.*, 1981, **41**, 3543–3545.

31 M. Salmon-Divon, Y. Nitzan and Z. Malik, *Photochem. Photobiol. Sci.*, 2004, **3**, 423–429.

32 M. Schafer, C. Schmitz and G. Horneck, *Int. J. Radiat. Biol.*, 1998, **74**, 249–253.

33 H. Ashkenazi, I. Pechatnikov and Y. Nitzan, *Curr. Microbiol.*, 2006, **52**, 317–323.

Fluorescent proteins as singlet oxygen photosensitizers: mechanistic studies in photodynamic inactivation of bacteria

Rubén Ruiz-González[a], John H. White[b], Aitziber L. Cortajarena[c], Montserrat Agut[a], Santi Nonell[a], Cristina Flors*[c]

[a]Institut Químic de Sarrià, Universitat Ramon Llull, Via Augusta 390, E-08017 Barcelona, Spain; [b]School of Chemistry, University of Edinburgh, Joseph Black Building, The King's Buildings, West Mains Rd, Edinburgh EH9 3JJ, United Kingdom; [c]Madrid Institute for Advanced Studies in Nanoscience (IMDEA Nanoscience), C/ Faraday 9, E-28049 Madrid, Spain

ABSTRACT

Antimicrobial photodynamic therapy (aPDT) combines a photosensitizer, light and oxygen to produce reactive oxygen species (ROS), mainly singlet oxygen ($^1O_2$), to photo-oxidize important biomolecules and induce cell death. aPDT is a promising alternative to standard antimicrobial strategies, but its mechanisms of action are not well understood. One of the reasons for that is the lack of control of the photosensitizing drugs location. Here we report the use of genetically-encoded fluorescent proteins that are also $^1O_2$ photosensitizers to address the latter issue. First, we have chosen the red fluorescent protein TagRFP as a photosensitizer, which unlike other fluorescent proteins such as KillerRed, is able to produce $^1O_2$ but not other ROS. TagRFP photosensitizes $^1O_2$ with a small, but not negligible, quantum yield. In addition, we have used miniSOG, a more efficient $^1O_2$ photosensitizing fluorescent flavoprotein that has been recently engineered from phototropin 2. We have genetically incorporated these two photosensitizers into the cytosol of *E. coli* and demonstrated that intracellular $^1O_2$ is sufficient to kill bacteria. Additional assays have provided further insight into the mechanism of cell death. Photodamage seems to occur primarily in the inner membrane, and extends to the outer membrane if the photosensitizer's efficiency is high enough. These observations are markedly different to those reported for external photosensitizers, suggesting that the site where $^1O_2$ is primarily generated proves crucial for inflicting different types of cell damage.

Keywords: antimicrobial photodynamic therapy, singlet oxygen, fluorescent proteins, miniSOG, photosensitization, TagRFP

1. INTRODUCTION

Fluorescent proteins are invaluable tools for fluorescence microscopy and related techniques to monitor cellular processes in living cells, owing to their ability to be genetically-fused to virtually any protein in a cell. They are mostly used as tags, sensors and reporters, but recently other interesting properties of fluorescent proteins are being exploited. In particular, their capability to act as singlet oxygen ($^1O_2$) photosensitizers is generating increasing interest.[1] $^1O_2$ is produced when a photosensitizer (in this case the fluorescent protein) is excited by light, and transfers its excitation energy to molecular dioxygen. $^1O_2$ is highly reactive, and can photo-oxidize substrates such as proteins, lipids and nucleic acids, which is relevant in the context of photodynamic therapy (PDT) and chromophore-assisted laser inactivation (CALI).

We have previously shown that some variants from the green fluorescent protein (GFP) family are able to photosensitize $^1O_2$, although with very low efficiency.[2-4] For example, TagRFP photosensitizes $^1O_2$ with a quantum yield (Φ_Δ) of 0.004,[4] similar to that of the free GFP chromophore.[2] The photosensitizing protein KillerRed,[5] although initially thought to produce $^1O_2$, is now acknowledged to produce other ROS.[6, 7]

Recently, efforts to produce genetically-encodable tags that generate $^1O_2$ have turned to the engineering of flavin mononucleotide (FMN)-binding fluorescent proteins, since FMN is an efficient $^1O_2$ photosensitizer ($\Phi_\Delta = 0.51$).[8] MiniSOG (for "mini Singlet Oxygen Generator") is a 15 kDa flavoprotein not structurally related to GFP.[9] Although its

value of Φ_Δ had been initially reported as 0.47, this value has been recently revised to 0.03, still an order of magnitude higher than that of TagRFP.[10]

Owing to the ability to genetically-encode them, fluorescent proteins that are able to photosensitize $^1O_2$ offer an advantage in a number of applications where full control of the site for $^1O_2$ generation is important (e.g. chromophore-assisted laser inactivation, photodynamic therapy, or electron microscopy).[1] In this paper, we take advantage of the genetic control of the photosensitizer location in mechanistic studies of antimicrobial photodynamic therapy (aPDT). aPDT is regarded as a very promising antimicrobial strategy because its mechanism of action involves non-specific photooxidation of cellular components, which strongly reduces the likelihood to develop resistance.[11] Photodynamic action involves the photosensitization of reactive oxygen species (ROS) such as $^1O_2$, superoxide radical anion, hydrogen peroxide, or hydroxyl radicals. Almost every cell component is a potential target for these ROS, as they react readily with proteins, carbohydrates, cell-membrane components, and nucleic acids.[12]

Despite decades of research, the mechanistic details of cell death triggered by these early photochemical steps is poorly understood and it is not clear whether bacterial death requires damage to the external wall and/or of inner cell components.[13, 14] Crucially, it has been difficult to establish the role of the photosensitizer location, and thus the primary site of photodamage, since the small size of bacteria precludes the use of fluorescence microscopy techniques due to their limited spatial resolution. On the other hand, time-resolved studies of the formation and decay of $^1O_2$ have been instrumental in establishing the coexistence of externally-bound and internalized photosensitizer molecules in *E. coli*.[15] Because the photosensitizer is delivered from the cell exterior it has not been possible so far to separately study the contributions of external and internal damage, nor has it been possible to control the location of the photosensitizer. As a result, a sound understanding of the role of drug location in the mechanism of cell death has been elusive to date. In this paper, we use two different fluorescent proteins, TagRFP and miniSOG, as genetically-encoded $^1O_2$ photosensitizer in aPDT. The proteins, which have very different structures and $^1O_2$ photosensitizing efficiencies, are expressed in the bacterial cytosol. We quantify the extent of photoinduced cell death inflicted by both fluorescent proteins, and we perform mechanistic studies to better understand how photodynamic damage occurs in aPDT.

2. MATERIALS AND METHODS

2.1 Bacterial expression and culture conditions

pET20bTagRFPHis1 or pET20b plasmids were transformed into competent *E. coli* strain BL21 (DE3). The pBAD-Myc-HisA plasmid encoding miniSOG[9] was transformed into *E. coli* DH5α cells. *E. coli* were aerobically grown overnight at 37 ℃ in an orbital shaking incubator (250 rpm) in luria-bertani (LB) broth (Fischer Scientific) in the presence of the appropriate amount of antibiotic (100 µg/mL disodium carbenicillin; Sigma) to stationary phase. A reinoculum was then grown in fresh LB medium at 37 ℃ to an OD600 = 0.2 (start of log phase). TagRFPHis expression was induced with 50 µM solution of isopropyl β-D-1-thiogalactopyranoside (IPTG; Sigma) and miniSOGHis expression with 0.1 % arabinose for 1 hour at 37°C to an OD600 ≈ 0.6-0.7 The suspensions were then centrifuged (10 min, 5000 rpm) and resuspended with sterile PBS or D-PBS at pH 7.4 to *ca.* 10^8 colony forming units per milliliter (CFU)/mLfor aPDT experiments.

2.2 Photodynamic inactivation studies

Cell suspension aliquots were placed in optical non-treated glass plates (Lab-Tek, Nalgene NUNC international, Rochester, New York). For Figure 1A, the wells with TagRFP-tagged samples were illuminated from the bottom of the plates by means of an expanded CW 532 nm laser beam (Cobolt Samba) at fluences ranging from 0 to 3500 J•cm^{-2}. For Figure 1B, the wells containing miniSOG- and TagRFP-tagged bacteria were illuminated from the top by means of a LED light source (Sorisa Photocare) using a 35 mW•cm^{-2} fluence rate either in the green for TagRFP (535 ± 15 nm) or in the blue for miniSOG (470 ± 10 nm). No significant temperature increase was observed during the experiments. At different time intervals during the illumination, when the desired fluences had been delivered, aliquots were taken from the well (the suspensions were thoroughly mixed before sampling to avoid cell settlement). For determination of cell viability after treatments, aliquots were serially diluted (1:10 dilutions until single colonies could be observed), streaked on nutrient agar, and incubated in the dark for 18-20 h at 37 ℃.

2.3 Integrity of cell membrane

After photodynamic treatments, samples were centrifuged (13000 rpm, 10 min) and the supernatant was monitored by UV—vis spectroscopy (Cary, Varian, Palo Alto) in order to measure the absorbance values at 260 nm, which indicates leakage of small cellular components due to inner membrane damage.[16] To test the integrity of the outer membrane, the pellet was resuspended and 1-N-phenylnaphthylamine (NPN; sigma) was added to a final concentration of 15 µM.[14, 17] Fluorescence spectra were readily measured after NPN addition upon excitation at 350 nm (Figure S2). Cell lysate (3 x 1 minute sonication) was used as a positive control.

3. RESULTS

3.1 Quantification of photodynamic bacterial inactivation

When cells expressing TagRFP were irradiated no significant damage was observed for light doses below 750 J·cm^{-2}.[18] However, a population reduction of *ca.* 4-log$_{10}$ in colony-forming units (CFU) per milliliter was achieved after a light dose of 3200 J·cm^{-2} in D-PBS suspensions (*ca.* 2.5-log$_{10}$ CFU/mL reduction in normal PBS; Fig. 1). It is well known that solvent deuteration extends the $^1O_2$ lifetime[19, 20] such that the enhancement of oxidative damage upon deuteration has long been used as a mechanistic test for the involvement of $^1O_2$. The light dose used is orders of magnitude higher than that used in typical aPDT treatments[11] but comparable to that in chromophore-assisted light inactivation (CALI) assays,[21] and is consistent with the low quantum yield of $^1O_2$ generation by TagRFP (0.004±0.0001).[4] *E. coli* cells transformed with the control pET20b plasmid, devoid of the TagRFP sequence, were tested under the same experimental conditions. As shown in Fig. 1, a CFU/mL reduction of less than 0.5-log$_{10}$ units was observed in all cases. In addition, bacteria expressing TagRFP which were not irradiated did not significantly lose viability (data not shown). These negative controls confirm that damage is inflicted by a photodynamic reaction, i.e., by the combination of light, oxygen and TagRFP acting as photosensitizer.

Our observation of *ca.*1-log$_{10}$ population reduction difference between PBS- and D-PBS-suspended cells is consistent with a $^1O_2$ lifetime of 3.5 µs in H$_2$O and 65 µs in D$_2$O.[20] This agrees also with our previous report that TagRFP is a pure $^1O_2$ photosensitizer[4] and suggests that cytoplasmic location of a $^1O_2$ photosensitizer is sufficient to induce bacterial cell death following light irradiation.
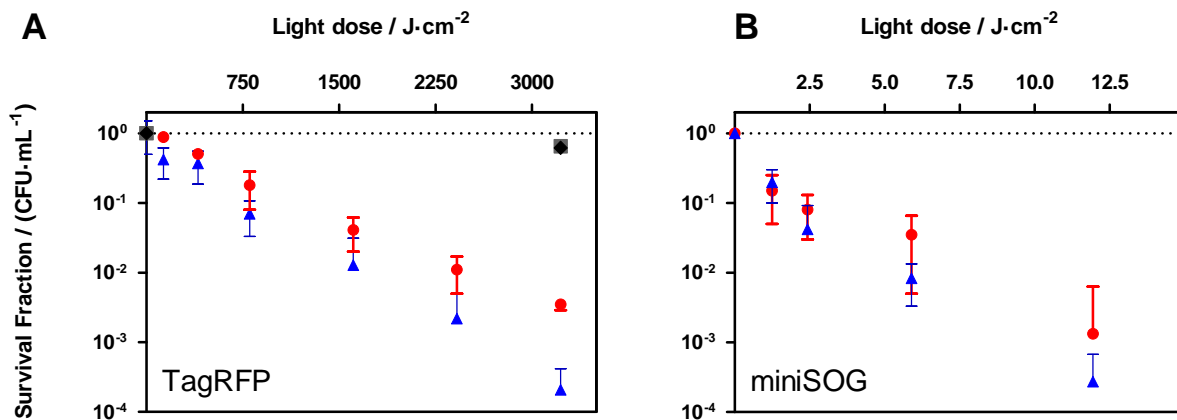
Figure 1. A) Photoinactivation of *E. coli* BL21 (DE3) expressing TagRFP in the cytosol upon irradiation with 532-nm laser light. Light-dose dependence on cell death transformed with pET20TagRFPhis in PBS (red circles) or D-PBS (blue triangles). Control with only pET20b in PBS (black diamonds) or dPBS (gray squares). B) Light-dose dependence (475 nm LED irradiation) on bacterial cell death in *E. coli* DH5α expressing miniSOG in the cytosol in PBS (red circles) and D-PBS (blue triangles).

A similar experiment was performed with *E. coli* DH5α cells expressing miniSOG in the cytosol. A population reduction of over 1-log$_{10}$ units was achieved even after a light doses as mild as 2.5 J·cm^{-2} and up to 3.5-log$_{10}$ units was observed

after 12 J·cm^{-2} treatment. Such a light dose is orders of magnitude lower than that used in previous aPDT treatments with red fluorescent proteins and comparable to the dose of KillerRed.[22] As above, an enhancement of photoinduced cell death was observed when the experiment was performed in D-PBS.No damage was observed at maximum light dose without miniSOG, nor for *E. coli* BL21 (DE3) transformed with pET20TagRFPhis plasmid (irradiated at 535 ± 15 nm) even at doses of 70 J•cm^{-2}. Moreover, no damage could be effected to bacteria expressing miniSOG in the absence of light (data not shown).

3.2 Mechanistic studies of photodynamic damage

In order to obtain further insight into the mechanism of cell death photosensitized by both fluorescent proteins, several additional assays were performed. First, we focused on the cytoplasmic cell membrane. Damage to the inner bacterial membrane is accompanied by leaching-out of low molecular-weight species and DNA and RNA fragments, which are also able to permeate the external membrane. Release of such intracellular components can be conveniently monitored by spectroscopic means, and the onset of UV absorption at 260 nm in the supernatant is taken as a strong indication of membrane damage.[14, 16] The results of this assay are shown in Fig. 2 (red circles), where the 260-nm absorbance of the supernatants of irradiated bacteria suspensions is plotted as a function of the light dose. The data have been normalized against the values for non-irradiated samples. In both cases, TagRFP- and miniSOG-expressing bacteria, a clear growth in the 260-nm absorbance can be observed almost from the outset, which indicates that photodynamic damage to the inner cell membrane occurs in both types of cells.

In a second series of assays, the integrity of the outer membrane was assessed. It is well known that gram-negative bacteria are markedly more resistant to photodynamic inactivation than gram-positive species, due to the highly organized structure of its cell envelope.[11] Specifically, many studies have shown that the presence of an additional outer membrane prevents many photosensitizers from reaching and/or binding to the inner membrane, resulting in lowered photosensitization efficiency.[11] The outer membrane is thus a typical target in gram-negative bacteria.[23] The fluorescent probe 1-N-phenylnaphthylamine (NPN), which increases its fluorescence upon binding to cells with a damaged outer membrane, was used to this end.[14, 17] As shown in Fig. 2 (blue circles), there is a markedly different behaviour between TagRFP- and miniSOG-expressing bacteria. For TagRFP, no increase in NPN fluorescence was observed relative to dark control suspensions. However, over 2-fold increase in NPN fluorescence was observed in miniSOG-tagged bacteria. This indicates that the more efficient photosensitizing properties of miniSOG result in a significant amount of $^1O_2$ being able to reach the outer membrane and inflict damage, which is not the case for TagRFP-tagged bacteria. NPN fluorescence measurements in water and in lysed cells served as further controls.[18]
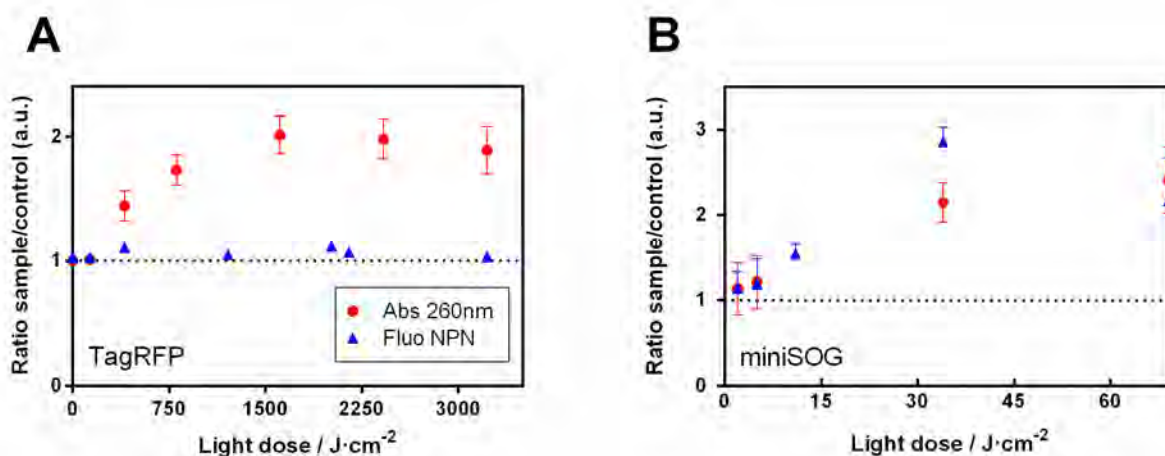
Figure 2. Bacterial cell envelope integrity assays after different aPDT light dose treatments. Red circles: absorbance of supernatants at 260 nm. Blue triangles: fluorescence of NPN. Data are normalized to values measured for non-irradiated samples. A)TagRFP in *E. coli* BL21 (DE3), laser irradiation at 532 nm; B) miniSOG in *E. coli* DH5α. LED irradiation at 475 nm.

Finally, damage to genomic DNA from *E. coli* cells was studied, since some authors have reported photodamage to genetic material in aPDT.[13, 24] DNA from irradiated cells was extracted by standard procedures and electrophoresis of the extracts was run in a 0.6 % agarose gel. No differences could be observed between samples irradiated at the maximum light dose and dark controls (not shown). This indicates that TagRFP- or miniSOG-induced photodamage to genomic DNA does not occur to any measurable extent. Our results are in line with those of previous studies where it was concluded that DNA damage is not the primary cause of bacterial cell photoinactivation.[25] However, we cannot exclude that a lethal effect may be produced by localized DNA damage that could not be detected in our assay.[26]

4. CONCLUSIONS

Purely endogenous $^1O_2$ produced by genetically-encoded photosensitizing proteins expressed in the bacterial cytosol is able to induce bacterial cell death. Photodamage seems to occur mainly in the bacterial membrane, the extent of which correlates with the photosensitizing efficiency of the protein. Both TagRFP and miniSOG can induce damage the inner membrane, but only miniSOG in the outer membrane. No damage of genomic DNA could be observed. Our observations are markedly different to those reported for an external photosensitizer.[14] Thus, the site where $^1O_2$ is primarily generated proves crucial for inflicting different types of cell damage.

This work supports the potential of genetically-encoded strategies in mechanistic studies of aPDT, and using appropriate gene transfer methods could be extended to therapeutic strategies.

ACKNOWLEDGMENTS

REFERENCES

[1] Flors, C. and Nonell, S., "Genetically-encoded photosensitizers: structure, photosensitization mechanisms and potential application to photodynamic therapy," in *Handbook of Photomedicine*. vol. in press, M. R. Hamblin and S. K. Sharma, Eds.: Taylor & Francis, 2013.

[2] Jimenez-Banzo, A., Nonell, S., Hofkens, J., and Flors, C., "Singlet oxygen photosensitization by EGFP and its chromophore HBDI," Biophys. J.*,* 94(1), 168-172 (2008).

[3] Jimenez-Banzo, A., Ragas, X., Abbruzzetti, S., Viappiani, C., Campanini, B., Flors, C., and Nonell, S., "Singlet oxygen photosensitisation by GFP mutants: oxygen accessibility to the chromophore," Photochem Photobiol Sci, 9(10), 1336-41 (2010).

[4] Ragas, X., Cooper, L. P., White, J. H., Nonell, S., and Flors, C., "Quantification of photosensitized singlet oxygen production by a fluorescent protein," Chemphyschem, 12(1), 161-5 (2011).

[5] Bulina, M. E., Chudakov, D. M., Britanova, O. V., Yanushevich, Y. G., Staroverov, D. B., Chepurnykh, T. V., Merzlyak, E. M., Shkrob, M. A., Lukyanov, S., and Lukyanov, K. A., "A genetically encoded photosensitizer," Nat .Biotechnol., 24(1), 95-99 (2006).

[6] Serebrovskaya, E. O., Edelweiss, E. F., Stremovskiy, O. A., Lukyanov, K. A., Chudakov, D. M., and Deyev, S. M., "Targeting cancer cells by using an antireceptor antibody-photosensitizer fusion protein," Proc Natl Acad Sci U S A, 106(23), 9221-9225 (2009).

[7] Vegh, R. B., Solntsev, K. M., Kuimova, M. K., Cho, S., Liang, Y., Loo, B. L., Tolbert, L. M., and Bommarius, A. S., "Reactive oxygen species in photochemistry of the red fluorescent protein Killer Red," Chem Commun, 47, 4887-4889 (2011).

[8] Baier, J., Maisch, T., Maier, M., Engel, E., Landthaler, M., and Baumler, W., "Singlet oxygen generation by UVA light exposure of endogenous photosensitizers," Biophys J, 91(4), 1452-9 (2006).

[9] Shu, X., Lev-Ram, V., Deerinck, T. J., Qi, Y., Ramko, E. B., Davidson, M. W., Jin, Y., Ellisman, M. H., and Tsien, R. Y., "A genetically encoded tag for correlated light and electron microscopy of intact cells, tissues, and organisms," PLoS Biol, 9(4), e1001041 (2011).

[10] Ruiz-Gonzalez, R., Cortajarena, A. L., Mejias, S. H., Agut, M., Nonell, S., and Flors, C., "Singlet oxygen generation by the genetically-encoded tag miniSOG," submitted.

[11] Jori, G., Fabris, C., Soncin, M., Ferro, S., Coppellotti, O., Dei, D., Fantetti, L., Chiti, G., and Roncucci, G., "Photodynamic therapy in the treatment of microbial infections: basic principles and perspective applications," Lasers Surg Med, 38(5), 468-81 (2006).

[12] Redmond, R. W. and Gamlin, J. N., "A compilation of singlet oxygen yields from biologically relevant molecules," Photochem. Photobiol., 70(4), 391-475 (1999).

[13] Salmon-Divon, M., Nitzan, Y., and Malik, Z., "Mechanistic aspects of Escherichia coli photodynamic inactivation by cationic tetra-meso(N-methylpyridyl)porphine," Photochem Photobiol Sci, 3(5), 423-9 (2004).

[14] Spesia, M. B., Caminos, D. A., Pons, P., and Durantini, E. N., "Mechanistic insight of the photodynamic inactivation of Escherichia coli by a tetracationic zinc(II) phthalocyanine derivative," Photodiagnosis Photodyn Ther, 6(1), 52-61 (2009).

[15] Ragas, X., Agut, M., and Nonell, S., "Singlet oxygen in Escherichia coli: New insights for antimicrobial photodynamic therapy," Free Radic Biol Med, 49(5), 770-6 (2010).

[16] Chen, C. Z. and Cooper, S. L., "Interactions between dendrimer biocides and bacterial membranes," Biomaterials, 23(16), 3359-68 (2002).

[17] Loh, B., Grant, C., and Hancock, R. E., "Use of the fluorescent probe 1-N-phenylnaphthylamine to study the interactions of aminoglycoside antibiotics with the outer membrane of Pseudomonas aeruginosa," Antimicrob Agents Chemother, 26(4), 546-51 (1984).

[18] Ruiz-Gonzalez, R., White, J. H., Agut, M., Nonell, S., and Flors, C., "A genetically-encoded photosensitiser demonstrates killing of bacteria by purely endogenous singlet oxygen," Photochem Photobiol Sci, 11(9), 1411-3 (2012).

[19] Schweitzer, C. and Schmidt, R., "Physical Mechanisms of generation and deactivation of singlet oxygen," Chem. Rev., 103(5), 1685-1757 (2003).

[20] Ogilby, P. R., "Singlet oxygen: there is still something new under the sun, and it is better than ever," Photochem Photobiol Sci, 9(12), 1543-60 (2010).

[21] McLean, M. A., Rajfur, Z., Chen, Z. Z., Humphrey, D., Yang, B., Sligar, S. G., and Jacobson, K., "Mechanism of Chromophore Assisted Laser Inactivation Employing Fluorescent Proteins," Anal. Chem., 81(5), 1755-1761 (2009).

[22] Waldeck, W., Heidenreich, E., Mueller, G., Wiessler, M., Toth, K., and Braun, K., "ROS-mediated killing efficiency with visible light of bacteria carrying different red fluorochrome proteins," J Photochem Photobiol B, 10928-33 (2012).

[23] Segalla, A., Borsarelli, C. D., Braslavsky, S. E., Spikes, J. D., Roncucci, G., Dei, D., Chiti, G., Jori, G., and Reddi, E., "Photophysical, photochemical and antibacterial photosensitizing properties of a novel octacationic Zn(II)-phthalocyanine," Photochem Photobiol Sci, 1(9), 641-8 (2002).

[24] Fiel, R. J., Datta-Gupta, N., Mark, E. H., and Howard, J. C., "Induction of DNA damage by porphyrin photosensitizers," Cancer Res, 41(9 Pt 1), 3543-5 (1981).

[25] Schafer, M., Schmitz, C., and Horneck, G., "High sensitivity of Deinococcus radiodurans to photodynamically-produced singlet oxygen," Int J Radiat Biol, 74(2), 249-53 (1998).

[26] Ashkenazi, H., Pechatnikov, I., and Nitzan, Y., "Low-intensity photosensitization may enhance RecA production," Curr Microbiol, 52(4), 317-23 (2006).

Synthesis, Characterization, and Photoinduced Antibacterial Activity of Porphyrin-Type Photosensitizers Conjugated to the Antimicrobial Peptide Apidaecin 1b

Ryan Dosselli,[†,||] Cristiano Tampieri,[‡] Rubén Ruiz-González,[§] Sonia De Munari,[‡,⊥] Xavier Ragàs,[§] David Sánchez-García,[§] Montserrat Agut,[§] Santi Nonell,[§] Elena Reddi,[†] and Marina Gobbo*[,‡]

[†]Department of Biology, University of Padova, via U. Bassi 58/B, I-35121 Padova, Italy
[‡]Department of Chemical Sciences, University of Padova, via F. Marzolo 1, I-35131 Padova, Italy
[§]Institut Químic de Sarrià, Universitat Ramon Llull, Vía Augusta 390, E-08017 Barcelona, Spain

S *Supporting Information*

ABSTRACT: Antimicrobial photodynamic therapy (aPDT) is an emerging treatment for bacterial infections that is becoming increasingly more attractive because of its effectiveness against multi-antibiotic-resistant strains and unlikelihood of inducing bacterial resistance. Among the strategies to enhance the efficacy of PDT against Gram-negative bacteria, the binding to a cationic antimicrobial peptide offers the attractive prospect for improving both the water solubilty and the localization of the photoactive drug in bacteria. In this work we have compared a number of free and apidaecin-conjugated photosensitizers (PSs) differing in structure and charge. Our results indicate that the conjugation of per se ineffective highly hydrophobic PSs to a cationic peptide produces a photosensitizing agent effective against Gram-negative bacteria. Apidaecin cannot improve the phototoxic activity of cationic PSs, which mainly depends on a very high yield of singlet oxygen production in the surroundings of the bacterial outer membrane. Apidaecin−PS conjugates appear most promising for treatment protocols requiring repeated washing after sensitizer delivery.
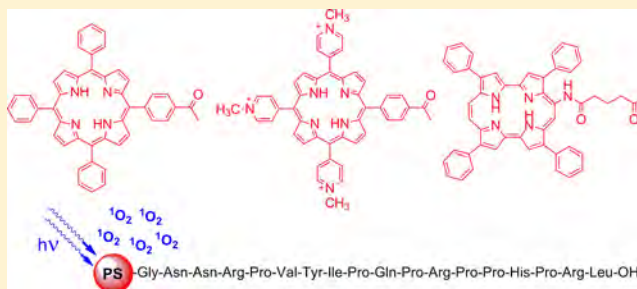
INTRODUCTION

The global diffusion of new antimicrobial infections as well as the continuously increasing resistance of pathogens against many of the commonly used antibiotics imposes a considerable effort to develop alternative therapies to the use of classical drugs. In this area antimicrobial photodynamic therapy (aPDT; also termed photodynamic antimicrobial chemotherapy, PACT) represents a very promising strategy, particularly for the treatment of superficial and localized infectious diseases.[1] The PDT concept comprises the action of three components: a photosensitizer (PS), a light source of appropriate wavelength, and oxygen. The interaction between light and the PS leads to the generation of reactive oxygen species (ROS), e.g., singlet oxygen, by two possible mechanisms involving either electron-transfer (type I) or energy-transfer (type II) reactions.[2] These ROS are highly reactive and can damage a variety of cellular components, e.g., proteins, nucleic acids, and lipids, resulting in cytotoxicity.[3−5] Advantages of aPDT over traditional antibiotics include a broad-spectrum activity, also against antibiotic-resistant species,[6] and the lack of development of resistance mechanisms due to the multitarget process.[7,8]

Porphyrins, commonly used as PSs in PDT, can efficiently kill Gram-positive bacteria, whereas only cationic PSs, or noncationic PSs in combination with agents that permeabilize the highly organized outer membrane of Gram-negative

bacteria, are able to kill Gram-negative species.[9−11] An alternative approach to improve the susceptibility of Gram-negative bacteria to the photodynamic action of neutral porphyrins involves the covalent attachment of the PS to a polymer molecule containing basic amino groups[12] or, as we recently proposed, to a cationic antimicrobial peptide.[13] Cationic antimicrobial peptides (CAMPs) are components of the innate defense of many organisms, and they are being considered a promising source of new antibiotics.[14] In addition to exerting direct antimicrobial effects, many studies have documented their ability to affect various host cell activity and to have a key modulatory role in the innate immune response.[44,45] Their overall positive charge ensures accumulation at the polyanionic microbial cell surfaces that contain acidic polymers, such as lipopolysaccharides, and wall-associated teichoic acids in Gram-negative and Gram-positive bacteria, respectively. Beyond the presence of several cationic amino acids, a substantial proportion of hydrophobic amino acid residues permit most of the CAMPs to fold into an amphipathic structure, which allows them to insert into the phospholipid bilayer of the cell membranes. After insertion, antimicrobial peptides act by either disrupting the physical

a, R = -OCH₃   b, R= -OH

c, R = -Gly-Asn-Asn-Arg-Pro-Val-Tyr-Ile-Pro-Gln-Pro-Arg-Pro-Pro-His-Pro-Arg-Leu-OH

d, R = -Gly-Pro-Arg-Pro-Pro-His-Pro-Arg-Leu-OH

e, R = -Gly-Asn-Asn-Arg-Pro-Val-Tyr-Ile-Pro-Gln-Pro-Arg-Pro-Pro-His(N^πCH₃)-Pro-Arg-Leu-OH
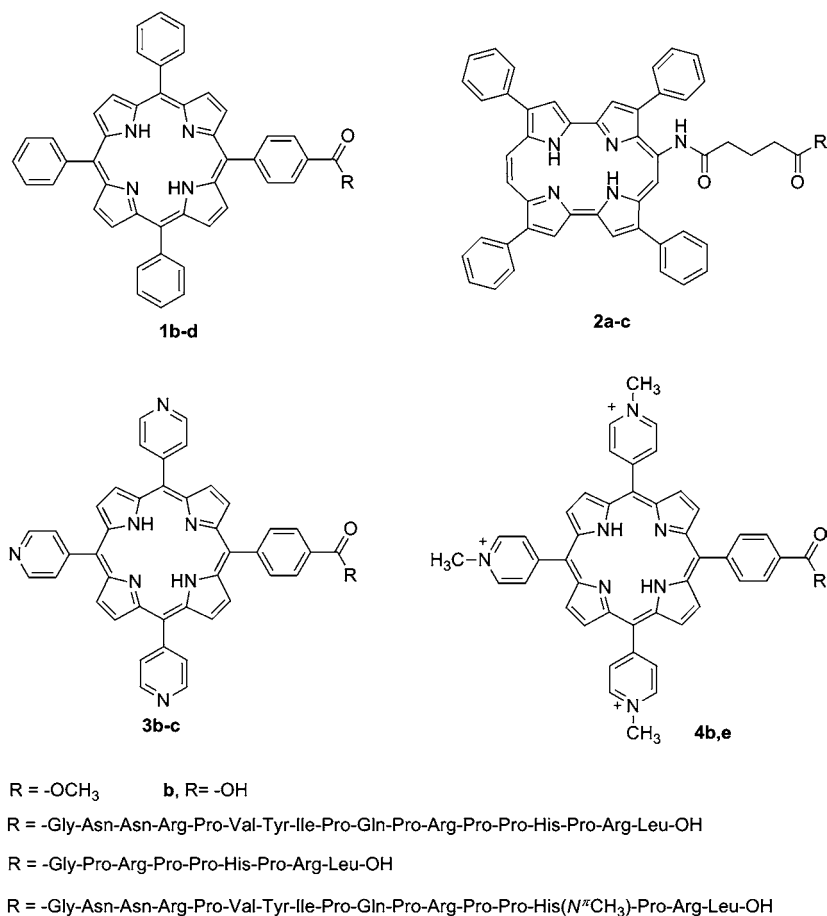
Figure 1. Structures of the photosensitizers and their peptide conjugates.

integrity of the membrane or translocating across the membrane to hit internal bacterial targets. This multitarget mode of action promises both low susceptibility to antibiotic resistance and a broad spectrum of activity against a variety of microorganisms. Among CAMPs, the family of short proline–arginine-rich peptides attracts particular interest because of some unique features, such as a higher activity against Gram-negative bacteria, a relative stability against proteolysis, and a very low toxicity against mammalian cells.[15] Apidaecin 1b, an insect 18-residue-long peptide belonging to this family, is effective against a large number of Gram-negative bacteria and a few Gram-positive bacteria,[16] where it acts by a non-pore-forming mechanism only partially elucidated.[17,18] Mutagenesis[19,20] and structure–activity relationship studies[21–24] have identified the C-terminal half of apidaecin as essential for its antimicrobial activity, and several studies have shown that the peptide is able to translocate a fluorescent tag into a bacterial cell.[22,24–26] In a preliminary communication we have shown that the conjugation of apidaecin to 5-(4′-carboxyphenyl)-10,15,20-triphenylporphyrin affords a new water-soluble PS (1c in Figure 1) that, upon light activation, is able to kill both Gram-positive and Gram-negative bacteria at concentrations at which the antimicrobial peptide and, on Gram-negative bacteria, the porphyrin alone are not effective.[13] Herein we report the synthesis, characterization, and phototoxicity studies against *Escherichia coli* and methicillin-resistant *Staphylococcus aureus* (MRSA) of new conjugates in which apidaecin and its C-terminal octapeptide were modified at the N-terminus with neutral or charged porphyrin and porphycene PSs.

■ RESULTS

Synthesis and Characterization of the Conjugates. Porphyrins 1b and 3b, properly functionalized for the covalent binding to the peptide, were prepared by established methods using the Lindsey[27] and Adler−Longo conditions,[28] respectively. We synthesized three new PS−peptide conjugates in which the porphycene 2b or the cationic porphyrin 4b was covalently linked to the N-terminal end of the antimicrobial peptide apidaecin and 5-(4′-carboxyphenyl)-10,15,20-triphenylporphyrin (1b) to its C-terminal segment (Figure 1). The trimethylated porphyrin 4b was prepared from 3b by treatment with an excess of methyl iodide in DMF, whereas alkaline hydrolysis of the porphycene 2a released the functional group from the subsequent conjugation. The synthesis of 2a has been reported elsewhere.[29] The side-chain-protected peptide sequences were automatically synthesized on a solid phase by the standard Fmoc protocol,[30] and after removal of the N-terminal amino protecting group, the selected PS (1−4b, 2.5 equiv) was coupled to the peptide chain using diisopropylcarbodiimide/N-hydroxybenzotriazole as the activating agent. The yields of the coupling reactions were in the range of 75−80% (based on HPLC) except in the case of the cationic porphyrin 4b, which apparently did not react with the peptide even using different coupling reagents and reaction conditions. The conjugate between apidaecin and this cationic PS was obtained from 3c, side-chain-protected and still attached to the solid support, by treatment with an excess of methyl iodide. Besides on pyridine nitrogens, methylation also occurred on the π-nitrogen of the histidine side chain, which usually remains unprotected during

the peptide chain assembly. After cleavage and deprotection from the solid support, the conjugates **1c**, **1d**, **2c**, and **4e** were purified by reversed-phase HPLC and characterized by analytical HPLC, electrospray mass spectrometry, and UV–vis absorption spectroscopy.

Absorption and Fluorescence of the Conjugates. The spectroscopic and photophysical properties of the PSs and their conjugates were measured in aqueous and organic media and in cell suspensions to assess the structural and environmental effects as well as their correlation with antibacterial activity.

Methanol. Figures 2 and 3 show the absorption and fluorescence spectra of the free PSs and of their peptide conjugates in methanol. While the spectra of porphyrins are essentially insensitive to conjugation (panels A, C, and D), clear changes can be observed for the porphycene (panel B). In turn, the fluorescence quantum yield does not change appreciably for the porphyrins, while it drops by ca. 50% for the porphycene (Table 1). Finally, all porphyrins show monoexponential fluorescence decay kinetics, and conjugation does not change the lifetime values either (Supporting Information, Figure S1A,C,D). Again, the situation is different for the porphycenes in that the conjugate **2c** shows biexponential kinetics unlike the free porphycene **2a** (Figure S1B), and on average the singlet state decays faster (Table 1).

Aqueous Solutions (PBS). Porphyrin **4b** is water-soluble as a consequence of its positively and negatively charged groups. It remains water-soluble after conjugation (**4e**) with small but clear shifts in the position of the Soret and Q absorption bands and changes in their relative intensities (Figure 2E). The fluorescence spectrum of **4b** shows a single, structureless broad band (Figure 3E), a behavior strikingly different from that in methanol but in line with that of the related tetracationic *meso*-tetrakis(*N*-methylpyridinium-yl)porphyrin (TMPyP).[32] Conjugation to the peptide (**4e**) leads to partial recovery of the two well-resolved fluorescence bands observed in methanol. The fluorescence decay kinetics of **4b** is monoexponential, albeit with a lifetime much shorter than that in methanol. For the conjugate **4e** two decay components can be observed, whose lifetimes are close to those of **4b** in methanol and in PBS, respectively (Figure S1E, Supporting Information, and Table 1). The kinetics is independent of concentration over 3 orders of magnitude (Figure S2A and Table S1, Supporting Information).

On the other hand, porphyrin **1b** and porphycene **2a** are insoluble in water, and therefore, no fluorescence can be recorded in this solvent. Conjugation to the peptides (**1c**, **1d**, and **2c**, respectively) renders them water-soluble, but the spectroscopic and photophysical properties change substantially relative to those in methanol: the absorption spectra show broadening of the Soret band and loss of structure in the Q region (Figure 2F–H), and the fluorescence is dramatically quenched. In addition, the fluorescence spectra of **1c** and **1d** are slightly red-shifted (Figure 3G,H), and the decays are biexponential (Figure S1G,H, Supporting Information, and Table 1) and show a clear concentration trend (Figure S2B,C and Table S1, Supporting Information).

E. coli Suspensions. The conjugate **4e** shows in cell suspensions the same absorption and fluorescence properties as it does in PBS (Figures 2I and 3I and Table 1). On the other hand, there are evident changes for conjugates **1c** and **1d** in cell suspensions relative to PBS, particularly in the absorption spectrum and in the fluorescence kinetics, which shows a third decay component not present in PBS or in methanol (Table 1).
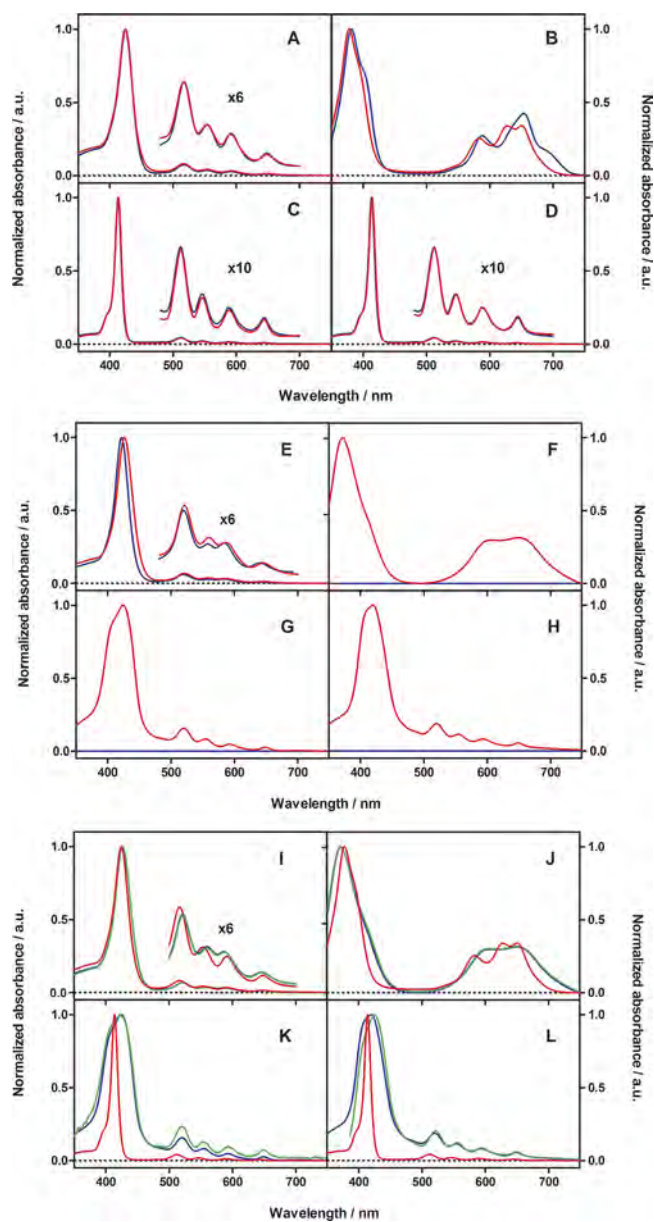
Figure 2. Absorption spectra in methanol (A–D), PBS (E–H), and *E. coli* suspensions (I–L), normalized to facilitate their comparison. The concentration is 5 μM for all compounds. Methanol: (A) **4e** (red) and **4b** (blue); (B) **2c** (red) and **2a** (blue; dichloromethane as solvent); (C) **1d** (red) and **1b** (blue); (D) **1c** (red) and **1b** (blue). PBS: (E) **4e** (red) and **4b** (blue); (F) **2c** (red) and **2a** (blue); (G) **1d** (red) and **1b** (blue); (H) **1c** (red) and **1b** (blue). *E. coli* suspensions (green): (I) **4e**; (J) **2c**; (K) **1d**; (L) **1c**. Spectra in methanol (red) and PBS (blue) are given for comparison.

Finally, the porphycene conjugate **2c** shows very similar absorption spectra in PBS and in *E. coli* suspensions (Figure 2J). However, while we could record no fluorescence in PBS, we were nevertheless able to observe extremely weak biexponential fluorescence decay in the cells (Figure 3, Figure S1J, Supporting Information, and Table 1).

Singlet Oxygen Production and Decay. All free and conjugated PSs were able to photosensitize the formation of $^1O_2$ in methanol as evidenced by its phosphorescence at 1275 nm. The quantum yields of $^1O_2$ production (Φ_Δ) were in the 0.6–0.7 range for the porphyrins and the 0.1–0.3 range for the
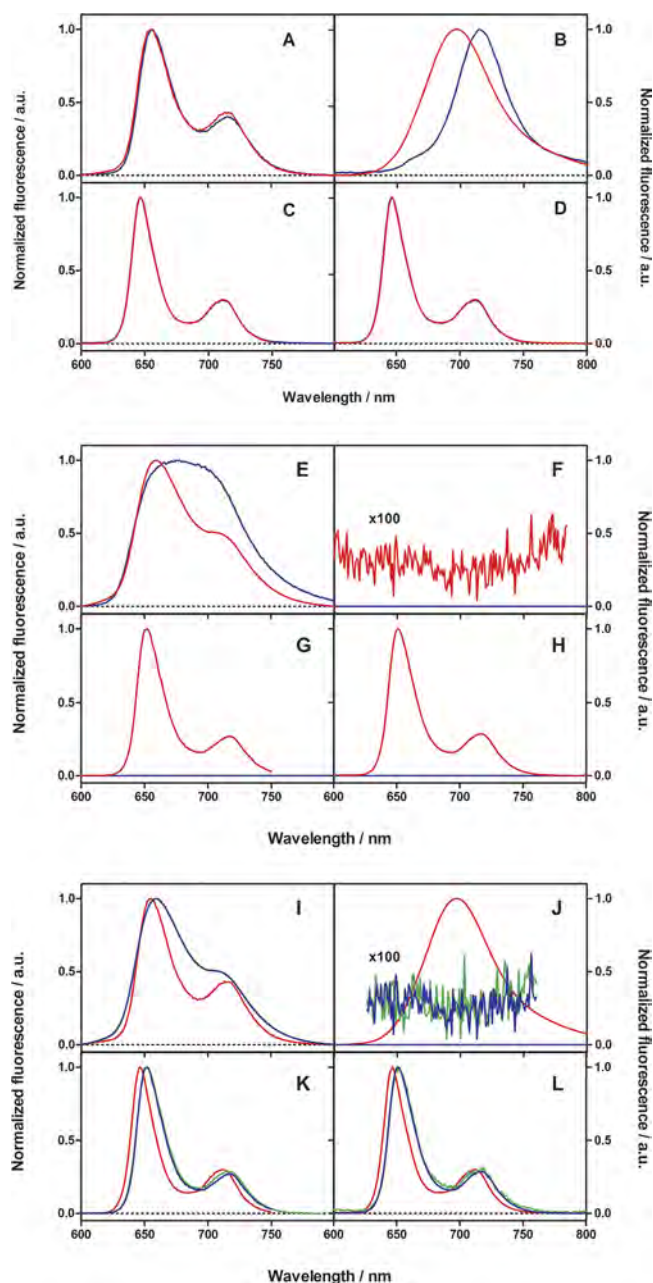
Figure 3. Emission spectra in methanol (A−D), PBS (E−H), and *E. coli* suspensions (I−L), normalized to facilitate their comparison. The concentration is 5 μM for all compounds. Methanol: (A) **4e** (red) and **4b** (blue); (B) **2c** (red) and **2a** (blue; dichloromethane as solvent); (C) **1d** (red) and **1b** (blue); (D) **1c** (red) and **1b** (blue). PBS: (E) **4e** (red) and **4b** (blue); (F) **2c** (red) and **2a** (blue); (G) **1d** (red) and **1b** (blue); (H) **1c** (red) and **1b** (blue). *E. coli* suspensions (green): (I) **4e**; (J) **2c**; (K) **1d**; (L) **1c**. Spectra in methanol (red) and PBS (blue) are given for comparison.

porphycenes (Table 2). The kinetics of $^1O_2$ production matched the results of laser flash photolysis experiments for the triplet PS decay (see the Supporting Information, Table S2). Likewise, an excellent match was found between the observed lifetime of $^1O_2$ and the literature values. In PBS, only porphyrins **4b** and **4e** retained their high ability to produce $^1O_2$; all other compounds experienced a decrease of the Φ_Δ value by 20−30-fold (porphyrins **1c** and **1d**) or even 100-fold (porphycene **2c**; Table 2). Inspection of the kinetics of $^1O_2$

(Figure S3, Supporting Information) reveals that production of singlet oxygen by conjugate **4e** is as fast as that by the free porphyrin **4b** (Table 2), yet for the conjugates **1c**, **1d**, and **2c** it is 1 order of magnitude slower. On the other hand, the lifetime of $^1O_2$ for all conjugates in deuterated PBS is shorter than the value expected in this solvent (67 μs),[34] which is actually observed only for the free porphyrin **4b**. When *E. coli* suspensions were studied, the $^1O_2$ signals showed essentially the same pattern as that in PBS solutions (Figure S4, Supporting Information, and Table 2).

Circular Dichroism (CD) Studies. The conformational properties of the conjugates were investigated by CD spectroscopy in different environments, including water and membrane-mimicking solvents, and compared to those of the parent peptide. As a consequence of the high proline content (6 out of 18 residues), in water apidaecin assumes a prevalently disordered, extended structure (Figure 4A), and in membrane-mimicking environments it exists as a mixture of conformers with a high percentage of nonrepetitive bent structures, most probably β-turns (Figure 4C,D).[23,25] The CD spectra of the conjugates in water are characterized by a broad negative band around 200 nm, much more intense for those with the cationic porphyrin than for those with the neutral PS (Figure 4A). Moreover, **1c** and **2c** showed a split Cotton effect in the Soret band region (Figure 4B), indicating that porphyrins are chirally oriented and close to one another in space.[35] These results suggest that while **4e** can assume in water a fully extended structure, conjugates **1c** and **2c** show the tendency to form aggregates with the peptide chain probably folded over the hydrophobic porphyrin platform[36] and the porphyrins close to one another to reduce the exposure to the solvent. Aggregation was confirmed by a change in the UV spectra of these conjugates moving from methanol to water. In organic solvent (2,2,2-trifluoroethanol, TFE) and in the presence of SDS micelles, the CD spectrum of the conjugates is similar to that of the parent peptide, with a broad band at 202 nm, a shoulder at 220 nm, and comparable intensities (Figure 4C,D). This suggests that in membrane-mimicking environments the conformational preferences of the peptide are minimally affected by the intramolecular interactions with the PS.

Photoinactivation of *E. coli*. To determine the photosensitizing efficiency of our PSs and peptide−PS conjugates against Gram-negative bacteria, *E. coli* suspensions were incubated in the dark for 60 min with different concentrations (1.5, 5, 10, and 15 μM) of the agents and then illuminated (light dose of 36 J/cm² of red light for **2a** and **2c**, 13.5 J/cm² of blue light for all other compounds) with or without washings. At the concentrations used, apidaecin alone did not cause any decrease of *E. coli* survival,[13] as did its C-terminal segment **1d**, in both the dark and light conditions (Table S3, Supporting Information). In addition, neither **1b** nor **2a** caused any bacteria photokilling in their unconjugated form. All conjugates exhibited markedly concentration-dependent abilities to kill *E. coli* under illumination with an efficiency that largely depended on the type of conjugate (Figure 5A). Indeed, considering the unwashed samples, **4b** and **4e** caused complete killing of bacteria at 5 and 10 μM concentrations, respectively, while all other agents were considerably less potent and at 15 μM reduced the survival of *E. coli* by 4 log at maximum. Moreover, it is interesting to notice that **1c** was slightly more efficient than **1d** and caused a bacterial mortality similar to that of **2c**. However, when illumination was carried out after three washings of the cells to remove the unbound PS (Figure 5B;

Table 1. Fluorescence Properties of the Peptide Conjugates and Model Compounds in Methanol, PBS, and *E. coli* Suspensions (Fractional Amplitudes in Parentheses)

compd	$\lambda_{F,max}$/nm			Φ_F		τ_S/ns		
	MeOH	PBS	*E. coli*	MeOH[a]	PBS[b]	MeOH	PBS	*E. coli*
1b	647	ns[c]		0.040	ns	10.1	ns	
1c	647	651	651	0.050	0.006	9.8	10.7 (0.82)	10.5 (0.46)
							3.1 (0.18)	7.5 (0.33)
								3.1 (0.21)
1d	646	652	652	0.044	0.006	9.8	6.1 (0.61)	5.9 (0.11)
							2.6 (0.39)	4.9 (0.48)
								2.5 (0.41)
2a	715	ns		0.030[d]		1.46[d]		
2c	697			0.016	<0.0001	0.9 (0.94)		0.9 (0.75)
						9.6 (0.06)		5.2 (0.25)
4b	656	675		0.022	0.008	7.9	4.2	
4e	655	660	660	0.024	0.018	8.1	4.2 (0.49)	4.2 (0.48)
							7.1 (0.51)	7.1 (0.52)

[a]Cresyl violet as standard (Φ_F(methanol) = 0.54).[31] [b]TMPyP as standard (Φ_F(PBS) = 0.017).[9] [c]Not soluble. [d]In toluene.

Table 2. Kinetics of Singlet Oxygen Production (Φ_Δ) and Decay (τ_Δ) of the Peptide Conjugates and Model Compounds in Air-Saturated Methanol, PBS, and *E. coli* Suspensions

| compd	Φ_Δ		τ_Δ/μs		
	MeOH[a]	PBS[b]	MeOH[c]	PBS[d]	*E. coli*[e]
1b	0.63	ns[f]	9.8	ns	
1c	0.70	0.020	9.8	3.0	2.3
				43[g]	
1d	0.66	0.036	9.5	45[g]	
2a	0.26[h]	ns		ns	
2c	0.14	0.001	9.8	42[g]	
4b	0.69	0.73	9.6	3.6	3.6
				60[g]	
4e	0.67	0.89	9.6	3.6	3.6
				36[g]	

[a]TMPyP as standard (Φ_Δ(methanol) = 0.74).[3] [b]TPPS as standard (Φ_Δ(water) = 0.69).[3] [c]Literature value 10.4 μs.[33] [d]Literature value 3.3 μs in PBS and 67 μs in D-PBS.[33] [e]In PBS. [f]Not soluble. [g]In D-PBS. [h]Toluene as solvent.

Figure S5, Supporting Information), only **1d** retained an efficacy similar to that observed in unwashed samples, while all other PSs were considerably less potent. In particular, the loss of efficacy of **4b** and **4e** in killing bacteria was drastic, with a decreased killing ability of 6 log at the 10 μM concentration. On the other hand, **1c** and **2c**, which were less photoactive without washings, were less hampered by the washing treatment. We also studied the photoinactivation of *E. coli* as a function of the incubation times and using a concentration of 5 μM for **4b** and **4e** and 10 μM for all other compounds (Figure S6, Supporting Information). The results showed that the time of dark incubation of the cells with the PSs and their conjugates before irradiation does not affect to a great extent the photokilling efficiency of *E. coli*. Incubation times ranging from 15 to 120 min gave very similar decreases of bacterial survival when irradiation was carried out leaving the unbound PS in solution. Only with **4b** and **4e** was the photoinactivation ability slightly improved by increasing the incubation time, but this effect was lost after the repeated washing treatment.

Photoinactivation of MRSA. The photoinactivation of MRSA was studied by using the same experimental approach

used for *E. coli*. Contrary to *E. coli*, both **1b** and **4b** were highly photoactive against MRSA; they caused complete killing of unwashed bacteria at, respectively, 50 nM and 0.5 μM concentrations (Figure 6A). These findings are in agreement with the well-known susceptibility of Gram-positive bacteria to many cationic and neutral PSs. However, the photoactivities of the two porphyrins were differently affected by the washing treatments: **1b** did not show any appreciable change, while the potency of **4b** was dramatically reduced (Figure S7A, Supporting Information). Both **1b** and **4b** lost part of their activity when conjugated to apidaecin or its C-terminal segment. In particular, at a 0.5 μM concentration the unconjugated porphyrins caused complete cell killing, while **4e**, **1c**, and **1d** caused only about a 3 log reduction of survival (Figure 6A). The washing of *S. aureus* before illumination did not appreciably reduce the killing efficiency of **1c** and **1d**, while it significantly affected that of **4e**, as was observed with *E. coli* (Figure S7A). **2a** and its apidaecin conjugate **2c** were less effective than the porphyrin counterparts, being active in the range of 1.5−15 μM, i.e., at 10-fold higher concentrations (Figure 6B). However, conjugation with apidaecin strengthened the action of the PS (Figure S7B). As for *E. coli*, also with *S. aureus* the photoinactivation experiments were performed as a function of the incubation time, and no major differences in the efficiency of *S. aureus* photoinactivation with conjugated and unconjugated PSs were found by changing the incubation times from 15 to 120 min (Figure S8, Supporting Information).

Uptake Experiments. Flow cytometry experiments were carried out to evaluate the interaction of the PSs (free or conjugated to apidaecin) following incubation with *E. coli* and *S. aureus* cells under the same experimental conditions as in the photoinactivation experiments. The measurements showed that **1b** does not associate with *E. coli* cells very efficiently. As shown in Figure 7, after incubation with 5 μM **1b**, only a small fraction of *E. coli* cells exhibited a fluorescence signal higher than the basal value in both washed and unwashed cells. On the contrary, MRSA cells incubated with **1b** exhibited a fluorescence signal whose intensity was orders of magnitude higher than the background signal, suggesting efficient porphyrin association/binding either before or after the washings. The conjugation of **1b** to apidaecin or its C-terminal segment did not affect to a great extent the association of **1b** with MRSA, while it increased the association with *E. coli*, as
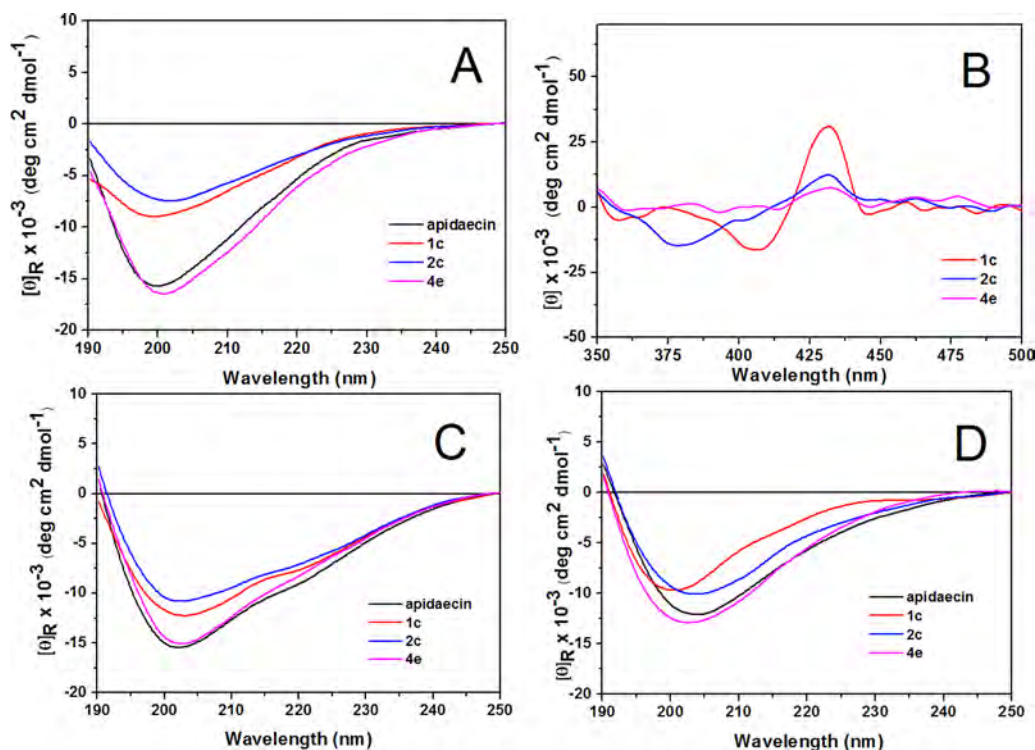
Figure 4. CD spectra of apidaecin and its conjugates in 10% methanol (A, amide region; B, Soret region), TFE (C), and 30 mM aqueous SDS (D). The peptide concentration is 10 μM.

clearly shown by the higher fluorescence signals exhibited by a large fraction of cells incubated with **1c** and **1d**. Both free and apidaecin-conjugated **4b** did not appreciably interact with *E. coli* since only in unwashed cells was the measured mean fluorescence intensity slightly higher than the background signal. Similar results were observed with MRSA cells, suggesting that **4b** and its conjugate exhibit a very poor ability to interact with both Gram-positive and Gram-negative bacteria.

■ DISCUSSION

In our previous paper[13] we have already shown that the conjugate **1c** is endowed with antibacterial activity following light activation. In this paper we have extended our investigations to other PS—apidaecin conjugates, containing either a neutral porphycene or a cationic porphyrin (respectively **2a** and **4b** in Figure 1) to assess the effects of structural modifications. Porphycene, a structural isomer of porphyrin, was chosen for its larger absorption coefficients in the red part of the spectrum, where light can deeply penetrate into tissues.[37] Because positively charged PSs are effective in PDT against Gram-negative bacteria without the addition of outer-membrane-disrupting agents,[38] we hypothesized that a conjugate between apidaecin and a cationic porphyrin could further promote the uptake of the PS in Gram-negative bacteria, thereby reducing the minimum effective dose. Moreover, to establish whether the antimicrobial peptide is able to direct the PS against specific bacterial targets, we also synthesized a conjugate between porphyrin **1b** and a short cationic peptide (PRPPHPRL) corresponding to the C-terminal segment of apidaecin. Although the mode of action of apidaecin has not been determined in detail, several points of evidence suggest that this peptide enters *E. coli* cells by a non-pore-forming mechanism and, once inside the cell, interacts

with components of the protein synthesis machinery, impairing protein synthesis and folding.[17,18] The full-length apidaecin sequence is very important, and the C-terminal octapeptide does not possess any antibacterial activity,[21] nor is it able to translocate a fluorescent cargo into bacterial cells.[24] Thus, most probably, the conjugate with this cationic peptide (**1d**) can effectively bind to the bacterial cell wall without being able to reach the cytosol.

Efficient PSs for PDT must have appropriate photophysical properties, such as an intense red-light absorption band and a high quantum yield of generation of both the long-lived excited triplet state and cytotoxic ROS, in particular singlet oxygen, $^1O_2$. To establish whether the peptide moiety negatively affects the PS photosensitizing efficiency, the porphyrin—peptide conjugates were submitted to a detailed photophysical characterization. The fluorescence properties and the singlet oxygen production ability of the peptide conjugates **1c—d** and **4e** in methanol (Tables 1 and 2) are essentially identical to those of free PSs, demonstrating that the peptide moiety exerts no influence on the PS photosensitizing efficiency in this solvent. Only in the case of porphycene **2a** did we observe changes in the absorption spectrum and a reduction by about 50% of the fluorescence quantum yield of the PS and in $^1O_2$ production after conjugation to the peptide, which may be ascribed to interactions between the peptide and the macrocyclic core. The situation is different in an aqueous environment (PBS) where the photophysical data change considerably relative to those in methanol for all conjugates and particularly for those containing a neutral PS. The decrease in the fluorescence quantum yield, the concentration dependence of the fluorescence kinetics, and the slow kinetics of $^1O_2$ production in **1c—d** and **2c** reveal the presence of intermolecular interactions, as observed also by CD spectros-
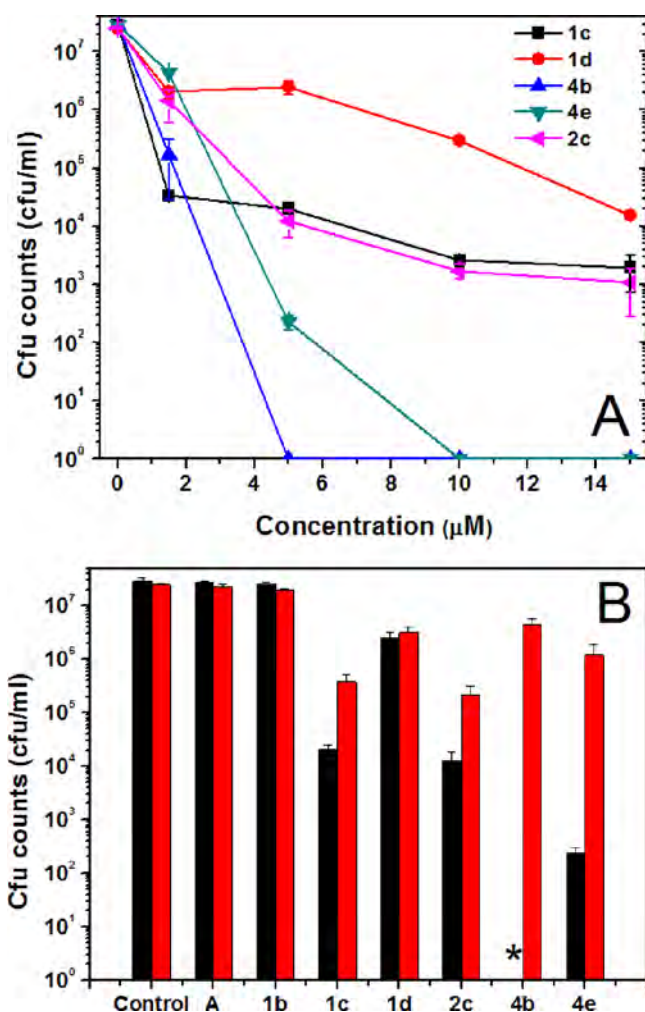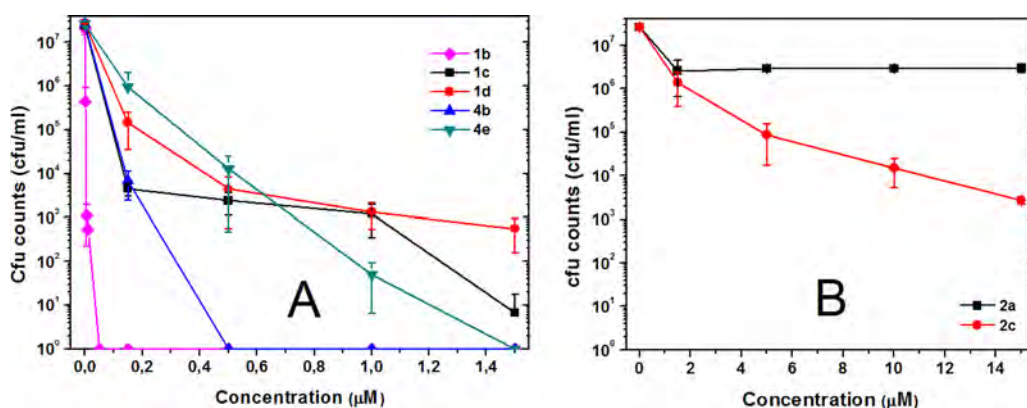
Figure 5. (A) *E. coli* photoinactivation with different concentrations (1.5–15 μM) of **2c**, **1c**, **1d**, **4b**, and **4e**. *E. coli* cells were incubated for 60 min with the PS and irradiated with a fixed light dose (36 J/cm² of 600–750 nm red light for **2c**, 13.5 J/cm² of 390–460 nm blue light for all other compounds). (B) *E. coli* photoinactivation with a 5 μM concentration of apidaecin or the tested PSs. Irradiation with a fixed light dose, as described above, was carried out without washing (black bars) or after three washings with PBS (red bars); the asterisk means a sterile solution.

copy (Figure 4B). Such interactions account also for the 20-fold lower production of $^1O_2$ in PBS relative to methanol (Table 2).

Nevertheless, following illumination (with blue light for **1c**–**d** and red light for **2c**), the conjugates were phototoxic against *E. coli* cells, inducing a decrease of survival of 3–4 log at a 15 μM concentration (Figure 5). On the other hand, the unconjugated PS **2a** was completely ineffective toward *E. coli* (data not shown), consistent with data previously reported for **1b**[13] and other neutral porphyrins, which are unable to diffuse through the highly organized outer membrane of Gram-negative bacteria.[39] Peptide conjugates **1c**–**d** and **2c** associate efficiently with *E. coli* cells, as suggested by the observation that repetitive washing of bacteria treated with conjugates, before illumination, caused only a moderate reduction of phototoxicity (Figure 5B; Figure S5, Supporting Information). In the case of **1c**–**d** this is also supported by the flow cytometry results (Figure 7). Porphycene was not fluorescent enough for cytometry studies, but the detection of fluorescence by time-resolved techniques in the *E. coli* suspensions, but not in PBS (Table 1), must be taken as proof of binding. A deeper understanding of the type of binding/association of **1c**–**d** to *E. coli* cells was obtained by analyzing the fluorescence decay kinetics: unlike PBS or methanol, three decay components were observed in cell suspensions, which suggest multiple binding sites (Table 1). The match between two of the three observed lifetimes with those detected in PBS indicates that one binding site is located in an aqueous-like environment. Thus, the third decay component suggests that an additional binding site exists where the conjugates experience a less hydrophilic environment.

However, the phototoxicity and the photophysical and flow cytometry results for the apidaecin conjugate **1c** and its truncated analogue **1d** are so similar that it is difficult to propose a different localization of these conjugates in *E. coli* cells. Most probably both conjugates can diffuse through the outer membrane and localize in different environments, but since the C-terminal apidaecin fragment is unable to translocate a PS across the cytoplasmic membrane, we are led to conclude that the apidaecin conjugate is also not able to reach the bacterial targets of apidaecin in cytosol.

The conjugate between the cationic porphyrin **4e** and apidaecin possesses a +6 net positive charge, well-distributed along the whole molecule, that is expected to discourage the aggregation phenomena observed in conjugates **1c** and **2c**. In

Figure 6. MRSA photoinactivation with different concentrations of (A) **1b**, **1c**, **1d**, **4b**, and **4e** (1 nM to 1.5 μM) and (B) **2b** and **2c** (1.5–15 μM). MRSA cells were incubated with the PS for 60 min and irradiated with a fixed light dose (36 J/cm² of 600–750 nm red light for **2b** and **2c**, 13.5 J/cm² of 390–460 nm blue light for all other compounds).
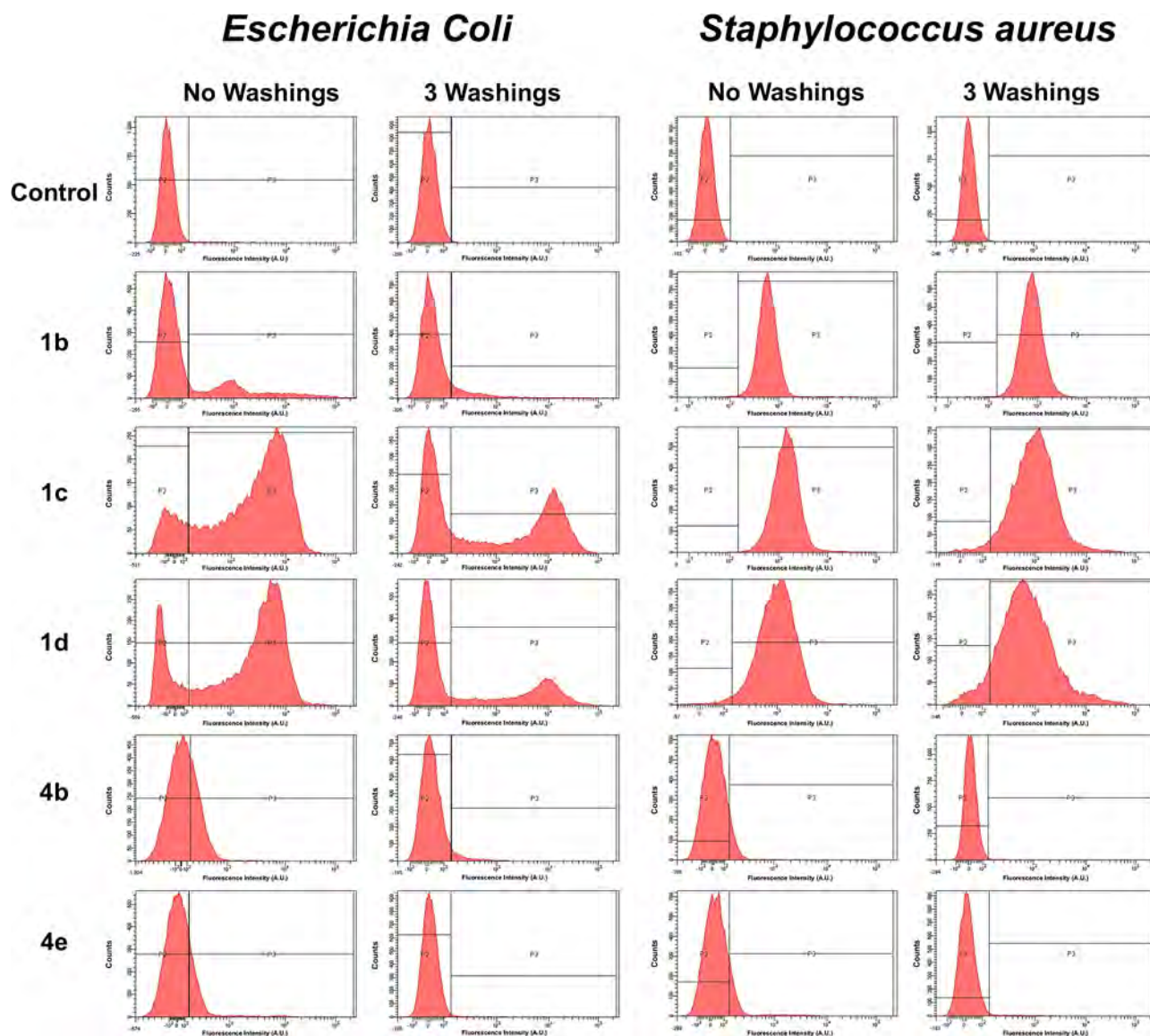
Figure 7. Uptake of the peptide conjugates and model PSs in *E. coli* and MRSA. The cells were incubated with the compounds for 60 min and then analyzed by flow cytometry. Concentrations of the compounds: 5 μM for *E. coli* and 1.5 μM for MRSA.

confirmation of this, the far-UV CD spectrum of **4e** in water is very similar to that of the free peptide and no dichroic signal, indicative of porphyrin−porphyrin interactions, was detected in the Soret band region (Figure 4 A,B). Aggregation can also be ruled out by the lack of concentration effects on the decay kinetics (Figure S2A and Table S1, Supporting Information). It can therefore be safely concluded that the major differences observed between **4b** and **4e** (Table 1) are due to interactions between apidaecin and the porphyrin within the conjugate. Comparison of the fluorescence spectrum, quantum yield, and kinetics for **4b** and **4e** reveals that two populations of conjugates coexist, in which the porphyrin is either exposed to water or shielded from it by the peptide. This conclusion is consistent with the well-known solvent-polarity effects on the fluorescence of tetrapyridinium porphyrins.[32] Nevertheless, the production of $^1O_2$ was very high in PBS, comparable to or even higher than that in methanol (Table 2). In fact, the conjugate **4e** caused total photokilling of *E. coli* cells at a concentration (10 μM) at which **1c** induced a strong (4 log) but incomplete reduction of cell survival (Figure 5A). The cationic porphyrin

4b proved to be even more potent than its apidaecin conjugate **4e** (Figure 5A). The $^1O_2$ lifetime data in Table 2, particularly in deuterated PBS, indicate that apidaecin is able to quench $^1O_2$. Thus, because $^1O_2$ molecules are generated in the vicinity of apidaecin, some of them will be quenched by the peptide during their lifetime rather than by cell components.

The washing of the cells before illumination, to remove the unbound or weakly associated PS, caused a tremendous reduction of photokilling of *E. coli* cells, and under these conditions **4b** became the least efficient PS (Figure 5B; Figure S5, Supporting Information). Flow cytometry measurements showed that only unwashed cells exhibited red fluorescence slightly above the background after incubation with these compounds (Figure 7). Thus, the results indicate that **4b** and **4e** associate very weakly with *E. coli* cells and the killing of unwashed cells is caused mainly by singlet oxygen generated by the PS molecules not associated with or loosely associated with the bacteria. Several reports of PDT on Gram-negative bacteria have pointed out that if singlet oxygen can be generated in sufficient quantities near the bacterial outer membrane, it will

be able to diffuse into the cell to inflict damage to the vital structure.[1,40] Our photophysical data thus support this hypothesis.

Testing the above PS against MRSA reveals a number of differences relative to *E. coli*. First, except for the porphycene, the concentration needed to inactivate bacteria was 1 order of magnitude lower. Interestingly, the porphycene conjugate was almost equally active against both kinds of bacteria. The higher susceptibility of Gram-positive bacteria to photodynamic damage has long been known for a large number of PSs.[41] Second, it is interesting to recall that washings did not appreciably remove **1b** and its conjugates (**1c** and **1d**) from the cells (Figure 7), nor did it decrease the photodynamic inactivation of MRSA (Figure S7, Supporting Information). In addition, the nonconjugated porphyrin **1b** was the most active PS. This probably can be related to its more hydrophobic character, which helps in penetration of the cell wall and the cytoplasmic membrane of Gram-positive bacteria. The porphycene **2a** was probably too hydrophobic, and its strong aggregation in the external medium prevented cell entrance. Concerning PSs **4b** and **4e**, the observations are similar to those of *E. coli*: the nonconjugated PS **4b** is more active than **4e** on account of its lower ability to quench $^1O_2$, and both lose their activity after washings due to the very poor binding to the bacterial cells (Figure 7).

CONCLUSIONS

The search for more effective antimicrobial PSs has led to a number of strategies. Among them, binding to an antimicrobial peptide offers the attractive prospect of enhancing both the water solubility of the PS and the efficiency of the PDT treatments through a synergistic effect. In this work we have compared a number of free and apidaecin-conjugated PSs differing in structure and charge. Our results confirm previous findings that the conjugation of per se ineffective highly hydrophobic PSs to a cationic peptide produces a photosensitizing agent effective against Gram-negative bacteria. MRSA are even more susceptible to the action of conjugates, which produce the same reduction of bacterial growth at one-tenth the concentration. The apidaecin ability to penetrate Gram-negative bacteria is unfortunately lost after conjugation to a bulky PS, but the amphiphilic character conferred by the peptide enforces the binding of the PS to the bacterial outer membrane. Apidaecin−PS conjugates appear most promising for treatment protocols requiring repetitive washing after sensitizer delivery, where the most active cationic PSs, such as **4b** and its apidaecin conjugate **4e**, are rapidly washed out. On the other hand, apidaecin cannot improve the phototoxic activity of the cationic porphyrin, which is mainly determined by a very high yield of singlet oxygen production in the surroundings of the bacterial outer membrane.

EXPERIMENTAL SECTION

General Methods. All chemicals were commercial products of the best grade available, and unless otherwise indicated, they were used directly without further purification. The starting porphyrins, 5-(4-carboxyphenyl)-10,15,20-triphenylporphyrin (**1b**),[42] 9-(glutaric methylesteramide)-2,7,12,17-tetraphenylporphycene (**2a**),[29] and 5-(4-carboxyphenyl)-10,15,20-tris(4-pyridyl)porphyrin (**3b**) and its tris-*N*-methylpyridinium iodide (**4b**),[28] were prepared according to literature procedures. 9-Fluorenylmethoxycarbonyl (Fmoc)-amino acids and all other chemicals for the solid-phase synthesis were supplied by Sigma-Aldrich. Fmoc-Leu-Wang resin was purchased from Novabiochem (Merck Biosciences). Analytical HPLC separations were carried out on

a Dionex Summit dual-gradient HPLC instrument, equipped with a four-channel UV−vis detector, using a Vydac 218TP54 column (250 × 4.6 mm, 5 μm, flow rate at 1.5 mL/min). Mobile phases A (aqueous 0.1% trifluoroacetic acid (TFA)) and B (90% aqueous acetonitrile containing 0.1% TFA) were used for preparing binary gradients. All analyses were carried out under gradient conditions (10−50% B in 20 min, except as otherwise indicated). All crude peptides were purified to 95% or more homogeneity for analytical and other experimental purposes. Semipreparative HPLC was carried out on a Shimadzu series LC-6A chromatograph, equipped with two independent pump units, a UV−vis detector, and a Vydac 218TP1022 column (250 × 22 mm, 10 μm, flow rate at 15 mL/min). Elutions were carried out by the same mobile phases described above. All the purified peptides were analyzed again by HPLC and HRMS. Mass spectral analyses were carried out on a Mariner API-TOF workstation (PerSeptive Biosystems Inc.), operating with ESI techniques in positive mode. NMR spectra were recorded on a Varian Gemini 300 spectrometer (300 and 75.5 MHz for ^{1}H and ^{13}C, respectively). UV−vis spectra were recorded at rt on a Shimadzu UV-2501PC spectrophotometer or on a Lambda 5 spectrophotometer (Perkin-Elmer), in 0.1 or 1 cm quartz cells.

Chemical Synthesis. *19-Glutaramide-2,7,12,17-tetraphenylporphycene (2b).* A 44 mg (0.1 mmol) sample of **2a** was dissolved in 14 mL of THF and combined with 14 mL of methanol, and 9 mL of 4 N aqueous sodium hydroxide was added dropwise with stirring at rt within 5 min. The reaction was stirred for an additional 45 min, neutralized, and then precipitated under acidic conditions with the complete addition of 50 mL of ice-cold 5% acetic acid. The flaky precipitate was filtered, washed with water and then with water/methanol (1:1), and dried. The title compound was obtained in the form of a dark green powder. Yield: 27 mg (70%). ^{1}H NMR (400 MHz, DMSO-d_6): δ = 12.10 (br s, 1H), 10.96 (s, 1H), 10.08 (s, 1H), 10.07 (s, 1H), 10.05 (s, 1H), 9.93 (d, J = 12, 1H), 9.91 (d, J = 12, 1H), 9.85 (s, 1H), 9.82 (s, 1H), 8.37 (m, 6H), 7.98 (d, J = 8, 2H), 7.88 (m, 5H), 7.74 (m, 5H), 7.60 (m, 2H), 4.29 (s, 1H), 3.93 (s, 1H), 2.25 (t, J = 8, 2H), 2.16 (t, J = 8, 2H), 1.72 (q, J = 8, 2H). ^{13}C NMR (100 MHz, DMSO-d_6): δ = 174.1, 171.9, 158.0, 144.7, 143.7, 142.8, 142.7, 141.3, 139.1, 137.7, 135.6, 135.4, 135.3, 134.8, 134.3, 133.3, 132.8, 131.1, 131.0, 130.3, 129.2, 129.2, 129.1, 128.0, 127.4, 127.1, 123.1, 125.0, 124.5, 116.0, 115.5, 113.9, 33.9, 33.06, 19.8. HRMS (ESI-TOF): m/z calcd for $C_{49}H_{38}N_5O_3$ 744.2969 [M + H]$^+$, found 744.2970.

Synthesis of PS−Peptide Conjugates (General Procedure). The peptide sequences were prepared on an automated Advanced Chemtech 348Ω peptide synthesizer, on a 0.25 mmol scale, starting from Fmoc-Leu-Wang (substitution 0.6 mmol/g of resin). The *tert*-butyl group and 2,2,4,6,7-pentamethyldihydrobenzofuran-5-sulfonyl group were used to protect tyrosine and arginine side chains, respectively, and the trityl group to protect asparagine and histidine side chains. Fmoc deprotection was achieved with 20% piperidine in DMF (5 + 15 min). Couplings were performed in the presence of *O*-(benzotriazol-1-yl)-*N,N,N′,N′*-tetramethyluronium hexafluorophosphate/*N*-hydroxybenzotriazole/*N,N*-diisopropylethylamine (reaction time 45−60 min), using an excess of 4 equiv of the carboxyl component. After the coupling of the last amino acid and removal of the Fmoc group, the resin was washed with DMF and CH$_2$Cl$_2$ and then dried under vacuum. The dried resins containing the protected amino acid sequences were used in the coupling reaction to the porphyrin derivatives. The H-peptide-resin (0.025 mmol) was swelled in DMF for 1 h and then washed with DMF. To the peptidyl resin was added 600 μL of a DMF−CH$_2$Cl$_2$ (1:1, v/v) solution containing 0.05 mmol of porphyrin (**1b**, **2b** or **3b**), 0.05 mmol of diisopropylcarbodiimide, and 0.05 mmol of 1-hydroxybenzotriazole. The reaction mixture was shaken overnight and then filtered to remove the excess of reagents. The resin was repeatedly washed with DMF and CH$_2$Cl$_2$, until the filtrate was colorless, and then dried under vacuum. Cleavage and deprotection was carried out by treatment of the resin with a mixture of TFA−triisopropylsilane−water (95:2.5:2.5 by volume) for 1.5 h at rt. The resin was filtered and washed with TFA, and the filtrates were combined and reduced under vacuum to a small volume. Addition of cold ether yielded a green precipitate, which was repeatedly washed with ether and dried under vacuum. The conjugates

1−3c and **1d** were purified by semipreparative HPLC (linear gradient 50−80% B in 20 min), and the fractions containing the conjugate were collected and lyophilized to yield the pure compound. The purity was ≥95% as determined by analytical HPLC (isocratic 10% B for 3 min; linear gradient 10−90% B in 30 min). The conjugates were characterized as follows:

(**1c**) Yield: 75%. HPLC: t_R = 22.0 min. UV−vis (methanol): λ_{max}/nm (log ε/M^{-1} cm^{-1}) 414 (5.48), 513 (4.05), 546 (3.70), 591 (3.45), 642 (3.35). HRMS: m/z calcd for $C_{140}H_{179}N_{36}O_{24}$ 2748.38 [M + H]$^+$, found 2748.39.

(**1d**) Yield: 80%. HPLC: t_R = 24.3 min. UV−vis (methanol): λ_{max}/nm (log ε/M^{-1} cm^{-1}) 413 (5.41), 512 (4.02), 548 (3.68), 589 (3.54), 644 (3.34). HRMS: m/z calcd for $C_{91}H_{104}N_{21}O_{11}$ 1666.82 [M + H]$^+$, found 1666.84.

(**2c**) Yield: 50%. HPLC: t_R = 30.3 min. UV−vis (methanol): λ_{max}/nm (log ε/M^{-1} cm^{-1}) 378 (4.99), 583 (4.40), 628 (4.53), 650 (4.54). HRMS: m/z calcd for $C_{144}H_{186}N_{37}O_{25}$ 2833.44 [M + H]$^+$, found 2833.39.

(**3c**) Yield: 50%. HPLC: t_R = 13.7 min. UV−vis (methanol): λ_{max}/nm (log ε/M^{-1} cm^{-1}) 413 (5.11), 510 (3.81), 544 (3.30), 586 (3.27), 642 (2.89). HRMS: m/z calcd for $C_{137}H_{176}N_{39}O_{24}$ 2751.37 [M + H]$^+$, found 2751.39.

Conjugate 4e. The porphyrin−peptide conjugate **3c** (0.02 mmol), still attached to the solid support, was swelled in DMF, and a 10% solution of methyl iodide in DMF (2 mL) was added to the peptidyl resin. The reaction mixture was shaken overnight at rt and then filtered to remove the excess of reagents. The resin was repeatedly washed with DMF and CH_2Cl_2 and then dried under vacuum. After detachment from the resin, as described above, the conjugate was purified by semipreparative HPLC (linear gradient 17−30% B in 25 min). Yield: 50%. HPLC: t_R = 12.4 min. UV−vis (methanol): λ_{max}/nm (log ε/M^{-1} cm^{-1}) 424 (5.15), 515 (3.98), 556 (3.63), 590 (3.51), 647 (3.03). HRMS: m/z calcd for $C_{141}H_{187}N_{39}O_{24}$ 702.615 [M^{4+}], found 702.874.

Spectroscopic Measurements. Absorption spectra were recorded on a double-beam Cary 6000i spectrophotometer (Varian), equipped with a 110 mm diameter integrating sphere and a high-performance photomultiplier tube for diffuse transmittance measurements. Absorption coefficients were derived from the slopes of Lambert−Beer plots. Fluorescence emission spectra were recorded in a Spex Fluoromax-4 spectrofluorometer. Fluorescence decays were recorded with a time-correlated single-photon-counting system (Fluotime 200) equipped with a red-sensitive photomultiplier. Excitation was achieved by means of a 405 nm LED working at a 10 MHz repetition rate. The counting frequency was always below 1%. Fluorescence decays were analyzed using the PicoQuant FluoFit 4.0 data analysis software. $^1O_2$ phosphorescence was detected by means of a customized PicoQuant Fluotime 200 system described in detail elsewhere.[43] Briefly, a diode-pumped pulsed Nd:YAG laser (FTSS355-Q, Crystal Laser) working at a 10 kHz repetition rate at 532 nm (12 mW, 1.2 μJ per pulse) was used for excitation. A 1064 nm rugate notch filter (Edmund Optics) was placed at the exit port of the laser to remove any residual component of its fundamental emission in the near-IR region. The luminescence exiting from the side of the sample was filtered by a cold mirror (CVI Melles Griot) to remove any scattered laser radiation and focused on the entrance slit of a Science Tech 9055 dual-grating monochromator. A near-IR-sensitive photomultiplier tube assembly (H9170-45, Hamamatsu Photonics) was used as the detector at the exit port of the monochromator. Photon counting was achieved with a multichannel scaler (Becker&Hickl MSA 300 or PicoQuant's Nanoharp 250). The time-resolved emission signals were analyzed using the FluoFit software to extract lifetime values. Laser flash photolysis measurements were carried out using a Q-switched Nd:YAG laser (Surelite I-10, Continuum) with a right-angle geometry and an analyzing beam produced by a Xe lamp (PTI, 75 W) in combination with a dual-grating monochromator (model 101, PTI) coupled to a photomultiplier (Hamamatsu R928). Kinetic analysis of the individual transients was performed with software developed in our laboratory. All spectroscopic measurements were carried out in 1 cm quartz cuvettes (Hellma) at rt. For the measurements in bacterial suspensions, bacteria were incubated in the dark at the conditions employed for the photoinactivation experiments, namely, 5 μM PS for 1 h. When required, the cells were washed once and resuspended in PBS to a final concentration of ~1 × 10^7 cfu mL^{-1}, and 3 mL volumes of the suspensions were irradiated with 3 million laser pulses at 532 nm under gentle stirring. CD measurements were carried out on a Jasco-715 spectropolarimeter, using a quartz cell of 0.1 cm path length. The spectra were recorded at 298 K and were the average of a series of six scans made at 0.1 nm intervals in the 250−190 and 350−550 nm regions. Sample concentrations in water (pH 7), TFE, and aqueous 30 mM SDS were in the range of 10−13 μM. Ellipticity is reported as the mean residue ellipticity $[\theta]_R$ (deg cm^2 dmol^{-1}).

Bacteria Culture. *E. coli* ATCC 25922 and the methicillin-resistant strain of *S. aureus* ATCC BAA-44 were purchased from LGC Promochem (Teddington, U.K.). Cultures were maintained by two weeks of subcultures in brain heart infusion (BHI; Difco, Detroit, MI) agar. For spectroscopic measurements we used instead the *E. coli* ECT strain, purchased from the Spanish-type cell culture collection.

Bacteria Photoinactivation. For the photoinactivation experiments, the bacteria were grown overnight in BHI at 37 °C, harvested by centrifugation, washed twice, and resuspended in PBS (10 mM phosphate, 0.14 M NaCl, 2.7 mM KCl, pH 7.3) at a density of ~2 × 10^7 cells/mL. The cell density was evaluated by measuring the turbidity of the suspension in a Perkin-Elmer spectrophotometer (model Lambda 5). The bacteria used in the experiments were collected from cultures in the stationary phase of growth.

The bacteria were incubated with different concentrations of the PSs in the dark at rt for 60 min or with a fixed PS concentration for different times. After incubation, the suspensions were (i) directly exposed to light with the unbound PS left in the suspension (no washing) or (ii) centrifuged (10000g for 5 min), the pellet resuspended in 1 mL of PBS, and washed two additional times with PBS before illumination (three washings). For illumination, aliquots of cell samples obtained as described above were transferred into 96-well plates (200 μL/well). Samples incubated with porphycene and its conjugate with apidaecin 1b were irradiated with red light (600−750 nm) with the Waldmann PDT 1200 lamp supplied by Waldmann MedizintechNnik; the cells were illuminated from the top of the plates with a fluence rate at the level of the samples of 40 mW/cm^2, as measured with an International Light power meter, and for a total light dose of 36 J/cm^2. Bacteria incubated with porphyrins and their conjugates were irradiated with blue light (390−460 nm, with a maximum at 420 nm) emitted by a UV 236 lamp supplied by Waldmann Eclairage SA; the cells were illuminated from the bottom of the plates with a fluence rate of 15.2 mW/cm^2, as measured with the Waldmann UV-meter, and for a total light dose of 13.5 J/cm^2. After illumination, aliquots of bacteria suspensions were serially 10-fold-diluted in PBS, and 50 μL volumes of the appropriate dilutions were plated in duplicate onto BHI agar to determine colony-forming units (cfu). Treated and untreated cells were incubated overnight at 37 °C to allow colony formation. Suspensions of bacteria exposed to PSs but kept in the dark and subjected to the same procedure applied to the irradiated suspensions were also plated onto BHI agar after the appropriate serial dilutions. Controls also included bacteria not exposed to any agent and bacteria exposed to light or peptide only. Each experiment was performed at least three times with independent bacterial suspensions.

Flow Cytometry. The interaction of PSs with bacteria was evaluated by flow cytometry. For these experiments, the bacteria were subjected to the same treatments used for photoinactivation experiments, but instead of being illuminated after incubation and washings, they were analyzed with a FACSCanto II flow cytometer. Samples were excited with the 488 nm laser, and fluorescence emission signals were recorded at wavelengths higher than 670 nm. The bacteria population was isolated from the instrument noise by setting electronic gates on the dual-parameter dot plots of forward scatter against side scatter. For each sample, 20 000 events were acquired and analyzed with the FACSDiva software (BD). Samples not incubated with the PSs were used to determine the cell background fluorescence.

■ ASSOCIATED CONTENT

ⓢ Supporting Information

Fluorescence decay kinetics, singlet oxygen phosphorescence kinetics, and bacteria photoinactivation after repetitive washings and as a function of the incubation time. This material is available free of charge via Internet at http://pubs.acs.org.

■ AUTHOR INFORMATION

Corresponding Author

*Phone: +39 0498275741. Fax: +39 0498275829. E-mail: marina.gobbo@unipd.it.

Present Addresses

‖Centre for Integrative Bee Research (CIBER), ARC CoE in Plant Energy Biology, MCS Building M316, The University of Western Australia, 6009 Crawley, Australia.

⊥Chemistry Research Laboratory, Department of Chemistry, University of Oxford, Mansfield Road, Oxford OX1 3TA, United Kingdom.

Notes

The authors declare no competing financial interest.

■ ACKNOWLEDGMENTS

■ ABBREVIATIONS USED

BHI, brain heart infusion; CAMP, cationic antimicrobial peptide; cfu, colony-forming units; D-PBS, deuterated phosphate-buffered saline; PDT, photodynamic therapy; PS, photosensitizer; ROS, reactive oxygen species; TFE, 2,2,2-trifluoroethanol; TMPyP, *meso*-tetrakis(*N*-methylpyridinium-yl)porphyrin; TPPS, *meso*-tetrakis(4-sulfonatophenyl)-porphyrin

■ REFERENCES

(1) Hamblin, M. R.; Hasan, T. Photodynamic therapy: a new antimicrobial approach to infectious disease? *Photochem. Photobiol. Sci.* **2004**, *3*, 436−450.

(2) Foote, C. S. Definition of type I and type II photosensitized oxidation. *Photochem. Photobiol.* **1991**, *54*, 659−659.

(3) Redmond, R.; Gamlin, J. A compilation of singlet oxygen yields from biologically relevant molecules. *Photochem. Photobiol.* **1999**, *70*, 391−475.

(4) Stark, G. Functional consequences of oxidative membrane damage. *J. Membr. Biol.* **2005**, *205*, 1−16.

(5) Ravanat, J.; Di Mascio, P.; Martinez, G.; Medeiros, M.; Cadet, J. Singlet oxygen induces oxidation of cellular DNA. *J. Biol. Chem.* **2000**, *275*, 40601−40604.

(6) Maisch, T. A New strategy to destroy antibiotic resistant microorganisms: antimicrobial photodynamic treatment. *Mini-Rev. Med. Chem.* **2009**, *9*, 974−983.

(7) Lambrechts, S.; Demidova, T.; Aalders, M.; Hasan, T.; Hamblin, M. Photodynamic therapy for *Staphylococcus aureus* infected burn wounds in mice. *Photochem. Photobiol. Sci.* **2005**, *4*, 503−509.

(8) Tavares, A.; Carvalho, C. M. B.; Faustino, M. A.; Neves, M. G. P. M. S.; Tome, J. P. C.; Tome, A. C.; Cavaleiro, J. A. S.; Cunha, A.; Gomes, N. C. M.; Alves, E.; Almeida, A. Antimicrobial photodynamic therapy: study of bacterial recovery viability and potential development of resistance after treatment. *Mar. Drugs* **2010**, *8*, 91−105.

(9) Reddi, E.; Ceccon, M.; Valduga, G.; Jori, G.; Bommer, J.; Elisei, F.; Latterini, L.; Mazzucato, U. Photophysical properties and antibacterial activity of meso-substituted cationic porphyrins. *Photochem. Photobiol.* **2002**, *75*, 462−470.

(10) Bertoloni, G.; Rossi, F.; Valduga, G.; Jori, G.; Vanlier, J. Photosensitizing activity of water- and lipid-soluble phthalocyanines on *Escherichia coli*. *FEMS Microbiol. Lett.* **1990**, *71*, 149−155.

(11) Minnock, A.; Vernon, D.; Schofield, J.; Griffiths, J.; Parish, J.; Brown, S. Mechanism of uptake of a cationic water-soluble pyridinium zinc phthalocyanine across the outer membrane of *Escherichia coli*. *Antimicrob. Agents Chemother.* **2000**, *44*, 522−527.

(12) Tegos, G.; Anbe, M.; Yang, C.; Demidova, T.; Satti, M.; Mroz, P.; Janjua, S.; Gad, F.; Hamblin, M. Protease-stable polycationic photosensitizer conjugates between polyethyleneimine and chlorin-(e6) for broad-spectrum antimicrobial photoinactivation. *Antimicrob. Agents Chemother.* **2006**, *50*, 1402−1410.

(13) Dosselli, R.; Gobbo, M.; Bolognini, E.; Campestrini, S.; Reddi, E. Porphyrin−apidaecin conjugate as a new broad spectrum antibacterial agent. *ACS Med. Chem. Lett.* **2010**, *1*, 35−38.

(14) Hancock, R. E. W.; Sahl, H. Antimicrobial and host-defense peptides as new anti-infective therapeutic strategies. *Nat. Biotechnol.* **2006**, *24*, 1551−1557.

(15) Otvos, L. The short proline-rich antibacterial peptide family. *Cell. Mol. Life Sci.* **2002**, *59*, 1138−1150.

(16) Li, W.; Ma, G.; Zhou, X. Apidaecin-type peptides: biodiversity, structure-function relationships and mode of action. *Peptides* **2006**, *27*, 2350−2359.

(17) Castle, M.; Nazarian, A.; Yi, S.; Tempst, P. Lethal effects of apidaecin on *Escherichia coli* involve sequential molecular interactions with diverse targets. *J. Biol. Chem.* **1999**, *274*, 32555−32564.

(18) Otvos, L.; O, I.; Rogers, M.; Consolvo, P.; Condie, B.; Lovas, S.; Bulet, P.; Blaszczyk-Thurin, M. Interaction between heat shock proteins and antimicrobial peptides. *Biochemistry* **2000**, *39*, 14150−14159.

(19) Casteels, P.; Romagnolo, J.; Castle, M.; Casteels-Josson, K.; Erdjumentbromage, H.; Tempst, P. Biodiversity of apidaecin-type peptide antibiotics—prospects of manipulating the antibacterial spectrum and combating acquired resistance. *J. Biol. Chem.* **1994**, *269*, 26107−26115.

(20) Taguchi, S.; Mita, K.; Ichinohe, K.; Hashimoto, S. Targeted engineering of the antibacterial peptide apidaecin, based on an in vivo monitoring assay system. *Appl. Environ. Microbiol.* **2009**, *75*, 1460−1464.

(21) Dutta, R. C.; Nagpal, S.; Salunke, D. M. Functional mapping of apidaecin through secondary structure correlation. *Int. J. Biochem. Cell Biol.* **2008**, *40*, 1005−1015.

(22) Zhou, X.; Li, W.; Pan, Y. Functional and structural characterization of apidaecin and its N-terminal and C-terminal fragments. *J. Pept. Sci.* **2008**, *14*, 697−707.

(23) Gobbo, M.; Biondi, L.; Filira, F.; Gennaro, R.; Benincasa, M.; Scolaro, B.; Rocchi, R. Antimicrobial peptides: synthesis and antibacterial activity of linear and cyclic drosocin and apidaecin 1b analogues. *J. Med. Chem.* **2002**, *45*, 4494−4504.

(24) Czihal, P.; Hoffmann, R. Mapping of apidaecin regions relevant for antimicrobial activity and bacterial internalization. *Int. J. Pept. Res. Ther.* **2009**, *15*, 157−164.

(25) Gobbo, M.; Benincasa, M.; Bertoloni, G.; Biondi, B.; Dosselli, R.; Papini, E.; Reddi, E.; Rocchi, R.; Tavano, R.; Gennaro, R. Substitution of the arginine/leucine residues in apidaecin Ib with peptoid residues: effect on antimicrobial activity, cellular uptake, and proteolytic degradation. *J. Med. Chem.* **2009**, *52*, 5197−5206.

(26) Matsumoto, K.; Orikasa, Y.; Ichinohe, K.; Hashimoto, S.; Ooi, T.; Taguchi, S. Flow cytometric analysis of the contributing factors for antimicrobial activity enhancement of cell-penetrating type peptides: case study on engineered apidaecins. *Biochem. Biophys. Res. Commun.* **2010**, *395*, 7−10.

(27) Lindsey, J.; Schereiman, I.; Hsu, H.; Kearney, P.; Marguerettaz, A. Rothemund and Adler−Longo reactions revisited: synthesis of tetraphenylporphyrins under equilibrium conditions. *J. Org. Chem.* **1987**, *52*, 827−836.

(28) Ishikawa, Y.; Yamashita, A.; Uno, T. Efficient photocleavage of DNA by cationic porphyrin-acridine hybrids with the effective length of diamino alkyl linkage. *Chem. Pharm. Bull.* **2001**, *49*, 287−293.

(29) Anguera, G.; Llinàs, M. C.; Batllori, X.; Sánchez-García, D. Aryl nitroporphycenes and derivatives: first regioselective synthesis of dinitroporphycenes. *J. Porphyrins Phthalocyanines* **2011**, *15*, 1−6.

(30) Chan, W. C.; White, P. D. *Fmoc Solid Phase Peptide Synthesis*; Oxford University Press: New York, 2000; pp 41−74.

(31) Magde, D.; Brannon, J. H.; Cremers, T. L.; Olmsted, J. Absolute luminescence yield of cresyl violet. A standard for the red. *J. Phys. Chem.* **1979**, *83*, 696−699.

(32) Vergeldt, F. J.; Koehorst, R. B. M.; van Hoek, A.; Schaafsma, T. J. Intramolecular interactions in the ground and excited states of tetrakis(*N*-methylpyridyl)porphyrins. *J. Phys. Chem.* **1995**, *99*, 4397−4405.

(33) Scaiano, J. C., Ed. *CRC Handbook of Organic Photochemistry*; CRC Press: Boca Raton, FL, 1989; p 496.

(34) Ogilby, P. R.; Foote, C. S. Chemistry of singlet oxygen. 36. Singlet molecular oxygen ($^1\Delta_g$) luminescence in solution following pulsed laser excitation. Solvent deuterium isotope effects on the lifetime of singlet oxygen. *J. Am. Chem. Soc.* **1982**, *104*, 2069−2070.

(35) Arai, T.; Inudo, M.; Ishimatsu, T.; Akamatsu, C.; Tokusaki, Y.; Sasaki, T.; Nishino, N. Self-assembling of the porphyrin-linked acyclic penta- and heptapeptides in aqueous trifluoroethanol. *J. Org. Chem.* **2003**, *68*, 5540−5549.

(36) Sibrian-Vazquez, M.; Jensen, T.; Fronczek, F.; Hammer, R.; Vicente, M. Synthesis and characterization of positively charged porphyrin-peptide conjugates. *Bioconjugate Chem.* **2005**, *16*, 852−863.

(37) Jori, G. Far-red-absorbing photosensitizers—their use in the photodynamic therapy of tumors. *J. Photochem. Photobiol., A* **1992**, *62*, 371−378.

(38) Valduga, G.; Breda, B.; Giacometti, G.; Jori, G.; Reddi, E. Photosensitization of wild and mutant strains of *Escherichia coli* by meso-tetra (N-methyl-4-pyridyl)porphine. *Biochem. Biophys. Res. Commun.* **1999**, *256*, 84−88.

(39) George, S.; Hamblin, M. R.; Kishen, A. Uptake pathways of anionic and cationic photosensitizers into bacteria. *Photochem. Photobiol. Sci.* **2009**, *8*, 788−795.

(40) Dahl, T.; Midden, W.; Hartman, P. Pure singlet oxygen cytotoxicity for bacteria. *Photochem. Photobiol.* **1987**, *46*, 345−352.

(41) Dai, T.; Huang, Y.; Hamblin, M. R. Photodynamic therapy for localized infections—state of the art. *Photodiagn. Photodyn. Ther.* **2009**, *6*, 170−188.

(42) Swamy, N.; James, D.; Mohr, S.; Hanson, R.; Ray, R. An estradiol-porphyrin conjugate selectively localizes into estrogen receptor-positive breast cancer cells. *Bioorg. Med. Chem.* **2002**, *10*, 3237−3243.

(43) Jimenez-Banzo, A.; Ragas, X.; Kapusta, P.; Nonell, S. Time-resolved methods in biophysics. 7. Photon counting vs. analog time-resolved singlet oxygen phosphorescence detection. *Photochem. Photobiol. Sci.* **2008**, *7*, 1003−1010.

(44) Brown, K. L.; Hancock, R. E. W. Cationic host defense (antimicrobial) peptides. *Curr. Opin. Immunol.* **2006**, *18*, 24−30.

(45) Tavano, R.; Segat, D.; Gobbo, M.; Papini, E. The honeybee antimicrobial peptide apidaecin differentially immunomodulates human macrophages, monocytes and dendritic cells. *J. Innate Immun.* **2011**, *3*, 614−622.

Naphthoxazole-Based Singlet Oxygen Fluorescent Probes[†]

Rubén Ruiz-González[1], Renzo Zanocco[2], Yasser Gidi[2], Antonio L. Zanocco[2], Santi Nonell*[1] and Else Lemp*[2]

[1]Grup d'Enginyeria Molecular, Institut Químic de Sarrià, Universitat Ramon Llull, Barcelona, Spain
[2]Departamento de Química Orgánica y Fisicoquímica, Facultad de Ciencias Químicas y Farmacéuticas, Universidad de Chile, Santiago, Chile

ABSTRACT

In this study, we report the synthesis and photochemical behavior of a new family of photoactive compounds to assess its potential as singlet oxygen ($^1O_2$) probes. The candidate dyads are composed by a $^1O_2$ trap plus a naphthoxazole moiety linked directly or through an unsaturated bond to the oxazole ring. In the native state, the inherent great fluorescence of the naphthoxazole moiety is quenched; but in the presence of $^1O_2$, generated by the addition and appropriate irradiation of an external photosensitizer, a photooxidation reaction occurs leading to the formation of a new chemical entity whose fluorescence is two orders of magnitude higher than that of the initial compound, at the optimal selected wavelength. The presented dyads outperform the commonly used indirect fluorescent $^1O_2$ probes in terms of fluorescence enhancement maintaining the required specificity for $^1O_2$ detection in solution.

INTRODUCTION

Reactive oxygen species (ROS) are present and participate in many biological processes. Among them, singlet oxygen ($^1O_2$), also well known because its use as a synthetic reagent, plays a key role in the pathological and physiological processes. It can oxidize various kinds of biological molecules (*i.e.* proteins, DNA and lipids), leading to a plethora of deleterious effects that can result in *e.g.* cell death or degenerative diseases (1). Over the years, insight has been gained in the rules that obey its generation, the characters involved and the energy requirements, which has led, among others, to the development of $^1O_2$-based therapies such as photodynamic therapy, in which a drug referred to as the photosensitizer (PS) produces $^1O_2$ upon exposure to light of the appropriate wavelength (2). Despite the major progress made, a better understanding of $^1O_2$ behavior in biological systems is still needed. Of critical importance, techniques and/or methods able not only to detect but also to quantify the concentration of $^1O_2$ both in solution and *in vivo* are still needed (3,4).

Singlet oxygen can be detected through its intrinsic phosphorescence with maximum centered at 1275 nm (5). This is a robust, specific, noninvasive and direct method; but it suffers from weak sensitivity due to the low efficiency for $^1O_2$ emission, particularly in biological media, where the lifetime of $^1O_2$ is very short (3.1 μs) (6) and the phosphorescence quantum yield is very small, *ca* 10^{-7} (7).

Trapping $^1O_2$ with suitable chemical acceptors is also extensively used, as such traps and/or their oxidation products, can be monitored more easily through absorption (8,9), fluorescence (3) or ESR (10,11). Fluorogenic probes that develop a bright fluorescence upon reaction with $^1O_2$ have attracted much interest lately as they offer excellent sensitivity and convenience, given the widespread use of fluorescence microscopy techniques. Thus, a two-component system comprised a $^1O_2$ trapping moiety and a suitable fluorophore covalently bound to it is the current paradigm underlying fluorogenic $^1O_2$ probes. In their native state, the luminescence of the emitting moiety is quenched by the trap. Oxidation of the trap by $^1O_2$ eliminates this quenching channel and the luminescence of the fluorophore is recovered.

Several probes have been developed following this principle: DPAX and DMAX (12,13), MTTA-Eu^{3+} (14) and, more recently, SOSG (15–17). All use an anthracene moiety as $^1O_2$ trap that quenches the luminescence of the fluorophore by an electron transfer process. The same concept has been recently used to develop a near-infrared probe, His-Cy, where anthracene has been replaced by a histidine and a cyanine is chosen as fluorophore (18). A common drawback for all the above probes is that the fluorescence increases only moderately after reaction with $^1O_2$, *e.g.* from less than two-fold for His-Cy (18) to *ca* 10-fold for SOSG. Moreover, as electron transfer reactions are strongly dependent on solvent polarity, false-positive signals arise that merely reflect location of the probe in a less polar microenvironment rather than reaction with $^1O_2$, *e.g.* when the probe is in hydrophobic pockets of proteins (16). In addition, the presence of an anthracene moiety in the structure is potentially misleading as anthracene is itself a $^1O_2$ PS that may autooxidize the probe, which further complicates its use (19).

We reasoned that the above problems could be overcome by designing a probe with distinct absorption and fluorescence spectra for the native and oxidized forms. This would allow enhancing the fluorescence of the oxidized form relative to the native probe to an unprecedented level. We report herein the synthesis and characterization of representative members of a new family of $^1O_2$ fluorescence probes based on furan trapping moieties linked to naphthoxazole fluorophores (Fig. 1). Four naphthoxazole derivatives have been synthesized. 2-(2-(Furan-2-yl)ethyl) naphtho[1,2-d]oxazole, **FN-I1**, contains a naphthoxazole linked

2-(2-(furan-2-yl)ethyl)naphtho[1,2-*d*]oxazole
FN-I1

2-(furan-2-yl)naphtho[1,2-*d*]oxazole
FN-I2

(*E*)-2-(2-(furan-2-yl)vinyl)naphtho[1,2-*d*]oxazole
FN-4

(*E*)-2-(4-methylstyryl)naphtho[1,2-*d*]oxazole
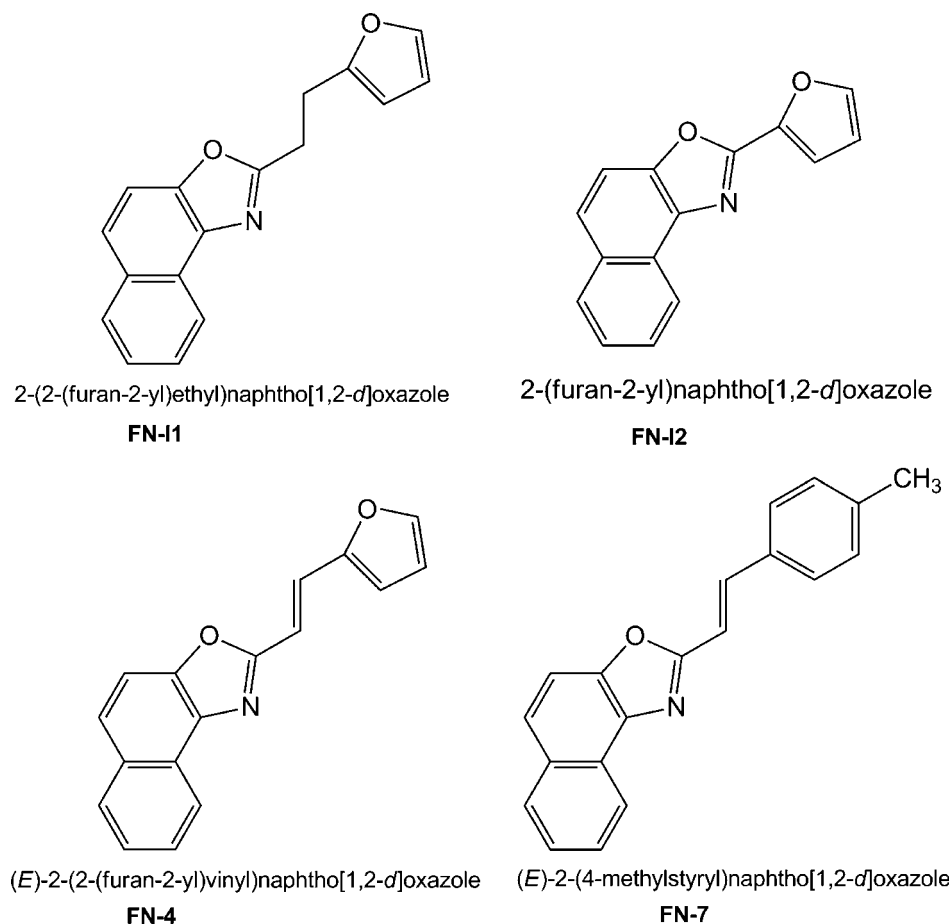**FN-7**

Figure 1. Structure of studied naphthoxazole derivatives.

to a furan through a saturated ethyl bridge. In 2-(furan-2-yl)naph-tho[1,2-d]oxazole, **FN-I2**, the furan moiety is bonded directly to the position 2 of the oxazole ring, whereas in (E)-2-(2-(furan-2-yl)vinyl)naphtho[1,2-d]oxazole, **FN-4**, the naphthoxazole and the furan are conjugated through an unsaturated ethylidene link. In the control molecule, (E)-2-(4-methylstyryl)naphtho[1,2-d]oxaz-ole, **FN-7**, the furan ring of **FN-4** has been replaced by a nonre-active tolyl group. Two candidates could be used as $^1O_2$ sensors namely **FN-I2** and **FN-4**, as their fluorescence is boosted by a factor of *ca* 135 and 300, respectively, upon reaction with $^1O_2$.

MATERIALS AND METHODS

Materials. Perinaphthenone, new methylene blue (NMB), anthracene and naphthalene were purchased from Sigma and used as received. All sol-vents used were UV grade.

(E)-2-(2-(furan-2-yl)vinyl)naphtho[1,2-d]oxazole, FN-4. To a mixture of 2-methylnaphthoxazole (1 mM, 0.15 mL) and furylcarboxaldehyde (0.09 mM, 0.075 mL) in 6 mL of dimethyl sulfoxide, 0.15 mL of aque-ous KOH 50% was added. The mixture was stirred by 12 h at room tem-perature. Addition of 15 mL of water afforded a yellow precipitate which was washed with cold water and cold methanol. Recrystallization from acetonitrile afforded 135 mg of the yellow product, yield 57%, m.p. = 124–126°C. ^{1}H-NMR (CDCl$_3$); δ: 8.51 (d, J = 8.1 Hz, 1H); 7.96 (d, J = 8.1 Hz, 1H); 7.79 (d, J = 9.0 Hz, 1H); 7.69–7.64 (m, 2H); 7.60–7.53 (m, 3H); 7.08 (d, J = 15.9 Hz, 1H); 6.62 (d, J = 3.3 Hz, 1H); 6.51 (m, 1H). MS(ESI) *m/z*: 262.11 [M+H]+, 261.11 [M]+.

2-(2-(furan-2-yl)ethyl)naphtho[1,2-d]oxazole, FN-I1. A quantity of 100 mg (0.38 mmol) of (E)-2-(2-(furan-2-yl)vinyl)naphtho[1,2-d]oxazole,

FN-4, in 50 mL of dry methanol, was reduced under hydrogen employ-ing 50 mg of Pd-C catalyst. The mixture was stirred during 4 h at room temperature, then, the catalyst was removed by filtration and the solution concentrated *in vacuo*. Recrystallization of the solid residue from petro-leum ether 40–60°C, afforded 32 mg of white crystals, 32% yield, m.p. = 120–123°C. ^{1}H-NMR (CDCl$_3$); δ: 8.49 (d, J = 8.0 Hz, 1H); 7.96 (d, J = 8.1 Hz, 1H); 7.76 (d, J = 9.0 Hz, 1H); 7.64 (d, J = 14.2 Hz, 2H); 7.51 (d, J = 14.2 Hz, 1H); 7.33 (s, 1H); 6.27 (d, J = 3.6 Hz, 1H); 6.07 (d, J = 3.6 Hz, 1H); 3.38 (d, J = 7.8 Hz, 2H), 3.30 (d, J = 7.9 Hz, 2H); ppm.

*2-(furan-2-yl)naphtho[1,2-d]*oxazole, FN-I2. A mixture of 1-amino-2-naphthol (1 mmol), 2-furylcarboxaldehyde (1 mmol) and triethylamine (2 mmol) in 10 mL of dry ethanol was refluxed 3 h under nitrogen. The end of reaction was monitored by thin layer chromatography up to disap-pearance of the aldehyde. After being cooled to room temperature, the solution was concentrated *in vacuo*, and the crude product recrystallized from acetonitrile to obtain 25% of the product, m.p. 134–136°C. ^{1}H-NMR (CDCl$_3$); δ: 8.54 (d, J = 8.2 Hz, 1H); 8.16 (d, J = 8.2 Hz, 1H); 7.98 (d, J = 8.8 Hz, 1H); 7.81 (d, J = 8.9 Hz, 1H); 7.62–7.54 (m, 3H); 6.66 (d, J = 3.6 Hz, 1H); 6.57 (m, 1H). MS(ESI) m/z: 236.09 [M+H]+, 235.09 [M]+.

(E)-2-(4-methylstyryl)naphtho[1,2-d]oxazole, FN-7. A quantity of 0.15 mL (1 mmol) of 2-methylnaftoxazole, 2 mL of KOH 50% aqueous and 0.11 mL (0.93 mmol) de 4-methyl-benzaldehyde in 6 mL of dimethyl sulfoxide were stirred at room temperature during 12 h to obtain a greenish yellow. Recrystallization from acetonitrile afforded 145 mg, 56% of the product, m.p. = 127–129°C. ^{1}H-RMN (CDCl$_3$); δ: 8.51 (d, J = 8.1 Hz, 1H); 7.94 (d, J = 8.1 Hz, 1H); 7.77 (d, J = 9.0 Hz, 1H); 7.77 (d, J = 16.2 Hz, 1H); 7.68–7.63 (m, 2H); 7.55–7.49 (m, 3H); 7.22 (d, J = 7.8 Hz, 2H), 7.13 (d, J = 16.2 Hz, 1H); δ 2.38 (s, 3H) ppm.^{13}C-RMN (CDCl$_3$) δ = 162.36, 147.63, 139.86, 138.29, 137.63, 132.61, 131.14, 129.68, 128.58, 127.39, 126.98, 126.29, 126.03, 125.32, 122.07, 113.02, 110.58, 21.44 ppm.

Spectroscopic measurements. Absorption spectra were recorded on a Cary 6000i spectrophotometer (Varian, Palo Alto, CA). Fluorescence emission spectra were recorded on a Spex Fluoromax-4 spectrofluorometer (Horiba Jobin-Ybon, Edison, NJ) or on a PC1 spectrofluorimeter (ISS, Champaign-Urbana). Fluorescence quantum yields (Φ_F) were measured by the comparative method described by Eaton and Demas (20,21), using quinine sulfate in 0.1 N sulfuric acid ($\Phi_F = 0.55$) or naphthalene in ethanol ($\Phi_F = 0.21$) as references (22). The absorbance of sample and reference solutions was set below 0.1 at the excitation wavelength and the fluorescence spectra were corrected using rhodamine G as reference. Sample quantum yields were evaluated using the following Eq. (1):

$$\Phi_x = \left(\frac{\text{Grad}_x}{\text{Grad}_{\text{Act}}}\right)\left(\frac{\eta_x^2}{\eta_{\text{Act}}^2}\right)\Phi_{\text{Act}} \quad (1)$$

where Grad_x and Grad_{Act} are the slope of integrated fluorescence *vs* absorbance plots for the sample and the actinometer and η_x and η_{Act} are the refractive index of sample and actinometer solutions respectively. All measurements were carried out in nitrogen-purged solutions at $(20.0 \pm 0.5)°C$. Fluorescence decays were recorded with a time-correlated single photon counting system (Fluotime 200; PicoQuant GmbH, Berlin, Germany) equipped with a red-sensitive photomultiplier. Excitation was achieved by means of a 375 nm picosecond diode laser working at 10 MHz repetition rate. The counting frequency was maintained always below 1%. Fluorescence lifetimes were analyzed using PicoQuant FluoFit 4.0 software. Light irradiations were performed by means of a SORISA Photocare LED light source applying a power of 25 mW cm^{-2} for every tested wavelength.

Singlet oxygen measurements. The phosphorescence of $^1O_2$ was detected by means of a customized PicoQuant Fluotime 200 system described in detail elsewhere (23). A diode-pumped pulsed Nd:YAG laser (FTSS355-Q; Crystal Laser, Berlin, Germany) working at 10 kHz repetition rate was used for excitation. A 1064 nm rugate notch filter (Edmund Optics, UK) was placed at the exit port of the laser to remove any residual component of its fundamental emission in the near-IR region. The luminescence exiting from the side of the sample was filtered by two long-pass filters of 355 and 532 nm (Edmund Optics, York, UK) and two narrow bandpass filters at 1275 nm (NB-1270-010, Spectrogon, Sweden; bk-1270-70-B, bk Interferenzoptik, Germany) to remove any scattered laser radiation. A near-IR sensitive photomultiplier tube assembly (H9170-45; Hamamatsu Photonics Hamamatsu City, Japan) was used as the detector at the exit port of the monochromator. Photon counting was achieved with a multichannel scaler (PicoQuant's Nanoharp 250). Time-resolved emission signals S_t were analyzed using the PicoQuant FluoFit 4.0 data analysis software to extract lifetime (τ_T and τ_Δ) and amplitude (*a*) values. Quantum yields for $^1O_2$ production (Φ_Δ) were calculated from the amplitudes using the following Eqs. (2)–(4):

$$S_t = a \times \frac{\tau_\Delta}{\tau_\Delta - \tau_T} \times \left(e^{-t/\tau_\Delta} - e^{-t/\tau_T}\right) \quad (2)$$

$$a \propto \Phi_\Delta \quad (3)$$

$$\Phi_\Delta(\text{sample}) = \Phi_\Delta(\text{ref}) \times \frac{a_{\text{sample}}}{a_{\text{ref}}} \quad (4)$$

Perinaphthenone was used as reference for which $\Phi_\Delta = 1$ was taken (24).

The rate constant for $^1O_2$ quenching by the dyads (k_q) was determined by measuring the $^1O_2$ lifetime as a function of the dyad concentration. $^1O_2$ was generated by 50 μM NMB and the concentration of the dyads was varied in the range (0.1–1 mM). A plot of the reciprocal lifetime *vs* the concentration of the dyad afforded k_q as the slope of the linear-fit Eq. (5),

$$\frac{1}{\tau_\Delta} = \frac{1}{\tau_\Delta^0} + k_q[\text{Dyad}] \quad (5)$$

where τ_Δ^0 is the $^1O_2$ lifetime in the neat solvent.

RESULTS

Photophysical characterization

FN-4 is a dyad composed by a furan ring linked to a naphthoxazole moiety through an ethylidene group. The absorption spectrum is dominated by a main band with maximum at 367 nm and a second weaker band at 314 nm (Fig. 2a) that compares reasonably well with the values of 387 and 314 nm obtained from TD-DFT calculations using G09W. The position of the bands follows no obvious trend with the solvent polarity (Table S1). The high values of molar absorptivity, *ca* 3×10^4 M^{-1} cm^{-1} in all solvents except in water, and the molecular orbital analysis of the minimum energy structure obtained from DFT calculations, indicate a π, π^* transition. A similar behavior of the absorption properties was observed for **FN-I2** (Table S2), in which the furan ring is linked directly to the naphthoxazole moiety, and for **FN-7**, in which a nonreactive tolyl substituent replaces the furan moiety. When the linker is saturated (**FN-I1**) spectral bands shift substantially to the blue ($\lambda_{\max} = 322$ nm) and become more structured. These results correlate with the distinct degree of electronic coupling between the aromatic moiety and the naphthoxazole fluorophore. Similar trends are observed in the maximum of the fluorescence spectra (Fig. 2b) consistent with the reports for related benzoxazole derivatives (25).
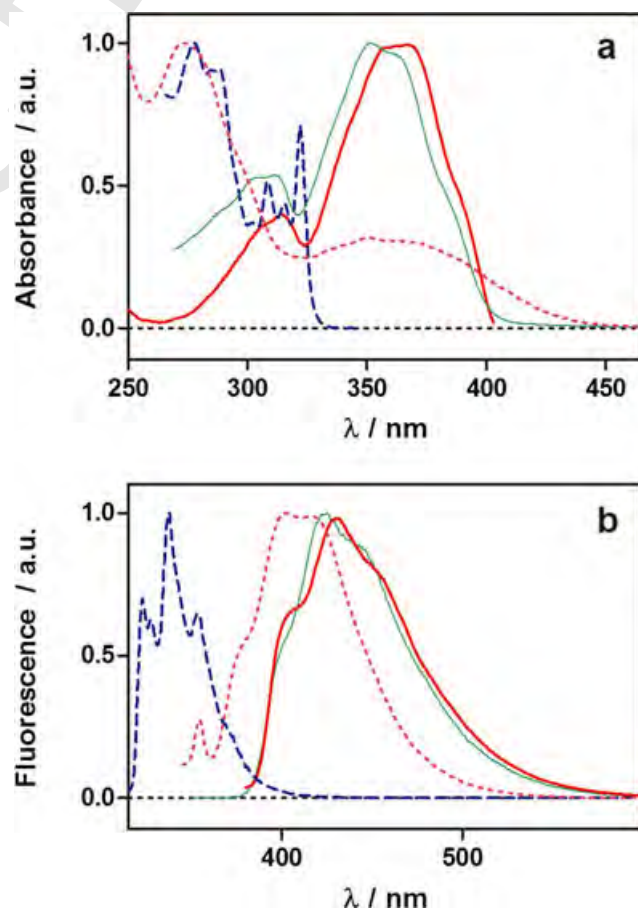
Figure 2. Normalized absorption (a) and fluorescence (b) spectra of **FN-I1** (dashed), **FN-I2** (dotted), **FN-4** (solid) and **FN-7** (light solid) in methanol.

Aryl oxazoles typically exhibit a very high fluorescence quantum yield (Φ_F), in the 0.7–1.0 range (26,27). Among all studied compounds, this is observed only for **FN-I1** ([Φ_F = 0.93] in methanol). In contrast, **FN-4** and **FN-7** show high Φ_F values in low-polarity solvents only, the quantum yield decreasing by 1–2 orders of magnitude as the solvent polarity increases (Tables S1 and S3). However, for (E)-4-(2-(naphtho[1,2-d]oxazol-2-yl)vinyl) benzonitrile, an **FN-7** analogue in which the methyl group is replaced by the strong electron-attractor cyano group, the fluorescence quantum yields are close to one in all solvents, irrespective of their polarity (A. L. Zanocco, unpublished). Finally, **FN-I2** is scantly fluorescent even in nonpolar solvents (Table S2). These results indicate that electron-rich aromatic moieties can act as effective quenchers of naphthoxazole fluorescence in conjugated dyads and, particularly, in polar protic environments, likely due to a charge–transfer interaction. Thus, furyl-oxazole dyads fulfill the first condition requested for a potential $^1O_2$ probe namely that the fluorescence is severely quenched in their native form, thus deserving further scrutiny.
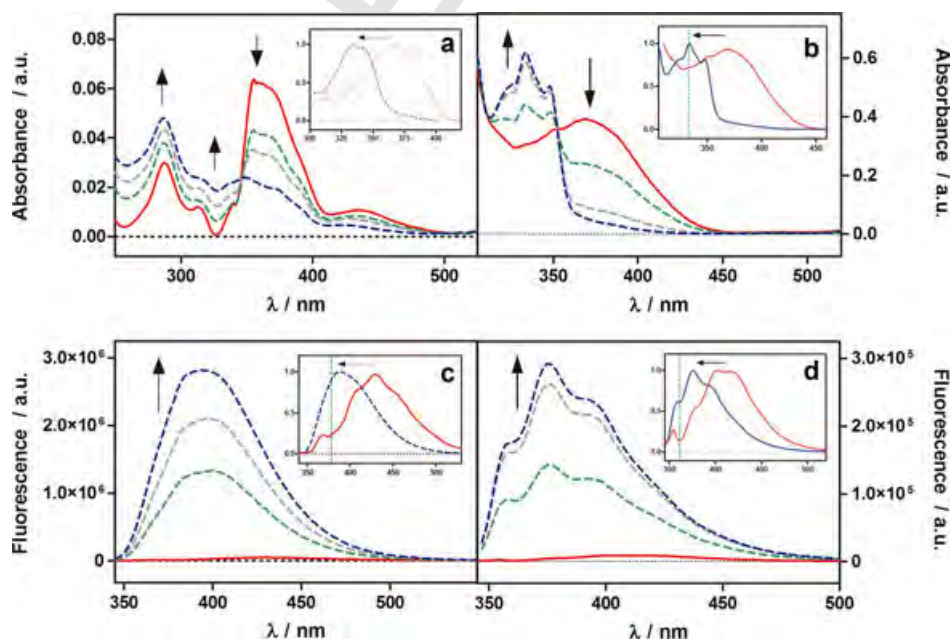
Reactivity toward singlet oxygen

The ability of the dyads to react with $^1O_2$ has been studied by monitoring changes in their absorption and fluorescence properties. No changes could be recorded for **FN-I1** and **FN7**, as expected. In the case of **FN-4**, reaction with $^1O_2$ in methanol caused bleaching of the main band at 367 nm and the growth of a new band in the 325–350 nm region (Fig. 3a). The clear isosbestic point at 348 nm suggests a clean transformation to a single photoproduct (hereafter **FN-4OX**). This was confirmed by HPLC experiments that, after 95% **FN-4** (t_r = 14.3 min) consumption, show the formation of a main product at t_r = 8.3 min and several minor secondary products (Figure S1). Experiments to identify reaction products are in progress; however, furan is well known to selectively react with $^1O_2$ through an endoperoxi-

dation reaction, whereby the primary endoperoxide evolves to different end products depending on the structure of the furan derivative and the solvent (28–30). Involvement of $^1O_2$ in the process was unequivocally demonstrated by the inhibitory effect of selective $^1O_2$ quenchers (Figure S2). Most effective were α-terpinene and sodium azide that inhibited the **FN-4** photooxidation by ca 90%. DABCO was able to diminish the **FN-4** consumption to a lesser extent. A strong fluorescence increase and a concomitant shift of the fluorescence peak to the blue could also be observed (Fig. 3c), the excitation spectra of the original and final fluorescence bands being markedly different, implying that they correspond to different chemical species (Fig. 3a, inset). The spectral overlap is minimized at 330 nm, which suggests that this excitation wavelength should be chosen to maximize the fluorescence of **FN-4OX**. As shown in Fig. 4, the fluorescence intensity at 378 nm is enhanced by more than 300-fold. Compared with SOSG, the fluorescence enhancement of **FN-4** is 30-fold larger.

In a similar fashion to that observed for **FN-4**, emission of **FN-I2** also increases considerably upon reaction with $^1O_2$ in methanol (Fig. 3d), concomitant with the bleaching of the low-energy absorption band at 367 nm (Fig. 3b). Both the absorption and fluorescence spectra reveal the appearance of new bands shifted to the blue. The absorption spectra show a clear isosbestic point at 352 nm, suggesting the formation of a single photoproduct as for **FN-4**. Excitation at 333 nm maximizes the system emission, which increases by a factor ca 135 at 363 nm (Fig. 4).

The results above demonstrate that the new family of naphthoxazole dyads represented by compounds **FN-4** and **FN-I2** outperform any other fluorescent probe currently available for monitoring $^1O_2$. The key novelty of the system relies on the fact that the fluorophore in the photooxidation adduct is different from that in the initial species. Thus, spectral changes arise that elicit the selection of optimal excitation wavelengths to enhance the fluorescence of the photoproducts.

Figure 3. Absorption (a,b) and fluorescence (c,d) spectra of **FN-4** (a,c) and **FN-I2** (b,d) before (solid line) and after (dashed lines) reaction with $^1O_2$. The photosensitizer was new methylene blue 1 μM, the irradiation wavelength was 635 ± 15 nm and the experiments were carried out in aerated methanol. Insets show normalized excitation (a,b) and fluorescence (c,d) spectra to facilitate their comparison.
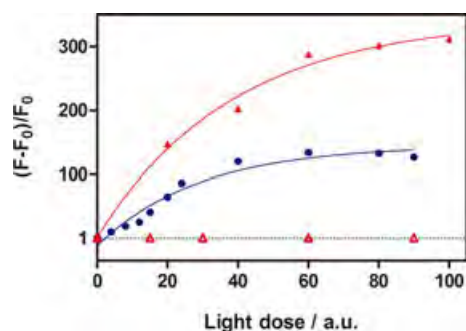
Figure 4. Fluorescence enhancement of **FN-4** (solid triangles; λ_{exc} = 330 nm; λ_{obs} = 378 nm) and **FN-I2** (solid circles; λ_{exc} = 333 nm; λ_{obs} = 363 nm) upon external generation of $^1O_2$ in methanol. Open triangles stand for **FN-4** fluorescence intensity changes upon cumulative irradiation at 355 nm. F stands for the fluorescence intensity at each point of study whereas F_0 refers to the background fluorescence.

Table 1. Summary of photophysical, $^1O_2$ production and reactivity data in MeOH for the compounds under study.

Compound	λ_{exc} (nm)	ε (M^{-1} cm^{-1})	Φ_F	k_q (M^{-1} s^{-1})	Φ_Δ*
FN-4	367	30 060	0.014	9.1×10^5	0.003
FN-I1	322	13 940	$0.930^\dagger$	1.9×10^7	0.070
FN-I2	367	31 721	0.032	2.1×10^7	0.009
FN-7	351	32 516	0.050	$0.0033^\ddagger$	0.004

*Perinaphthenone in methanol (Φ_Δ = 1.0) was used as standard; λ_{exc} = 355 nm (24); †Naphthalene in ethanol (Φ_F = 0.21) was used as standard (22). Excitation wavelength was λ_{exc} = 280 nm (for **FN-I1**); ‡Acetonitrile as solvent.

The rate constant for $^1O_2$ quenching by the dyads (k_q) was determined by time-resolved detection of $^1O_2$ phosphorescence at 1275 nm (5,23). Increasing concentrations of the dyads enhanced the decay rate of $^1O_2$ in a linear fashion. The slope of the plots afforded the k_q values, which are collected in Table 1. Interestingly, the value for **FN-4** (vinyl bridge) is 20-fold smaller than that for **FN-I1** (ethyl bridge) and for **FN-I2** (direct link), and about 40-fold smaller than for isolated 2-methylfuran: $k_q = 9.9 \times 10^7$ M^{-1} s^{-1} in methanol (31), which confirms the strong electronic delocalization of the furan ring across the vinyl bridge in **FN-4**. Notice that the fluorescence enhancements do not correlate with k_q. Finally, the low k_q value for **FN-7** confirms that naphthoxazole derivatives lacking the furyl substituent are essentially unreactive toward $^1O_2$.

Self-sensitization of $^1O_2$ by the dyads and reactivity toward other ROS

A drawback of SOSG is the growth of fluorescence due to self-sensitization of $^1O_2$ (19). Other dyads lack selectivity toward $^1O_2$ and react also with different ROS. We investigated whether the naphthoxazole dyads suffered from the same problems. All dyads sensitized the production of $^1O_2$, although with very small quantum yields (Φ_Δ, Table 1 and Figure S3). Nevertheless, Fig. 4 and Figure S4 show that the fluorescence of **FN-4** does not increase upon cumulative irradiation in methanol and that of **FN-I2** actually decreases.

Reactivity toward other ROS was also tested for **FN-I2** and **FN-4**. Negative results for both dyads *vs* both superoxide (KO_2)

and H_2O_2 were encountered (Figure S5) indicating a high degree of specificity for $^1O_2$

CONCLUSIONS

FN-4 and **FN-I2** are two examples of successful naphthoxazole-based dyads capable of monitoring $^1O_2$ in solution with unprecedented sensitivity. Photooxidation of the trapping moiety leads to the formation of a new chemical entity whose fluorescence is spectrally different from that of the nonirradiated conjugate. Fluorescence enhancement factors up to 300-fold have been observed taking advantage of the change in spectral properties upon photooxidation. Its added selectivity toward $^1O_2$ and the negligible effects of self-sensitization make naphthoxazole dyads worth of further development as $^1O_2$ fluorescent probes.

SUPPORTING INFORMATION

Additional Supporting Information may be found in the online version of this article:

Figure S1. HPLC chromatograms of **FN-4** before (solid line) and after photooxidation (dashed line) with MB as photosensitizer.

Figure S2. Inhibitory effect of $^1O_2$ selective quenchers for **FN4**.

Figure S3. $^1O_2$ self-sensitization by the dyads in methanol.

Figure S4. FN-4 fluorescence changes upon $^1O_2$ self-sensitization

Figure S5. Selectivity of **FN-4** and **FN-I2** toward other reactive oxygen species.

Table S1. Detailed photophysical characterization of **FN-4** in solution.

Table S2. Detailed photophysical characterization of **FN-I1** in solution.

Table S3. Detailed photophysical characterization of **FN-7** in solution.

REFERENCES

1. Redmond, R. W. and I. E. Kochevar (2006) Spatially resolved cellular responses to singlet oxygen. *Photochem. Photobiol.* **82**, 1178–1186.
2. Agostinis, P., K. Berg, K. A. Cengel, T. H. Foster, A. W. Girotti, S. O. Gollnick, S. M. Hahn, M. R. Hamblin, A. Juzeniene, D. Kessel, M. Korbelik, J. Moan, P. Mroz, D. Nowis, J. Piette, B. C. Wilson and J. Golab (2011) Photodynamic therapy of cancer: An update. *CA Cancer J. Clin.* **61**, 250–281.
3. Soh, N. (2006) Recent advances in fluorescent probes for the detection of reactive oxygen species. *Anal. Bioanal. Chem.* **386**, 532–543.
4. Wu, H., Q. Song, G. Ran, X. Lu and B. Xu (2011) Recent developments in the detection of singlet oxygen with molecular spectroscopic methods. *Trends Anal. Chem.* **30**, 133–141.
5. Nonell, S. and S. E. Braslavsky (2000) Time-resolved singlet oxygen detection. In *Singlet Oxygen, UV-A and Ozone*. (Edited by L. Packer

and H. Sies), *Methods Enzymol.* **319**, 37–49. Academic Press, San Diego.

6. Ogilby, P. R. (2010) Singlet oxygen: There is indeed something new under the sun. *Chem. Soc. Rev.* **39**, 3181–3209.

7. Schweitzer, C. and R. Schmidt (2003) Physical mechanisms of generation and deactivation of singlet oxygen. *Chem. Rev.* **103**, 1685–1758.

8. Gandin, E., Y. Lion and A. Van de Vorst (1983) Quantum yield of singlet oxygen production by xanthene derivatives. *Photochem. Photobiol.* **37**, 271–278.

9. Rabello, B. R., A. P. Gerola, D. S. Pellosi, A. L. Tessaro, J. L. Aparício, W. Caetano and N. Hioka (2012) Singlet oxygen dosimetry using uric acid as a chemical probe: Systematic evaluation. *J. Photochem. Photobiol. A* **238**, 53–62.

10. Kalai, T., E. Hideg, I. Vass and K. Hideg (1998) Double (fluorescent and spin) sensors for detection of reactive oxygen species in the thylakoid membrane. *Free Radic. Biol. Med.* **24**, 649–652.

11. Hideg, E. (2004) Detection of free radicals and reactive oxygen species. *Methods Mol. Biol.* **274**, 249–260.

12. Umezawa, N., K. Tanaka, Y. Urano, K. Kikuchi, T. Higuchi and T. Nagano (1999) Novel fluorescent probes for singlet oxygen. *Angew. Chem. Int. Ed. Eng.* **38**, 2899–2901.

13. Tanaka, K., T. Miura, N. Umezawa, Y. Urano, K. Kikuchi, T. Higuchi and T. Nagano (2001) Rational design of fluorescein-based fluorescence probes. Mechanism-based design of a maximum fluorescence probe for singlet oxygen. *J. Am. Chem. Soc.* **123**, 2530–2536.

14. Song, B., G. Wang, M. Tan and J. Yuan (2006) A europium(III) complex as an efficient singlet oxygen luminescence probe. *J. Am. Chem. Soc.* **128**, 13442–13450.

15. Invitrogen—Molecular Probes (2005) Singlet Oxygen Sensor Green Reagent. Available at: http://probes.invitrogen.com/media/pis/mp36002.pdf. Accessed on 18 March 2013.

16. Gollmer, A., J. Arnbjerg, F. H. Blaikie, B. W. Pedersen, T. Breitenbach, K. Daasbjerg, M. Glasius and P. R. Ogilby (2011) Singlet Oxygen Sensor Green®: Photochemical behavior in solution and in a mammalian cell. *Photochem. Photobiol.* **87**, 671–679.

17. Lin, H., Y. Shen, D. Chen, L. Lin, B. C. Wilson, B. Li and S. Xie (2013) Feasibility study on quantitative measurements of singlet oxygen generation using singlet oxygen sensor green. *J. Fluoresc.* **23**, 41–47.

18. Xu, K., L. Wang, M. Qiang, L. Wang, P. Li and B. Tang (2011) A selective near-infrared fluorescent probe for singlet oxygen in living cells. *Chem. Commun.* **47**, 7386–7388.

19. Ragàs, X., A. Jiménez-Banzo, D. Sanchez-Garcia, X. Batllori and S. Nonell (2009) Singlet oxygen photosensitisation by the fluorescent probe Singlet Oxygen Sensor Green®. *Chem. Commun.* **20**, 2920–2922.

20. Demas, J. N. and G. A. Crosby (1971) Measurement of photoluminescence quantum yields—Review. *J. Phys. Chem.* **75**, 991–1024.

21. Eaton, D. F. (1988) Reference materials for fluorescence measurement. *Pure Appl. Chem.* **60**, 1107–1114.

22. Montalti, M., A. Credi, L. Prodi and G. M.T (2006) *Handbook of Photochemistry*, 3rd edn. CRC Press, Boca Raton, FL.

23. Jiménez-Banzo, A., X. Ragàs, P. Kapusta and S. Nonell (2008) Time-resolved methods in biophysics. 7. Photon counting vs. analog time-resolved singlet oxygen phosphorescence detection. *Photochem. Photobiol. Sci.* **7**, 1003–1010.

24. Schmidt, R., C. Tanielian, R. Dunsbach and C. Wolff (1994) Phenalenone, a universal reference compound for the determination of quantum yields of singlet oxygen $O_2(1\Delta g)$ sensitization. *J. Photochem. Photobiol. A* **79**, 11–17.

25. Mac, M., B. Tokarczyk, T. Uchacz and A. Danel (2007) Charge transfer fluorescence of benzoxazol derivatives investigation of solvent effect on fluorescence of these dyes. *J. Photochem. Photobiol. A* **191**, 32–41.

26. Machado, A. E., J. de Miranda, S. Guilardi, D. Nicodem and D. Severino (2003) Photophysics and spectroscopic properties of 3-benzoxazol-2-yl-chromen-2-one. *Spectrochim. Acta A Mol. Biomol. Spectrosc.* **59**, 345–355.

27. Fayed, T. (2004) Probing of micellar and biological systems using 2-(p-dimethylaminostyryl)benzoxazole—An intramolecular charge transfer fluorescent probe. *Colloids Surf. A* **236**, 171–177.

28. Gollnick, K. and A. Griesbeck (1985) Singlet oxygen photooxygenation of furans—isolation and reactions of (4 2)-cycloaddition products (unsaturated sec-ozonides). *Tetrahedron* **41**, 2057–2068.

29. Lemp, E., A. Zanocco and E. Lissi (2003) Linear free energy relationship analysis of solvent effects on singlet oxygen reactions. *Curr. Org. Chem.* **7**, 799–819.

30. Clennan, E. L. and A. Pace (2005) Advances in singlet oxygen chemistry. *Tetrahedron* **61**, 6665–6691.

31. Wilkinson, F., W. P. Helman and A. B. Ross (1995) Rate constants for the decay and reactions of the lowest electronically excited singlet state of molecular oxygen in solution. An expanded and revised compilation. *J. Phys. Chem. Ref. Data* **24**, 663–677.